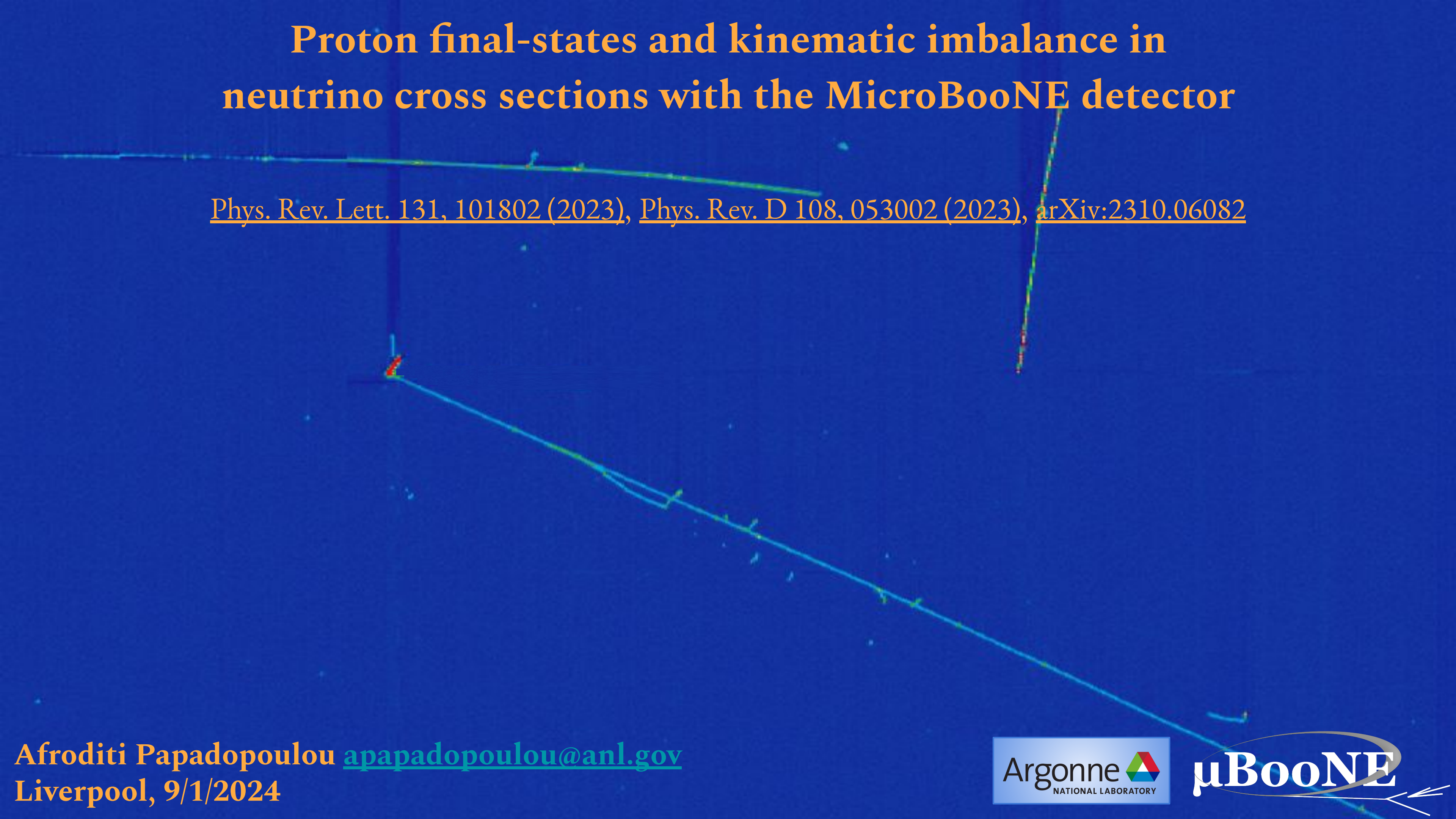

Proton final-states and kinematic imbalance in neutrino cross sections with the MicroBooNE detector

Phys. Rev. Lett. 131, 101802 (2023), Phys. Rev. D 108, 053002 (2023), arXiv:2310.06082

Afroditi Papadopoulou apapadopoulou@anl.gov
Liverpool, 9/1/2024

High-Precision Neutrino Measurements

Question: why matter dominated universe ?

(Potential) answer: Neutrino parameters lead to preferred matter production

Experimental test: Forthcoming DUNE experiment will measure neutrino (matter) and anti-neutrino (anti-matter) interaction rates

Challenge: unprecedented understanding of neutrino-nucleus interactions

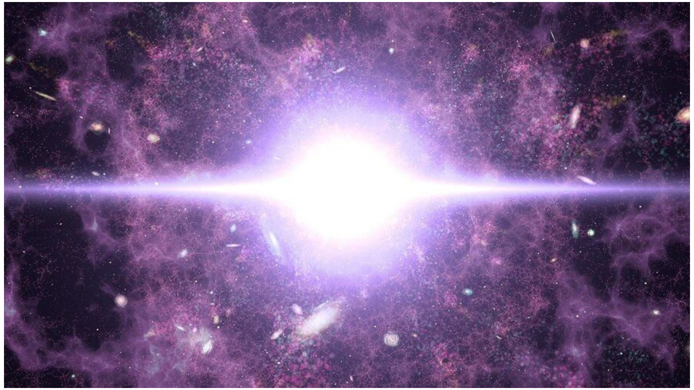

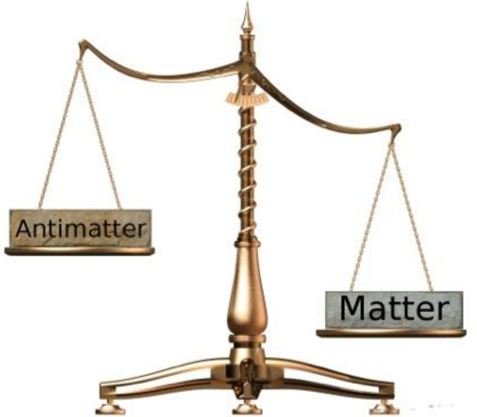

Neutrinos 101

Flavor eigenstates

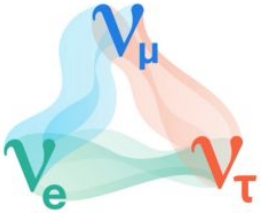

$$\begin{pmatrix} \nu_e \\ \nu_\mu \\ \nu_\tau \end{pmatrix} = U_{\text{PMNS}} \begin{pmatrix} \nu_1 \\ \nu_2 \\ \nu_3 \end{pmatrix}$$

Mass eigenstates

Mixing matrix

$$U_{\text{PMNS}} = \begin{bmatrix} 1 & 0 & 0 \\ 0 & c_{23} & s_{23} \\ 0 & -s_{23} & c_{23} \end{bmatrix} \begin{bmatrix} c_{13} & 0 & s_{13}e^{-i\delta_{\text{CP}}} \\ 0 & 1 & 0 \\ -s_{13}e^{i\delta_{\text{CP}}} & 0 & c_{13} \end{bmatrix} \begin{bmatrix} c_{12} & s_{12} & 0 \\ -s_{12} & c_{12} & 0 \\ 0 & 0 & 1 \end{bmatrix}$$

$c_{ij} = \cos\theta_{ij}$
$s_{ij} = \sin\theta_{ij}$
θ = mixing angle

Experimental Overview

Two-neutrino approximation

$$P(\nu_\alpha \rightarrow \nu_\beta) \sim \sin^2(2\theta)\sin^2\left(\frac{\Delta m^2_{ij} L}{4E}\right)$$

L: distance (baseline)
E: neutrino energy
Δm^2: neutrino mass splitting

$$U_{\mathrm{PMNS}} = \begin{bmatrix} 1 & 0 & 0 \\ 0 & c_{23} & s_{23} \\ 0 & -s_{23} & c_{23} \end{bmatrix} \begin{bmatrix} c_{13} & 0 & s_{13}e^{-i\delta_{\mathrm{CP}}} \\ 0 & 1 & 0 \\ -s_{13}e^{i\delta_{\mathrm{CP}}} & 0 & c_{13} \end{bmatrix} \begin{bmatrix} c_{12} & s_{12} & 0 \\ -s_{12} & c_{12} & 0 \\ 0 & 0 & 1 \end{bmatrix}$$

$c_{ij} = \cos\theta_{ij}$
$s_{ij} = \sin\theta_{ij}$
θ = mixing angle

Experimental Overview

Optimizing baseline L for a given neutrino source of energy E
Mass eigenstate splitting Δm^2 and mixing angles θ known to few %-level

$$U_{\mathrm{PMNS}} = \begin{bmatrix} 1 & 0 & 0 \\ 0 & c_{23} & s_{23} \\ 0 & -s_{23} & c_{23} \end{bmatrix} \begin{bmatrix} c_{13} & 0 & s_{13}e^{-i\delta_{\mathrm{CP}}} \\ 0 & 1 & 0 \\ -s_{13}e^{i\delta_{\mathrm{CP}}} & 0 & c_{13} \end{bmatrix} \begin{bmatrix} c_{12} & s_{12} & 0 \\ -s_{12} & c_{12} & 0 \\ 0 & 0 & 1 \end{bmatrix}$$

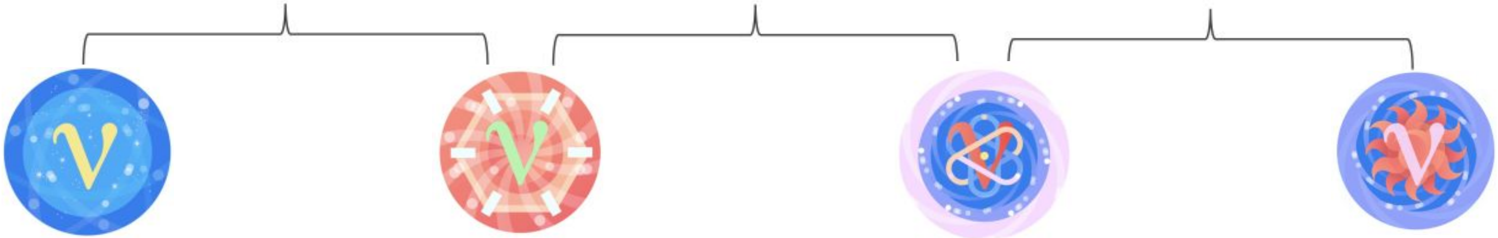

Atmospheric | Accelerator | Reactor | Solar

Open Questions

Charge parity violation

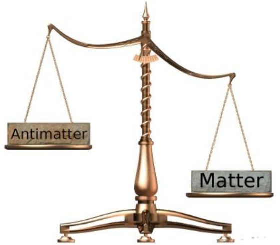

Quarks Leptons

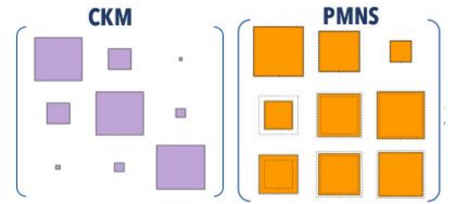

CKM vs PMNS matrix

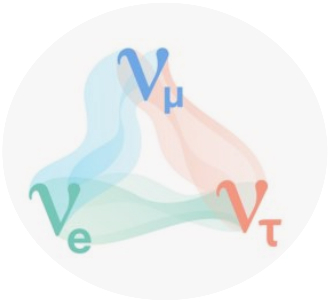

Neutrino nature

Sterile neutrinos & BSM

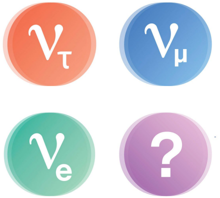

Mass mechanism

Mass ordering

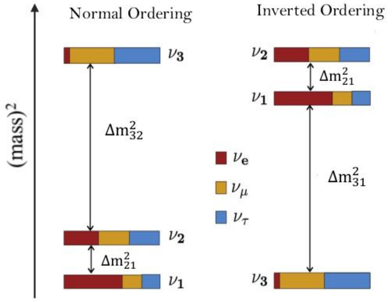

Open Questions

Charge parity violation

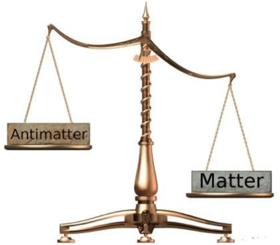

Quarks Leptons

CKM vs PMNS matrix

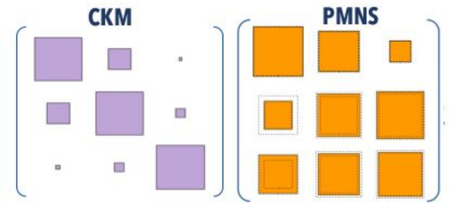

Investigated with high-precision
short- and long-baseline neutrino oscillation experiments

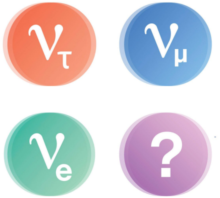

Sterile neutrinos & BSM

Mass ordering

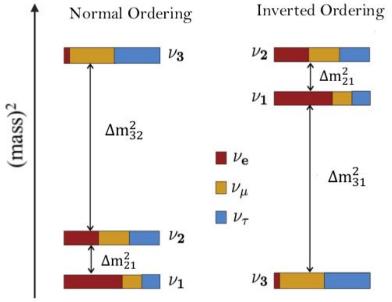

Neutrino Oscillation Experiments

$N_{ND}^{\alpha}(E_{rec})$: Number of events of flavor α

E_{rec} = Reconstructed ν energy

Near Detector

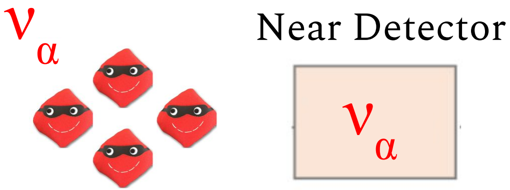

Neutrino flux prediction

Near detector selection efficiency

$$N_{ND}^{\alpha}(E_{rec}) \sim \Phi_{ND}(E_\nu)\, \sigma(E_\nu)\, \varepsilon_{ND}(E_\nu)$$

Neutrino cross section model

E_ν = True ν energy
Also dependence on detector observables

Neutrino Oscillation Experiments

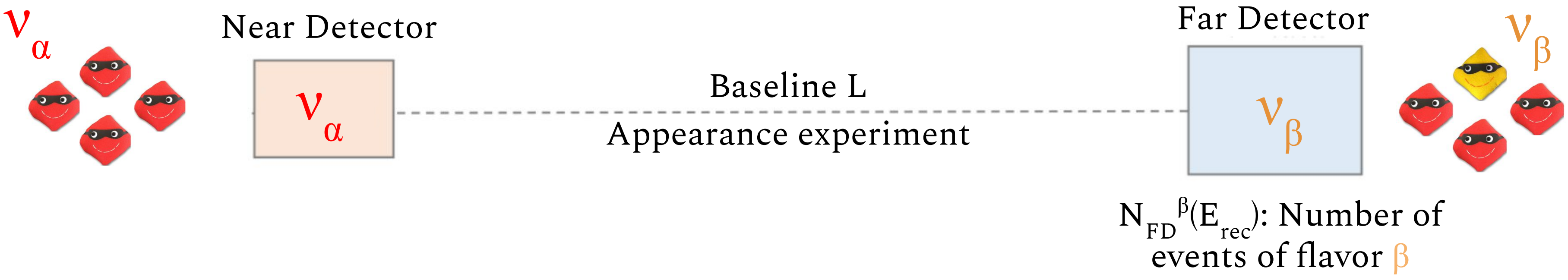

E_{rec} = Reconstructed ν energy

Far Detector

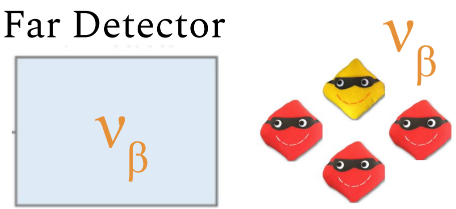

Neutrino flux prediction

Far detector selection efficiency

$$N_{FD}^{\beta}(E_{rec}) \sim \Phi_{FD}(L,E_\nu)\ \sigma(E_\nu)\ \varepsilon_{FD}(E_\nu)\ \mathbf{P}(\boldsymbol{\nu}_{\boldsymbol{\alpha}}\rightarrow\boldsymbol{\nu}_{\boldsymbol{\beta}})$$

Oscillation probability

Neutrino cross section Model

$$P(\nu_\alpha \to \nu_\beta) \sim \sin^2(2\theta)\sin^2\left(\frac{\Delta m_{ij}^2 L}{4E}\right)$$

E_ν = True ν energy

Also dependence on detector observables

Far Detector

Measured | Precise modeling input needed | Want to measure with high-precision

$$N_{FD}^{\beta}(E_{rec}) \sim \Phi_{FD}(L,E_\nu)\,\sigma(E_\nu)\,\varepsilon_{FD}(E_\nu)\,\mathbf{P}(\nu_\alpha \rightarrow \nu_\beta)$$

Oscillation probability

- Smearing relating E_ν to E_{rec}
- Neutrino signal topologies
- Neutrino backgrounds for BSM
- ...

Far Detector

$$N_{FD}^{\beta}(E_{rec}) \sim \Phi_{FD}(L,E_\nu)\ \sigma(E_\nu)\ \varepsilon_{FD}(E_\nu)\ \mathbf{P}(\boldsymbol{\nu_\alpha \rightarrow \nu_\beta})$$

Oscillation probability

Need for high precision
ν cross section measurements

Challenging ...

- Broad neutrino spectra
- Various complex interaction mechanisms

Any mismodeling in neutrino event generator simulation predictions can limit experimental sensitivity

Rev. Mod. Phys. 84, 1307 (2012)

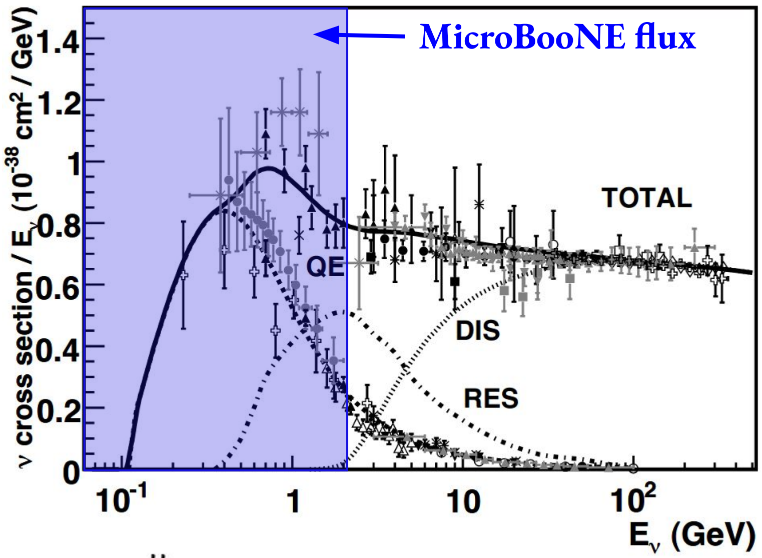

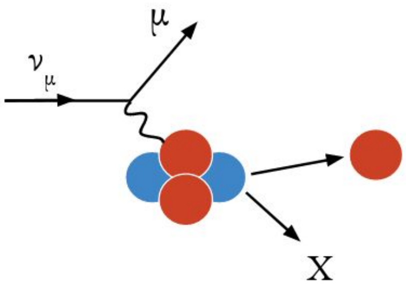

Quasi-elastic (QE)

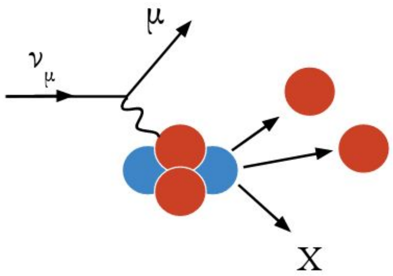

Meson Exchange Current (MEC)

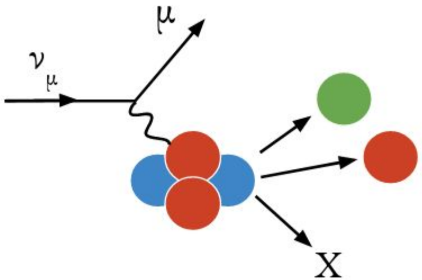

Resonance (RES)

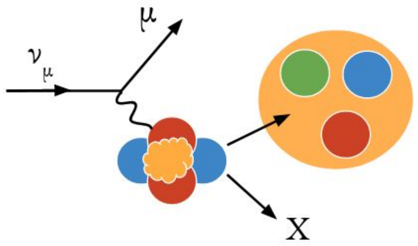

Deep Inelastic Scattering (DIS)

Future Experiments

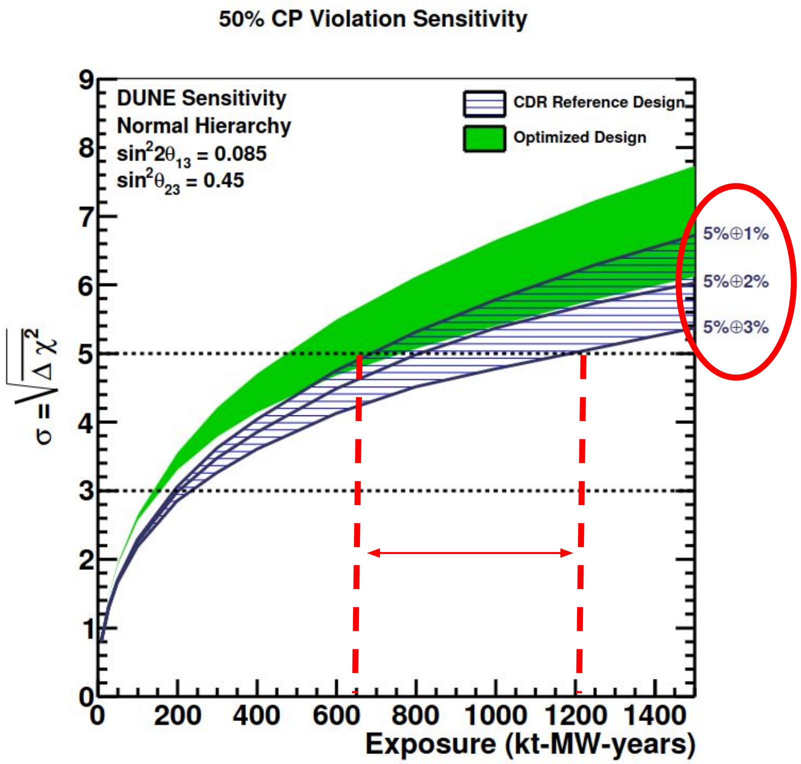

DUNE CDR, arXiv:1512.06148

- Mismodeling can impact required run time of forthcoming flagship experiments

- But … head start with Short-Baseline Neutrino (SBN) Program (MicroBooNE, SBND, ICARUS)

MicroBooNE@FNAL

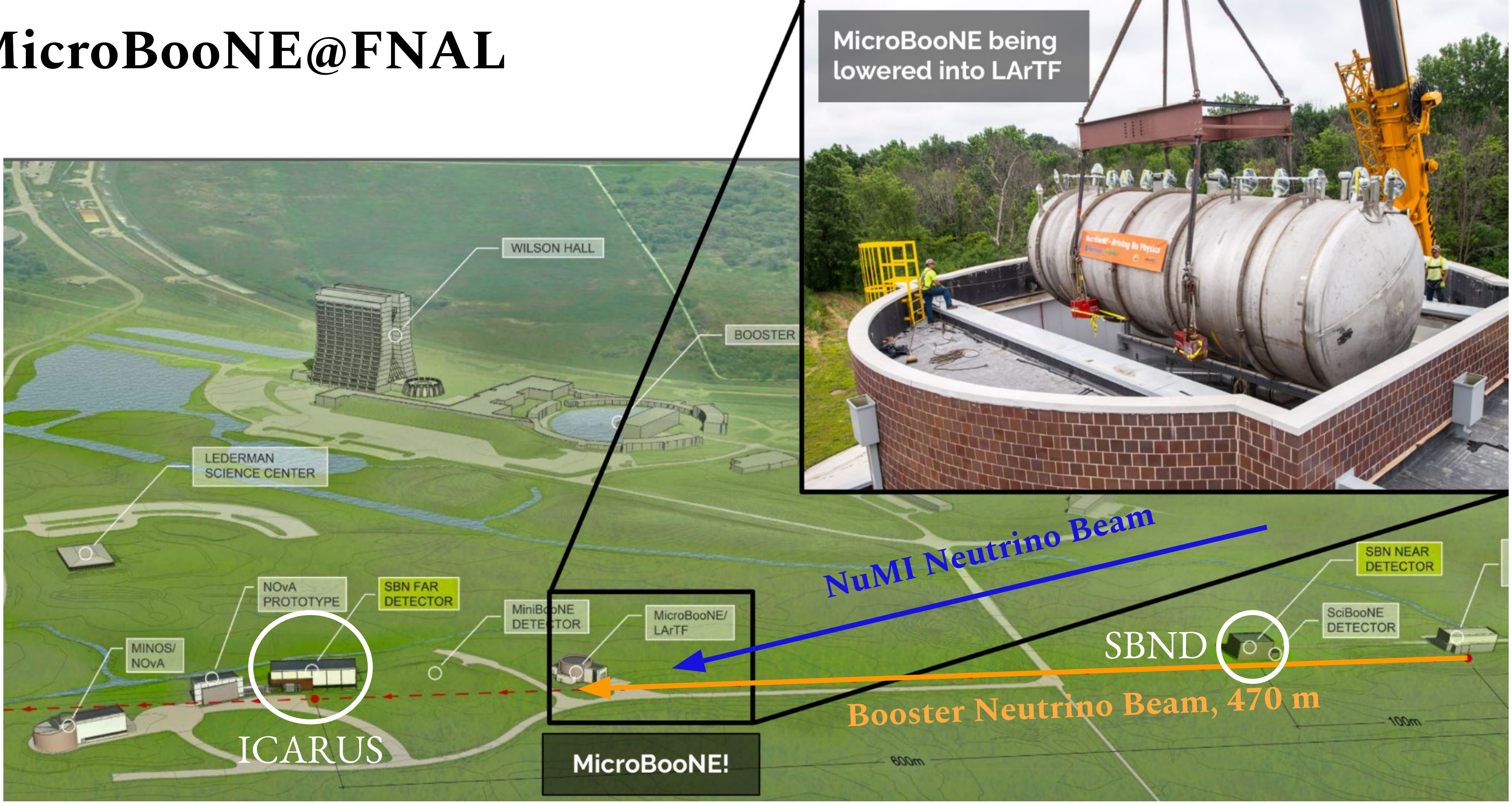

85 tonne Liquid Argon Time Projection Chamber (LArTPC)

JINST 12, P02017 (2017)

LArTPC Operation Principle

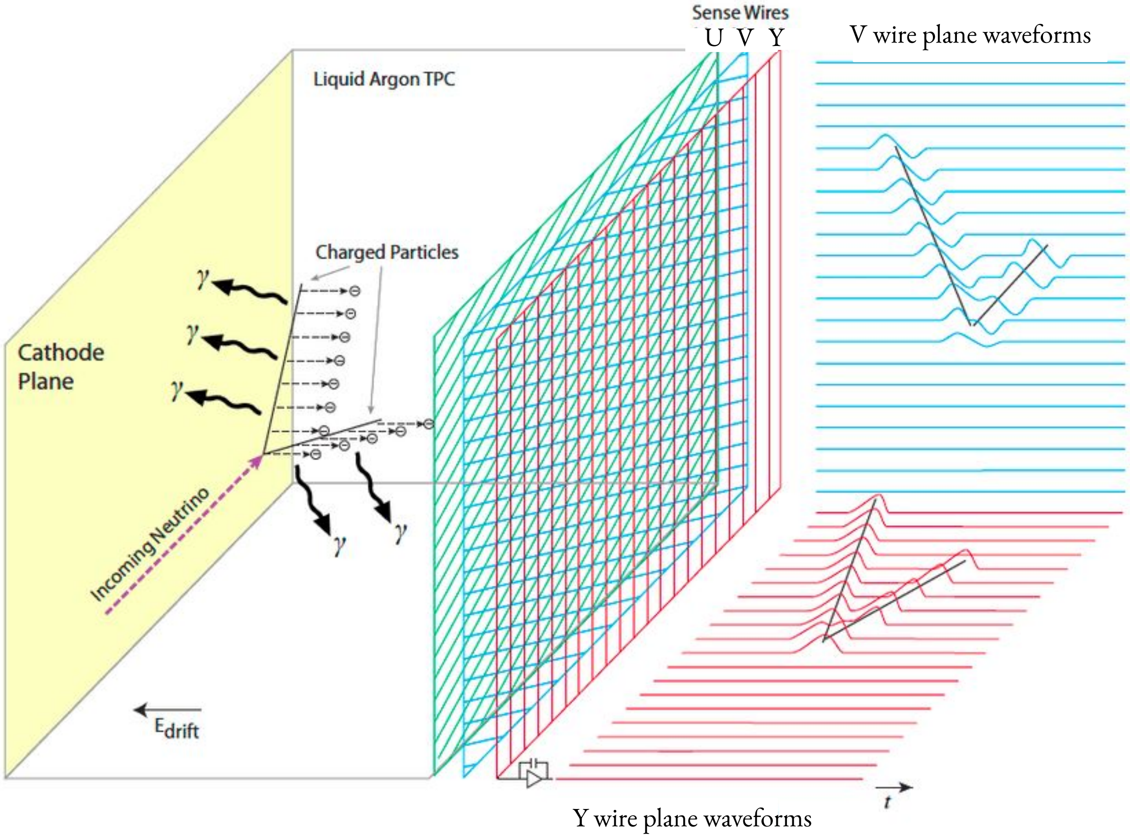

MicroBooNE

- 3 wire planes
- 8192 gold coated wires
- 3 mm wire spacing
- 32 PMTs

JINST 12, P02017 (2017)

MicroBooNE Data Events

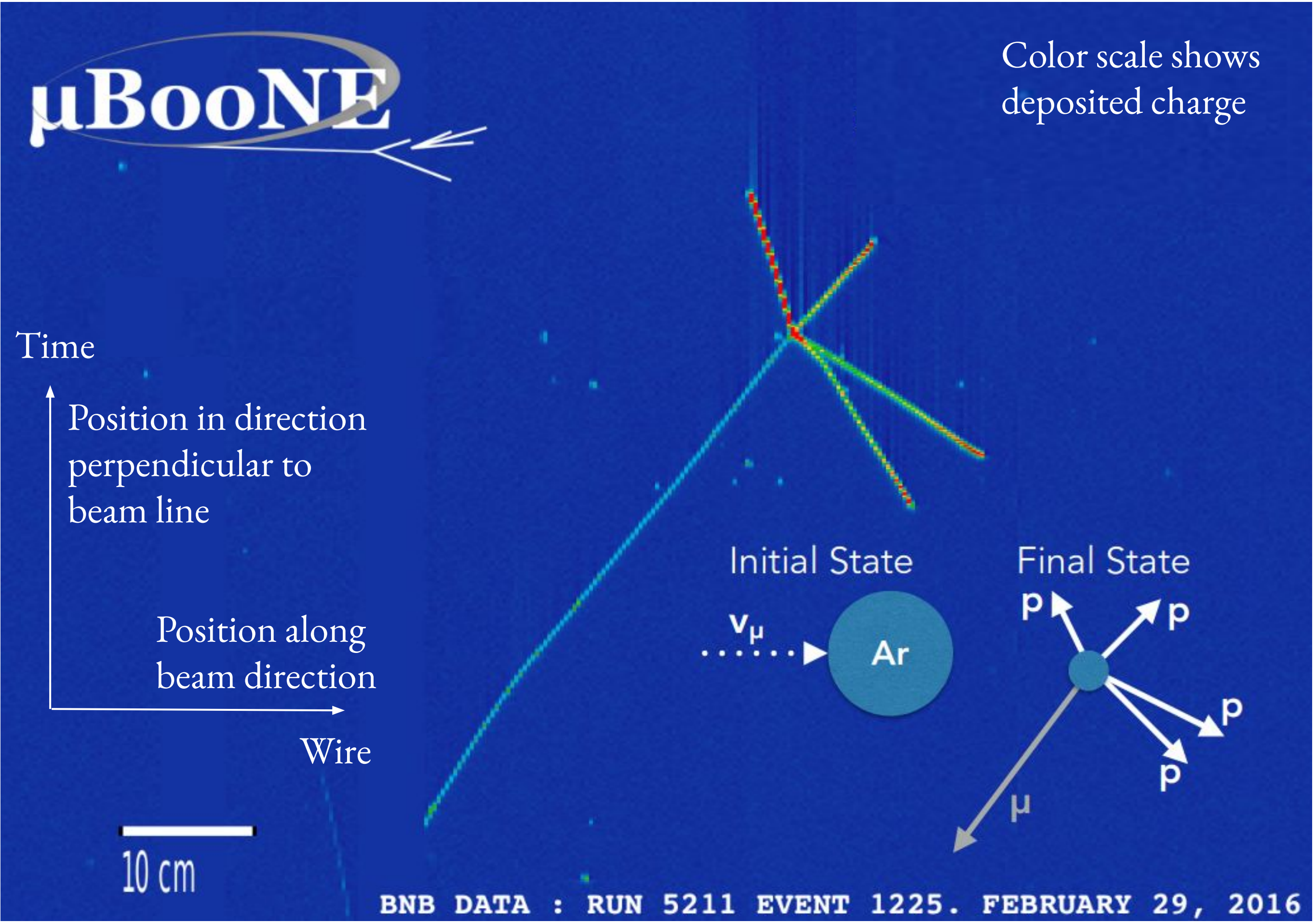

- Excellent spatial resolution
- Low detection thresholds
- Precise calorimetric information
- Powerful particle identification

MicroBooNE Data Events

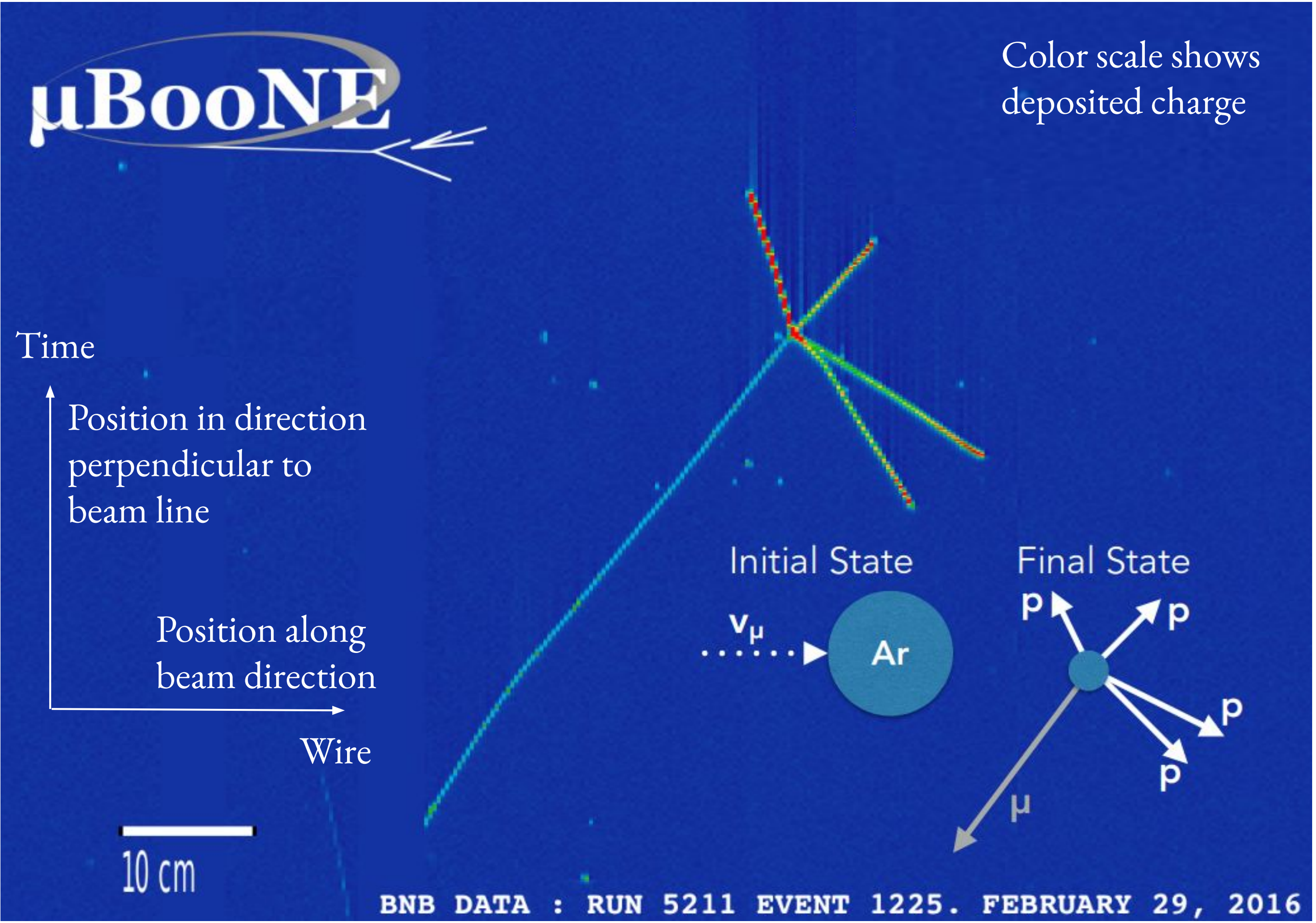

- Largest available neutrino-argon data set with ~500k recorded neutrino interactions
- 15 released and more than 30 active MicroBooNE cross section analyses
- Multiple topologies investigated

Already Public Results

CC inclusive

- 1D ν_μ CC inclusive @ BNB
  Phys. Rev. Lett. 123, 131801 (2019)
- 1D ν_μ CC E_ν @ BNB
  Phys. Rev. Lett. 128, 151801 (2022)
- 3D CC E_ν @ BNB
  arXiv:2307.06413 , submitted to PRL
- 1D ν_e CC inclusive @ NuMI
  Phys. Rev. D105, L051102 (2022)
  Phys. Rev. D104, 052002 (2021)

Pion production

- ν_μ NCπ^0 @ BNB
  Phys. Rev. D 107, 012004 (2023)

Rare channels

- η production @ BNB, submitted to PRL
  arXiv:2305.16249
- Λ production @ NuMI
  Phys. Rev. Lett. 130, 231802 (2023)

CC0π

- 1D ν_e CCNp0π @ BNB
  Phys. Rev. D 106, L051102 (2022)
- 1D & 2D ν_μ CC1p0π Transverse Imbalance @ BNB
  Phys. Rev. Lett. 131, 101802 (2023)
  Phys. Rev. D 108, 053002 (2023)
- 1D & 2D ν_μ CC1p0π Generalized Imbalance @ BNB
  arXiv:2310.06082, submitted to PRD
- 1D ν_μ CC1p0π @ BNB
  Phys. Rev. Lett. 125, 201803 (2020)
- 1D ν_μ CC2p @ BNB
  arXiv:2211.03734
- 1D ν_μ CCNp0π @ BNB
  Phys. Rev. D102, 112013 (2020)

15 cross section publications
and way more to come!

Already Public Results

μBooNE

CC inclusive

- 1D ν_μ CC inclusive @ BNB
  Phys. Rev. Lett. 123, 131801 (2019)
- 1D ν_μ CC E_ν @ BNB
  Phys. Rev. Lett. 128, 151801 (2022)
- 3D CC E_ν @ BNB
  arXiv:2307.06413 , submitted to PRL
- 1D ν_e CC inclusive @ NuMI
  Phys. Rev. D105, L05110
  Phys. Rev. D104, 052002

Pion production

- ν_μ NCπ^0 @ BNB
  Phys. Rev. D 107, 012004 (2023)

Rare channels

- η production @ BNB, submitted to PRL
  arXiv:2305.16249
- Λ production @ NuMI
  Phys. Rev. Lett. 130, 231802 (2023)

CC0π

- 1D ν_e CCNp0π @ BNB
  Phys. Rev. D 106, L051102 (2022)
- 1D & 2D ν_μ CC1p0π Transverse Imbalance @ BNB
  Phys. Rev. Lett. 131, 101802 (2023)
  Phys. Rev. D 108, 053002 (2023)
- 1D & 2D ν_μ CC1p0π Generalized Imbalance @ BNB
  arXiv:2310.06082, submitted to PRD

  0)

  arXiv:2211.03734
- 1D ν_μ CCNp0π @ BNB
  Phys. Rev. D102, 112013 (2020)

Opportunity to extensively benchmark neutrino event generator predictions

15 cross section publications
and way more to come!

Nuclear Effects in Event Generators

[Rev. Mod. Phys. 89, 045002 (2017)](https://journals.aps.org/rmp/abstract/10.1103/RevModPhys.89.045002)

- Fermi motion
- Final state interactions
- Meson exchange currents
- …

Known unknowns that need to be accurately simulated

Struck nucleon motion in argon

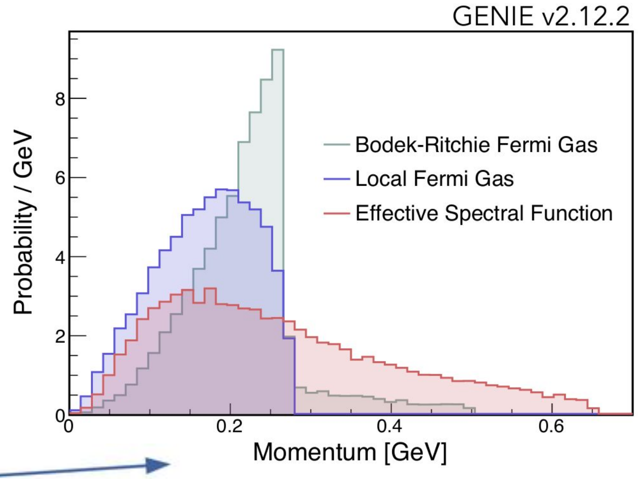

Hadron reinteractions

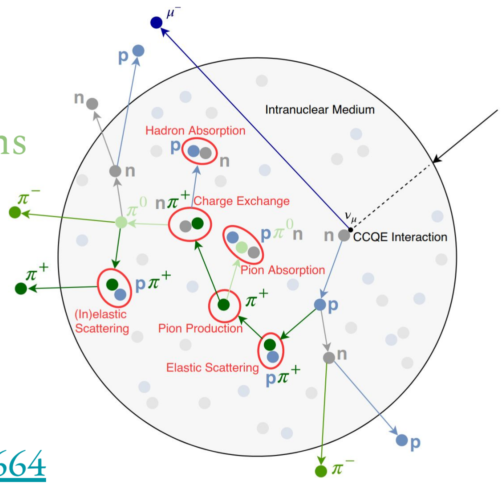

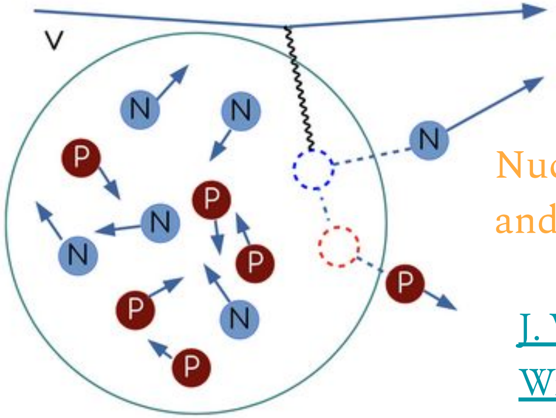

Nucleon-nucleon relative angle and momenta

J. Wolcott Wine & Cheese Seminar

arXiv:2201.04664

Double-Differential Single-Proton Knockout

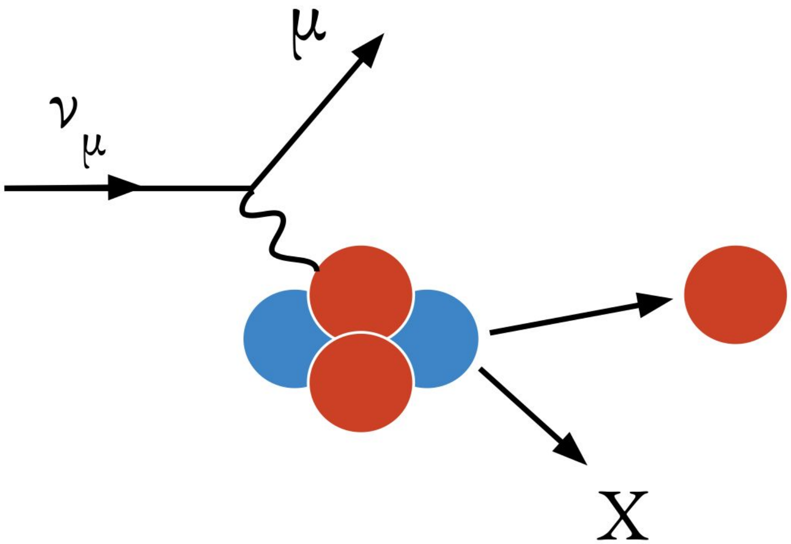

- First double-differential single-proton cross section measurement on argon
- Identified kinematic variables and phase-space regions with sensitivity to Fermi motion & final state interactions
- Uses ~50% of available MicroBooNE data sets & Booster Neutrino Beam (BNB)

Phys. Rev. Lett. 131, 101802 (2023)
Phys. Rev. D 108, 053002 (2023)
arXiv:2310.06082

Single-Proton Knockout

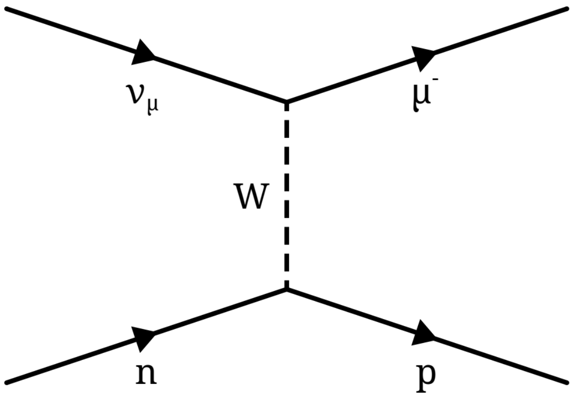

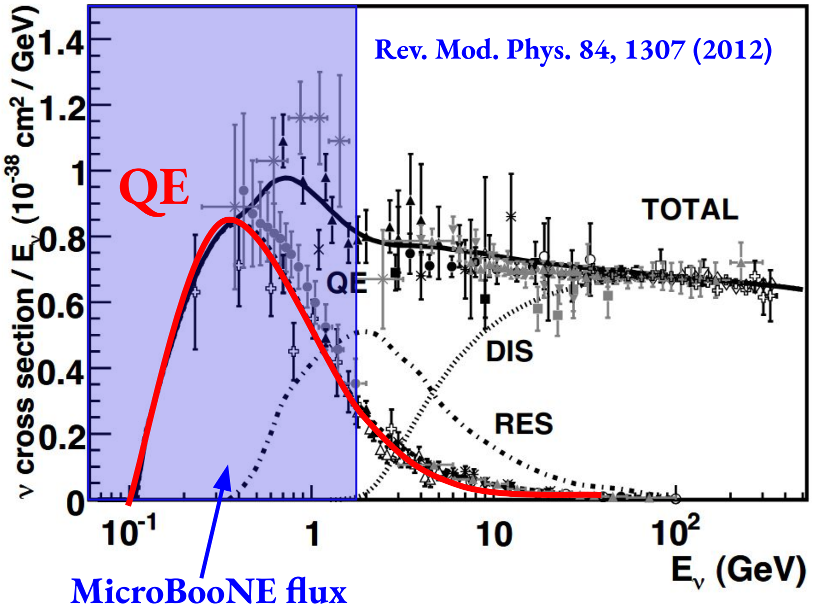

- Dominated by Charged Current Quasi-elastic (CCQE) interactions
- Simple single muon-proton events
- Dominant at MicroBooNE energies

CC1p0π Quasielastic-like Signal Definition

Ranges driven by minimum track length, track containment, hadronic reinteractions, and systematics

- 1 muon
  $100 < P_\mu < 1200$ MeV/c
- 1 proton
  $300 < P_p < 1000$ MeV/c
- No $\pi^\pm$ with $P_\pi > 70$ MeV/c
- No π^0 or heavier mesons
- Any number of neutrons

9051 CC1p0π candidate data events

CC1p0π ~10% efficiency

~70% purity

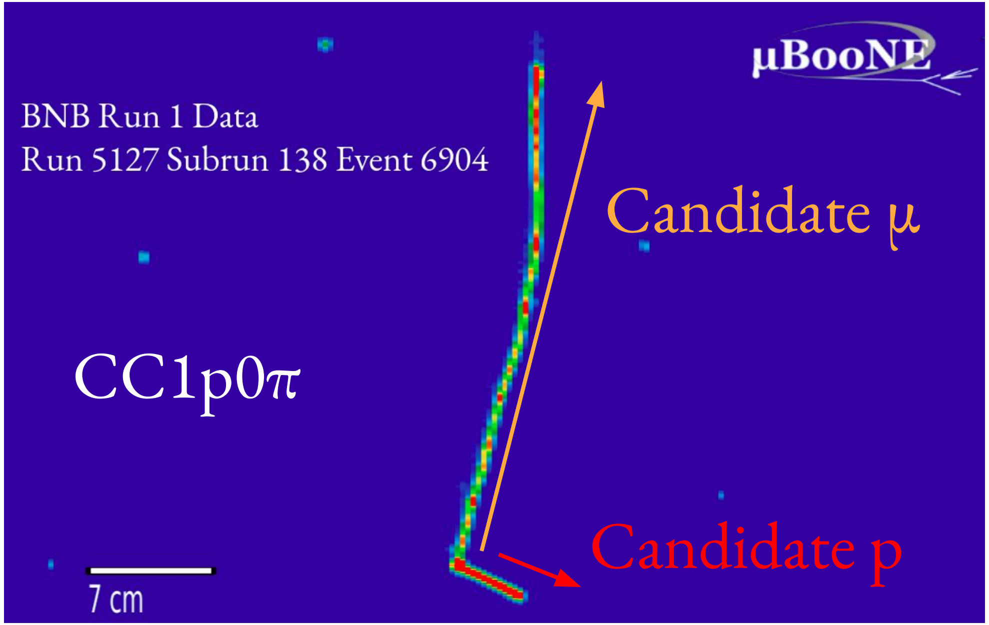

Phys. Rev. Lett. 131, 101802 (2023)
Phys. Rev. D 108, 053002 (2023)
* Phys. Rev. D 105, 072001 (2022)

MC: GENIE v3.0.6 G18_10a_02_11b + tune*
Nieves QE & MEC, Berger Sehgal RES

Transverse Kinematic Imbalance (TKI)

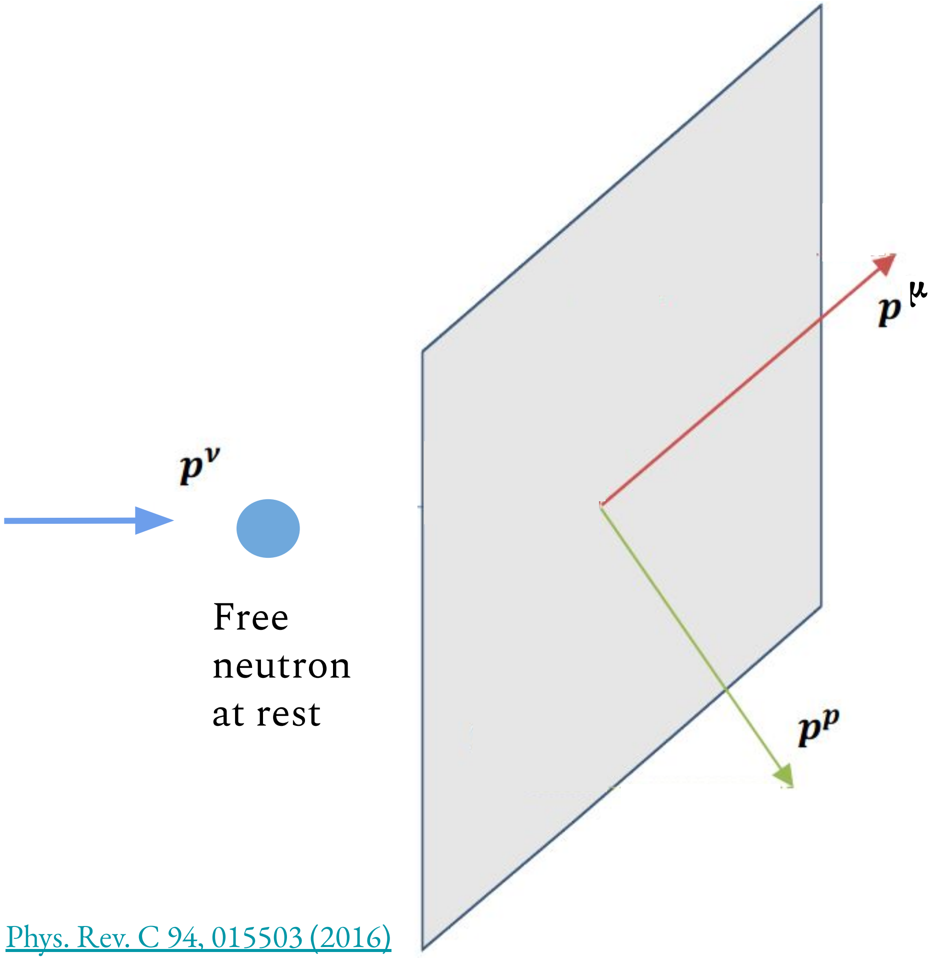

Free
neutron
at rest

Phys. Rev. C 94, 015503 (2016)

Transverse Kinematic Imbalance (TKI)

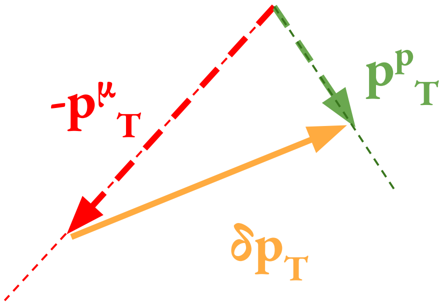

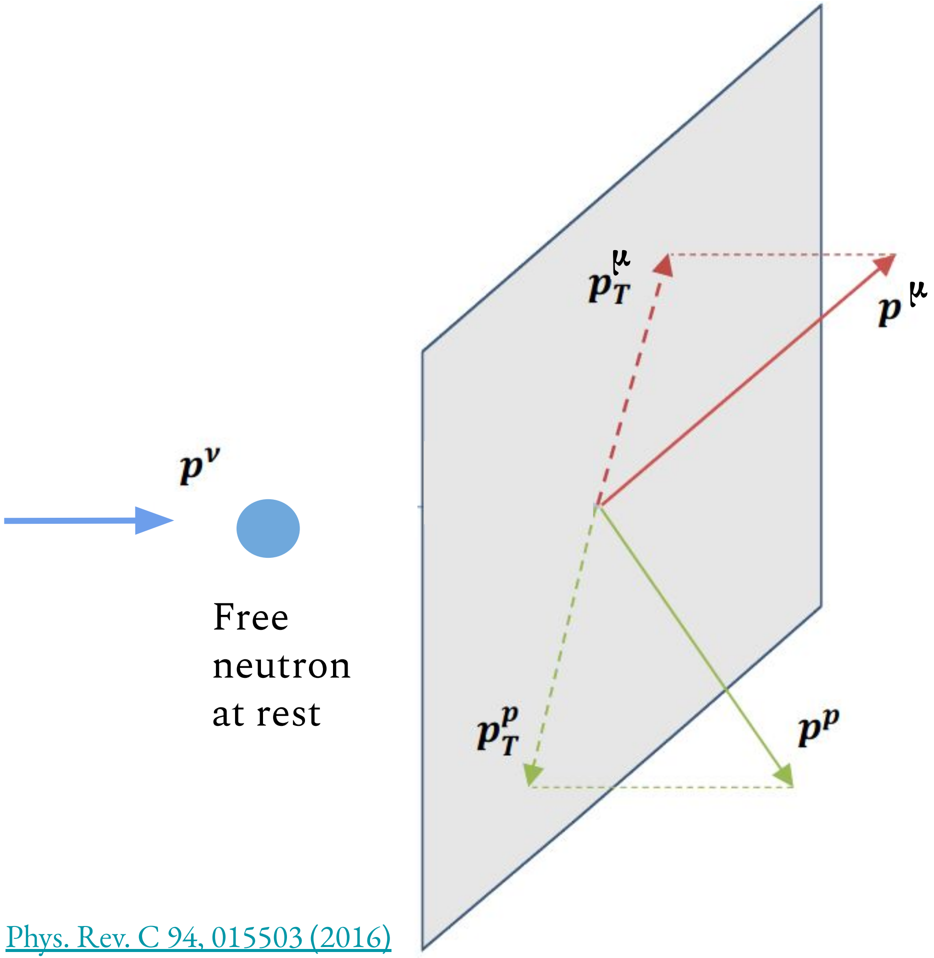

Free
neutron
at rest

Transverse missing momentum
$\delta p_T = | \mathbf{p_T}^{\mu} + \mathbf{p_T}^{p} | = 0$

Transverse projections equal and opposite due to momentum conservation

Phys. Rev. C 94, 015503 (2016)

Transverse Kinematic Imbalance (TKI)

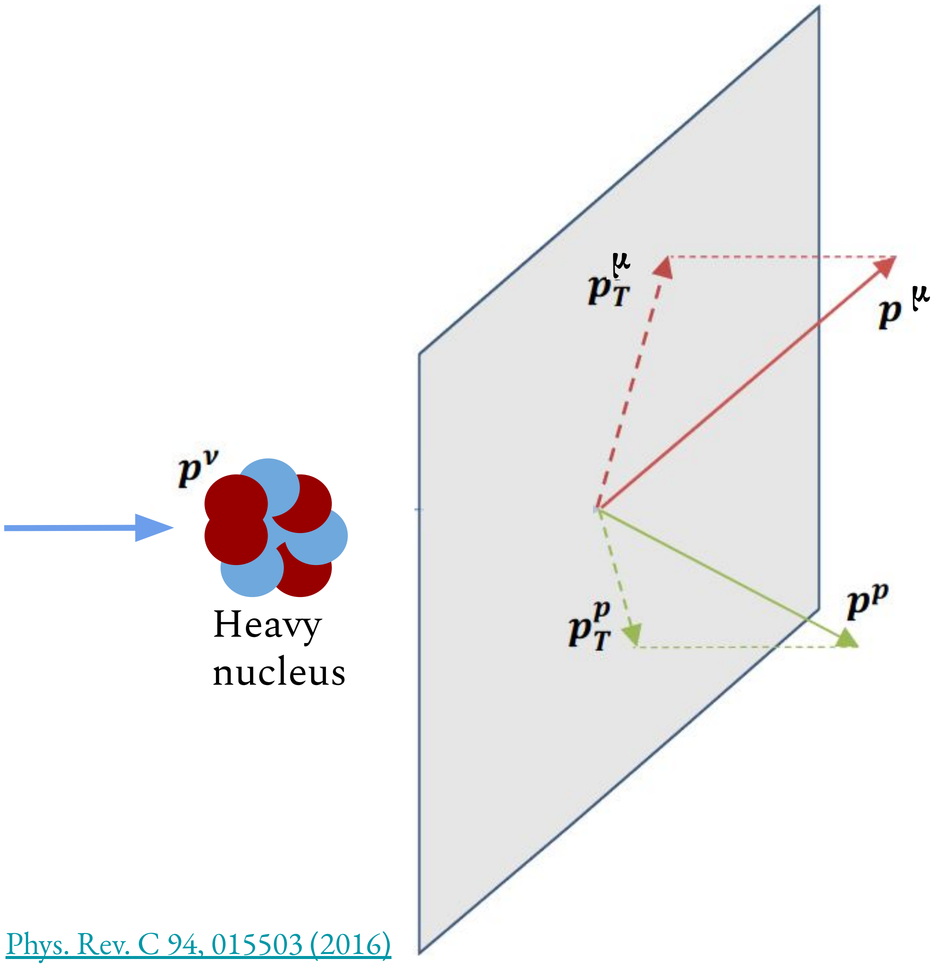

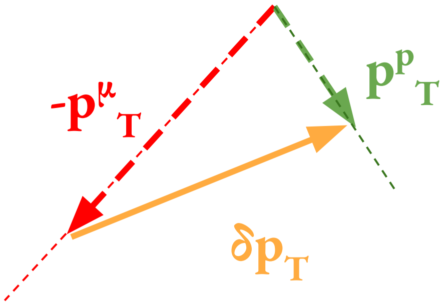

Transverse missing momentum
$\delta p_T = | \mathbf{p_T}^\mu + \mathbf{p_T}^p | > 0$

Broad distribution due to initial nucleon motion and other nuclear effects

[Phys. Rev. C 94, 015503 (2016)]

Transverse Kinematic Imbalance (TKI)

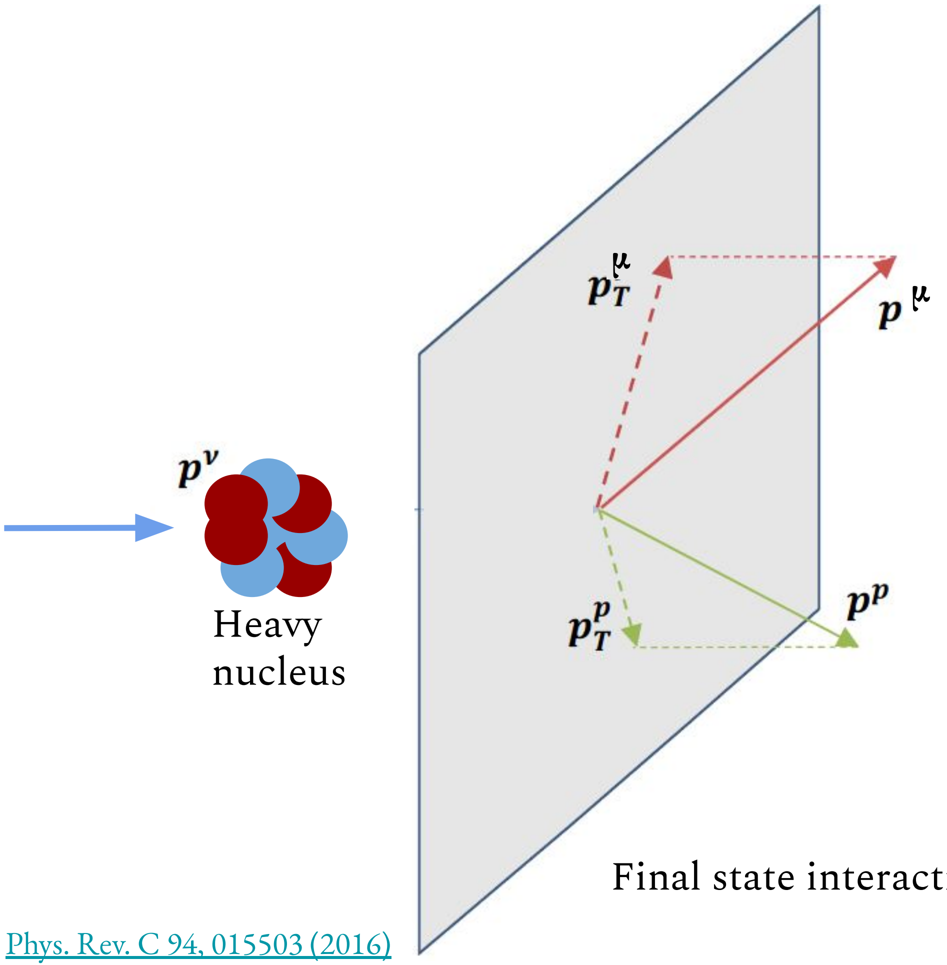

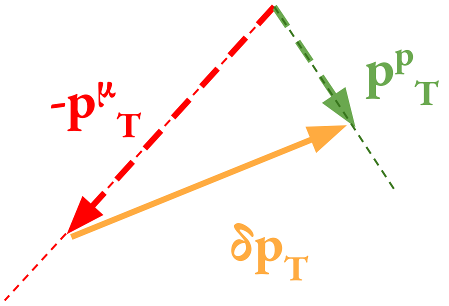

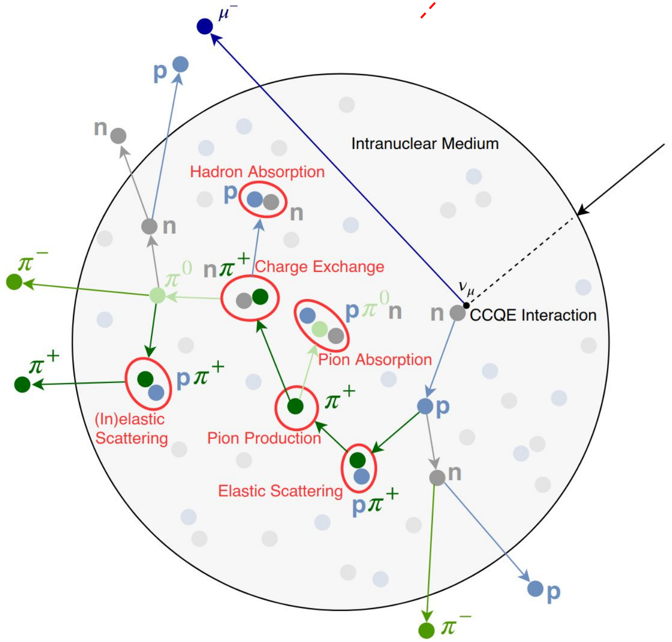

Final state interactions (FSI)

[arXiv:2201.04664](https://arxiv.org/abs/2201.04664)

[Phys. Rev. C 94, 015503 (2016)](https://doi.org/10.1103/PhysRevC.94.015503)

Transverse Kinematic Imbalance (TKI)

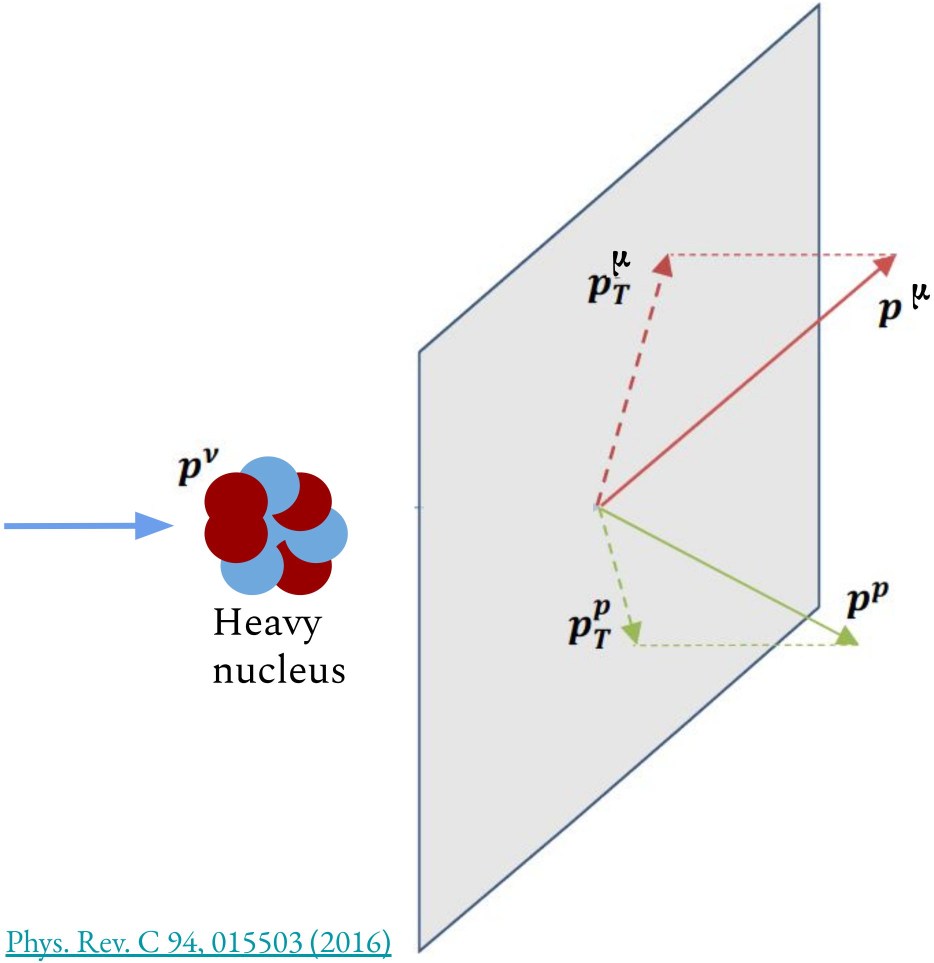

Orientation of the imbalance ($\delta\alpha_T$) also meaningful

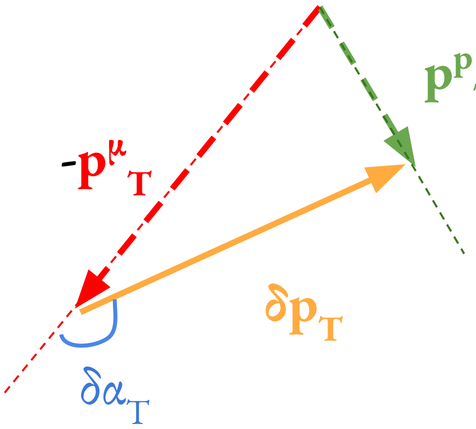

Phys. Rev. C 94, 015503 (2016)

Transverse Kinematic Imbalance (TKI)

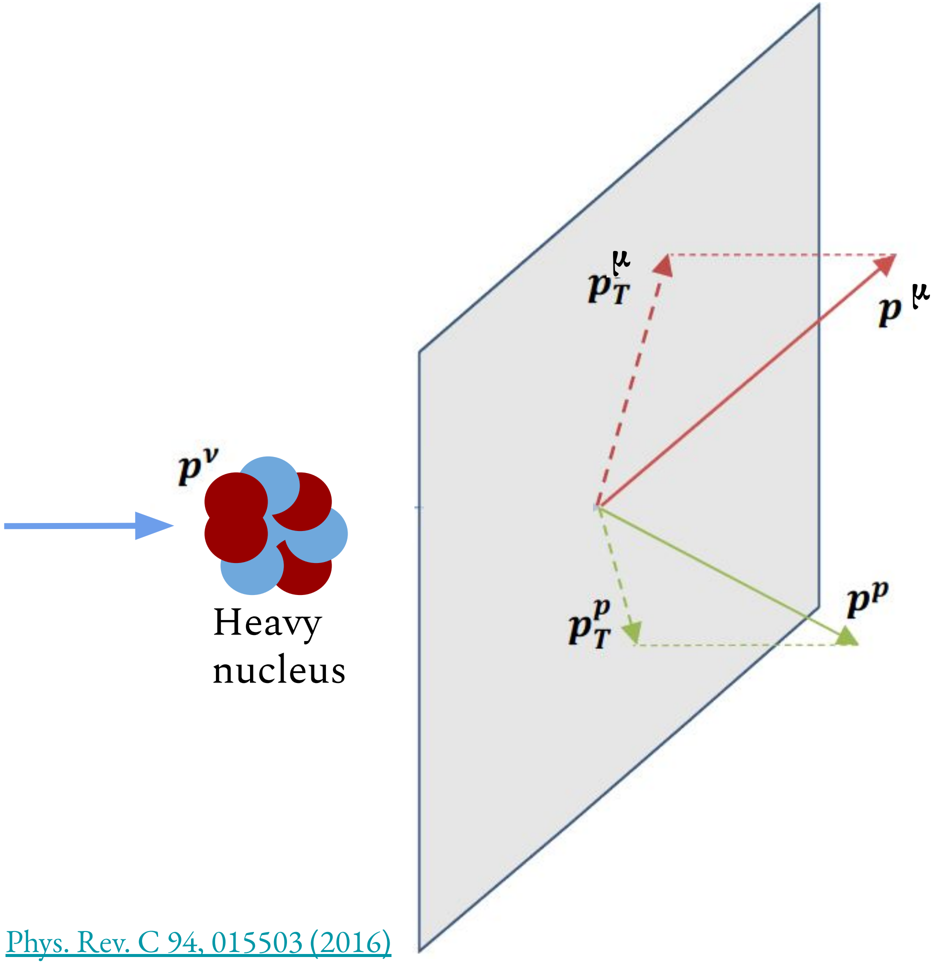

Lower proton momentum due to FSI leads to larger $\delta\alpha_T$ (closer to 180°)

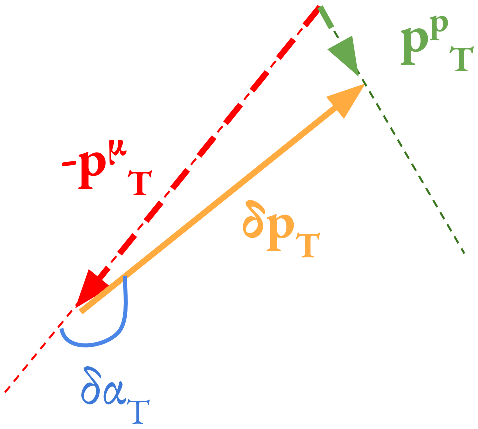

Phys. Rev. C 94, 015503 (2016)

Transverse Missing Momentum δp_T

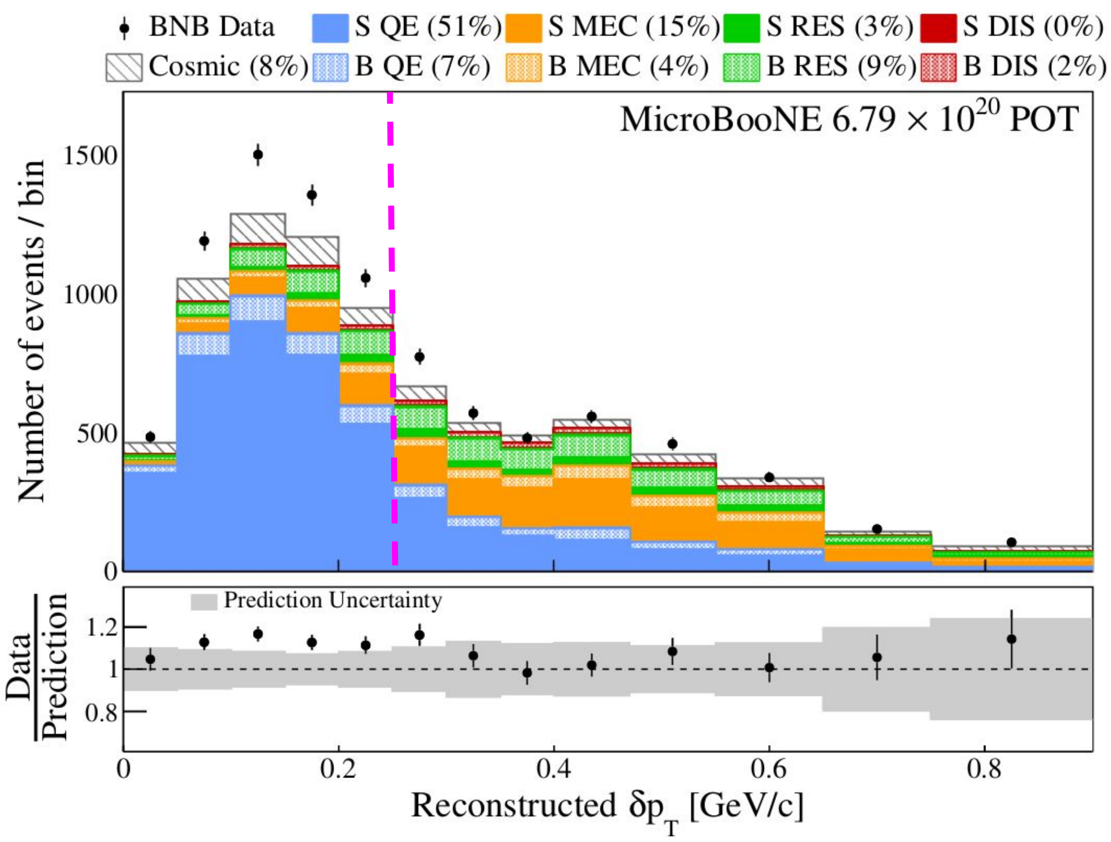

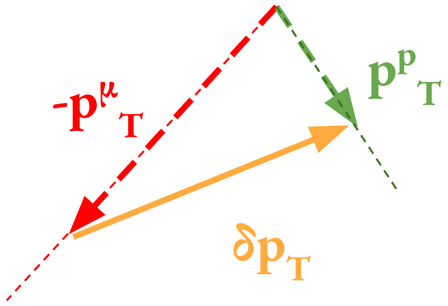

- S = Signal, B = Background
- QE dominance in peak below Fermi momentum (~250 MeV/c)
- MEC/RES mainly in high momentum tail

GENIE v3.0.6 G18_10a_02_11b + tune*
Nieves QE & MEC, Berger Sehgal RES

Phys. Rev. D 108, 053002 (2023)

* Phys. Rev. D 105, 072001 (2022)

Transverse Orientation $\delta\alpha_T$

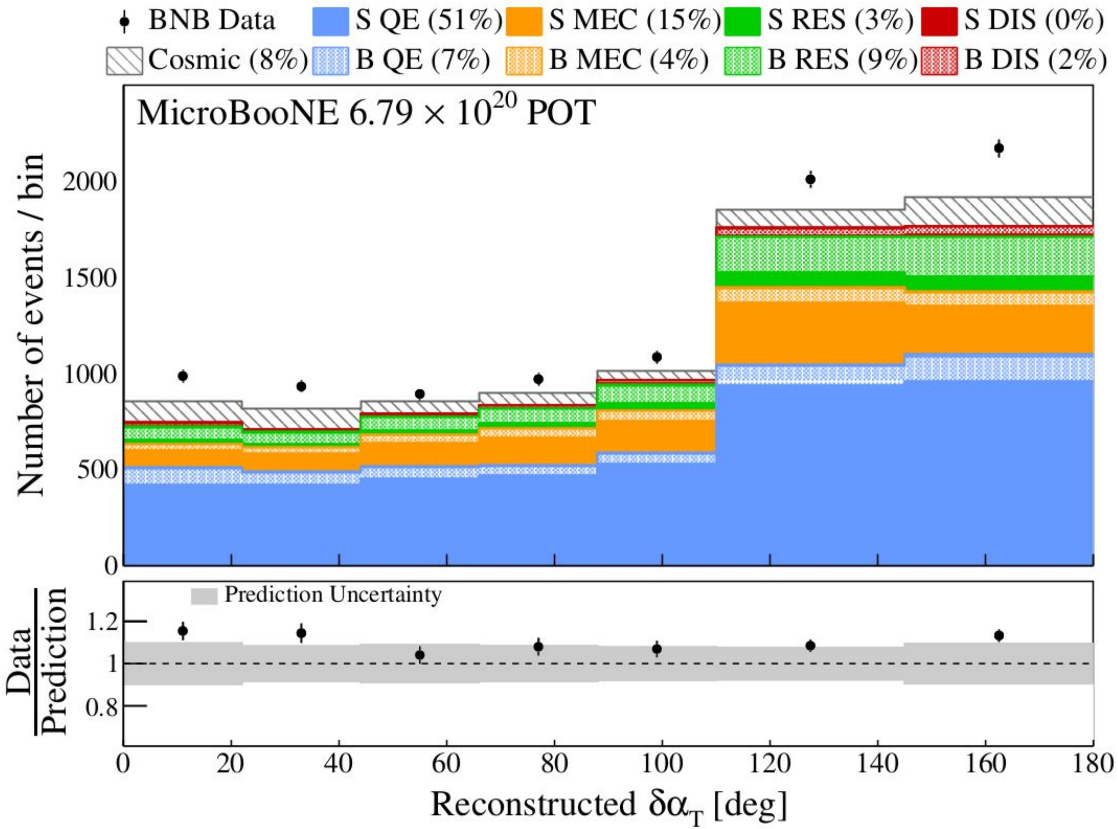

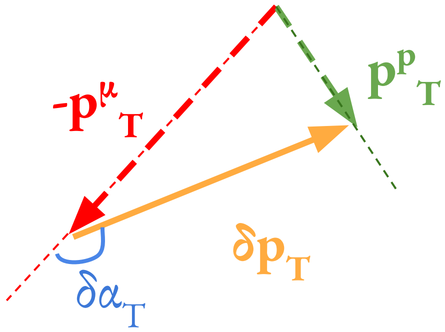

- $\delta\alpha_T$ asymmetry due to proton FSI
- **MEC**/**RES** fractional contribution enhanced in ~180° region

GENIE v3.0.6 G18_10a_02_11b + tune*
Nieves QE & MEC, Berger Sehgal RES

Phys. Rev. D 108, 053002 (2023)
* Phys. Rev. D 105, 072001 (2022)

Transverse Orientation $\delta\alpha_T$

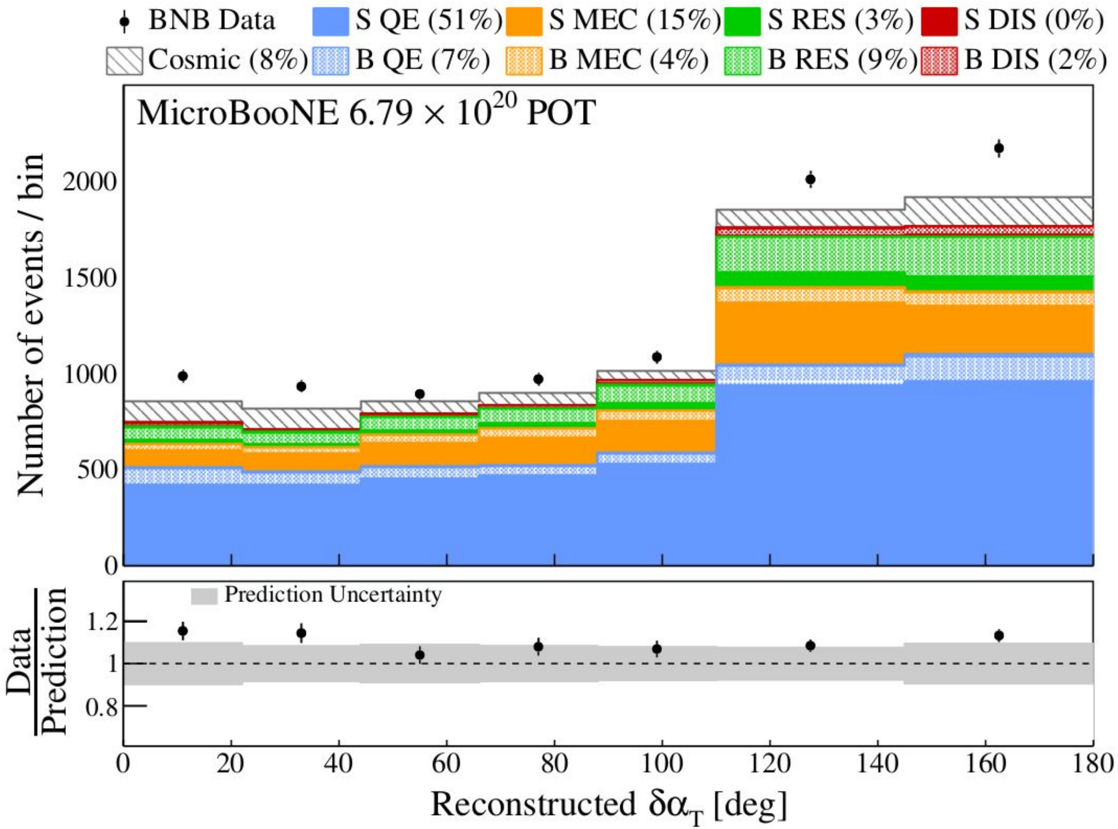

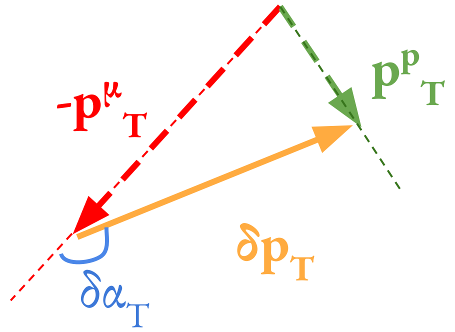

Need to move from event distributions to cross sections→ *unfolding*

[Phys. Rev. D 108, 053002 (2023)]

* [Phys. Rev. D 105, 072001 (2022)]

Cross Section Extraction with Wiener SVD Unfolding

JINST **12** P10002 (2017)

Input Quantities

- Measurement (Data)
- Background (Cosmics + MC)
- Response Matrix (MC)
- Total Covariance Matrix (MC)

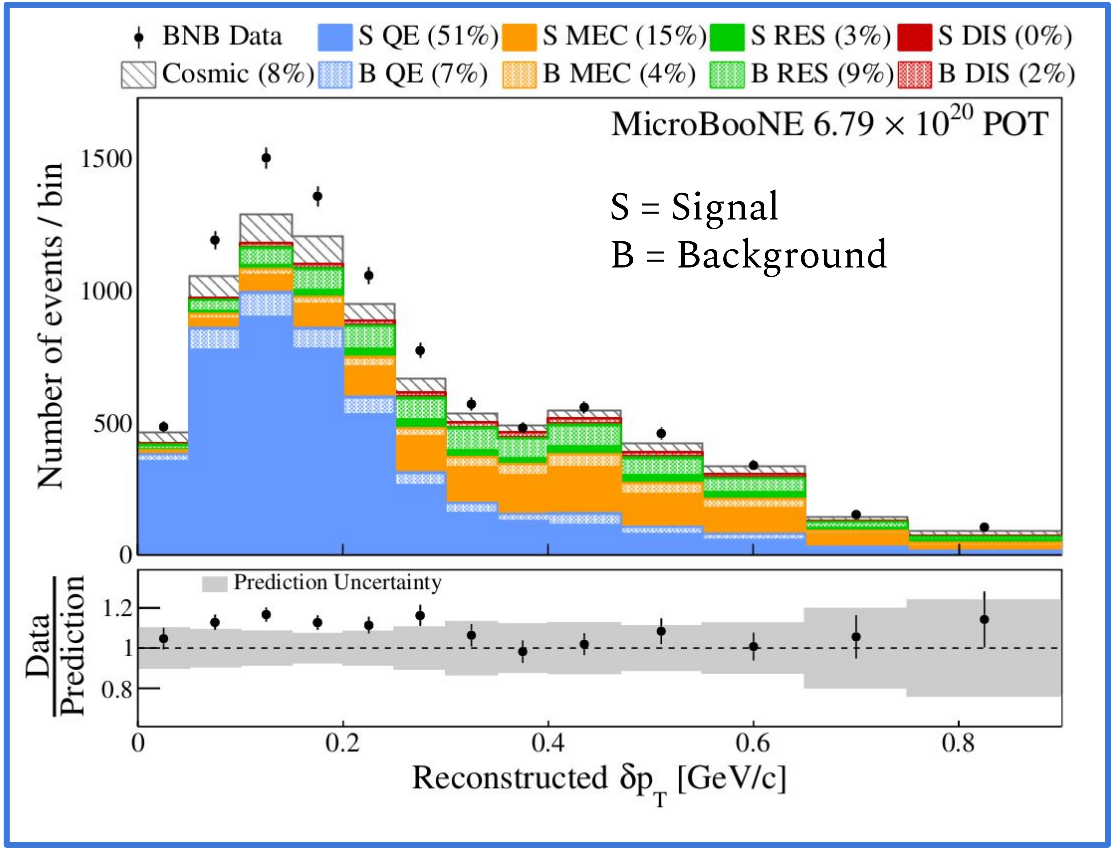

Phys. Rev. D 108, 053002 (2023)

Cross Section Extraction with Wiener SVD Unfolding

JINST **12** P10002 (2017)

Input Quantities

- Measurement (Data)
- Background (MC)
- Response Matrix (MC)
- Total Covariance Matrix (MC)

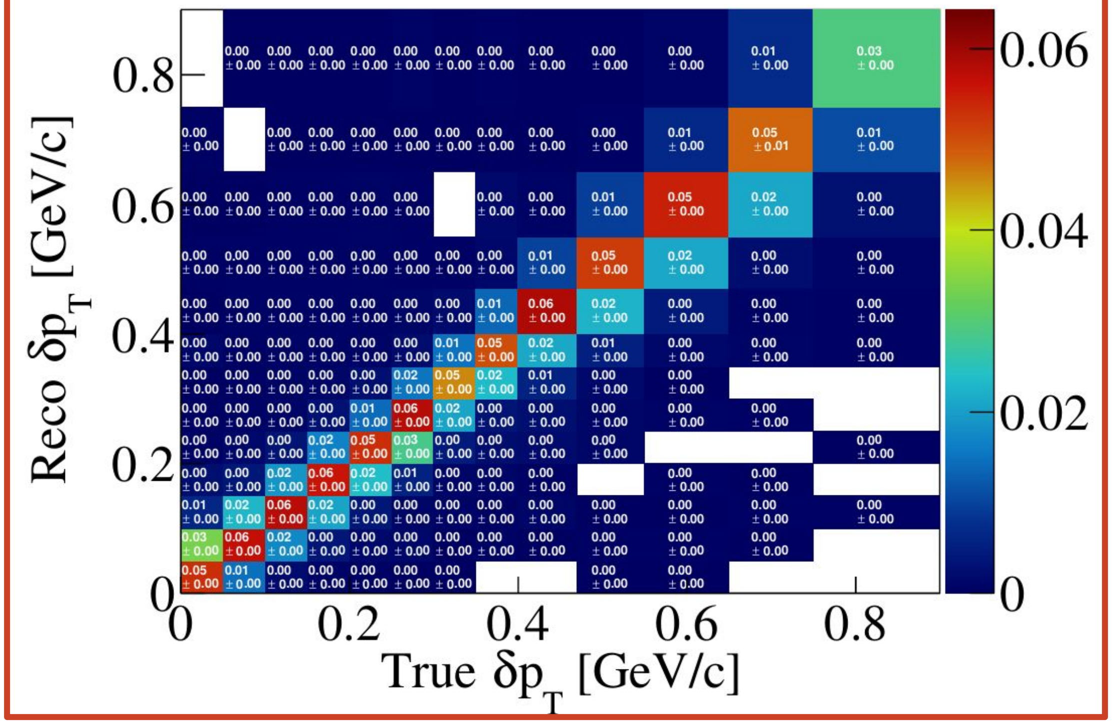

Probability that a generated event is reconstructed and selected

Diagonal matrix with flat ~6% efficiency

Phys. Rev. D 108, 053002 (2023)

Cross Section Extraction with Wiener SVD Unfolding

JINST **12** P10002 (2017)

Input Quantities

- Measurement (Data)
- Background (MC)
- Response Matrix (MC)
- Total Covariance Matrix (MC)

Includes information on statistical and systematic uncertainties

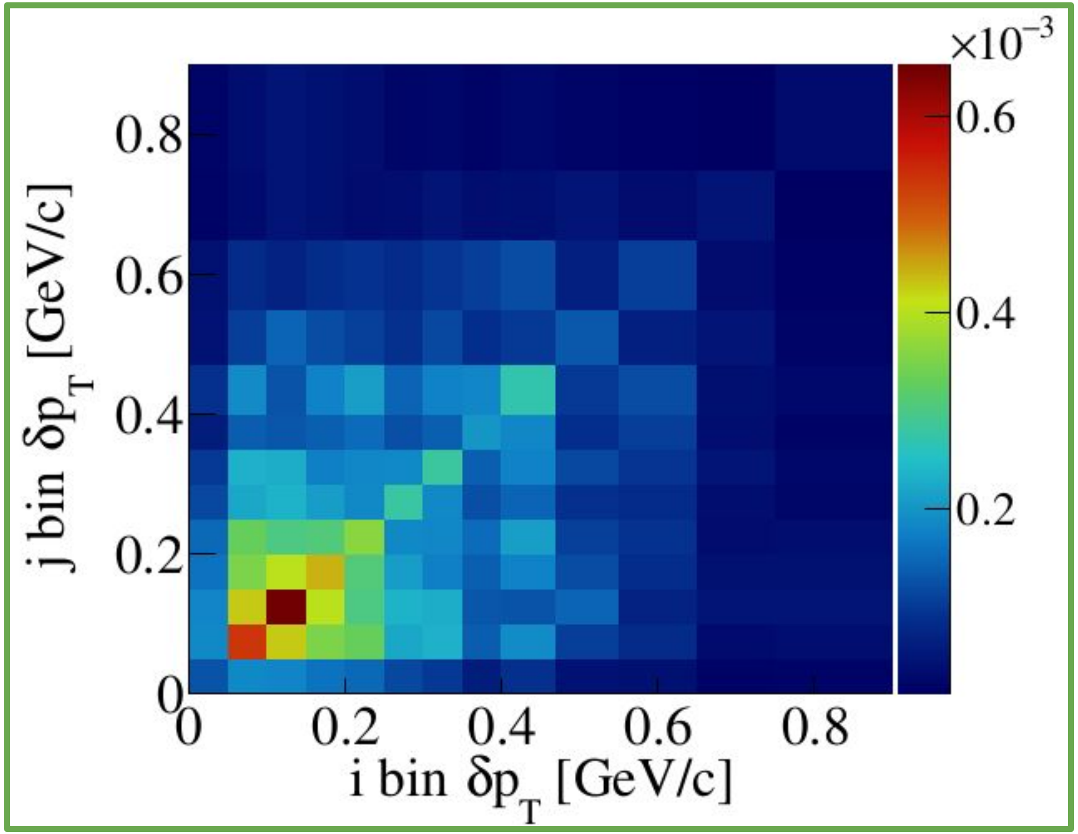

Phys. Rev. D 108, 053002 (2023)

Uncertainties

Flux

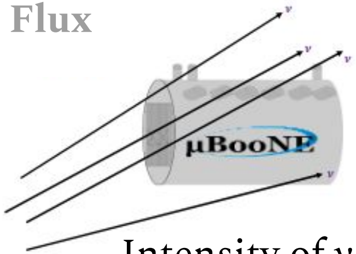

(7.3%)

Intensity of ν source

Detector

(4.9%)

TPC & light variations

Cross section

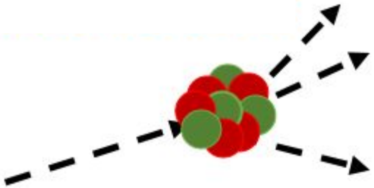

(6%)

Modeling accuracy

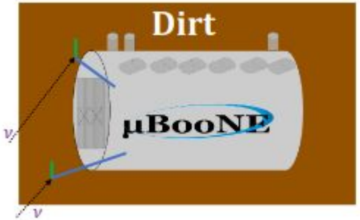

(0.2%)

Out-of-cryostat ν interactions

Reinteractions

(1%)

Hadron rescattering

POT counting

(2%)

Protons-on-target precision

- \+ Statistical (1.5%)
- \+ Number of argon targets (1%)

Total (11%)

Systematics-dominated analysis

Cross Section Extraction with Wiener SVD Unfolding

JINST **12** P10002 (2017)

Output quantities in regularized space

- Unfolded data spectrum
- Smearing Matrix A_C
  *Applied on theory predictions and included in data release

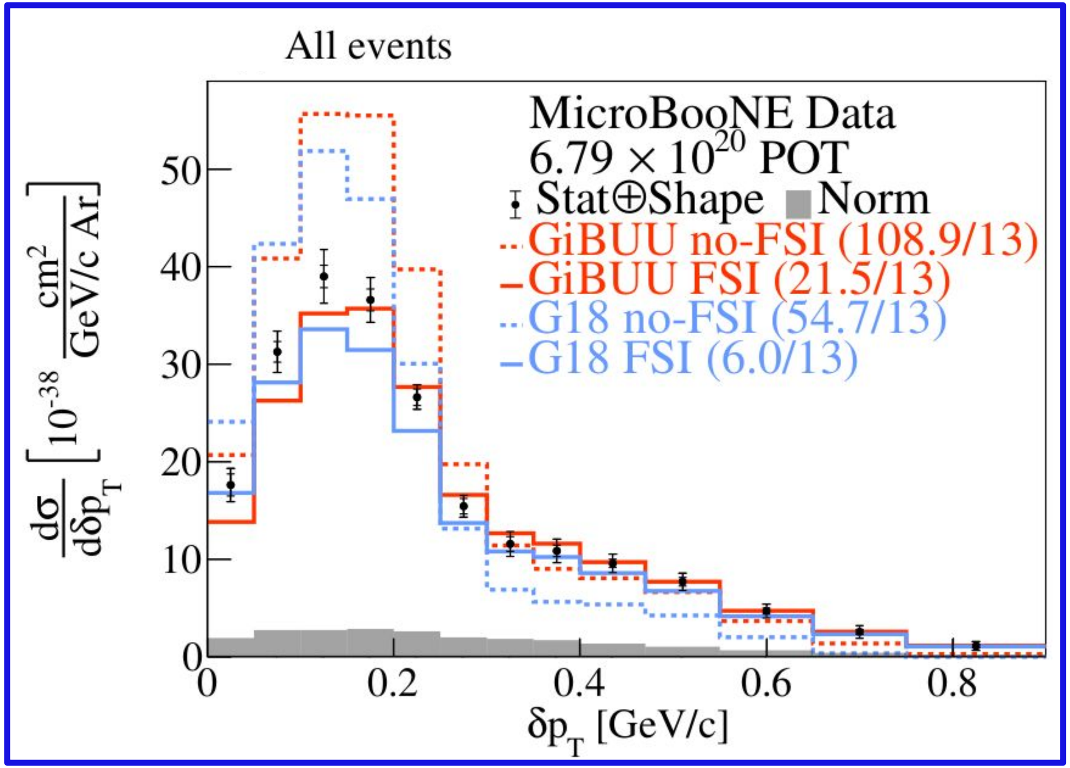

Phys. Rev. Lett. 131, 101802 (2023)

Cross Section Extraction with Wiener SVD Unfolding

[JINST **12** P10002 (2017)](#)

Output quantities in regularized space

- Unfolded data spectrum
- Smearing Matrix A_C

  *Applied on theory predictions and included in data release

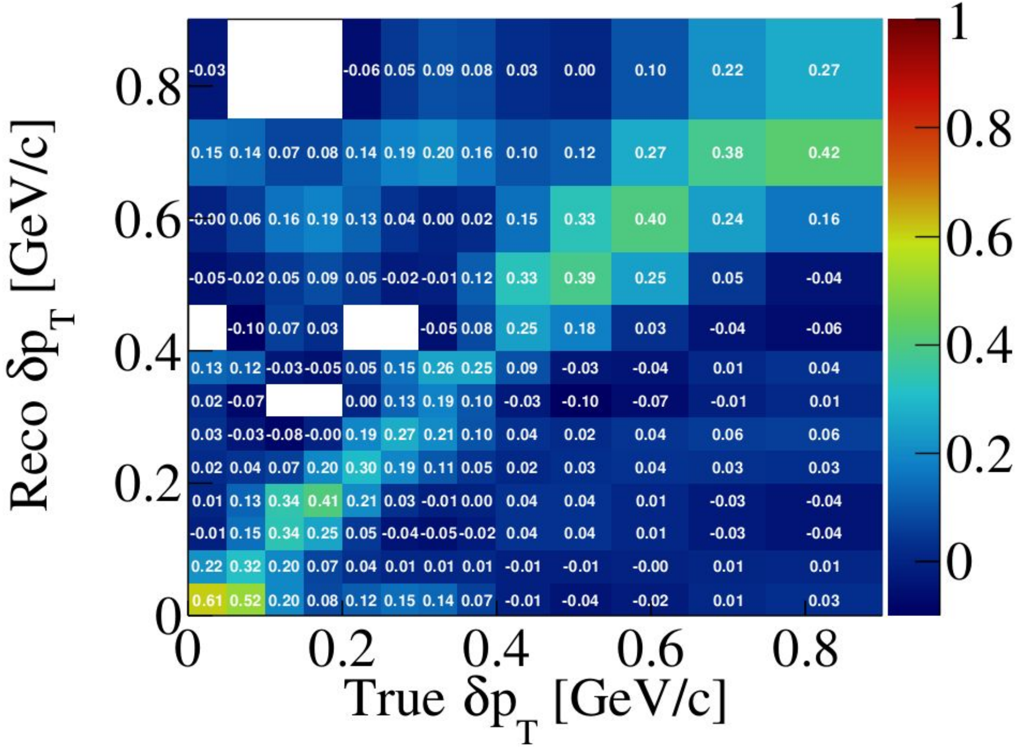

[arXiv:2301.03706](#)

Transverse Missing Momentum δp_T Cross Section

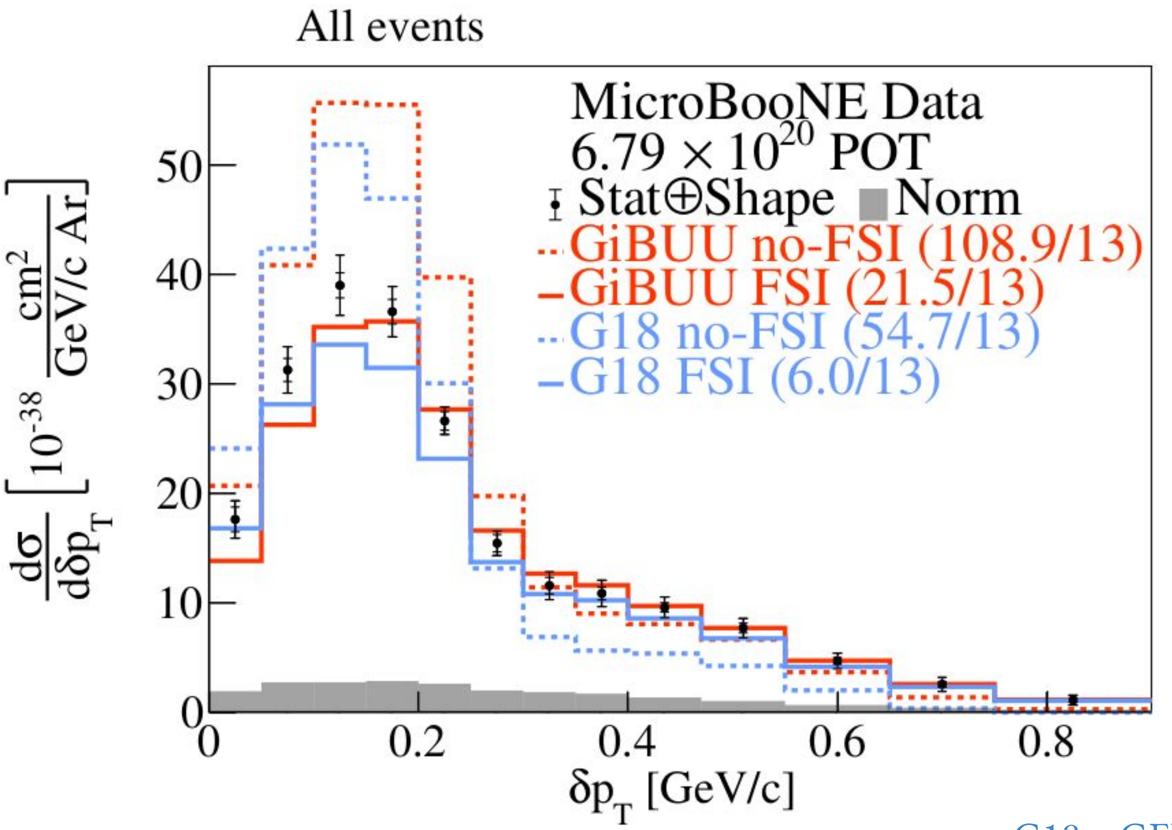

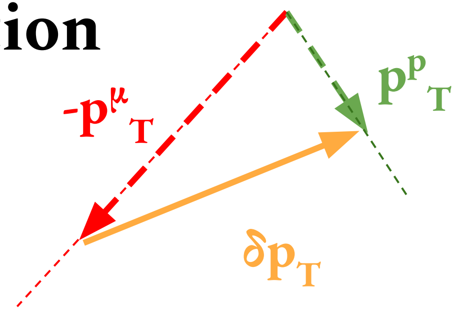

- First neutrino-argon differential cross section in δp_T
- FSI reduces strength of the peak
- Small changes in the tail
- Data favors FSI addition

G18 = GENIE v3.0.6 G18_10a_02_11b + tune*
GiBUU = GiBUU 2021

Phys. Rev. Lett. 131, 101802 (2023)
* Phys. Rev. D 105, 072001 (2022)

High Statistics→Into the Multiverse!

- **Extension to 2D** for the first time on argon
- Probe regions with greater model discrimination power

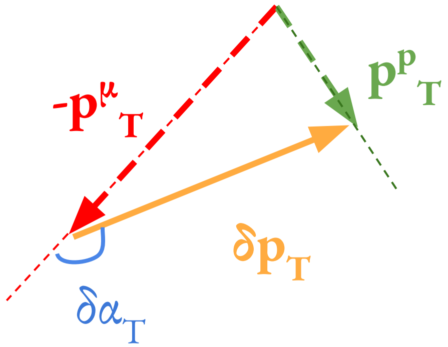

High Statistics→Into the Multiverse!

- **Extension to 2D** for the first time on argon
- Probe regions with greater model discrimination power

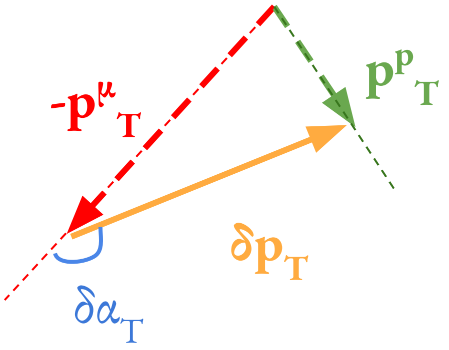

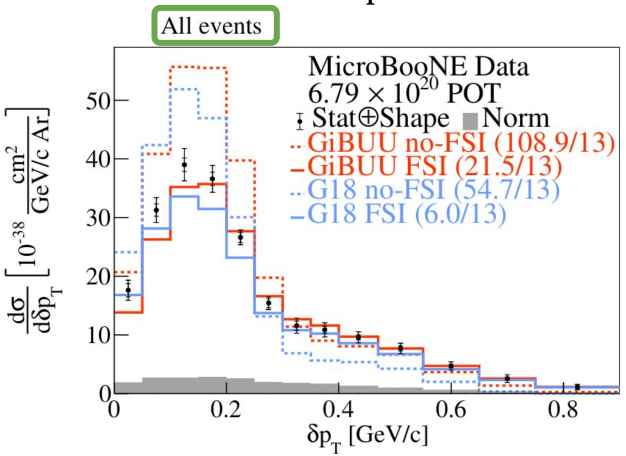

QE-dominated

MEC/RES/FSI-dominated

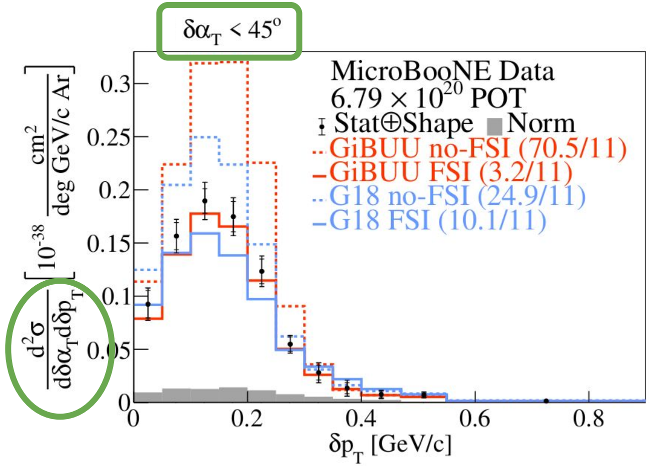

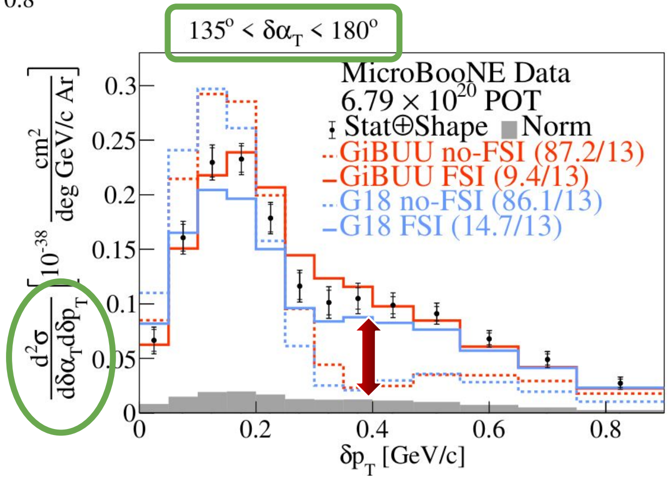

High Statistics→Into the Multiverse!

QE-dominated region

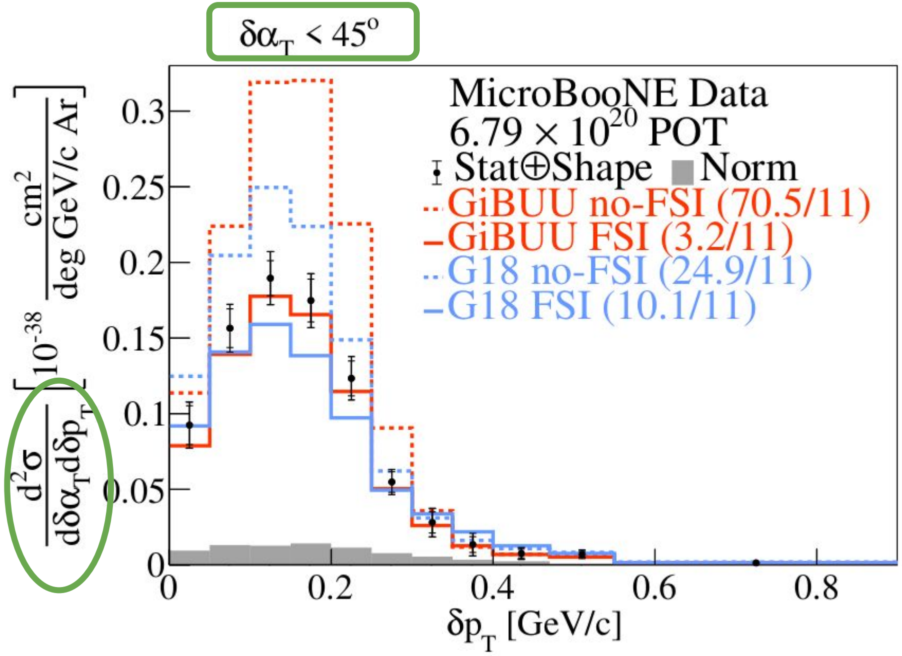

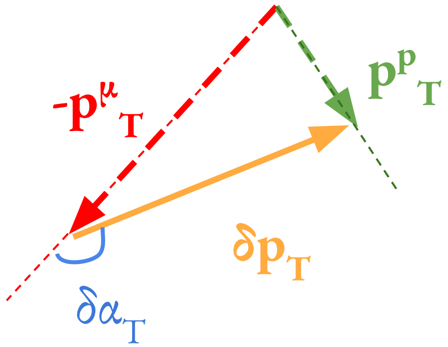

- No high transverse missing momentum tail
- Ideal part of phase-space to study Fermi motion
- Results consistent with local Fermi gas distribution

G18 = GENIE v3.0.6 G18_10a_02_11b + tune*
GiBUU = GiBUU 2021

Phys. Rev. Lett. 131, 101802 (2023)

* Phys. Rev. D 105, 072001 (2022)

High Statistics→Into the Multiverse!

MEC/RES/FSI-dominated

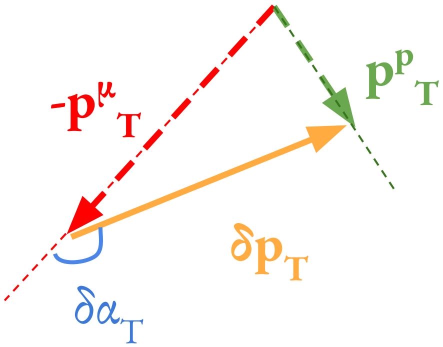

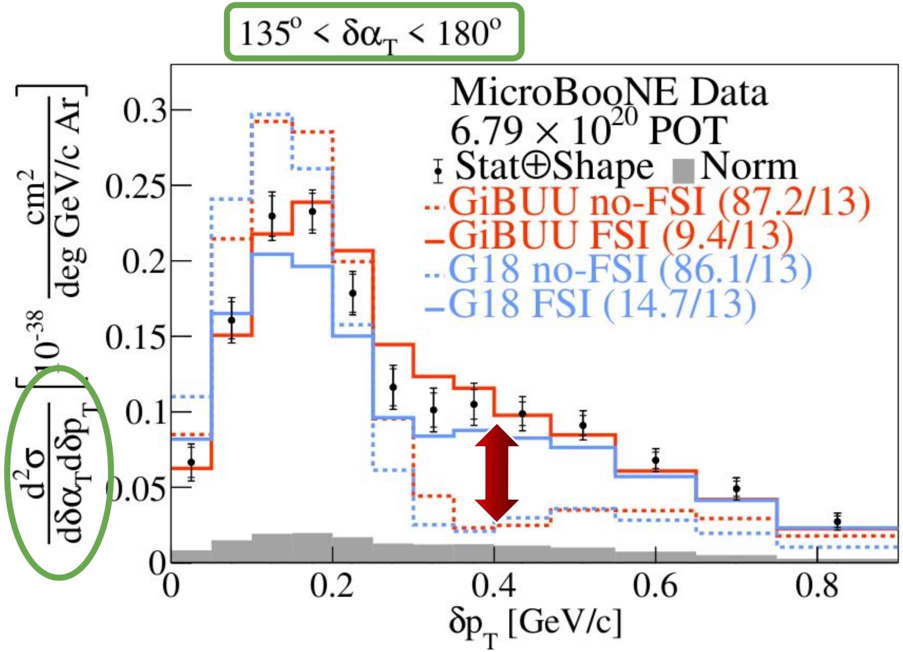

- FSI predictions in good agreement with data
- Minimal no-FSI contributions at high δp_T
- High $\delta\alpha_T$ & high δp_T part of phase-space ideal to test FSI / multinucleon effects

G18 = GENIE v3.0.6 G18_10a_02_11b + tune*

GiBUU = GiBUU 2021

Phys. Rev. Lett. 131, 101802 (2023)

* Phys. Rev. D 105, 072001 (2022)

CC1p0π TKI Summary

- First single- and double- differential neutrino-argon cross section measurements in TKI
- Fermi motion studied with 2D measurement in δp_T with $\delta\alpha_T < 45^o$
- FSI & multinucleon effects studied with 2D measurement in δp_T with $135^o < \delta\alpha_T < 180^o$
- Way more single- and double-differential results in Phys. Rev. Lett. 131, 101802 (2023) and Phys. Rev. D 108, 053002 (2023)!

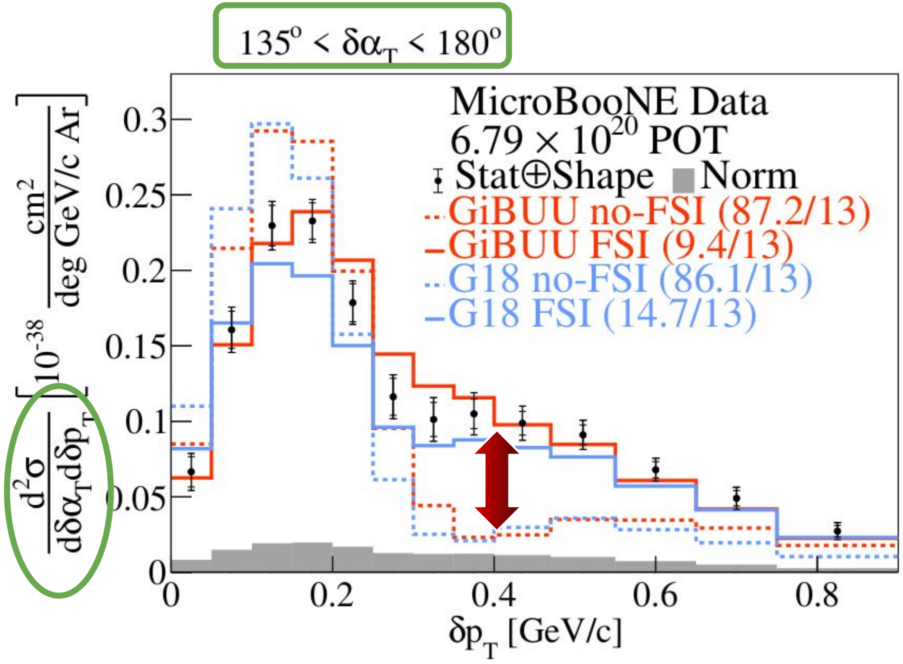

CC1p0π TKI Summary

- First single- and double- differential neutrino-argon cross section measurements in TKI
- Fermi motion studied w in δp_T with $\delta\alpha_T < 45^o$
- FSI & multinucleon effects studied with 2D measurement in δp_T with $135^o < \delta\alpha_T < 180^o$
- Way more single- and double-differential results in Phys. Rev. Lett. 131, 101802 (2023) and Phys. Rev. D 108, 053002 (2023)!

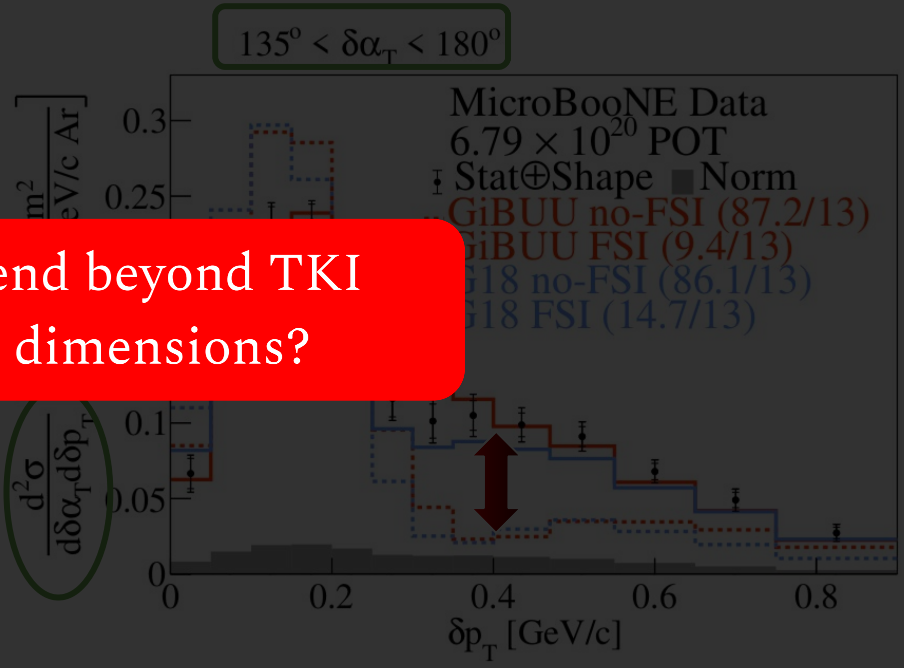

But why not extend beyond TKI by using three dimensions?

Generalized Kinematic Imbalance (GKI)

Phys. Rev. C 95, 065501 (2017)
arXiv:2310.06082

- Extension to 3D by considering longitudinal component of missing momentum and calorimetric assumption on the incoming energy

Generalized Kinematic Imbalance (GKI)

Phys. Rev. C 95, 065501 (2017)
arXiv:2310.06082

- Extension to 3D by considering longitudinal component of missing momentum and calorimetric assumption on the incoming energy

BE = 30.9 MeV

$$E_{\mathrm{cal}} = E_{\mu} + K_p + B$$

$$\vec{q} = E_{\mathrm{cal}}\hat{z} - \vec{p}_{\mu}$$

$$p_L = p_L^{\mu} + p_L^{p} - E_{\mathrm{cal}}$$

Generalized Kinematic Imbalance (GKI)

Phys. Rev. C 95, 065501 (2017)
arXiv:2310.06082

- Extension to 3D by considering longitudinal component of missing momentum and calorimetric assumption on the incoming energy

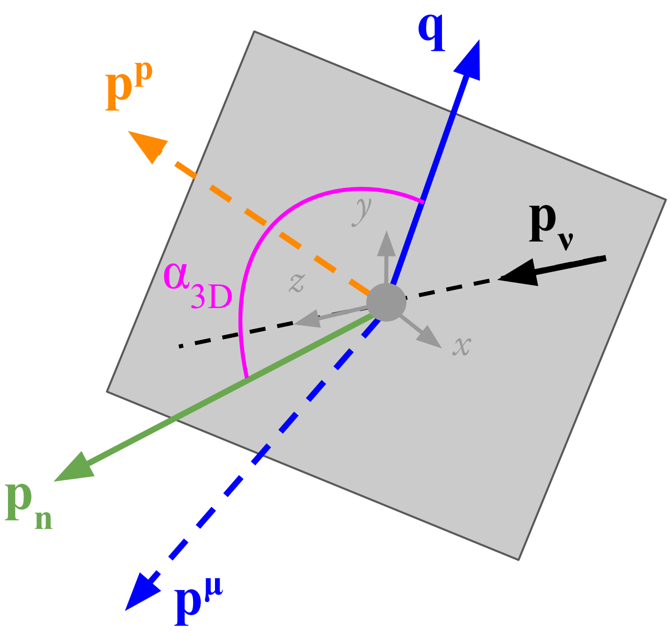

$$p_n = |\vec{p}_n| = \sqrt{p_L^2 + \delta p_T^2}$$

$$\alpha_{3D} = \cos^{-1}\left(\frac{\vec{q}\cdot\vec{p}_n}{|\vec{q}||\vec{p}_n|}\right)$$

Generalized Kinematic Imbalance (GKI)

Phys. Rev. C 95, 065501 (2017)
arXiv:2310.06082

- Extension to 3D by considering longitudinal component of missing momentum and calorimetric assumption on the incoming energy
- Extensively tested again several event generators and model configurations

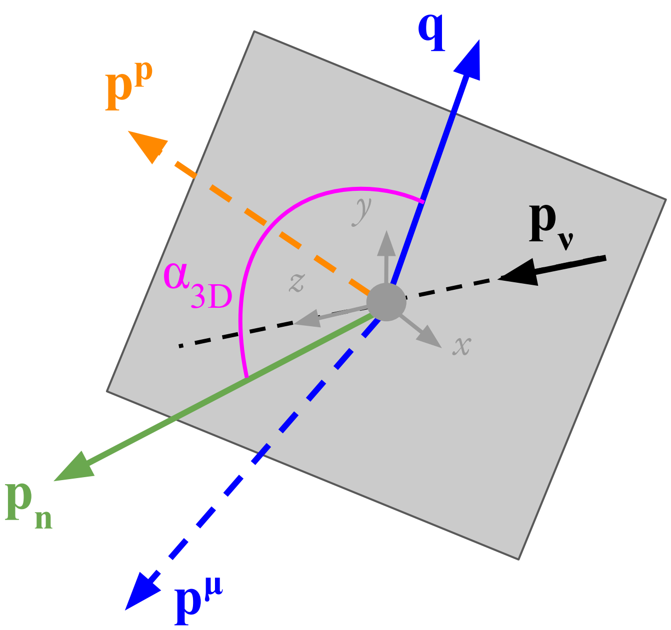

Name	Generator / Configuration
Gv2	GENIE v2.12.10
G18	GENIE v3.0.6 G18_10a_02_11a
G18T	G18 with tune
G21	GENIE v3.2.0 G21_11b_00_000
GiBUU	GiBUU 2021
NuWro	NuWro v19.02.1
NEUT	NEUT v5.4.0

Generalized Kinematic Imbalance (GKI)

Phys. Rev. C 95, 065501 (2017)
arXiv:2310.06082

- Extension to 3D by considering longitudinal component of missing moment and calorimetric assumption on the incoming energy
- Extensively tested again several event generators and model configurations

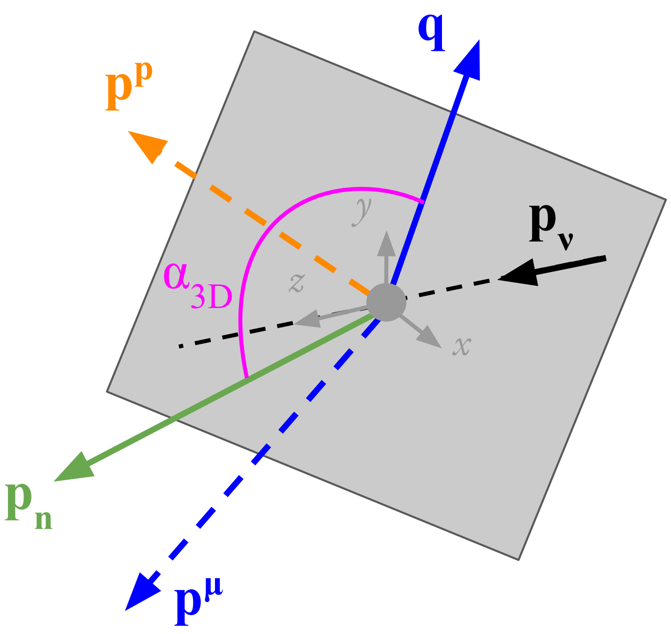

Name	Generator / Configuration
Gv2	GENIE v2.12.10
G18	GENIE v3.0.6 G18_10a_02_11a
G18T	G18 with tune
G21	GENIE v3.2.0 G21_11b_00_000
GiBUU	GiBUU 2021
NuWro	NuWro v19.02.1
NEUT	NEUT v5.4.0

Selected comparisons shown next using same CC1p0π selection

Missing momentum

arXiv:2310.06082

GENIE v3.0.6 G18_10a_02_11a (no tune)

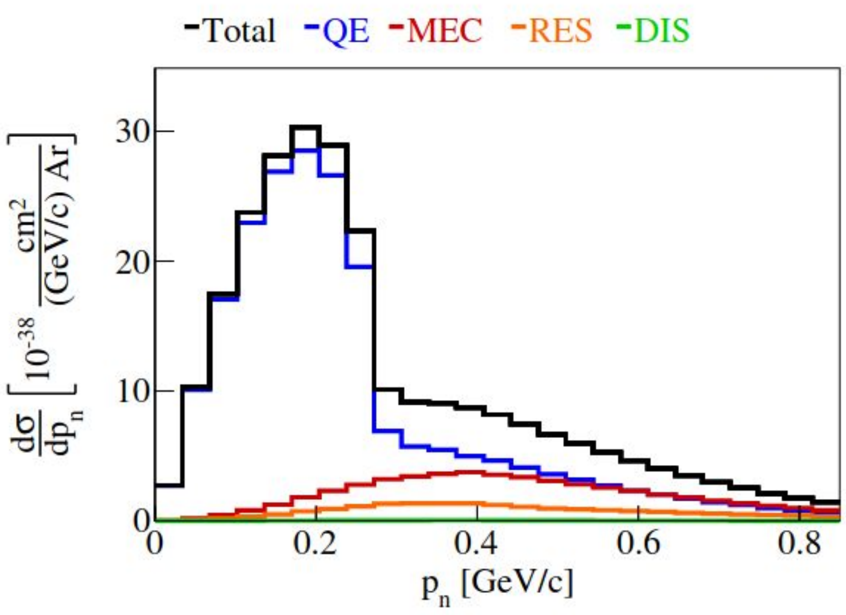

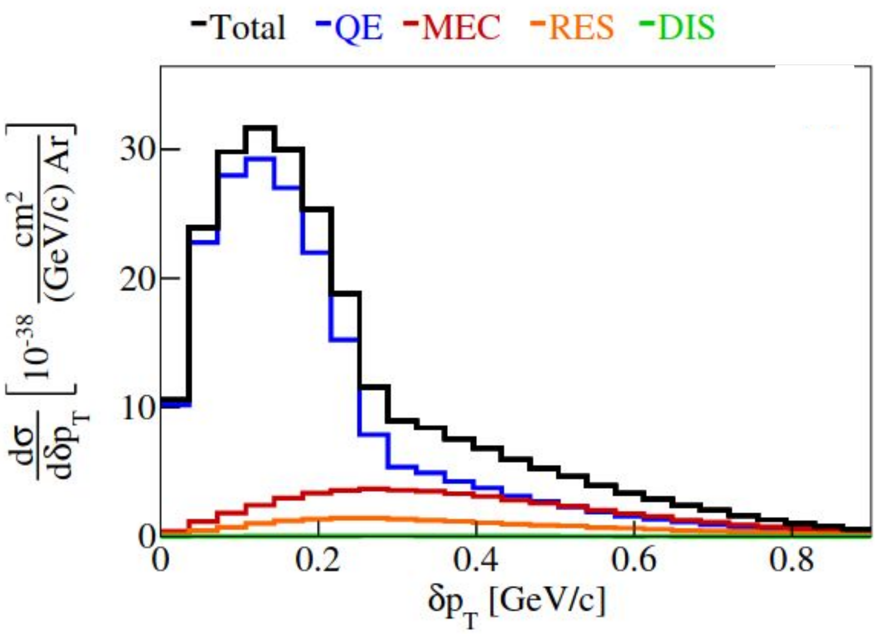

- QE dominance due to CC1p0π signal definition
- p_n pushes non-QE component to higher values

Into the GKI multiverse!

QE-dominated region

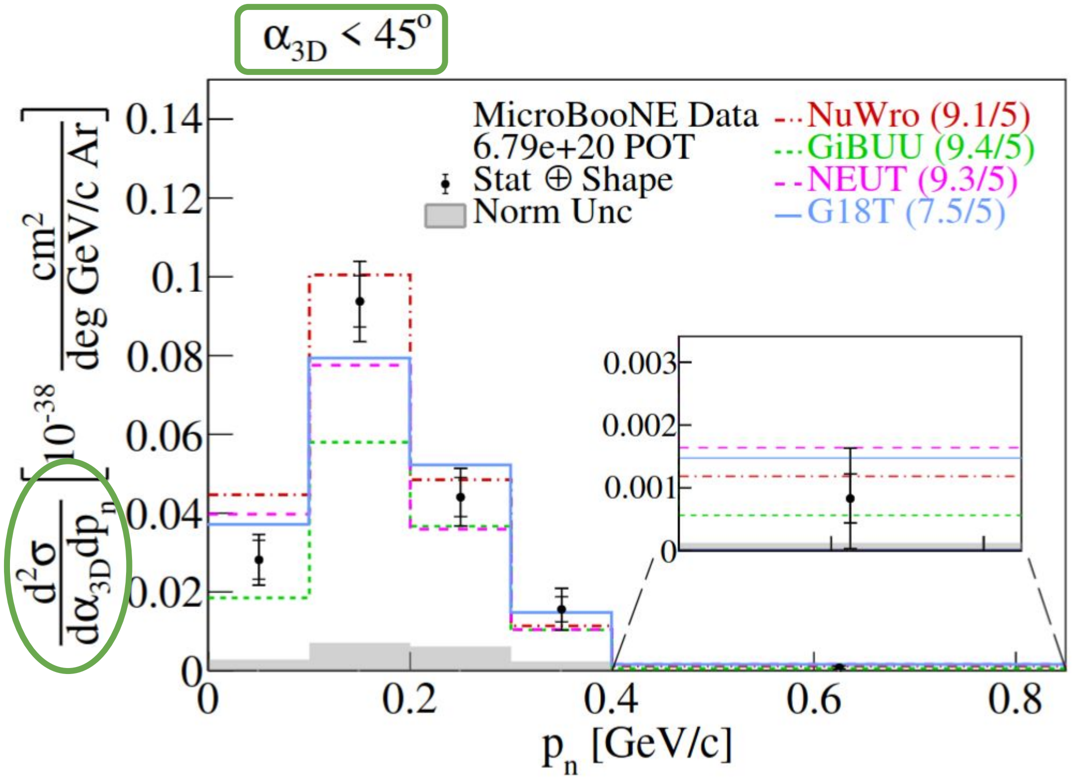

- Tail significantly suppressed
- Consistent with local Fermi gas
- G18T results in lowest χ^2

arXiv:2310.06082

Into the GKI multiverse!

MEC/RES/FSI-dominated

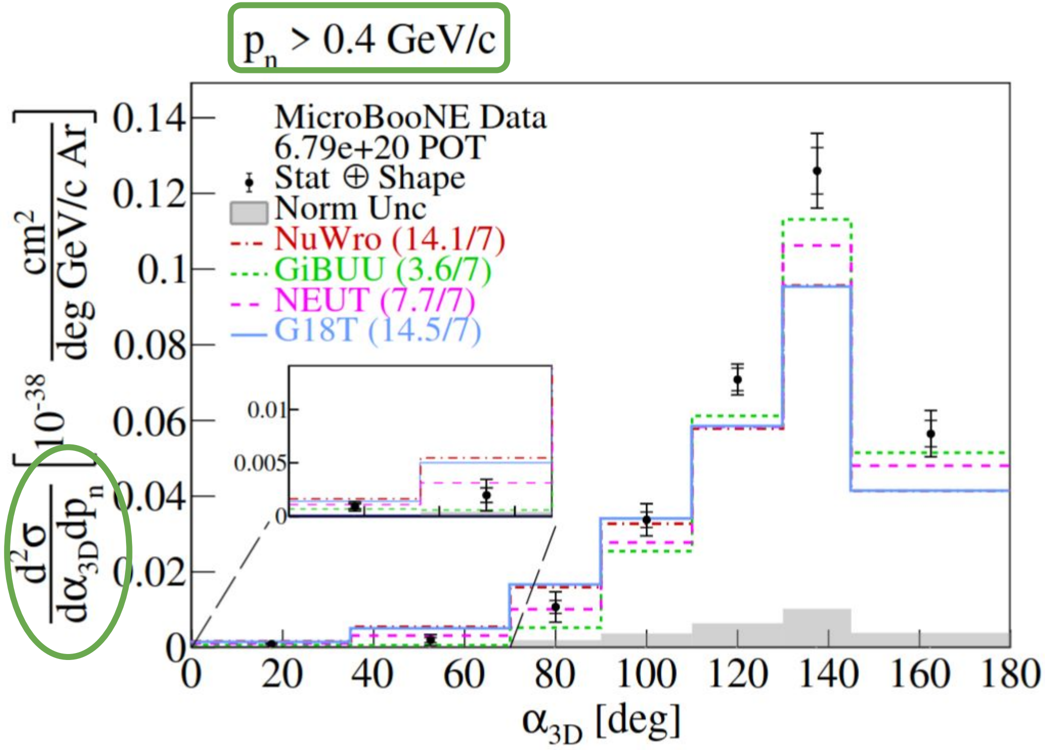

- Sharply peaked distribution to the right
- Driven by FSI
- GiBUU yields best result

arXiv:2310.06082

CC1p0π GKI Summary

- Introduction of generalized kinematic imbalance (GKI) variables in 3D space
- Enhanced sensitivity to nuclear effects
- First single- and double-differential cross section GKI measurement ever with MicroBooNE
- G18T results in good description in QE-dominated regions
- GiBUU yields best performance in FSI-dominated regions
- Way more results in arXiv:2310.06082!

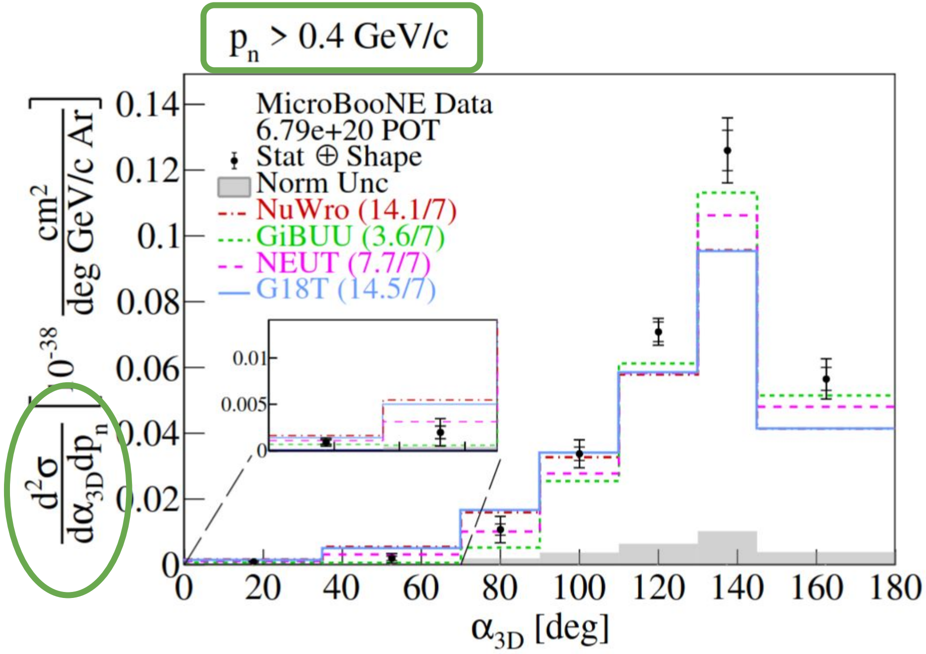

CC1p0π GKI Summary

- Introduction of generalized kinematic imbalance (GKI) variables in 3D space
- Enhanced sensitivity to nuclear effects
- First single- and double-differential ... GKI measurement ever
- G18T results in good d... in QE-dominated regions
- GiBUU yields best performance in FSI-dominated regions
- Way more results in arXiv:2310.06082!

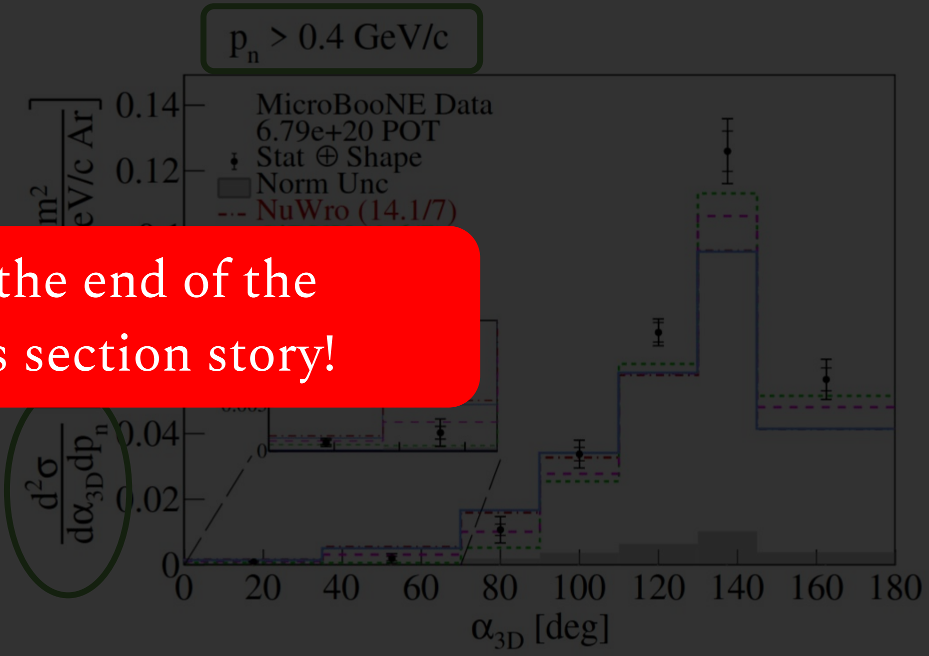

But far from the end of the neutrino cross section story!

SBN Experiments (SBND & ICARUS)

Common model configuration used by both experiments, systematics under development
High statistics cross section measurements planned using both BNB & NuMI beamlines

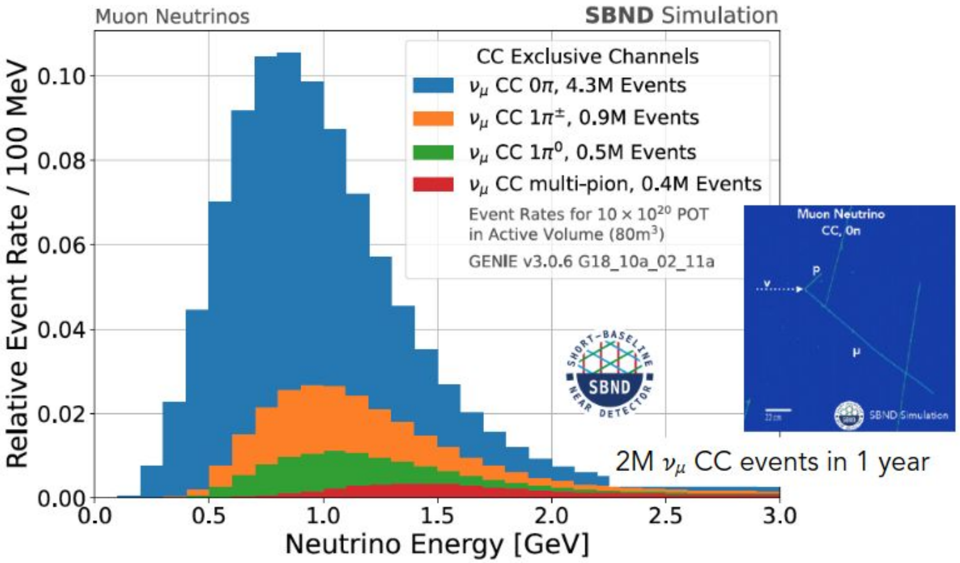

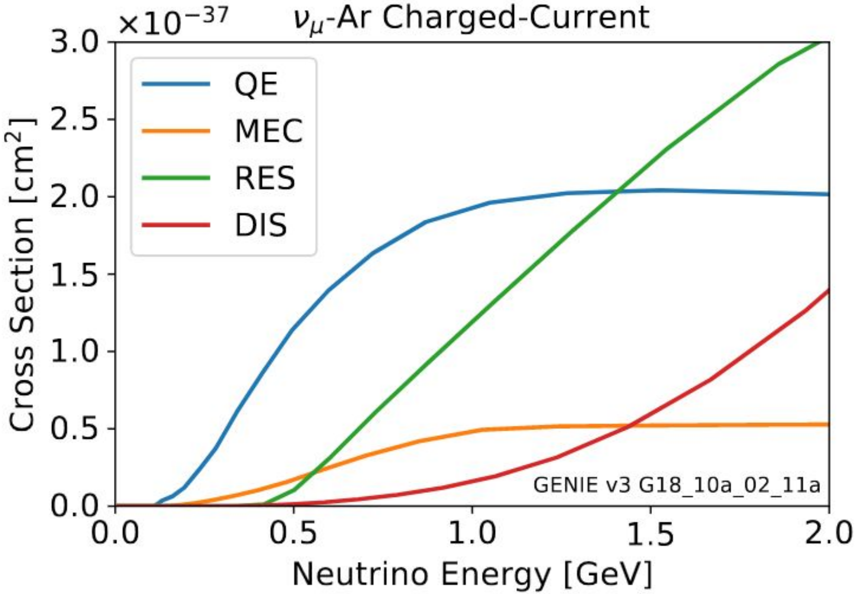

DUNE Near Detector

2x2 Near Detector prototype
Simulation studies on track multiplicity and inclusive selection
Cross section measurement targeting specific interactions

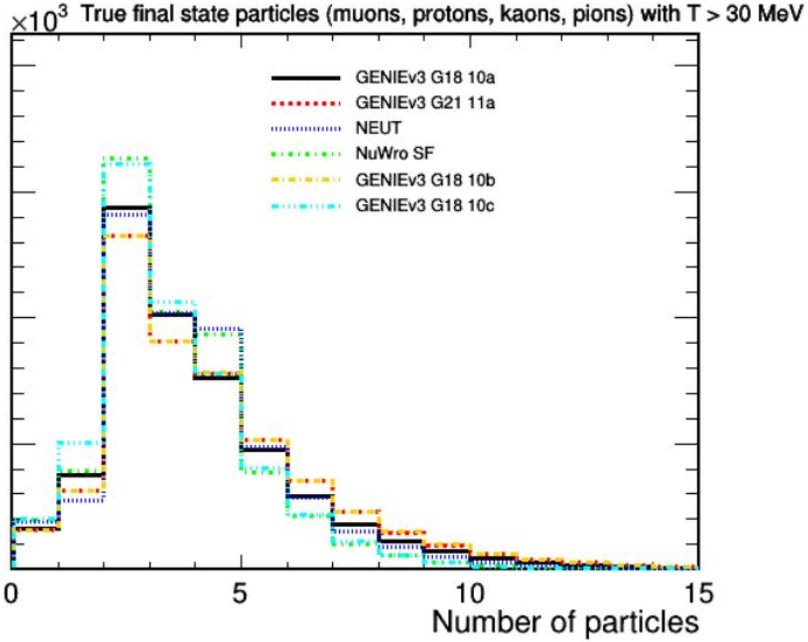

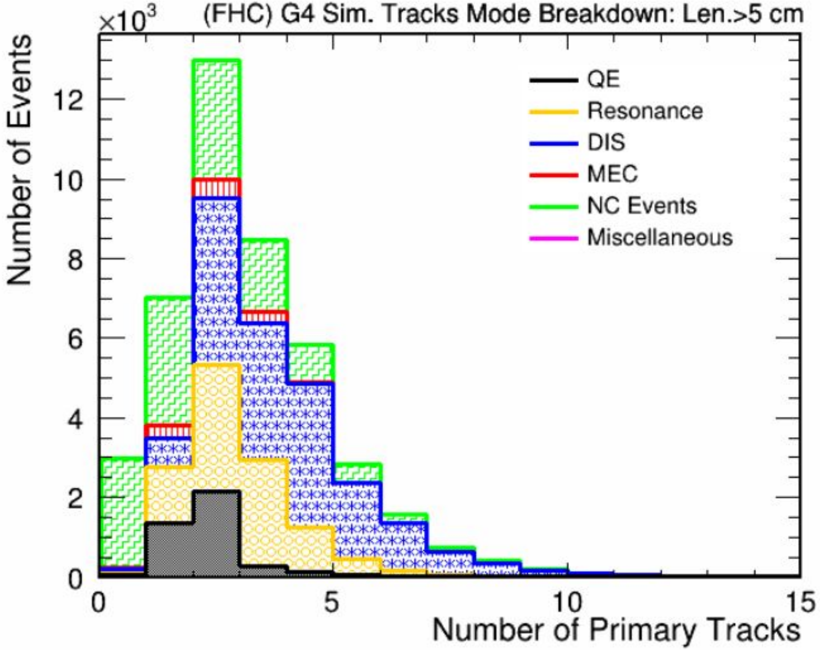

Electron Complementarity

μBooNE

Phys. Rev. Lett. 131, 101802 (2023)
Phys. Rev. D 108, 053002 (2023)

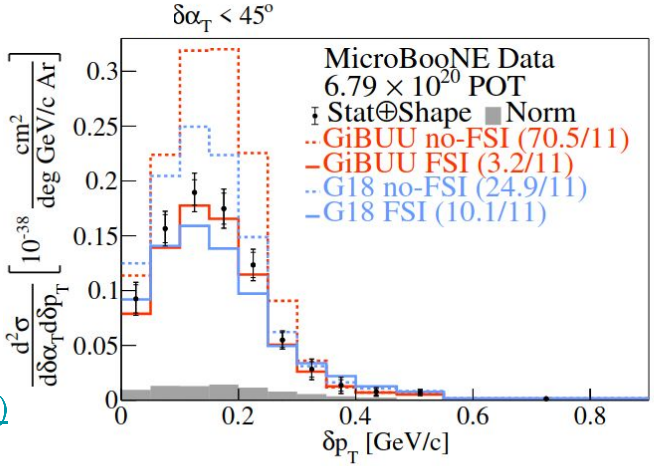

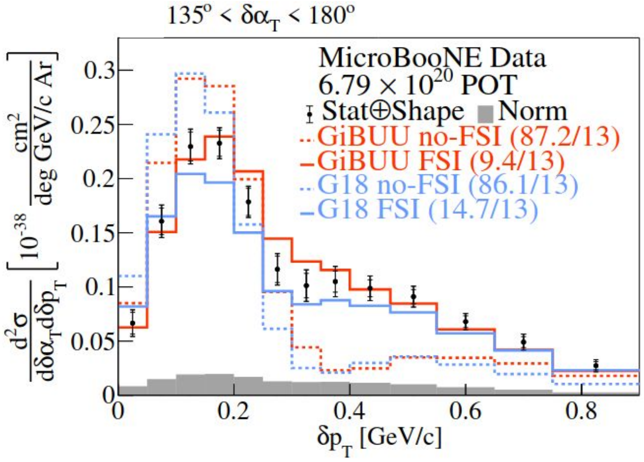

e4ν @ JLab

In preparation

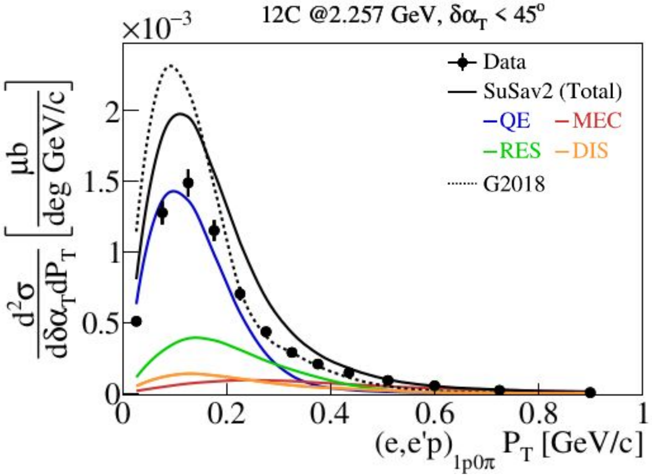

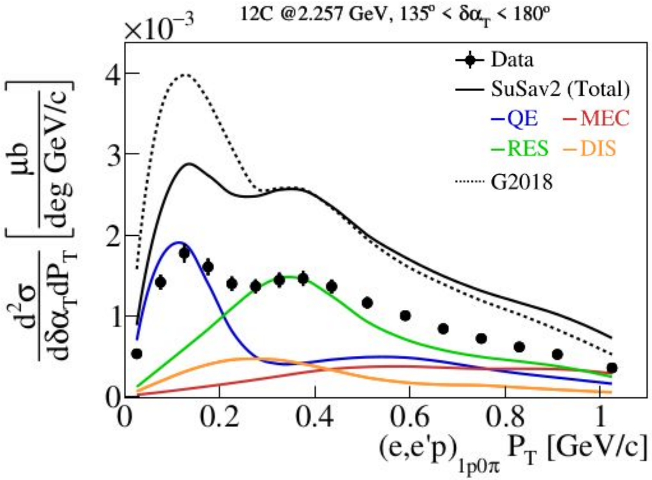

Thank you!

Backup Slides

Backup Slides: Table of Contents

3.6.3 Effect of Variation in Uncertainty

Figure 3.23 shows DUNE sensitivity to determination of neutrino mass hierarchy and discovery of CP violation as a function of exposure for several levels of signal normalization uncertainty. As seen in Figure 3.23, for early phases of DUNE with exposures less than 100 kt · MW · year, the experiment will be statistically limited. The impact of systematic uncertainty on the CP-violation sensitivity for large exposure is obvious in Figure 3.23; the ν_e signal normalization uncertainty must be understood at the level of $5\% \oplus 2\%$ in order to reach 5σ sensitivity for 75% of $\delta_{\rm CP}$ values with exposures less than ~900 kt · MW · year in the case of the Optimized Design. Specifically, the absolute normalization of the ν_μ sample must be known to ~5% and the normalization of the ν_e sample, relative to the $\bar{\nu}_e$, ν_μ, and $\bar{\nu}_\mu$ samples after all constraints from external, near detector, and far detector data have been applied, must be determined at the few-percent level. This level of systematic uncertainty sets the capability and design requirements for all components of the experiment, including the beam design and the near and far detectors.

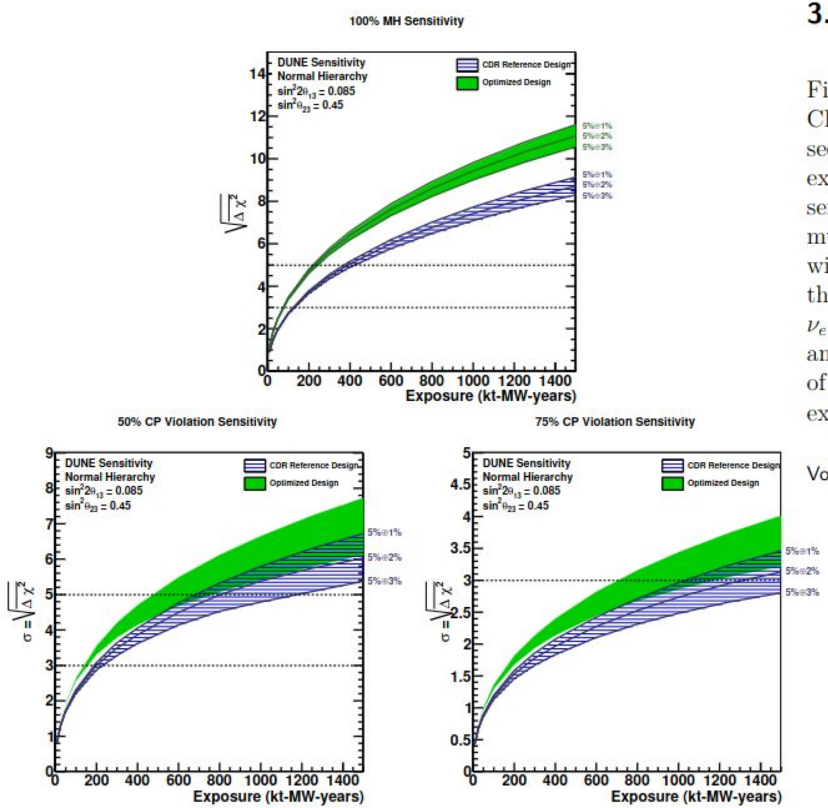

Figure 3.23: Expected sensitivity of DUNE to determination of the neutrino mass hierarchy (top) and discovery of CP violation, i.e., $\delta_{CP} \neq 0$ or π, (bottom) as a function of exposure in kt · MW · year, assuming equal running in neutrino and antineutrino mode, for a range of values for the ν_e and $\bar{\nu}_e$ signal normalization uncertainties from $5\% \oplus 3\%$ to $5\% \oplus 1\%$. The sensitivities quoted are the minimum sensitivity for 100% of $\delta_{\rm CP}$ values in the case of mass hierarchy and 50% (bottom left) or 75% (bottom right) of $\delta_{\rm CP}$ values in the case of CP violation. The two bands on each plot represent a range of potential beam designs: the blue hashed band is for the CDR Reference Design and the solid green band is for the Optimized Design. Sensitivities are for true normal hierarchy; neutrino mass hierarchy and θ_{23} octant are assumed to be unknown.

A short baseline neutrino detector

Studying accelerator neutrinos from two beams

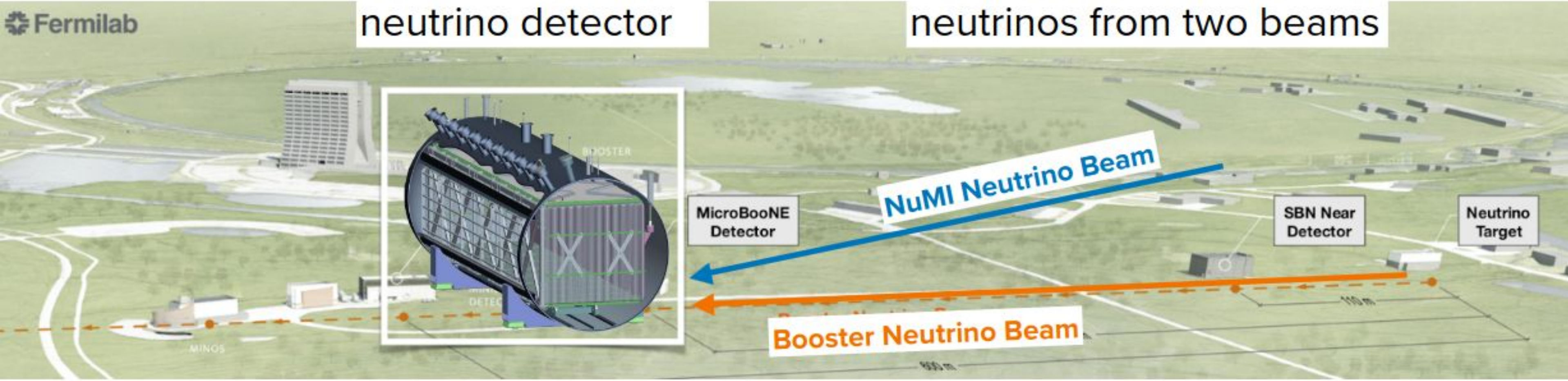

<u>MicroBooNE's physics program</u>

Non-standard neutrino oscillations

Cross-section measurements

Detector physics, R&D

Beyond Standard Model physics!

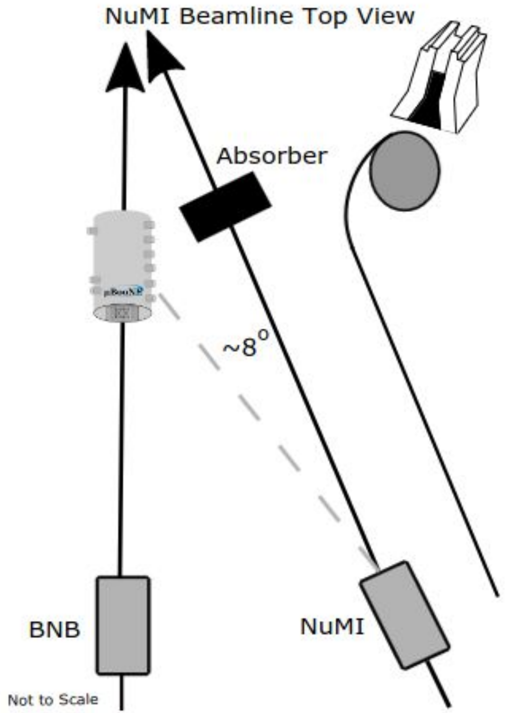

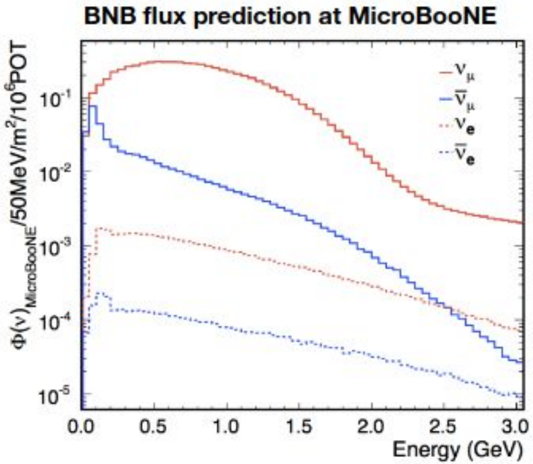

- 8 GeV protons
- ~470 m from MicroBooNE
- On-axis

- 120 GeV protons
- ~680 m from MicroBooNE
- ~8° off-axis from MicroBooNE

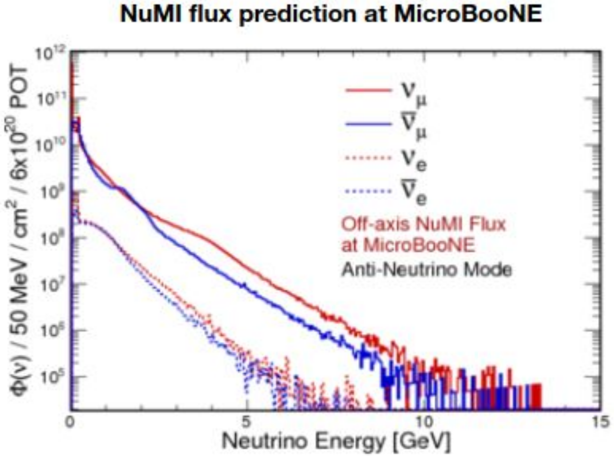

- MicroBooNE collected BNB and NuMI data between 2015 and 2020

- ~50% of the dataset (Runs 1-3) used in first wave of results

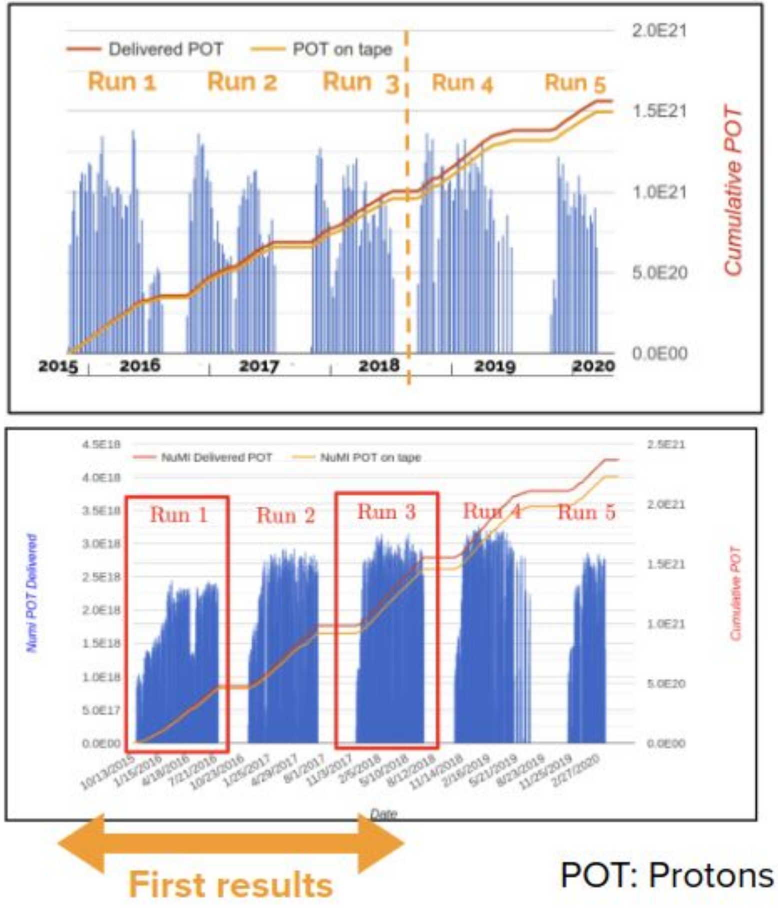

POT: Protons on Target

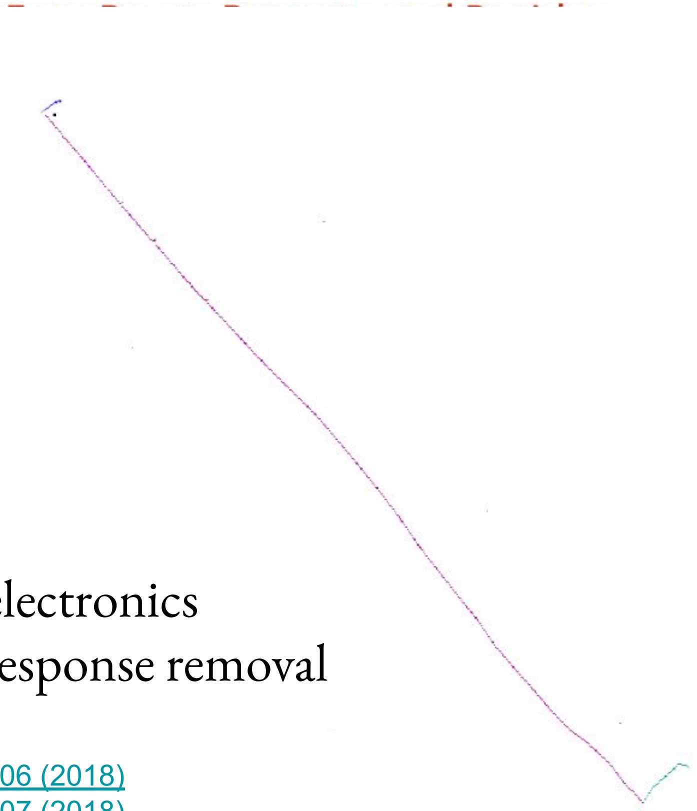

From raw hits to
particle reconstruction

Pandora Pattern Recognition

- Eur. Phys. J. C78, 1, 82 (2018)

Readout electronics
and field response removal

JINST 13, P07006 (2018)
JINST 13, P07007 (2018)

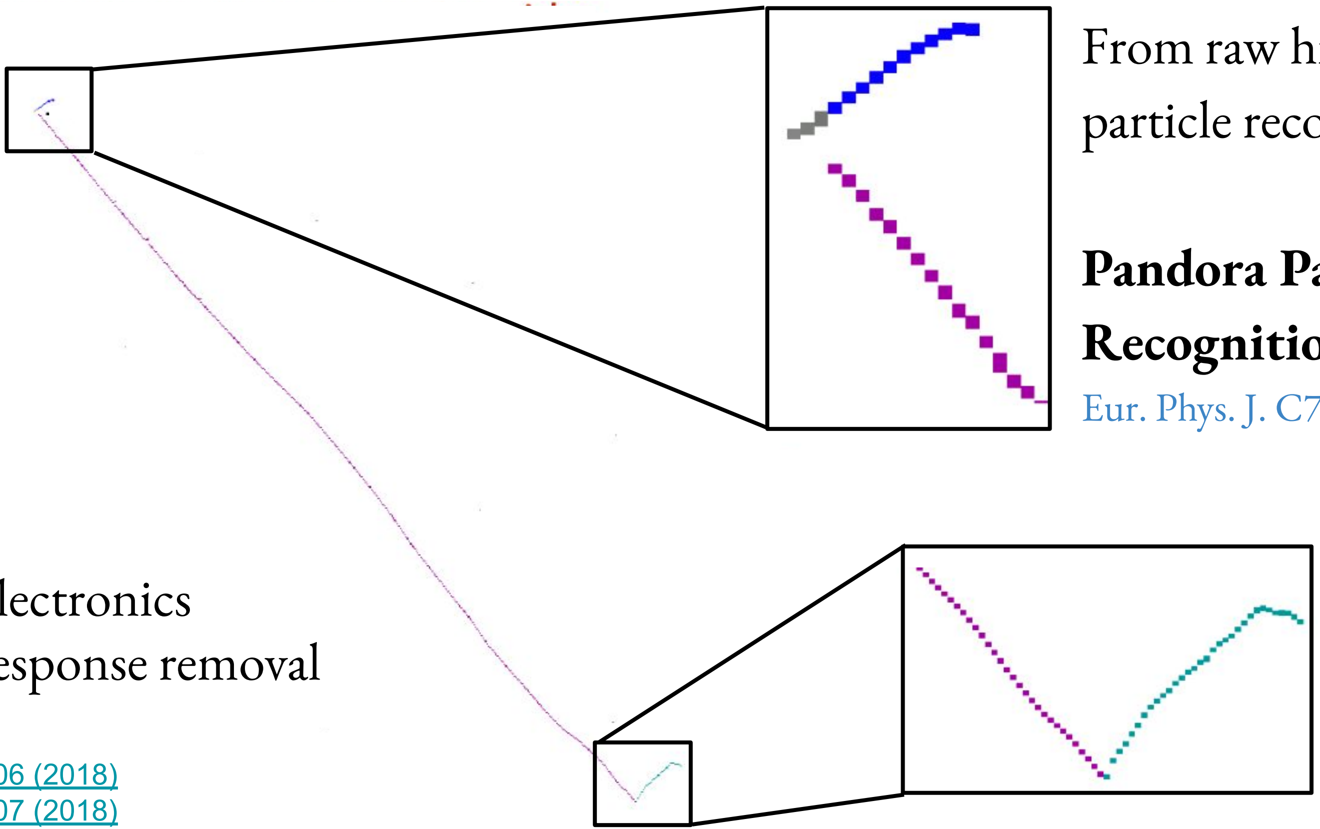

From raw hits to particle reconstruction

Pandora Pattern Recognition

Eur. Phys. J. C78, 1, 82 (2018)

Readout electronics and field response removal

JINST 13, P07006 (2018)

JINST 13, P07007 (2018)

Eur. Phys. J. C 79 673 (2019)

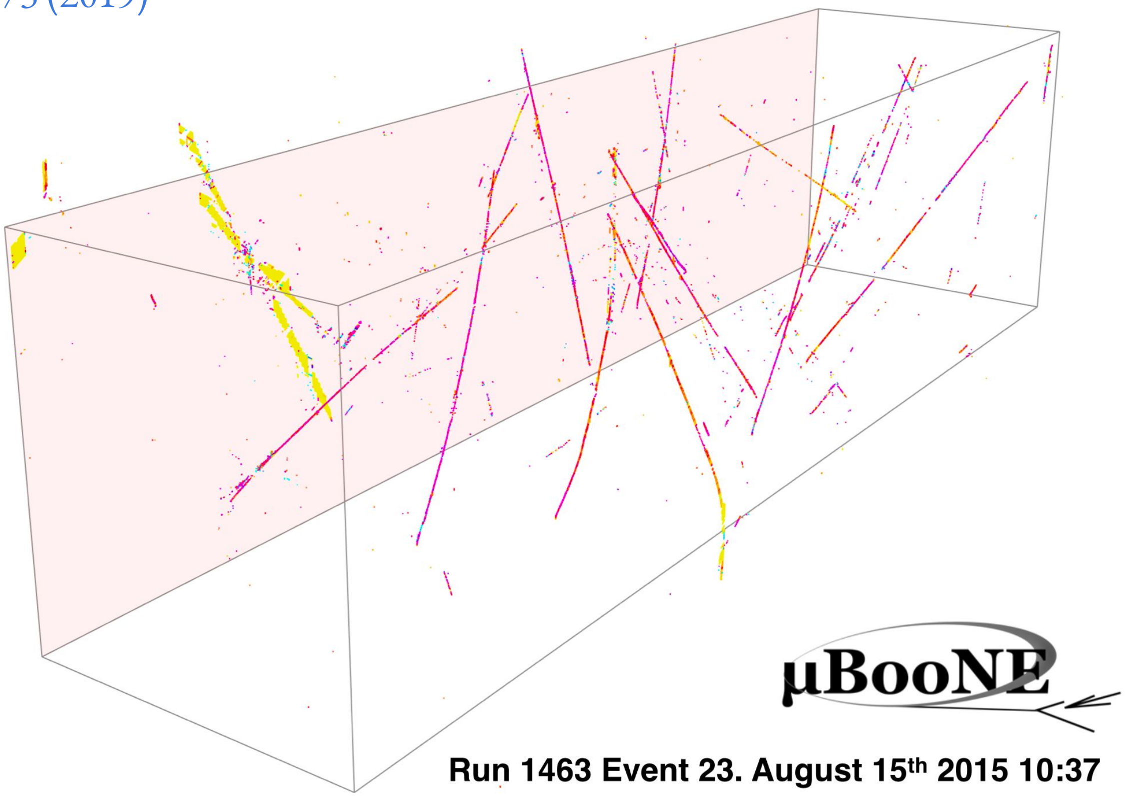

Readout window of 2.3 ms

- ~20 cosmic interactions
- ~0.0017 ν interactions

Significant reduction using optical information to 1 ν interaction in ~10 events

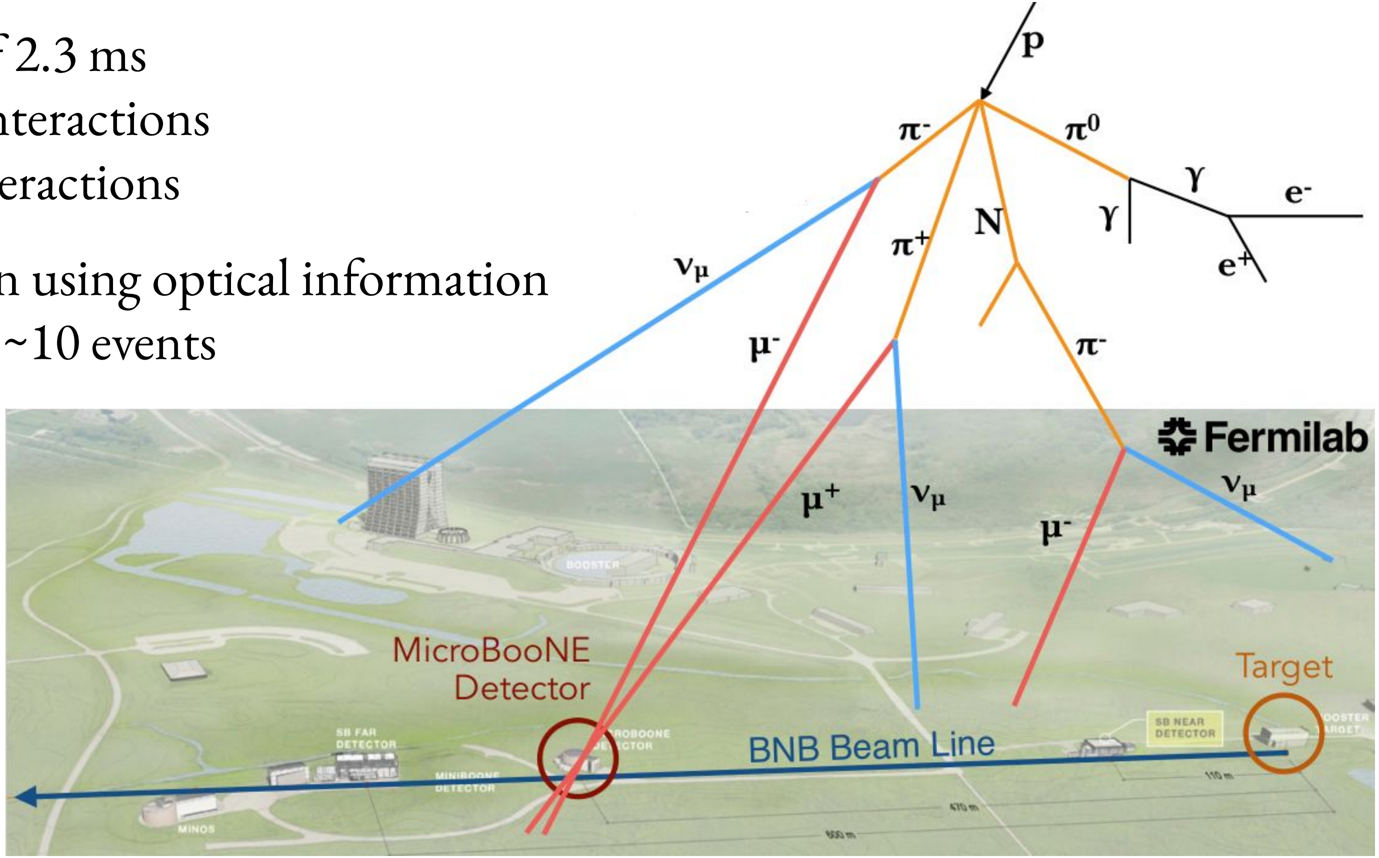

TABLE IV. Tuned parameter values and uncertainties after fitting to T2K CC0π data for the nominal simulation and three tunes that build to the final four parameter tune. Note that postfit χ^2 values are quoted here only for the 58 bins included in the fit (excluding the highest muon momentum bin in each cos θ bin), and using diagonal elements of the covariance matrix only. In the text and figures, pre- and postfit χ^2 comparisons are also quoted for the full T2K dataset of 67 bins. "Norm." is an abbreviation for normalization.

	MaCCQE fitted value	CC2p2h Norm. fitted value	CCQE RPA Strength fitted value	CC2p2h Shape fitted value	T2K $\chi^2_{\text{diag}}/N_{\text{bins}}$
Nominal (untuned)	0.961242 GeV	1	100%	0	106.7/58
Fit MaCCQE + CC2p2h Norm.	1.14 ± 0.07 GeV	1.61 ± 0.19	100% (fixed)	0 (fixed)	71.8/58
Fit MaCCQE + CC2p2h Norm + CCQE RPA Strength	1.18 ± 0.08 GeV	1.12 ± 0.38	(64 ± 23)%	0 (fixed)	69.7/58
Fit MaCCQE + CC2p2h Norm + CCQE RPA Strength + CC2p2h Shape	1.10 ± 0.07 GeV	1.66 ± 0.19	(85 ± 20)%	$1^{+0}_{-0.74}$	52.5/58

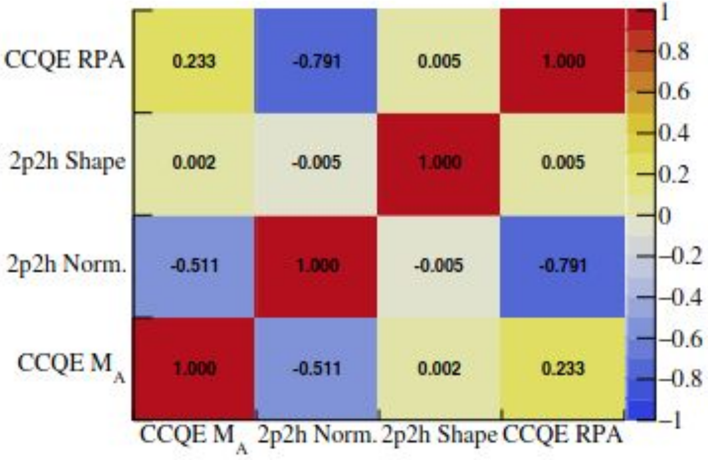

FIG. 7. Correlations between parameters after fitting to T2K CC0π data.

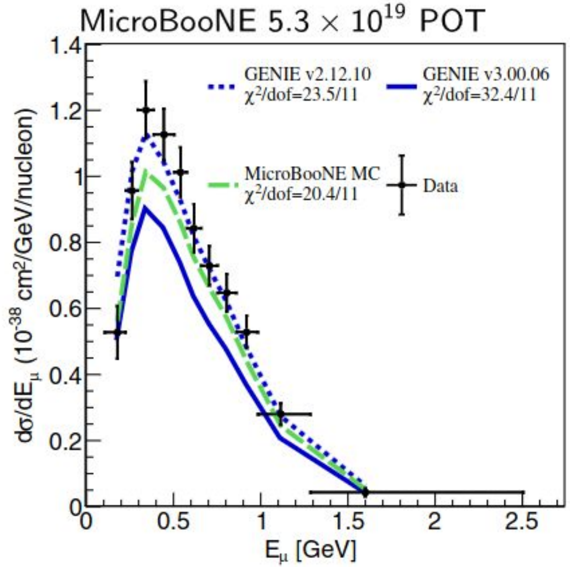

Phys. Rev. D 105, 072001 (2022)

Unfolding problem

- In practice, the data unfolding problem starts with

$$\chi^2(s) = (\boldsymbol{m} - \boldsymbol{r} \cdot s)^T Cov^{-1} (\boldsymbol{m} - \boldsymbol{r} \cdot s)$$

  - $\boldsymbol{m}$: measured spectrum, *m*-dimensional vector
  - $\boldsymbol{s}$: unknown spectrum, to be unfolded, *n*-dimensional vector
  - $\boldsymbol{r}$: smearing (response) matrix, $m \, X \, n$ and $m \geq n$
  - *Cov* : covariance matrix containing all statistical and systematic uncertainties associated with $\boldsymbol{m}$ and $\boldsymbol{r}$.

- Cholesky decomposition: $Cov^{-1} = Q^T Q$, Q is a lower triangular matrix

$$\chi^2(s) = (M - R \cdot s)^T \cdot (M - R \cdot s)$$

Pre-scaling

- $M \coloneqq Q \cdot \boldsymbol{m}$
- $R \coloneqq Q \cdot \boldsymbol{r}$

Solution (direct inversion)

$$\hat{s} = (R^T R)^{-1} R^T M$$

$$\hat{s} = (R^T R)^{-1} R^T (R \cdot s_{true} + N)$$

The response matrix R is unnecessary to be a square matrix

Unfolding problem

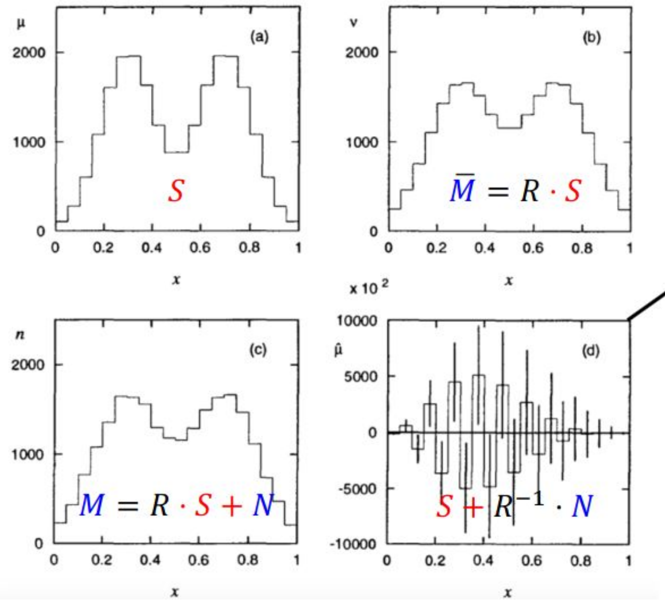

This is one unbiased solution (direct inversion) to an unfolding problem. However, it has catastrophic oscillations, i.e. huge variance, in the unfolded spectrum.

- Decrease the number of bins to suppress the “oscillation” --> Nyquist theorem
- Trade-off **bias** and **variance** to suppress the “oscillation” --> e.g. **regularization [unfolding method]**

Wiener-SVD unfolding

- To automatically minimize the Mean Square Error (MSE) given a model S

$$MSE = E\left[(\hat{S} - S)^2\right] = E\left[\left(F \cdot \frac{M}{R} - S\right)^2\right] = E\left[\left(F \cdot S + F \cdot \frac{N}{R} - S\right)^2\right]$$

$$= E\left[((\boldsymbol{F} - \boldsymbol{I}) \cdot \boldsymbol{S})^2 + \left(\boldsymbol{F} \cdot \frac{\boldsymbol{N}}{\boldsymbol{R}}\right)^2\right]$$

Bias — Variance

F = "filter" = additional smearing matrix = regularization

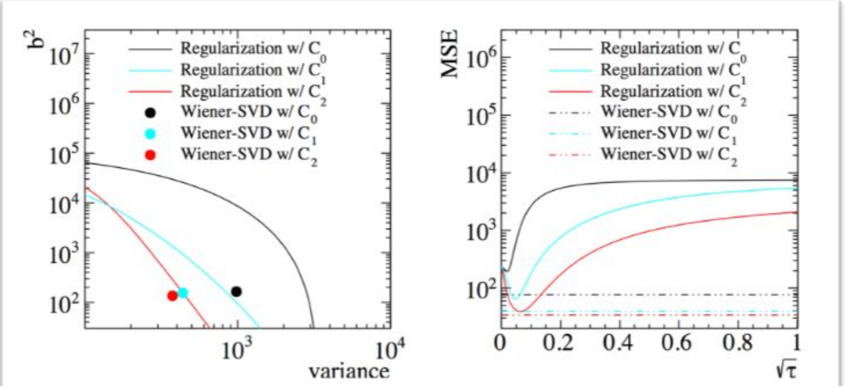

Given one model S

- General regularization, e.g. Tikhonov regularization, needs to "tune" a regularization strength parameter [curve in the left plot]
- Wiener-SVD regularization corresponds to a fixed point in the phase space of bias versus variance with **minimum MSE**

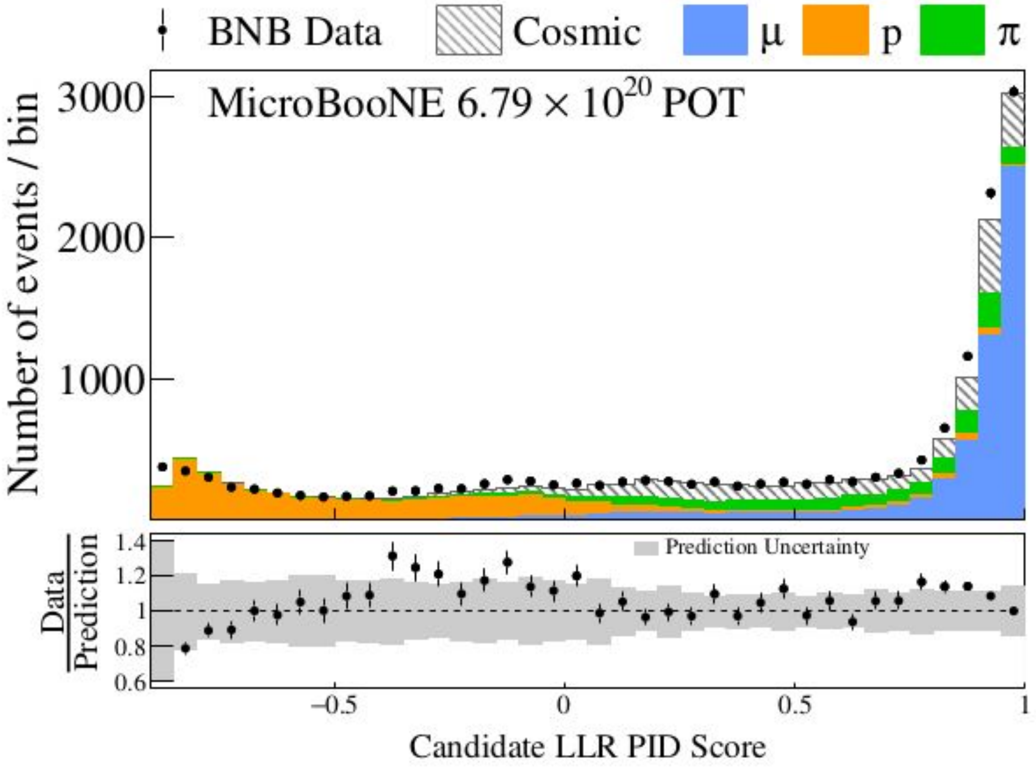

FIG. 1. The log-likelihood ratio (LLR) particle identification (PID) score distribution used to tag the muon and proton candidates.

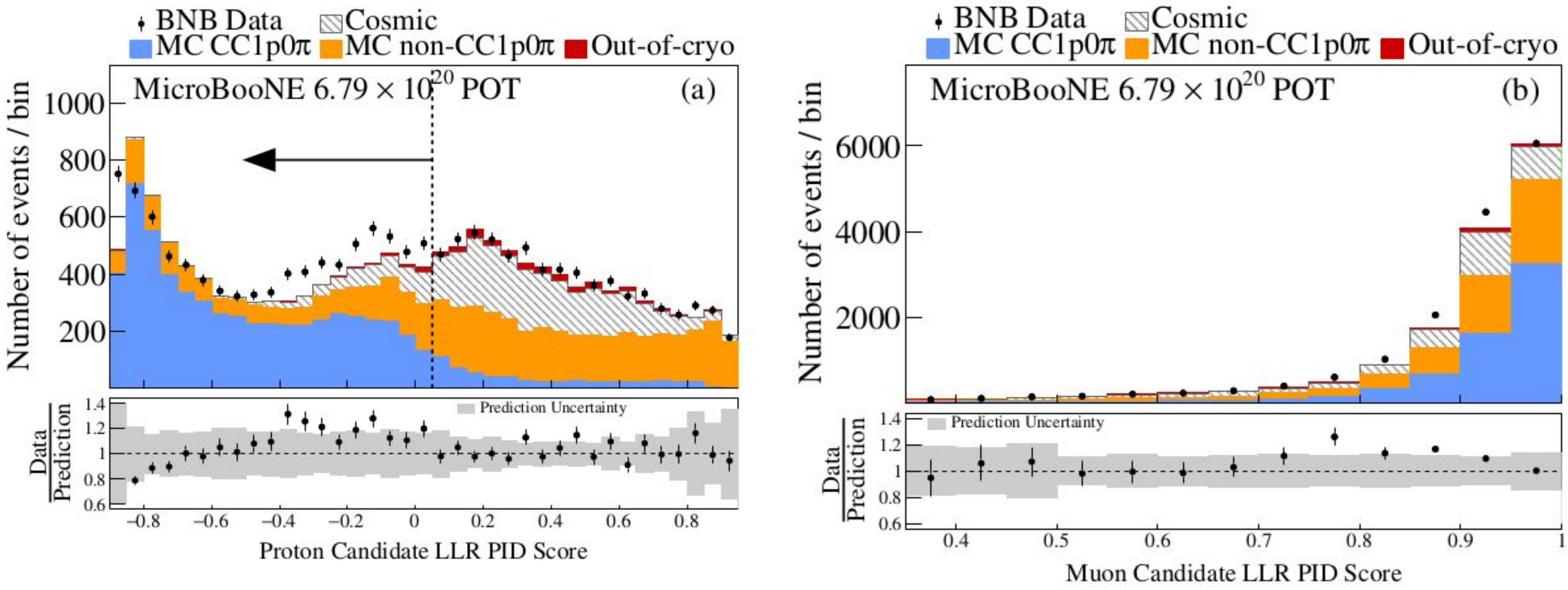

FIG. 2. (Top) the proton candidate LLR PID score distribution, illustrating the fitness of a cut at LLR PID < 0.05 to reject cosmic and non-CC1p0π background events. (Bottom) the muon candidate LLR PID score distribution, illustrating a peak close to one. Only statistical uncertainties are shown on the data. The bottom panel shows the ratio of data to prediction.

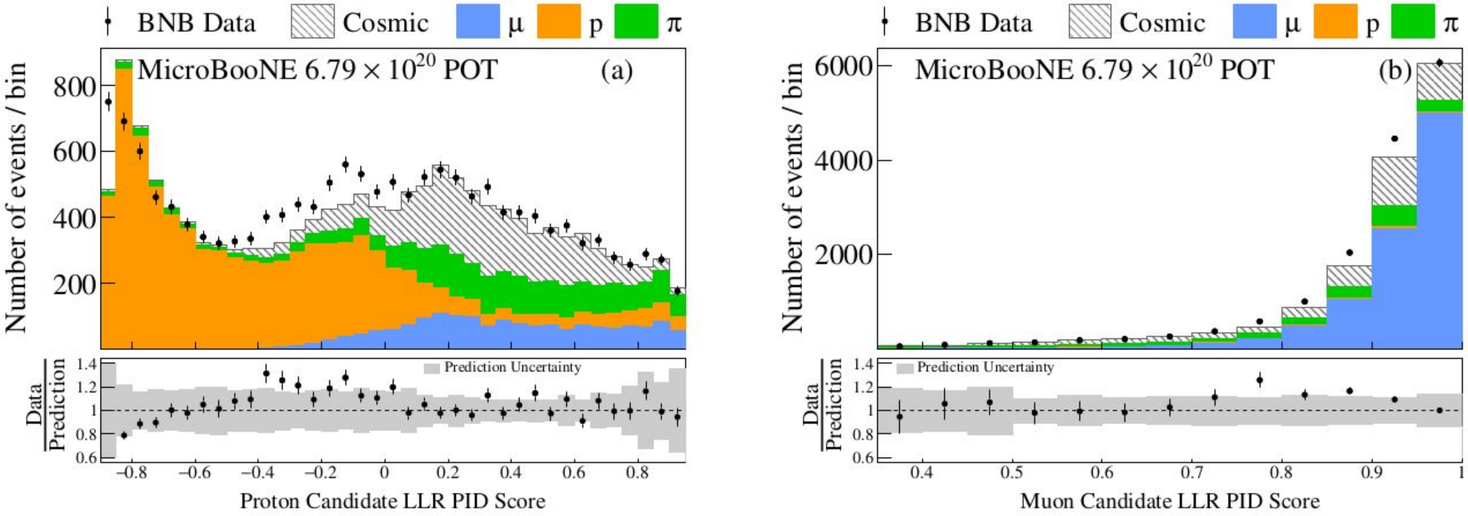

FIG. 1. (Left) the proton candidate LLR PID score distribution, illustrating the particle composition of the variable. (Right) the muon candidate LLR PID score distribution, illustrating a peak close to one. Only statistical uncertainties are shown on the data. The bottom panel shows the ratio of data to prediction.

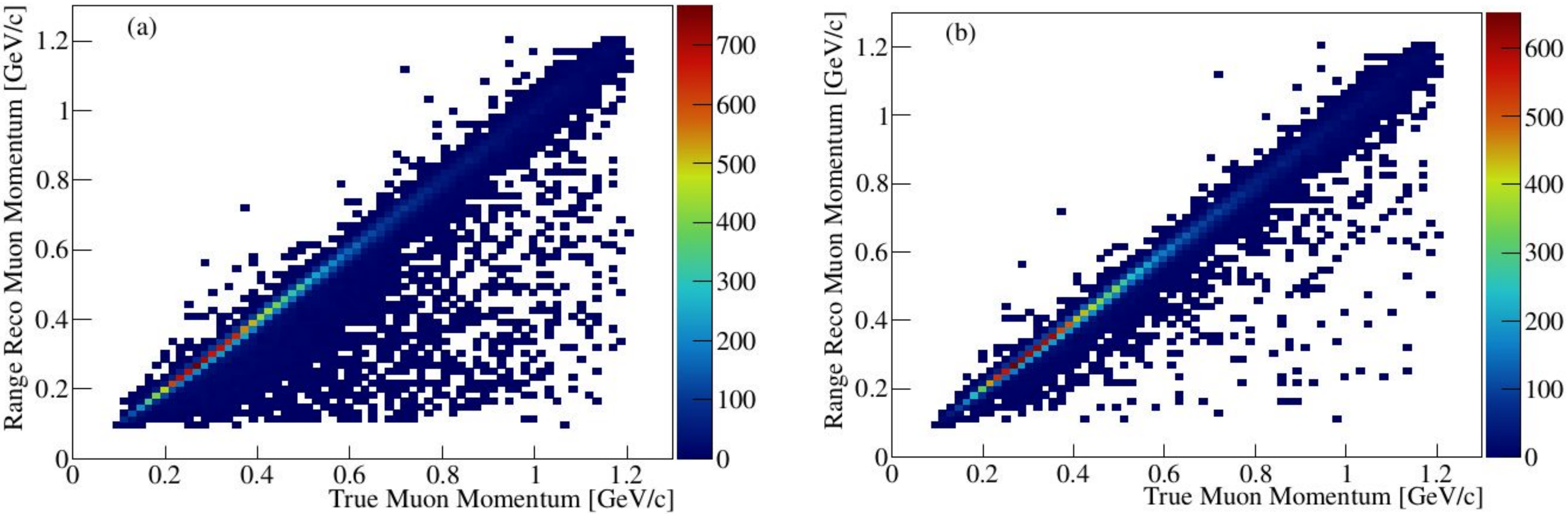

FIG. 3. Muon momentum reconstruction (top) before and (bottom) after the application of the muon momentum quality cut using contained muon tracks.

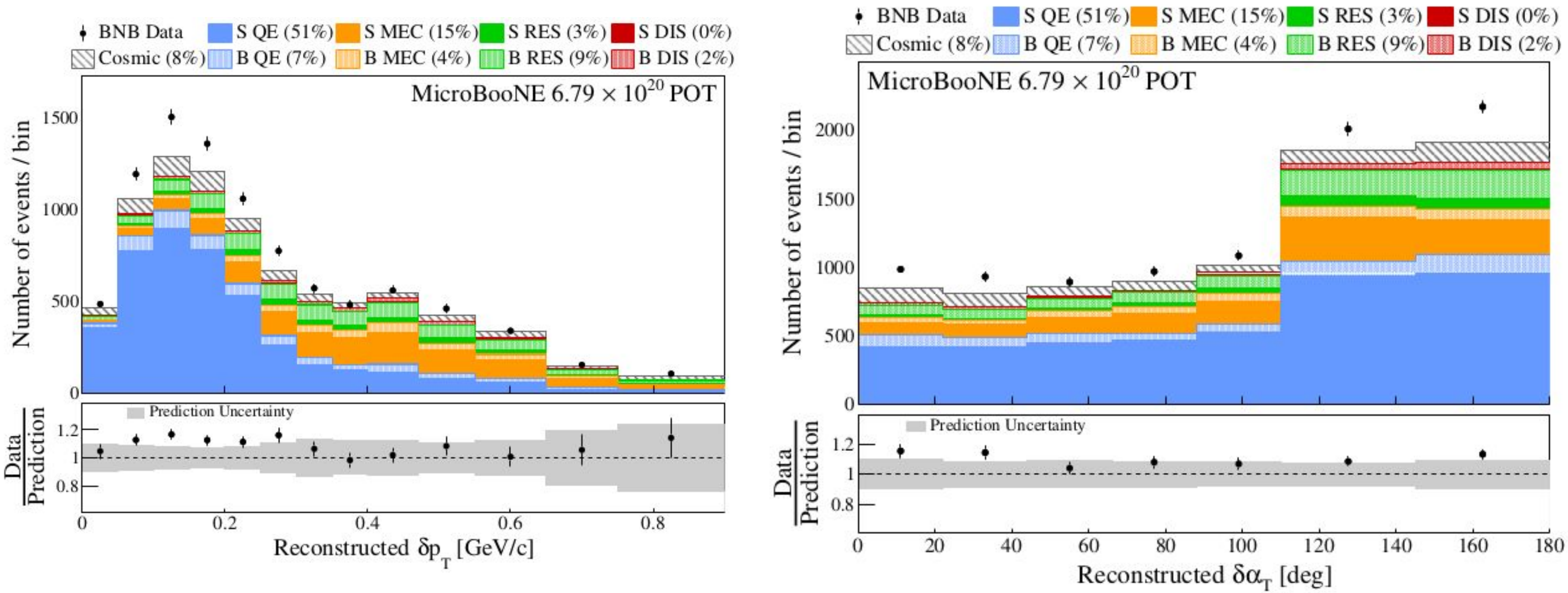

BNB Data
S QE (51%)
S MEC (15%)
S RES (3%)
S DIS (0%)
Cosmic (8%)
B QE (7%)
B MEC (4%)
B RES (9%)
B DIS (2%)
MicroBooNE 6.79 × 10^20 POT
Number of events / bin
Prediction Uncertainty
Data / Prediction
Reconstructed δp_T [GeV/c]
Reconstructed δα_T [deg]

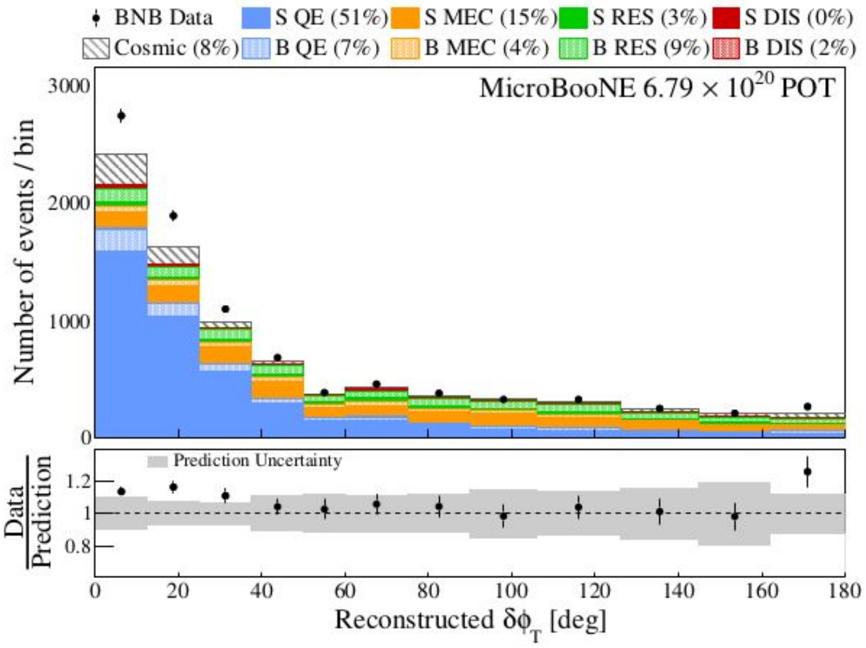
BNB Data
S QE (51%)
S MEC (15%)
S RES (3%)
S DIS (0%)
Cosmic (8%)
B QE (7%)
B MEC (4%)
B RES (9%)
B DIS (2%)
MicroBooNE 6.79 × 10^20 POT
Number of events / bin
Prediction Uncertainty
Data / Prediction
Reconstructed δφ_T [deg]

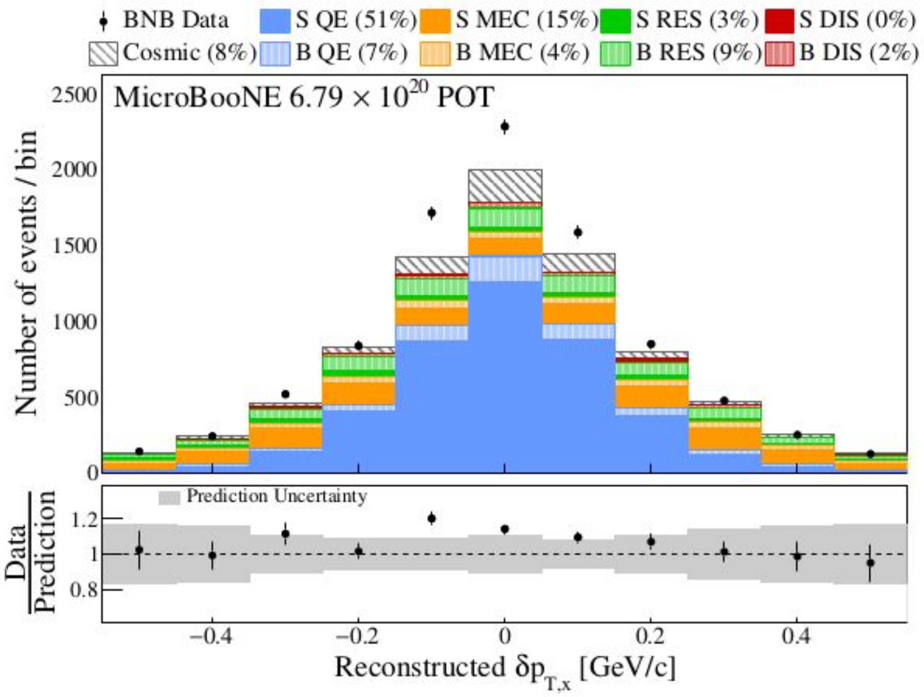
BNB Data
S QE (51%)
S MEC (15%)
S RES (3%)
S DIS (0%)
Cosmic (8%)
B QE (7%)
B MEC (4%)
B RES (9%)
B DIS (2%)
MicroBooNE 6.79 × 10^20 POT
Number of events / bin
Prediction Uncertainty
Data / Prediction
Reconstructed δp_T,x [GeV/c]

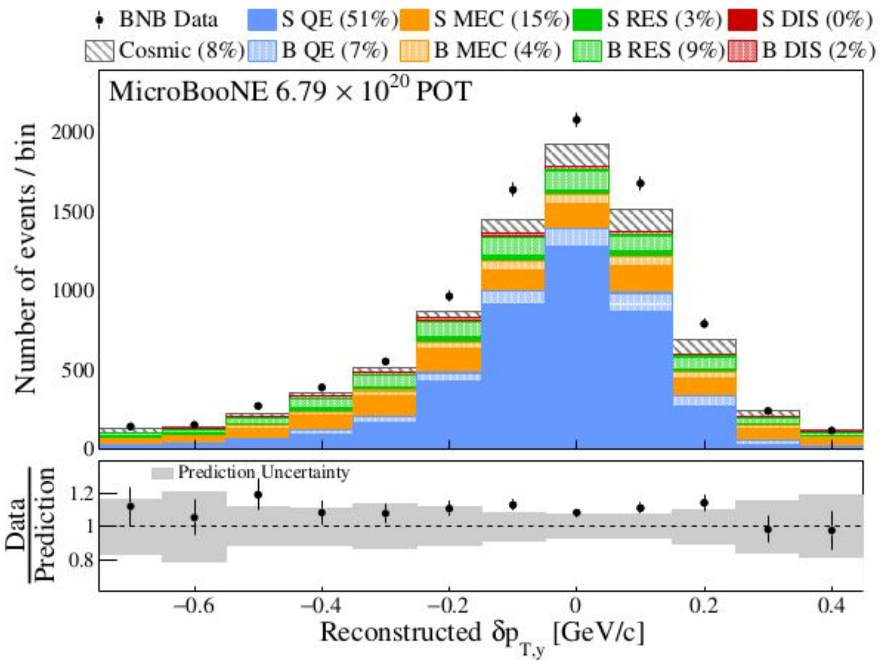
BNB Data
S QE (51%)
S MEC (15%)
S RES (3%)
S DIS (0%)
Cosmic (8%)
B QE (7%)
B MEC (4%)
B RES (9%)
B DIS (2%)
MicroBooNE 6.79 × 10^20 POT
Number of events / bin
Prediction Uncertainty
Data / Prediction
Reconstructed δp_T,y [GeV/c]

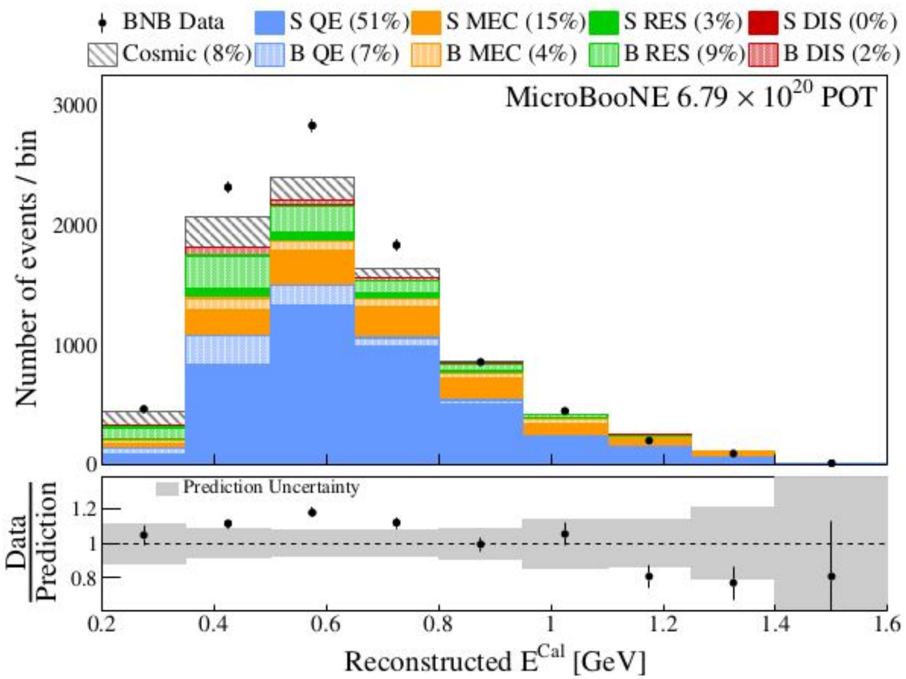
BNB Data
S QE (51%)
S MEC (15%)
S RES (3%)
S DIS (0%)
Cosmic (8%)
B QE (7%)
B MEC (4%)
B RES (9%)
B DIS (2%)
MicroBooNE 6.79 × 10^20 POT
Number of events / bin
Prediction Uncertainty
Data / Prediction
Reconstructed E^Cal [GeV]

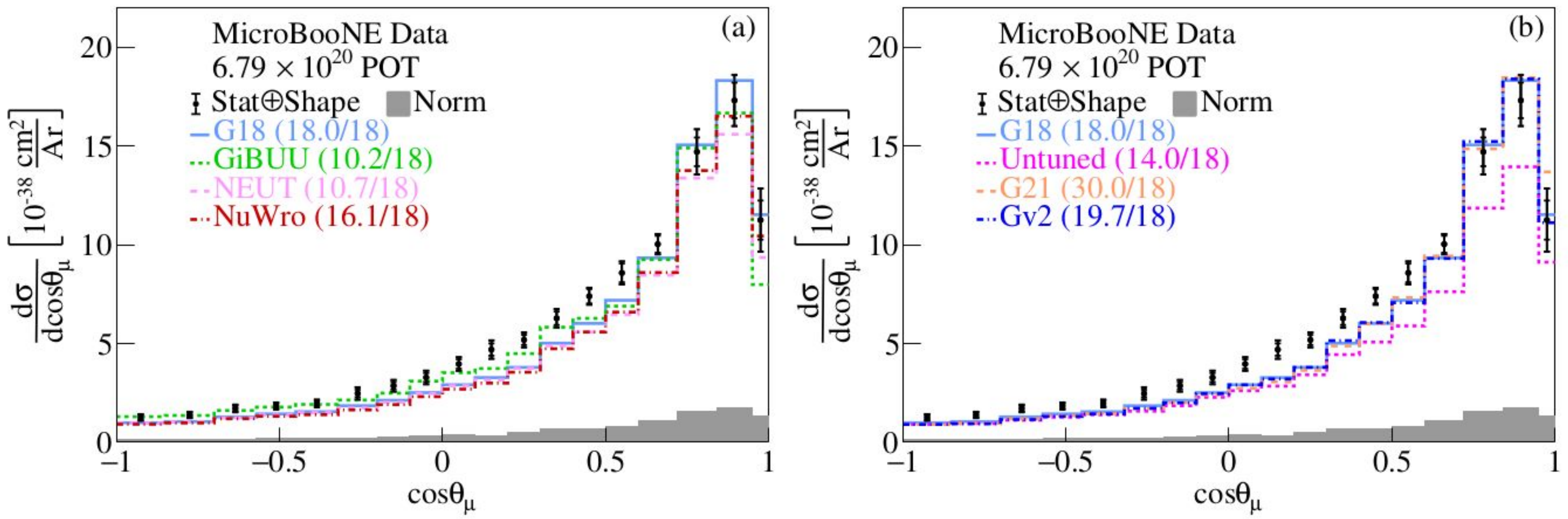
MicroBooNE Data
6.79 × 10^20 POT
Stat⊕Shape
Norm
G18 (18.0/18)
GiBUU (10.2/18)
NEUT (10.7/18)
NuWro (16.1/18)
(a)
MicroBooNE Data
6.79 × 10^20 POT
Stat⊕Shape
Norm
G18 (18.0/18)
Untuned (14.0/18)
G21 (30.0/18)
Gv2 (19.7/18)
(b)
dσ/dcosθ_μ [10^-38 cm²/Ar]
cosθ_μ
−1
−0.5
0
0.5
1
0
5
10
15
20

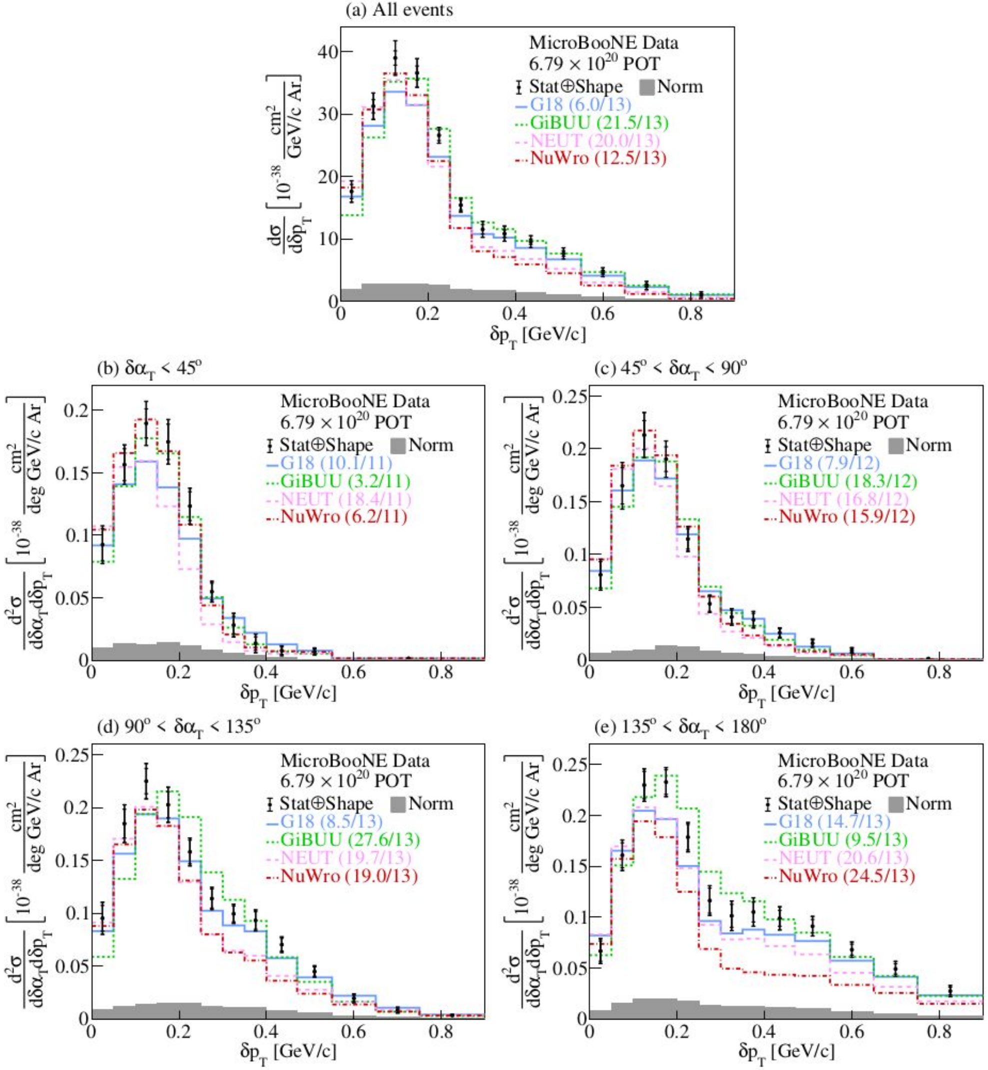

(a) All events
MicroBooNE Data
6.79 × 10^20 POT
Stat⊕Shape
Norm
G18 (6.0/13)
GiBUU (21.5/13)
NEUT (20.0/13)
NuWro (12.5/13)
δp_T [GeV/c]
(b) δα_T < 45°
G18 (10.1/11)
GiBUU (3.2/11)
NEUT (18.4/11)
NuWro (6.2/11)
(c) 45° < δα_T < 90°
G18 (7.9/12)
GiBUU (18.3/12)
NEUT (16.8/12)
NuWro (15.9/12)
(d) 90° < δα_T < 135°
G18 (8.5/13)
GiBUU (27.6/13)
NEUT (19.7/13)
NuWro (19.0/13)
(e) 135° < δα_T < 180°
G18 (14.7/13)
GiBUU (9.5/13)
NEUT (20.6/13)
NuWro (24.5/13)

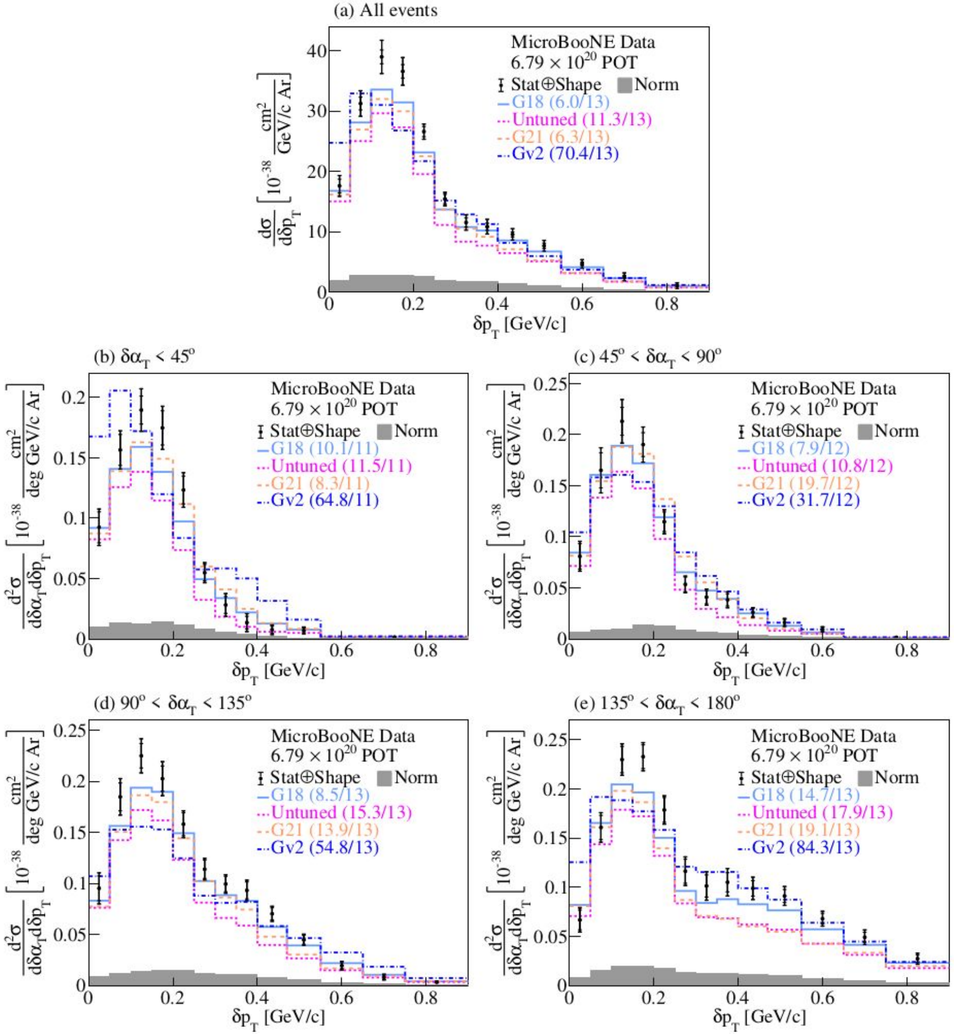
(a) All events
MicroBooNE Data
6.79 × 10^20 POT
Stat⊕Shape Norm
G18 (6.0/13)
Untuned (11.3/13)
G21 (6.3/13)
Gv2 (70.4/13)
dσ/dδp_T [10^-38 cm²/(GeV/c Ar)]
δp_T [GeV/c]
(b) δα_T < 45°
MicroBooNE Data
6.79 × 10^20 POT
Stat⊕Shape Norm
G18 (10.1/11)
Untuned (11.5/11)
G21 (8.3/11)
Gv2 (64.8/11)
(c) 45° < δα_T < 90°
MicroBooNE Data
6.79 × 10^20 POT
Stat⊕Shape Norm
G18 (7.9/12)
Untuned (10.8/12)
G21 (19.7/12)
Gv2 (31.7/12)
(d) 90° < δα_T < 135°
MicroBooNE Data
6.79 × 10^20 POT
Stat⊕Shape Norm
G18 (8.5/13)
Untuned (15.3/13)
G21 (13.9/13)
Gv2 (54.8/13)
(e) 135° < δα_T < 180°
MicroBooNE Data
6.79 × 10^20 POT
Stat⊕Shape Norm
G18 (14.7/13)
Untuned (17.9/13)
G21 (19.1/13)
Gv2 (84.3/13)
d²σ/dδα_T dδp_T [10^-38 cm²/(deg GeV/c Ar)]
δp_T [GeV/c]

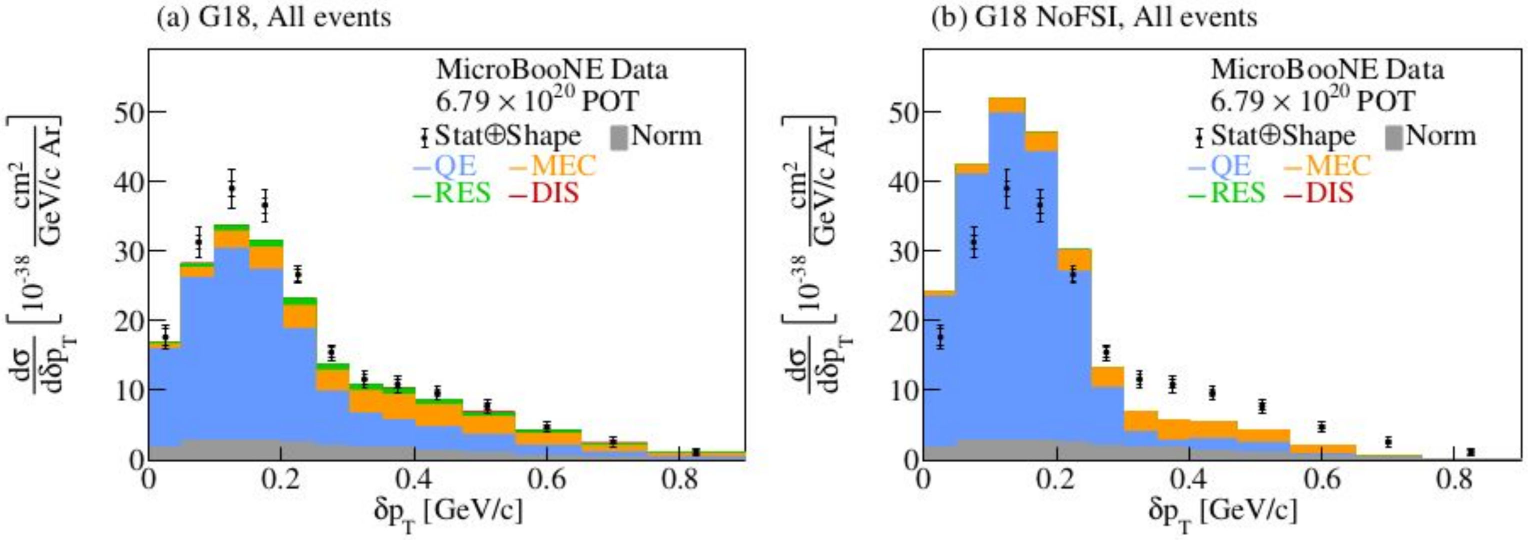
(a) G18, All events
(b) G18 NoFSI, All events
MicroBooNE Data
6.79 × 10^20 POT
Stat⊕Shape
Norm
QE
MEC
RES
DIS
dσ/dδp_T [10^-38 cm²/(GeV/c Ar)]
δp_T [GeV/c]
0
10
20
30
40
50
0.2
0.4
0.6
0.8

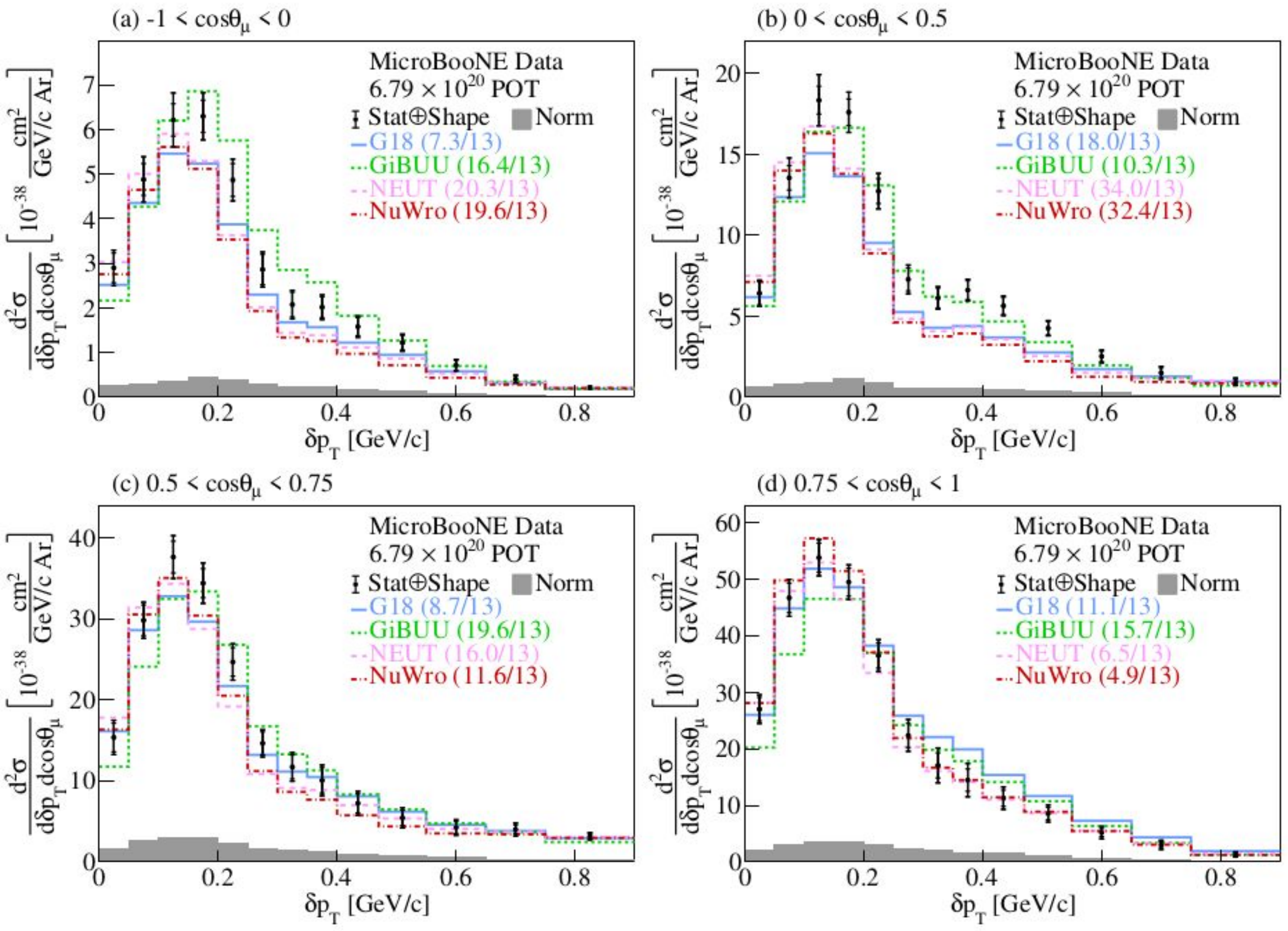

(a) -1 < cosθ_μ < 0
(b) 0 < cosθ_μ < 0.5
(c) 0.5 < cosθ_μ < 0.75
(d) 0.75 < cosθ_μ < 1
MicroBooNE Data
6.79 × 10^20 POT
Stat⊕Shape
Norm
G18 (7.3/13)
GiBUU (16.4/13)
NEUT (20.3/13)
NuWro (19.6/13)
G18 (18.0/13)
GiBUU (10.3/13)
NEUT (34.0/13)
NuWro (32.4/13)
G18 (8.7/13)
GiBUU (19.6/13)
NEUT (16.0/13)
NuWro (11.6/13)
G18 (11.1/13)
GiBUU (15.7/13)
NEUT (6.5/13)
NuWro (4.9/13)
d²σ / dδp_T dcosθ_μ [10^-38 cm² / GeV/c Ar]
δp_T [GeV/c]

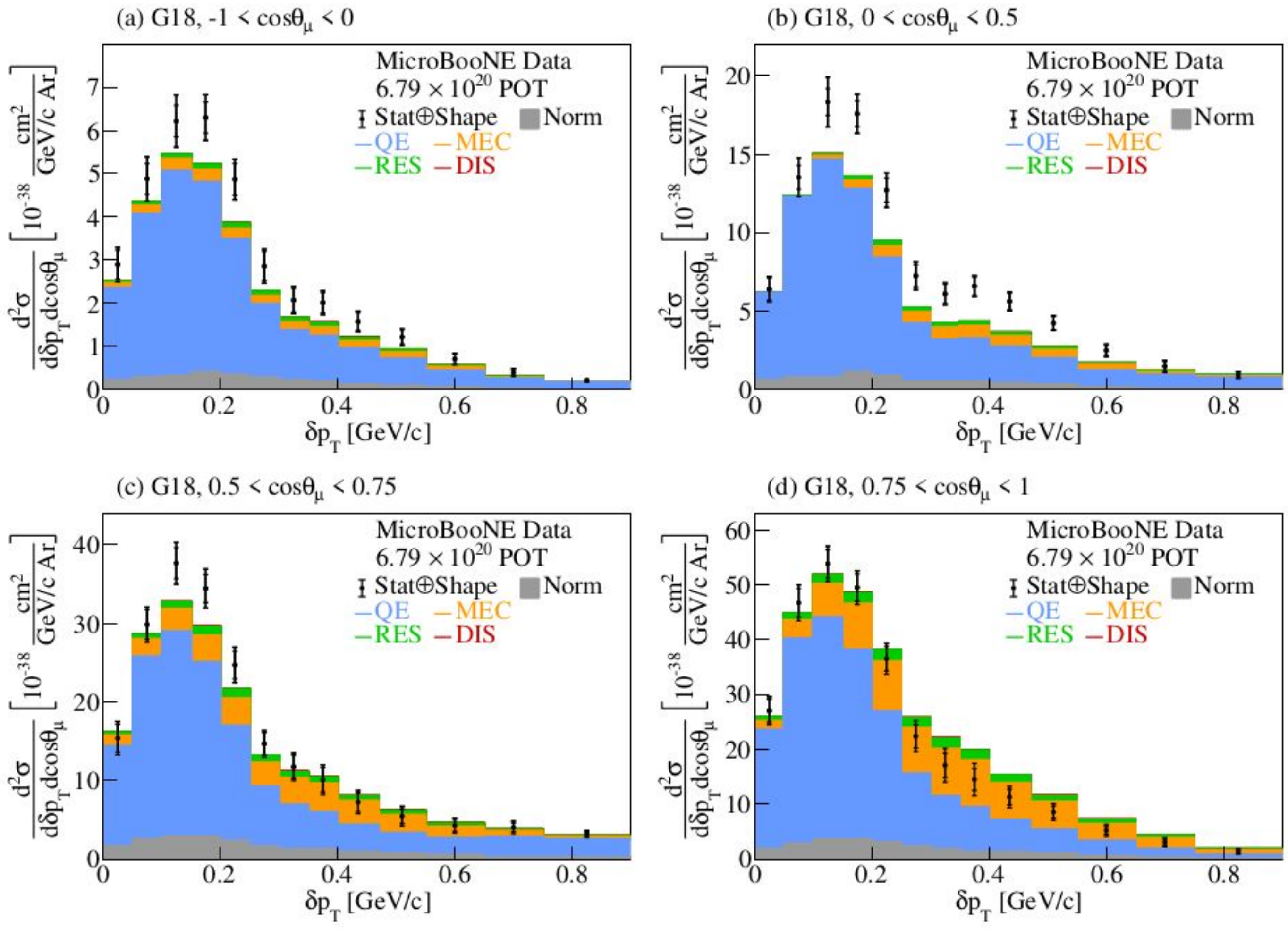

(a) G18, -1 < cosθμ < 0
(b) G18, 0 < cosθμ < 0.5
(c) G18, 0.5 < cosθμ < 0.75
(d) G18, 0.75 < cosθμ < 1
MicroBooNE Data
6.79 × 10^20 POT
Stat⊕Shape
Norm
QE
MEC
RES
DIS
d²σ / dδpT dcosθμ [10^-38 cm² / GeV/c Ar]
δpT [GeV/c]

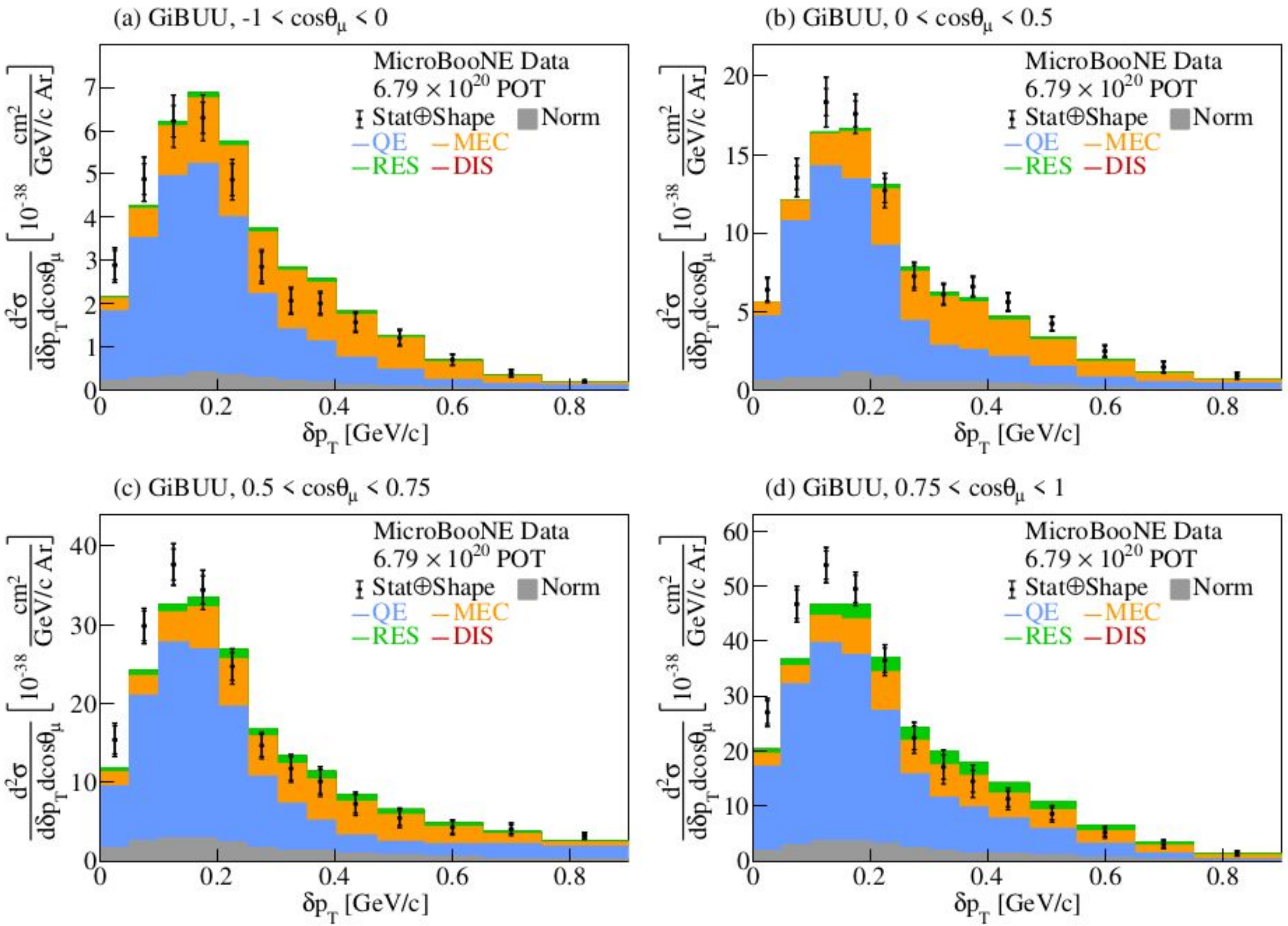

(a) GiBUU, -1 < cosθμ < 0
(b) GiBUU, 0 < cosθμ < 0.5
(c) GiBUU, 0.5 < cosθμ < 0.75
(d) GiBUU, 0.75 < cosθμ < 1
MicroBooNE Data
6.79 × 10^20 POT
Stat⊕Shape
Norm
QE
MEC
RES
DIS
d²σ/dδpT dcosθμ [10^-38 cm²/(GeV/c Ar)]
δpT [GeV/c]

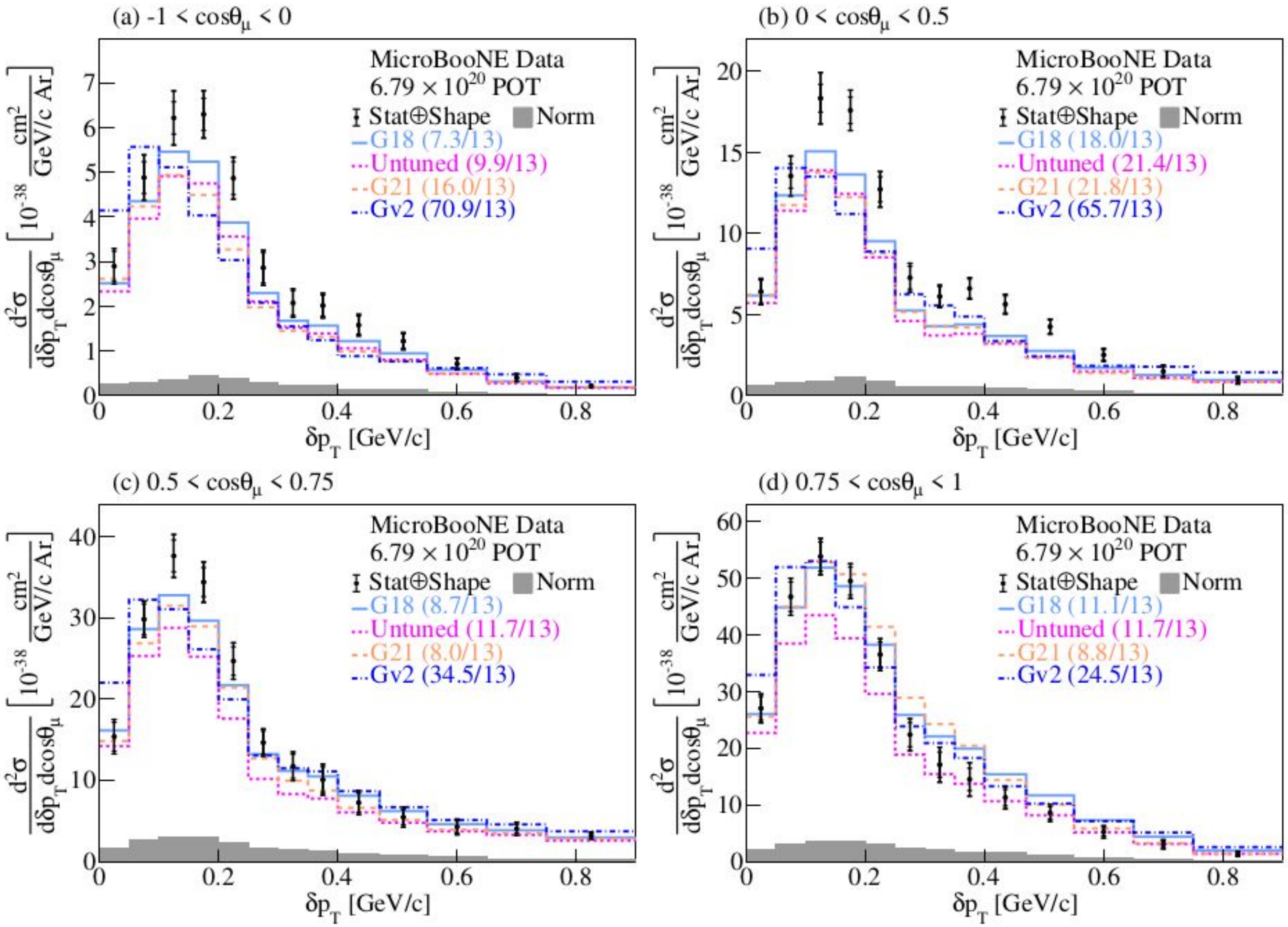
(a) -1 < cosθμ < 0
MicroBooNE Data
6.79 × 10^20 POT
Stat⊕Shape
Norm
G18 (7.3/13)
Untuned (9.9/13)
G21 (16.0/13)
Gv2 (70.9/13)
(b) 0 < cosθμ < 0.5
MicroBooNE Data
6.79 × 10^20 POT
Stat⊕Shape
Norm
G18 (18.0/13)
Untuned (21.4/13)
G21 (21.8/13)
Gv2 (65.7/13)
(c) 0.5 < cosθμ < 0.75
MicroBooNE Data
6.79 × 10^20 POT
Stat⊕Shape
Norm
G18 (8.7/13)
Untuned (11.7/13)
G21 (8.0/13)
Gv2 (34.5/13)
(d) 0.75 < cosθμ < 1
MicroBooNE Data
6.79 × 10^20 POT
Stat⊕Shape
Norm
G18 (11.1/13)
Untuned (11.7/13)
G21 (8.8/13)
Gv2 (24.5/13)
d²σ / dδpT dcosθμ [10^-38 cm² / GeV/c Ar]
δpT [GeV/c]

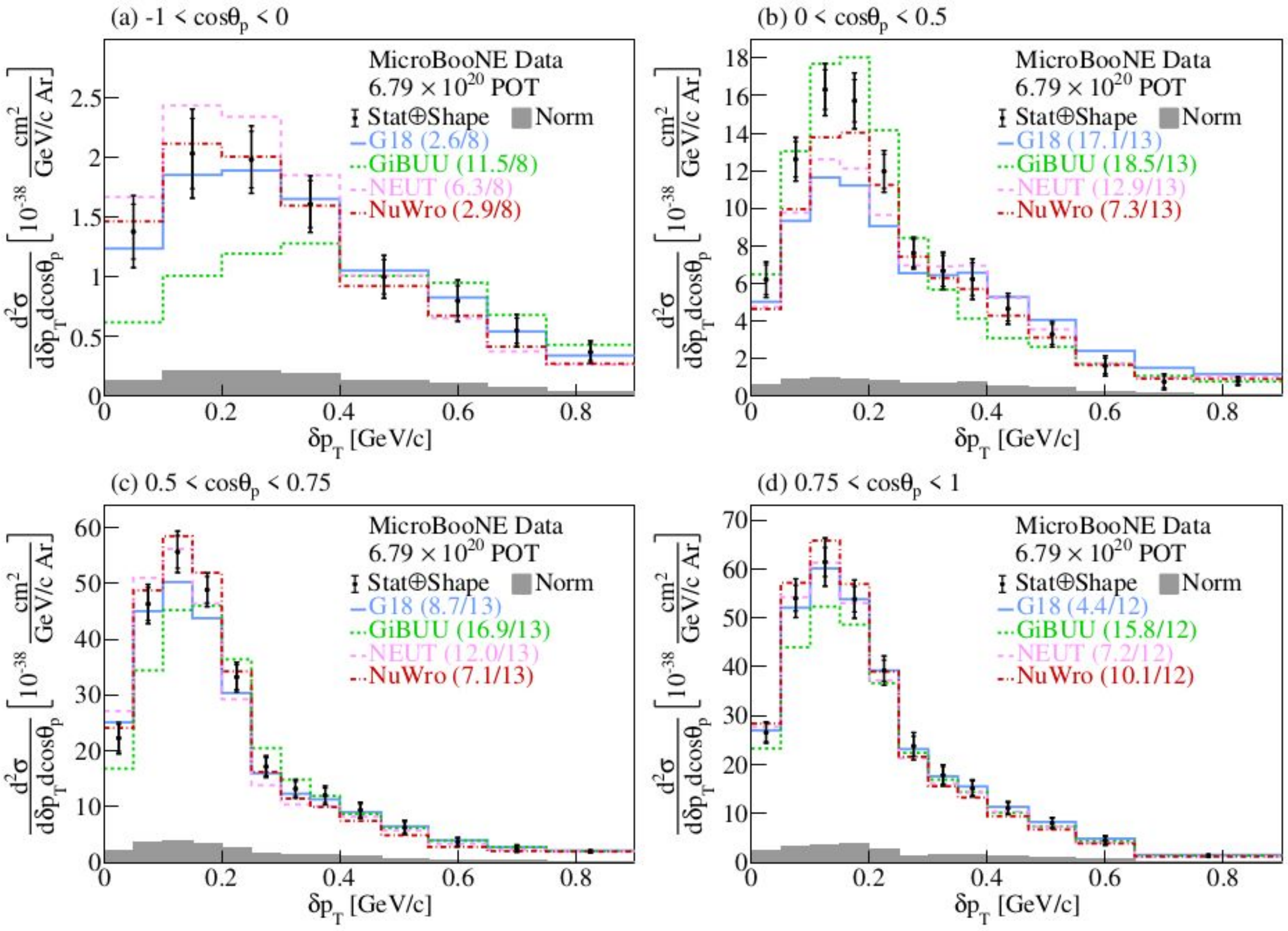

(a) -1 < cosθp < 0
(b) 0 < cosθp < 0.5
(c) 0.5 < cosθp < 0.75
(d) 0.75 < cosθp < 1
MicroBooNE Data
6.79 × 10^20 POT
Stat⊕Shape
Norm
G18 (2.6/8)
GiBUU (11.5/8)
NEUT (6.3/8)
NuWro (2.9/8)
G18 (17.1/13)
GiBUU (18.5/13)
NEUT (12.9/13)
NuWro (7.3/13)
G18 (8.7/13)
GiBUU (16.9/13)
NEUT (12.0/13)
NuWro (7.1/13)
G18 (4.4/12)
GiBUU (15.8/12)
NEUT (7.2/12)
NuWro (10.1/12)
δpT [GeV/c]
d²σ/dδpT dcosθp [10^-38 cm²/GeV/c Ar]

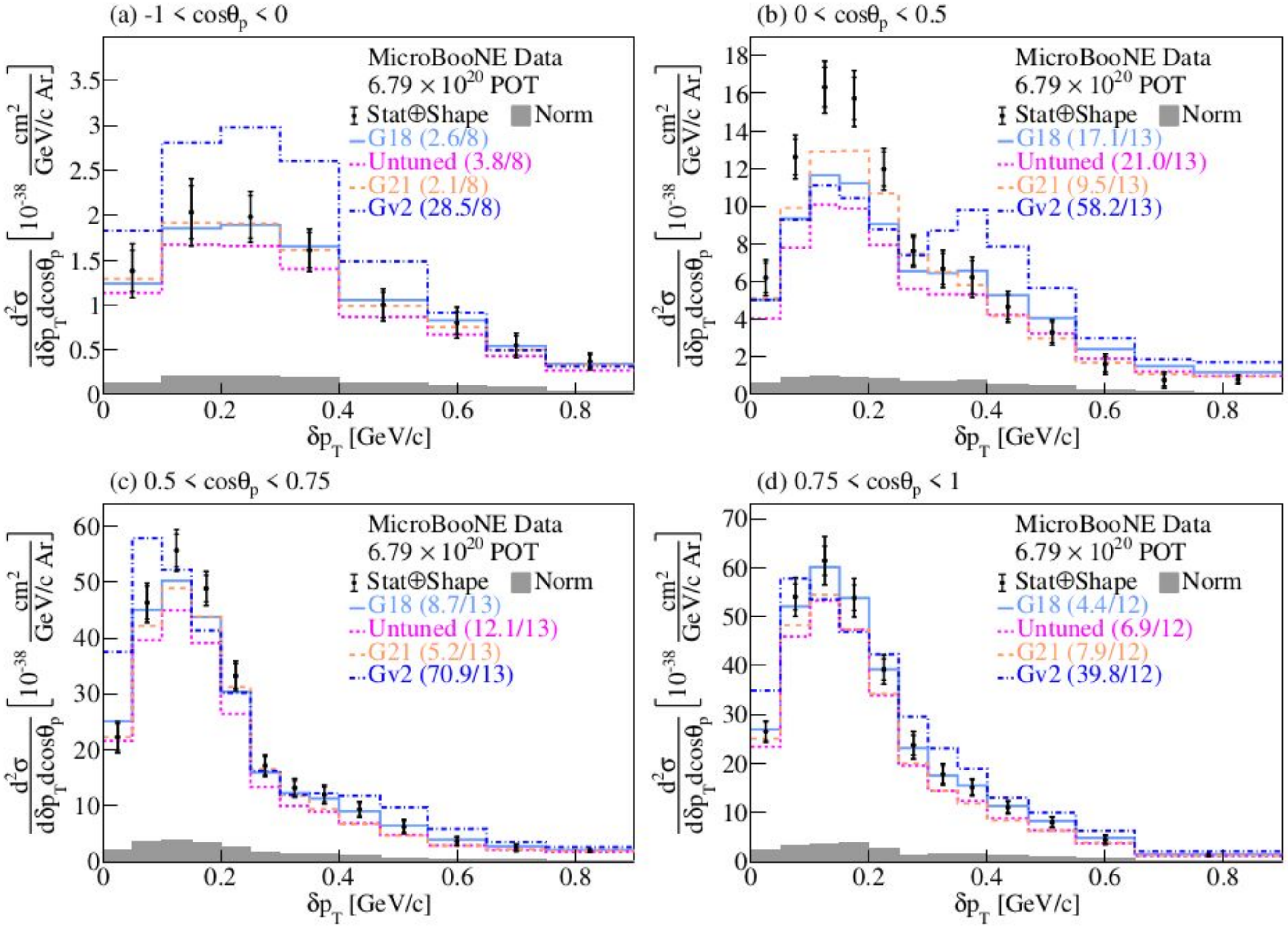

(a) -1 < cosθp < 0
(b) 0 < cosθp < 0.5
(c) 0.5 < cosθp < 0.75
(d) 0.75 < cosθp < 1
MicroBooNE Data
6.79 × 10^20 POT
Stat⊕Shape
Norm
G18 (2.6/8)
Untuned (3.8/8)
G21 (2.1/8)
Gv2 (28.5/8)
G18 (17.1/13)
Untuned (21.0/13)
G21 (9.5/13)
Gv2 (58.2/13)
G18 (8.7/13)
Untuned (12.1/13)
G21 (5.2/13)
Gv2 (70.9/13)
G18 (4.4/12)
Untuned (6.9/12)
G21 (7.9/12)
Gv2 (39.8/12)
d²σ/dδpT dcosθp [10^-38 cm²/GeV/c Ar]
δpT [GeV/c]

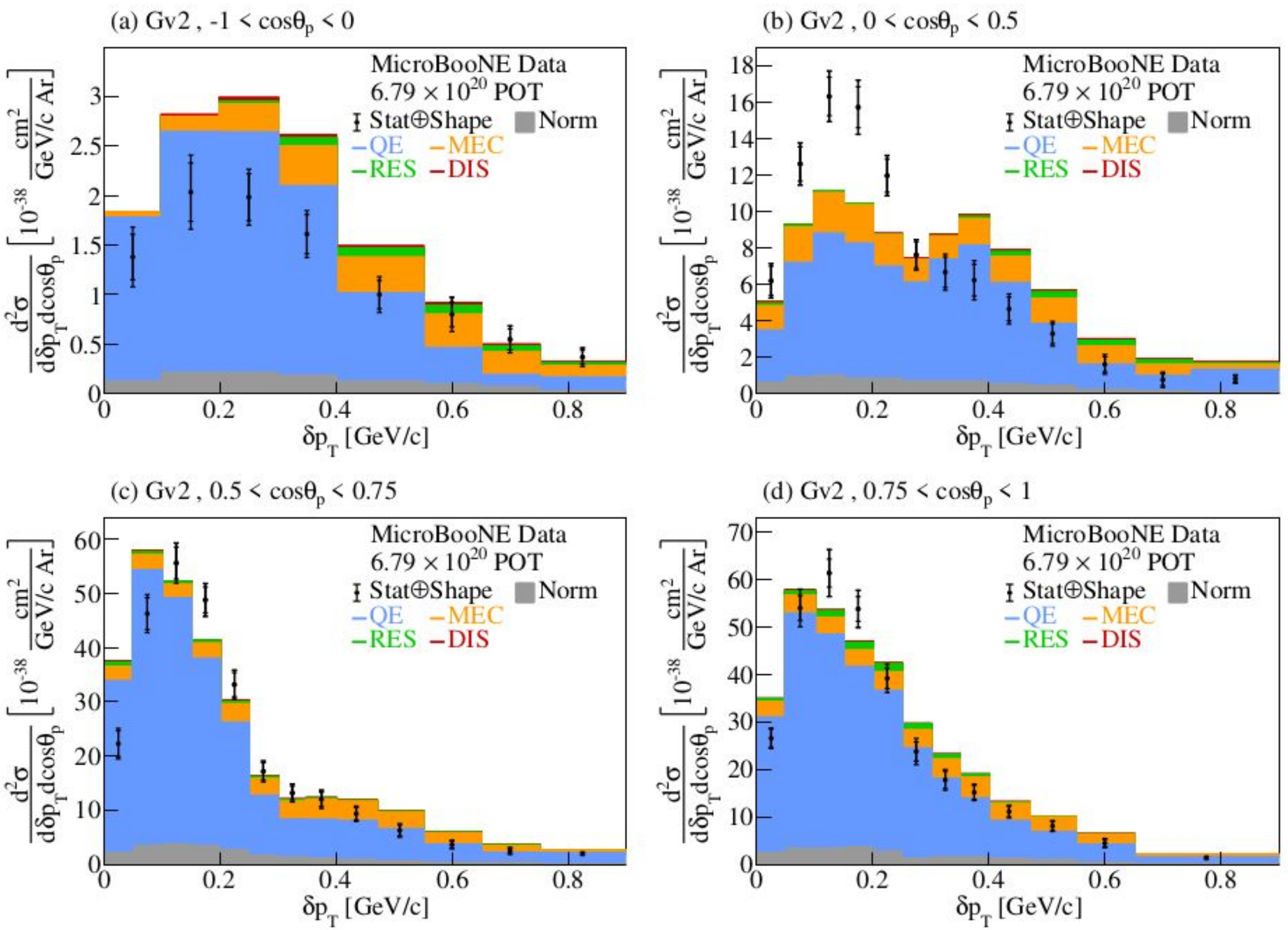

(a) Gv2 , -1 < cosθp < 0
(b) Gv2 , 0 < cosθp < 0.5
(c) Gv2 , 0.5 < cosθp < 0.75
(d) Gv2 , 0.75 < cosθp < 1
MicroBooNE Data
6.79 × 10^20 POT
Stat⊕Shape
Norm
QE
MEC
RES
DIS
$\frac{d^2\sigma}{d\delta p_T d\cos\theta_p}$ $\left[10^{-38} \frac{cm^2}{GeV/c\ Ar}\right]$
δp_T [GeV/c]

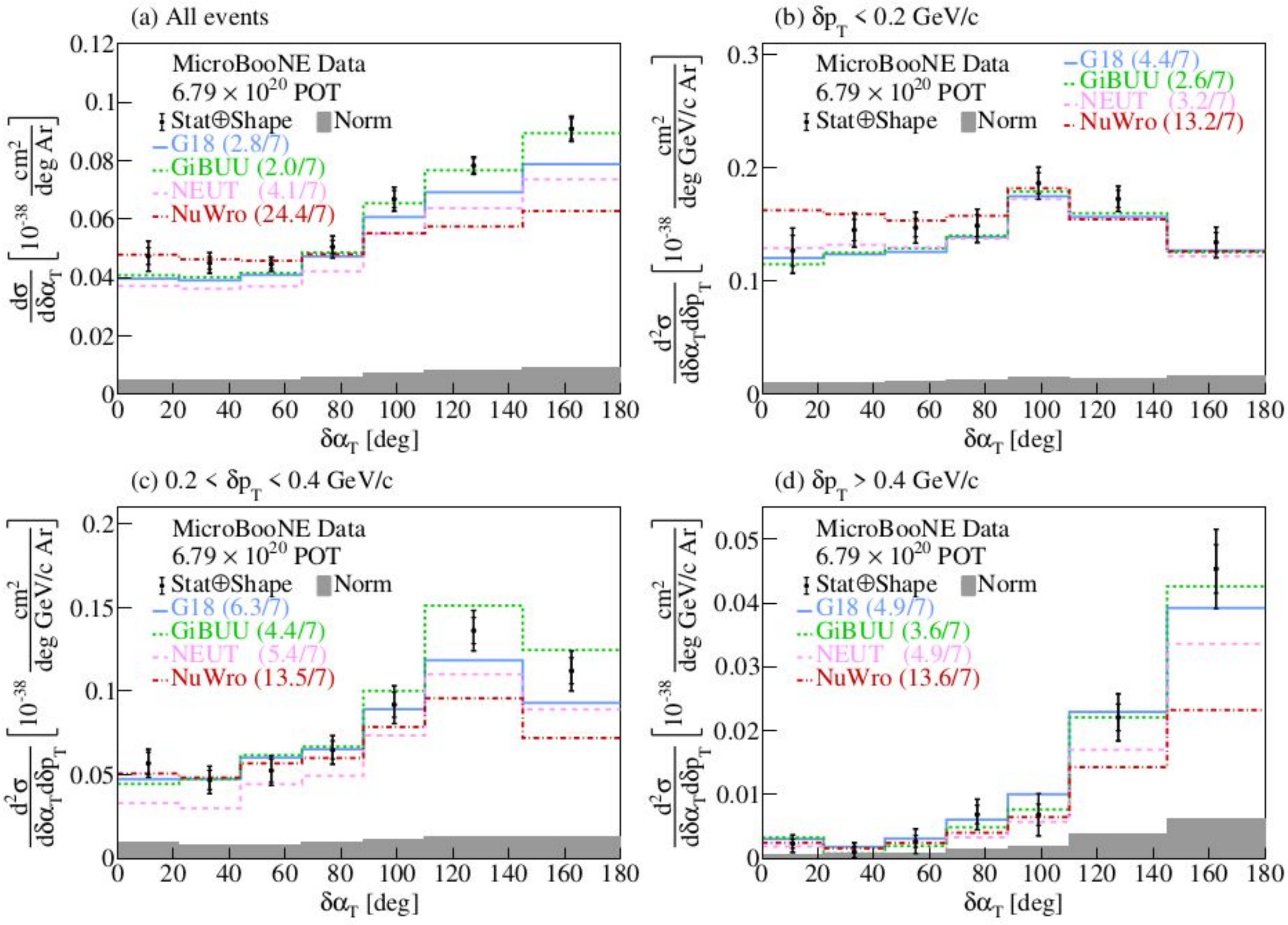

(a) All events
MicroBooNE Data
6.79 × 10^20 POT
Stat⊕Shape
Norm
G18 (2.8/7)
GiBUU (2.0/7)
NEUT (4.1/7)
NuWro (24.4/7)
dσ/dδα_T [10^-38 cm²/deg Ar]
δα_T [deg]
(b) δp_T < 0.2 GeV/c
MicroBooNE Data
6.79 × 10^20 POT
Stat⊕Shape
Norm
G18 (4.4/7)
GiBUU (2.6/7)
NEUT (3.2/7)
NuWro (13.2/7)
d²σ/dδα_T dδp_T [10^-38 cm²/deg GeV/c Ar]
δα_T [deg]
(c) 0.2 < δp_T < 0.4 GeV/c
MicroBooNE Data
6.79 × 10^20 POT
Stat⊕Shape
Norm
G18 (6.3/7)
GiBUU (4.4/7)
NEUT (5.4/7)
NuWro (13.5/7)
d²σ/dδα_T dδp_T [10^-38 cm²/deg GeV/c Ar]
δα_T [deg]
(d) δp_T > 0.4 GeV/c
MicroBooNE Data
6.79 × 10^20 POT
Stat⊕Shape
Norm
G18 (4.9/7)
GiBUU (3.6/7)
NEUT (4.9/7)
NuWro (13.6/7)
d²σ/dδα_T dδp_T [10^-38 cm²/deg GeV/c Ar]
δα_T [deg]

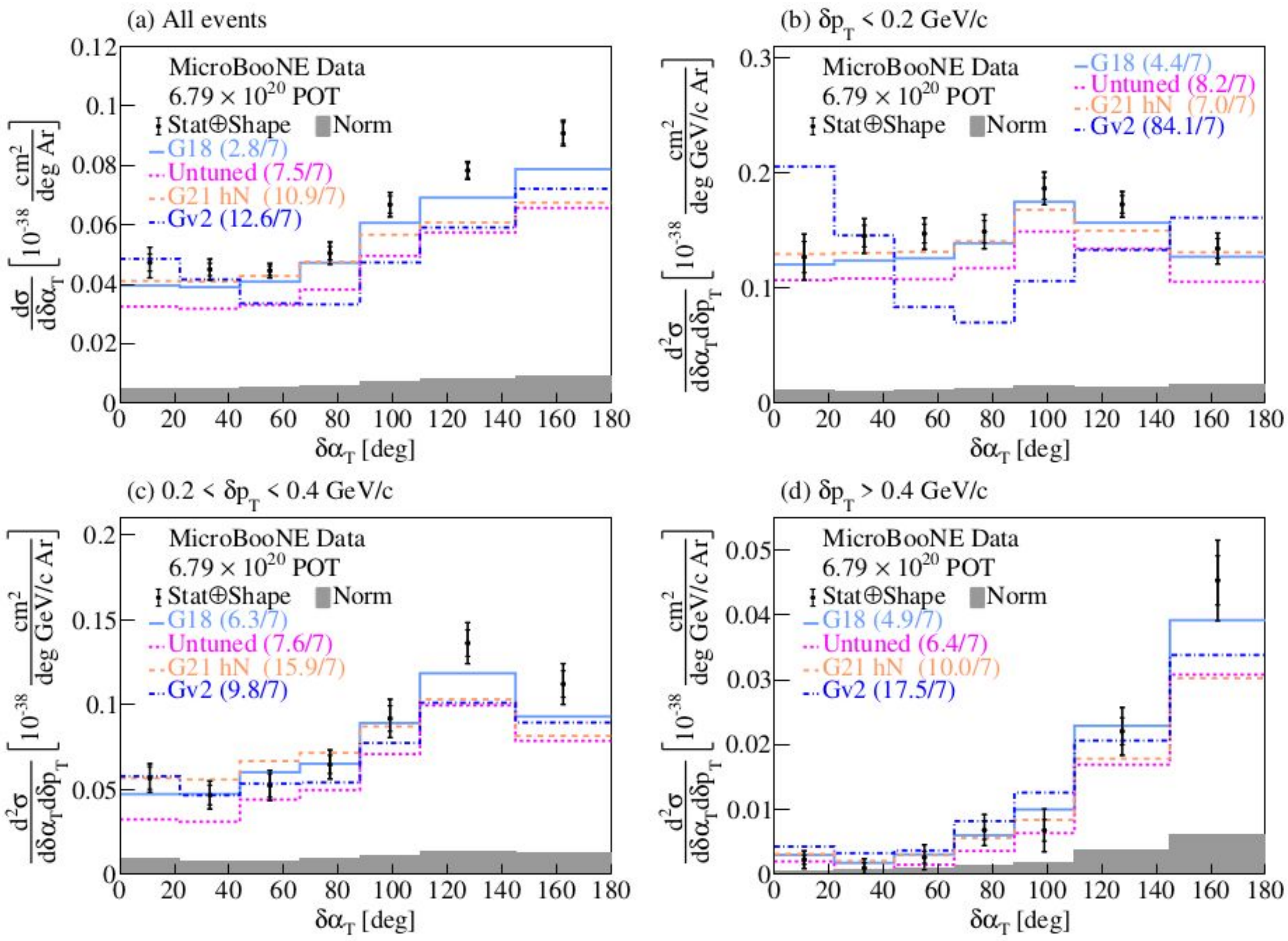
(a) All events
MicroBooNE Data
6.79 × 10^20 POT
Stat⊕Shape
Norm
G18 (2.8/7)
Untuned (7.5/7)
G21 hN (10.9/7)
Gv2 (12.6/7)
dσ/dδα_T [10^-38 cm^2/deg Ar]
δα_T [deg]
(b) δp_T < 0.2 GeV/c
MicroBooNE Data
6.79 × 10^20 POT
Stat⊕Shape
Norm
G18 (4.4/7)
Untuned (8.2/7)
G21 hN (7.0/7)
Gv2 (84.1/7)
d^2σ/dδα_T dδp_T [10^-38 cm^2/deg GeV/c Ar]
δα_T [deg]
(c) 0.2 < δp_T < 0.4 GeV/c
MicroBooNE Data
6.79 × 10^20 POT
Stat⊕Shape
Norm
G18 (6.3/7)
Untuned (7.6/7)
G21 hN (15.9/7)
Gv2 (9.8/7)
d^2σ/dδα_T dδp_T [10^-38 cm^2/deg GeV/c Ar]
δα_T [deg]
(d) δp_T > 0.4 GeV/c
MicroBooNE Data
6.79 × 10^20 POT
Stat⊕Shape
Norm
G18 (4.9/7)
Untuned (6.4/7)
G21 hN (10.0/7)
Gv2 (17.5/7)
d^2σ/dδα_T dδp_T [10^-38 cm^2/deg GeV/c Ar]
δα_T [deg]

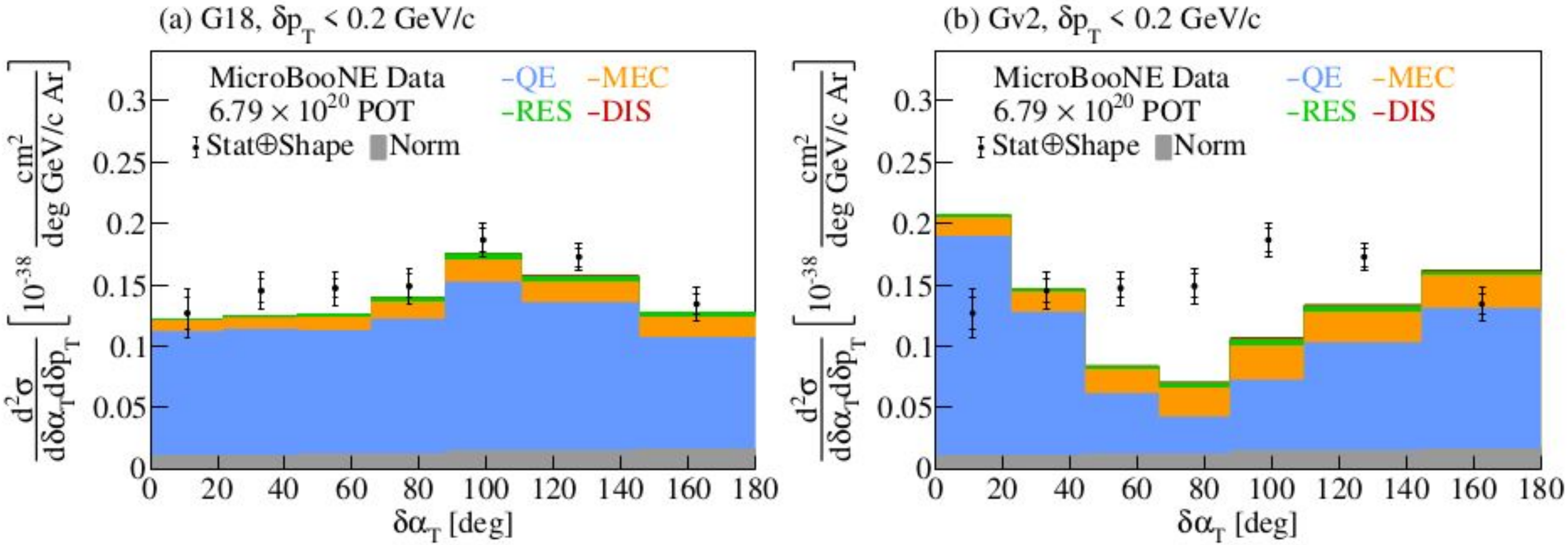

(a) G18, δp_T < 0.2 GeV/c
(b) Gv2, δp_T < 0.2 GeV/c
MicroBooNE Data
6.79×10^{20} POT
Stat⊕Shape
Norm
QE
MEC
RES
DIS
$\frac{d^2\sigma}{d\delta\alpha_T d\delta p_T} \left[10^{-38} \frac{cm^2}{deg\ GeV/c\ Ar}\right]$
$\delta\alpha_T$ [deg]
0
0.05
0.1
0.15
0.2
0.25
0.3
0
20
40
60
80
100
120
140
160
180

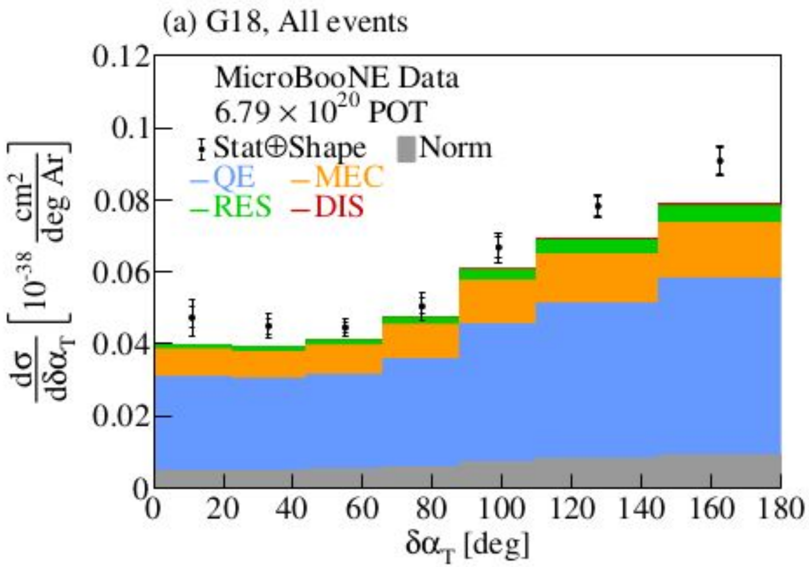

(a) G18, All events
MicroBooNE Data
6.79×10^{20} POT
Stat⊕Shape
Norm
QE
MEC
RES
DIS
$\frac{d\sigma}{d\delta\alpha_T}$ $\left[10^{-38} \frac{cm^2}{deg\ Ar}\right]$
0
0.02
0.04
0.06
0.08
0.1
0.12
0 20 40 60 80 100 120 140 160 180
$\delta\alpha_T$ [deg]

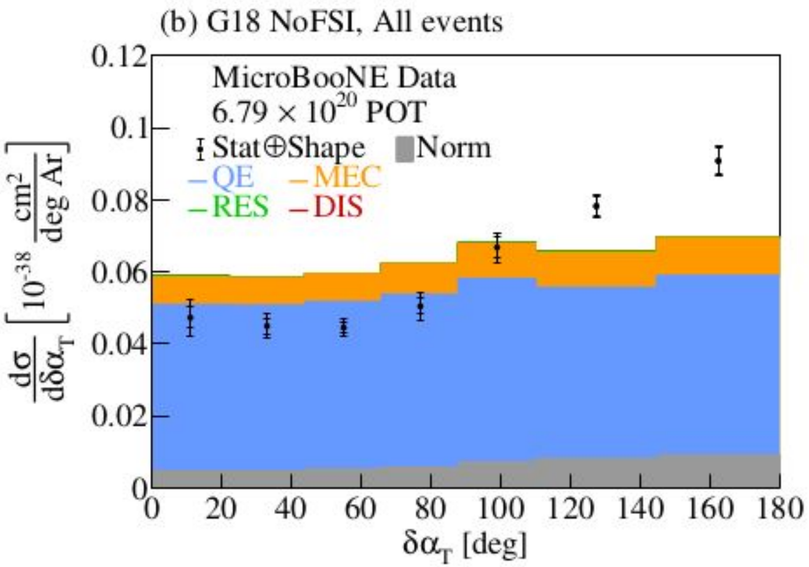

(b) G18 NoFSI, All events
MicroBooNE Data
6.79×10^{20} POT
Stat⊕Shape
Norm
QE
MEC
RES
DIS
$\frac{d\sigma}{d\delta\alpha_T}$ $\left[10^{-38} \frac{cm^2}{deg\ Ar}\right]$
0
0.02
0.04
0.06
0.08
0.1
0.12
0 20 40 60 80 100 120 140 160 180
$\delta\alpha_T$ [deg]

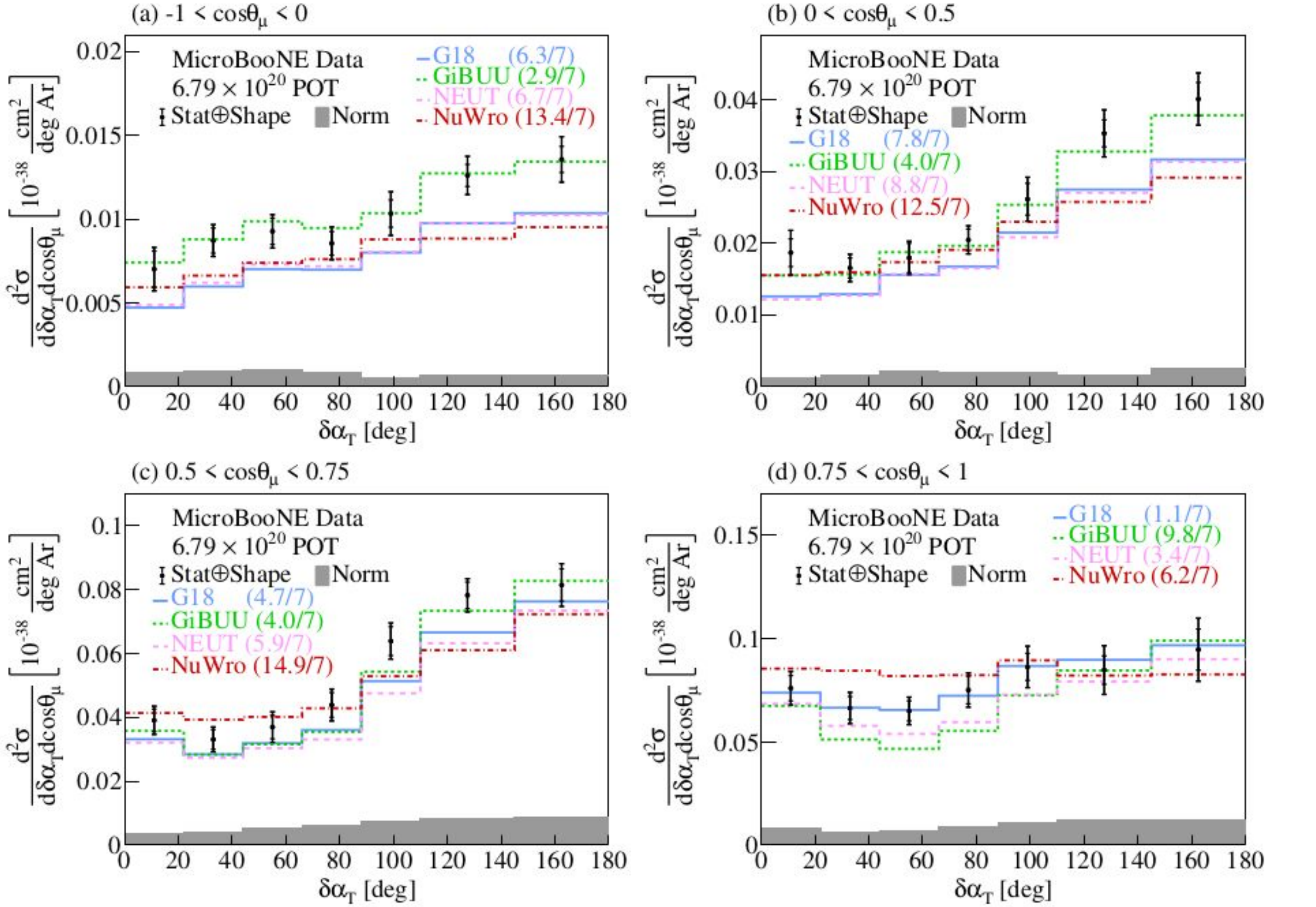

(a) -1 < cosθμ < 0
(b) 0 < cosθμ < 0.5
(c) 0.5 < cosθμ < 0.75
(d) 0.75 < cosθμ < 1
MicroBooNE Data
6.79 × 10^20 POT
Stat⊕Shape
Norm
G18 (6.3/7)
GiBUU (2.9/7)
NEUT (6.7/7)
NuWro (13.4/7)
G18 (7.8/7)
GiBUU (4.0/7)
NEUT (8.8/7)
NuWro (12.5/7)
G18 (4.7/7)
GiBUU (4.0/7)
NEUT (5.9/7)
NuWro (14.9/7)
G18 (1.1/7)
GiBUU (9.8/7)
NEUT (3.4/7)
NuWro (6.2/7)
d²σ/dδαT dcosθμ [10^-38 cm²/deg Ar]
δαT [deg]

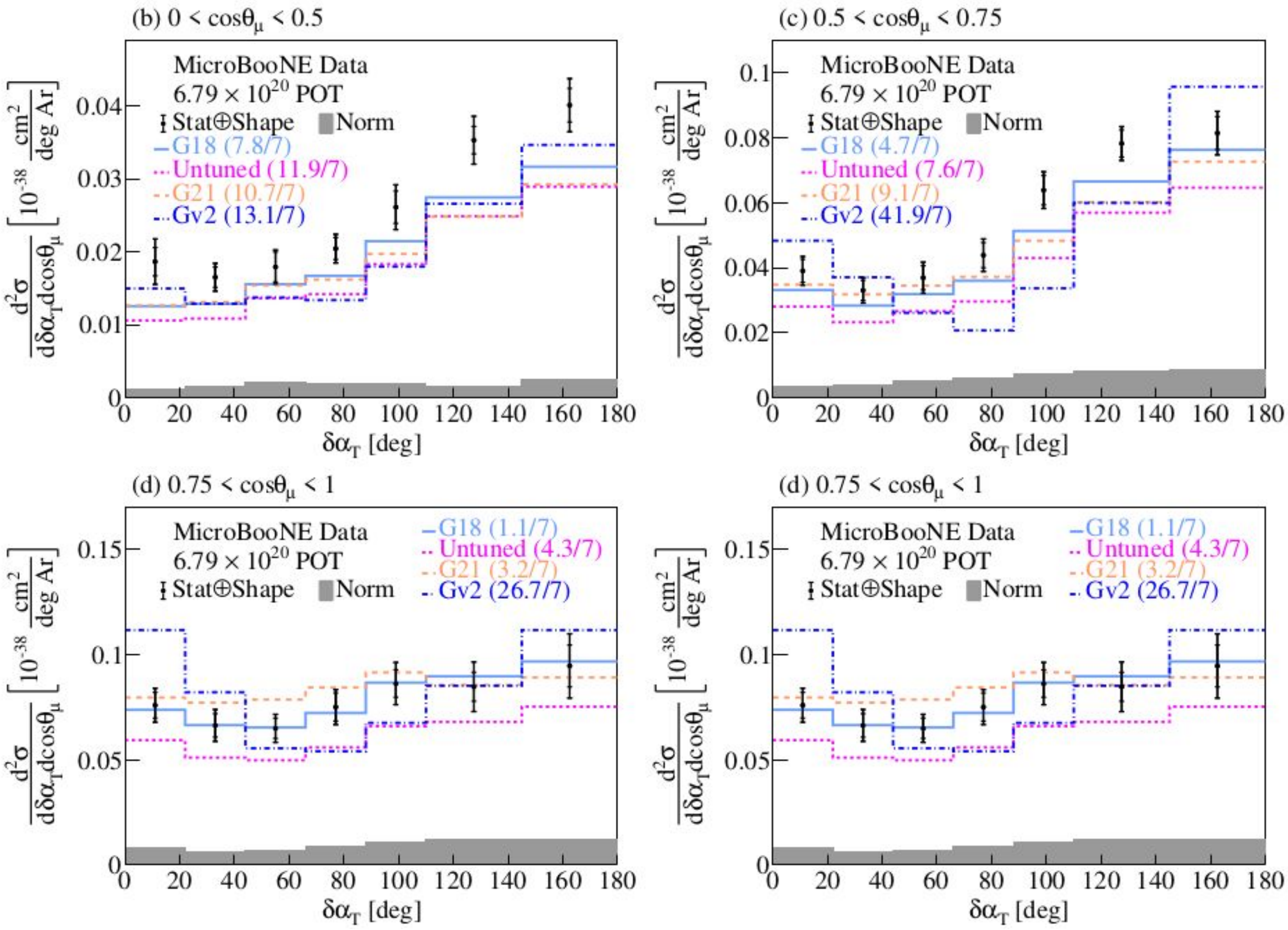

(b) 0 < cosθμ < 0.5
MicroBooNE Data
6.79 × 10^20 POT
Stat⊕Shape
Norm
G18 (7.8/7)
Untuned (11.9/7)
G21 (10.7/7)
Gv2 (13.1/7)
(c) 0.5 < cosθμ < 0.75
MicroBooNE Data
6.79 × 10^20 POT
Stat⊕Shape
Norm
G18 (4.7/7)
Untuned (7.6/7)
G21 (9.1/7)
Gv2 (41.9/7)
(d) 0.75 < cosθμ < 1
MicroBooNE Data
6.79 × 10^20 POT
Stat⊕Shape
Norm
G18 (1.1/7)
Untuned (4.3/7)
G21 (3.2/7)
Gv2 (26.7/7)
(d) 0.75 < cosθμ < 1
MicroBooNE Data
6.79 × 10^20 POT
Stat⊕Shape
Norm
G18 (1.1/7)
Untuned (4.3/7)
G21 (3.2/7)
Gv2 (26.7/7)
d²σ/dδαT dcosθμ [10^-38 cm²/deg Ar]
δαT [deg]

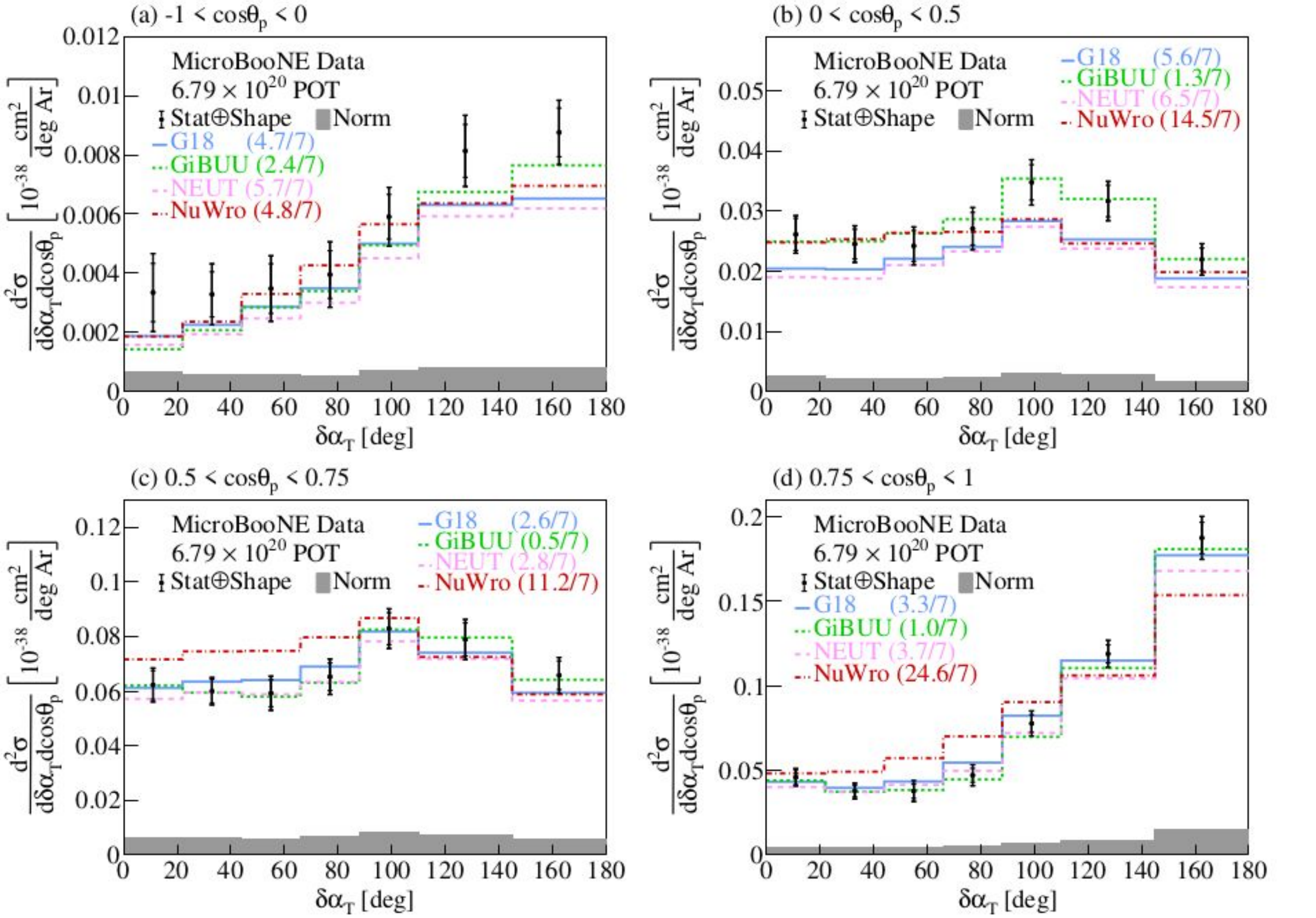

(a) -1 < cosθp < 0
(b) 0 < cosθp < 0.5
(c) 0.5 < cosθp < 0.75
(d) 0.75 < cosθp < 1
MicroBooNE Data
6.79 × 10^20 POT
Stat⊕Shape
Norm
G18 (4.7/7)
GiBUU (2.4/7)
NEUT (5.7/7)
NuWro (4.8/7)
G18 (5.6/7)
GiBUU (1.3/7)
NEUT (6.5/7)
NuWro (14.5/7)
G18 (2.6/7)
GiBUU (0.5/7)
NEUT (2.8/7)
NuWro (11.2/7)
G18 (3.3/7)
GiBUU (1.0/7)
NEUT (3.7/7)
NuWro (24.6/7)
d²σ / dδαT dcosθp [10^-38 cm² / deg Ar]
δαT [deg]

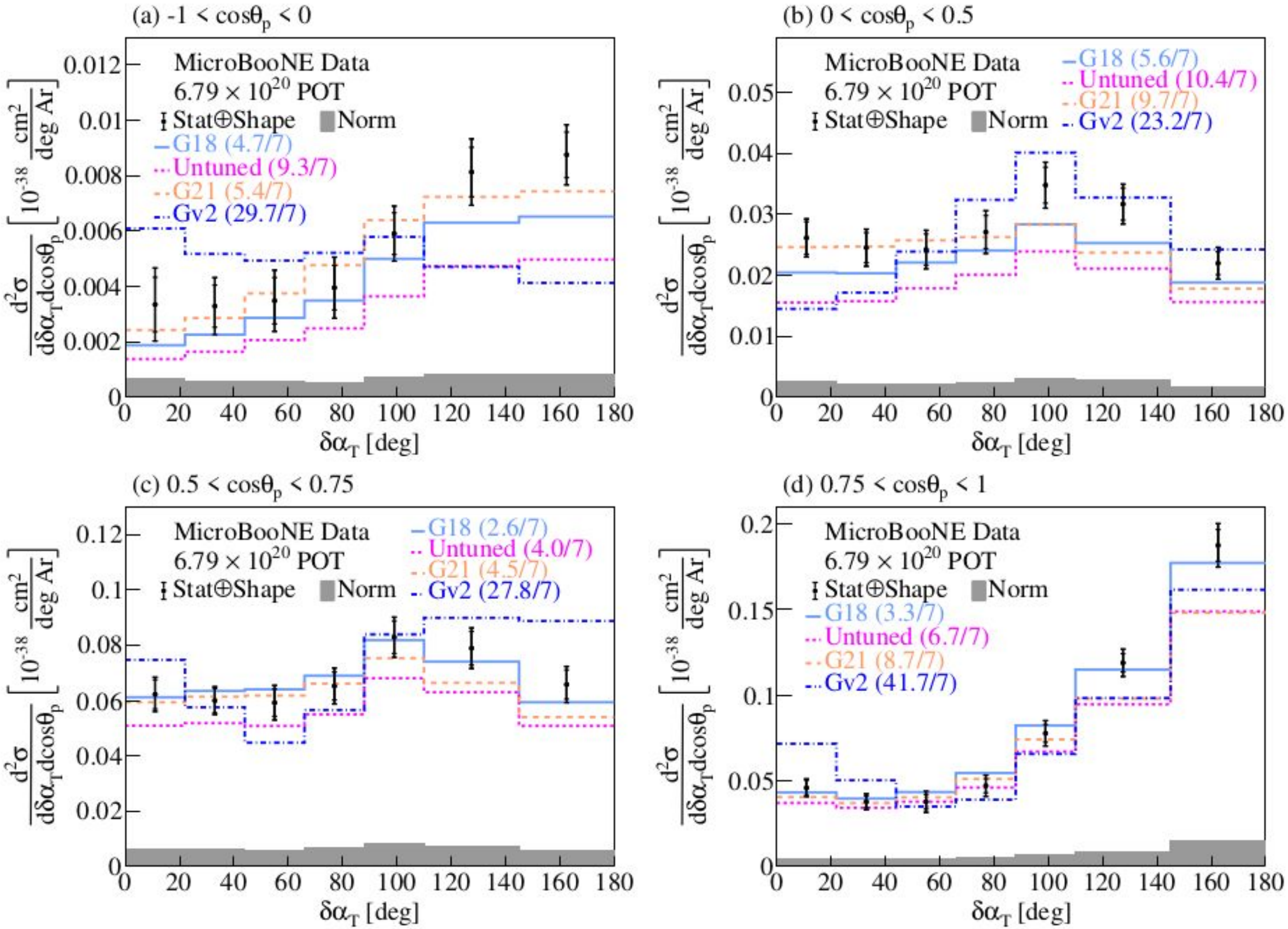
(a) -1 < cosθp < 0
(b) 0 < cosθp < 0.5
(c) 0.5 < cosθp < 0.75
(d) 0.75 < cosθp < 1
MicroBooNE Data
6.79 × 10^20 POT
Stat⊕Shape
Norm
G18 (4.7/7)
Untuned (9.3/7)
G21 (5.4/7)
Gv2 (29.7/7)
G18 (5.6/7)
Untuned (10.4/7)
G21 (9.7/7)
Gv2 (23.2/7)
G18 (2.6/7)
Untuned (4.0/7)
G21 (4.5/7)
Gv2 (27.8/7)
G18 (3.3/7)
Untuned (6.7/7)
G21 (8.7/7)
Gv2 (41.7/7)
d²σ/dδαT dcosθp [10^-38 cm²/deg Ar]
δαT [deg]

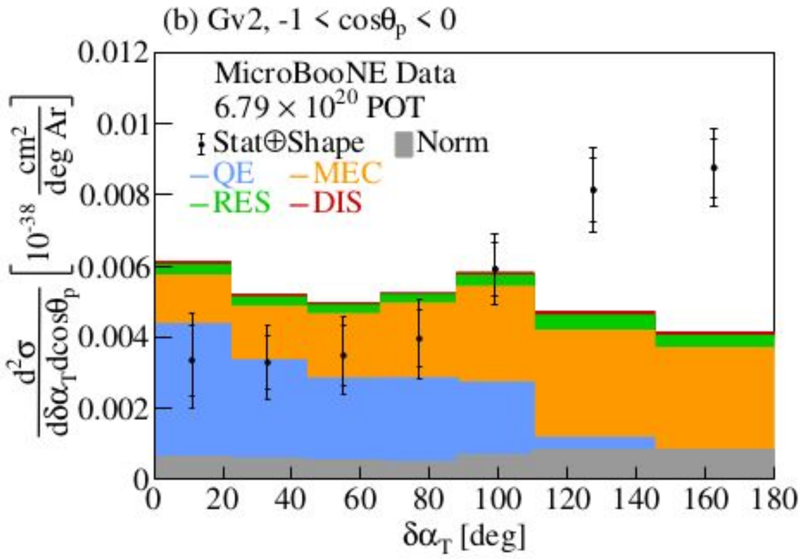

(b) Gv2, -1 < cosθp < 0
MicroBooNE Data
6.79 × 10^20 POT
Stat⊕Shape
Norm
QE
MEC
RES
DIS
0.012
0.01
0.008
0.006
0.004
0.002
0
0 20 40 60 80 100 120 140 160 180
δαT [deg]
d²σ/dδαTdcosθp [10⁻³⁸ cm²/deg Ar]

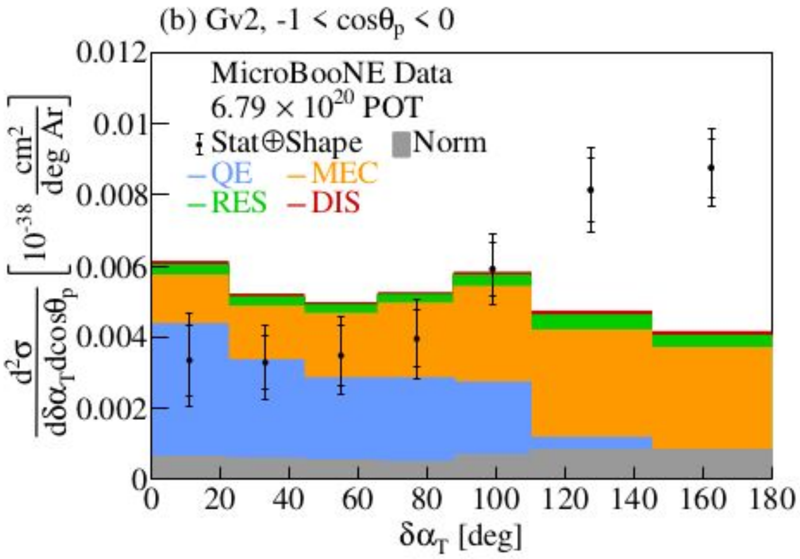

(b) Gv2, -1 < cosθp < 0
MicroBooNE Data
6.79 × 10^20 POT
Stat⊕Shape
Norm
QE
MEC
RES
DIS
0.012
0.01
0.008
0.006
0.004
0.002
0
0 20 40 60 80 100 120 140 160 180
δαT [deg]
d²σ/dδαTdcosθp [10⁻³⁸ cm²/deg Ar]

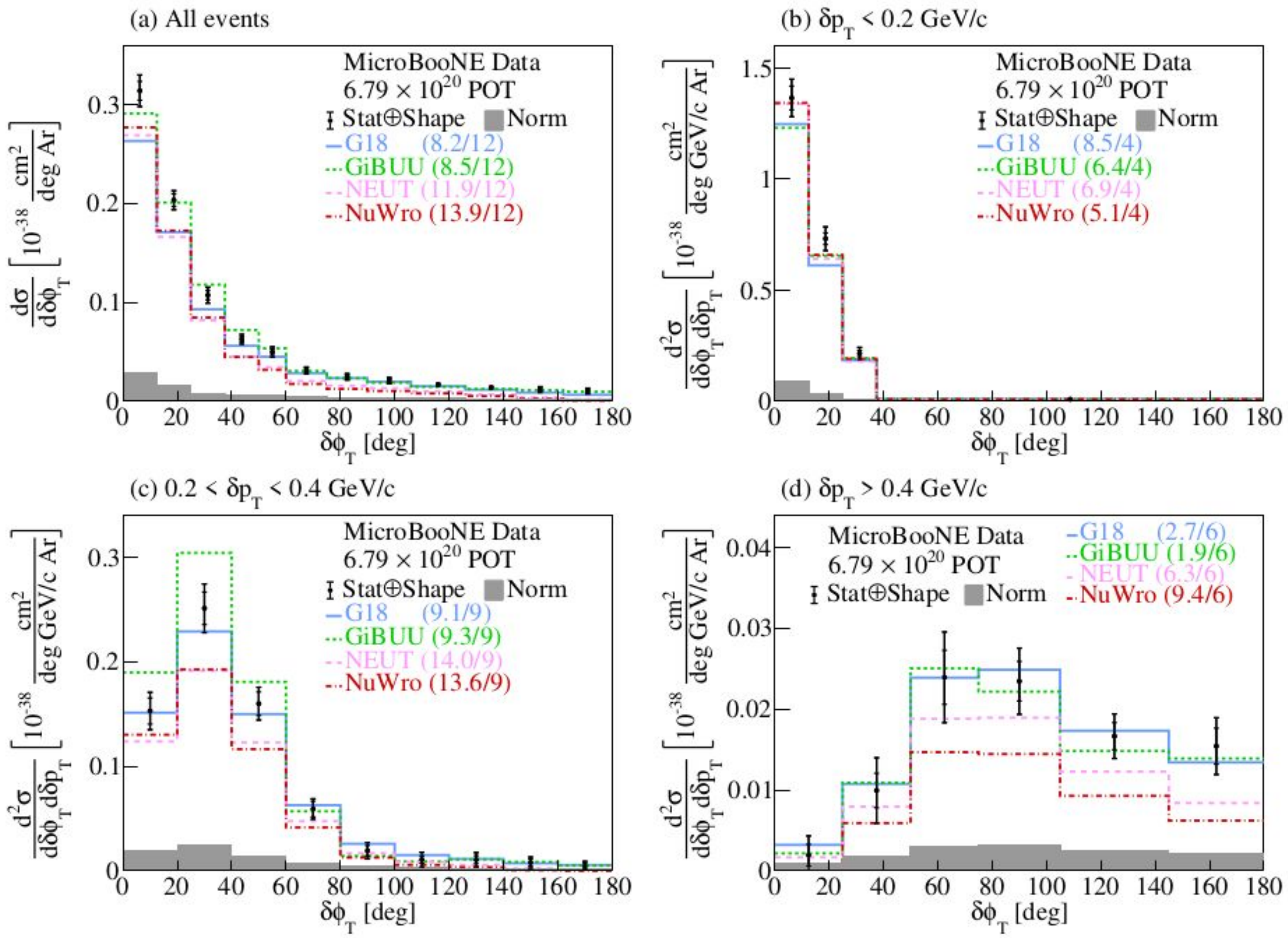
(a) All events
MicroBooNE Data
6.79 × 10^20 POT
Stat⊕Shape Norm
G18 (8.2/12)
GiBUU (8.5/12)
NEUT (11.9/12)
NuWro (13.9/12)
dσ/dδφ_T [10^-38 cm²/deg Ar]
δφ_T [deg]
(b) δp_T < 0.2 GeV/c
MicroBooNE Data
6.79 × 10^20 POT
Stat⊕Shape Norm
G18 (8.5/4)
GiBUU (6.4/4)
NEUT (6.9/4)
NuWro (5.1/4)
d²σ/dδφ_T dδp_T [10^-38 cm²/deg GeV/c Ar]
δφ_T [deg]
(c) 0.2 < δp_T < 0.4 GeV/c
MicroBooNE Data
6.79 × 10^20 POT
Stat⊕Shape Norm
G18 (9.1/9)
GiBUU (9.3/9)
NEUT (14.0/9)
NuWro (13.6/9)
d²σ/dδφ_T dδp_T [10^-38 cm²/deg GeV/c Ar]
δφ_T [deg]
(d) δp_T > 0.4 GeV/c
MicroBooNE Data
6.79 × 10^20 POT
Stat⊕Shape Norm
G18 (2.7/6)
GiBUU (1.9/6)
NEUT (6.3/6)
NuWro (9.4/6)
d²σ/dδφ_T dδp_T [10^-38 cm²/deg GeV/c Ar]
δφ_T [deg]

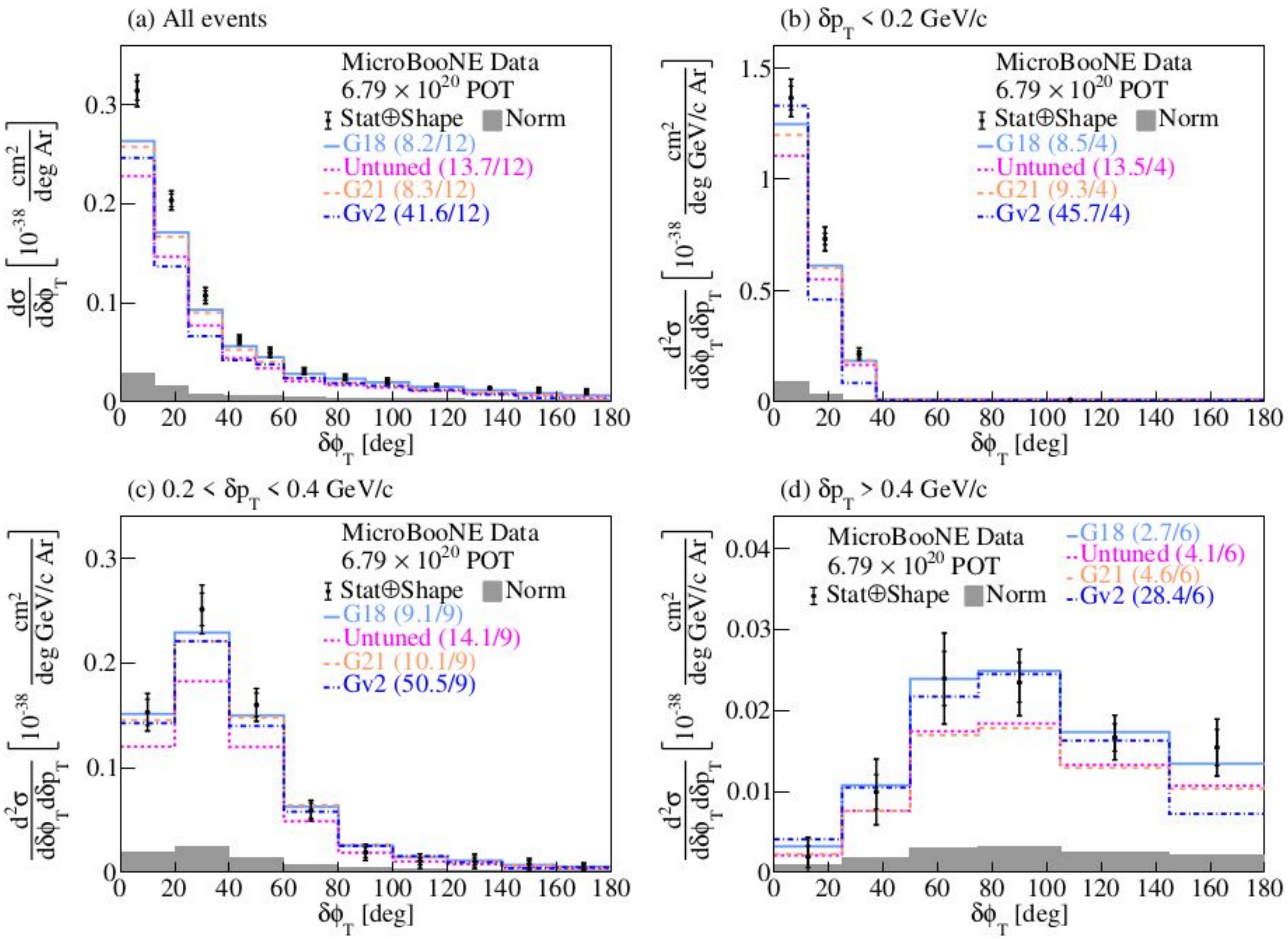

(a) All events
MicroBooNE Data
6.79 × 10^20 POT
Stat⊕Shape
Norm
G18 (8.2/12)
Untuned (13.7/12)
G21 (8.3/12)
Gv2 (41.6/12)
dσ/dδφ_T [10^-38 cm²/deg Ar]
δφ_T [deg]
(b) δp_T < 0.2 GeV/c
MicroBooNE Data
6.79 × 10^20 POT
Stat⊕Shape
Norm
G18 (8.5/4)
Untuned (13.5/4)
G21 (9.3/4)
Gv2 (45.7/4)
d²σ/dδφ_T dδp_T [10^-38 cm²/deg GeV/c Ar]
δφ_T [deg]
(c) 0.2 < δp_T < 0.4 GeV/c
MicroBooNE Data
6.79 × 10^20 POT
Stat⊕Shape
Norm
G18 (9.1/9)
Untuned (14.1/9)
G21 (10.1/9)
Gv2 (50.5/9)
d²σ/dδφ_T dδp_T [10^-38 cm²/deg GeV/c Ar]
δφ_T [deg]
(d) δp_T > 0.4 GeV/c
MicroBooNE Data
6.79 × 10^20 POT
Stat⊕Shape
Norm
G18 (2.7/6)
Untuned (4.1/6)
G21 (4.6/6)
Gv2 (28.4/6)
d²σ/dδφ_T dδp_T [10^-38 cm²/deg GeV/c Ar]
δφ_T [deg]

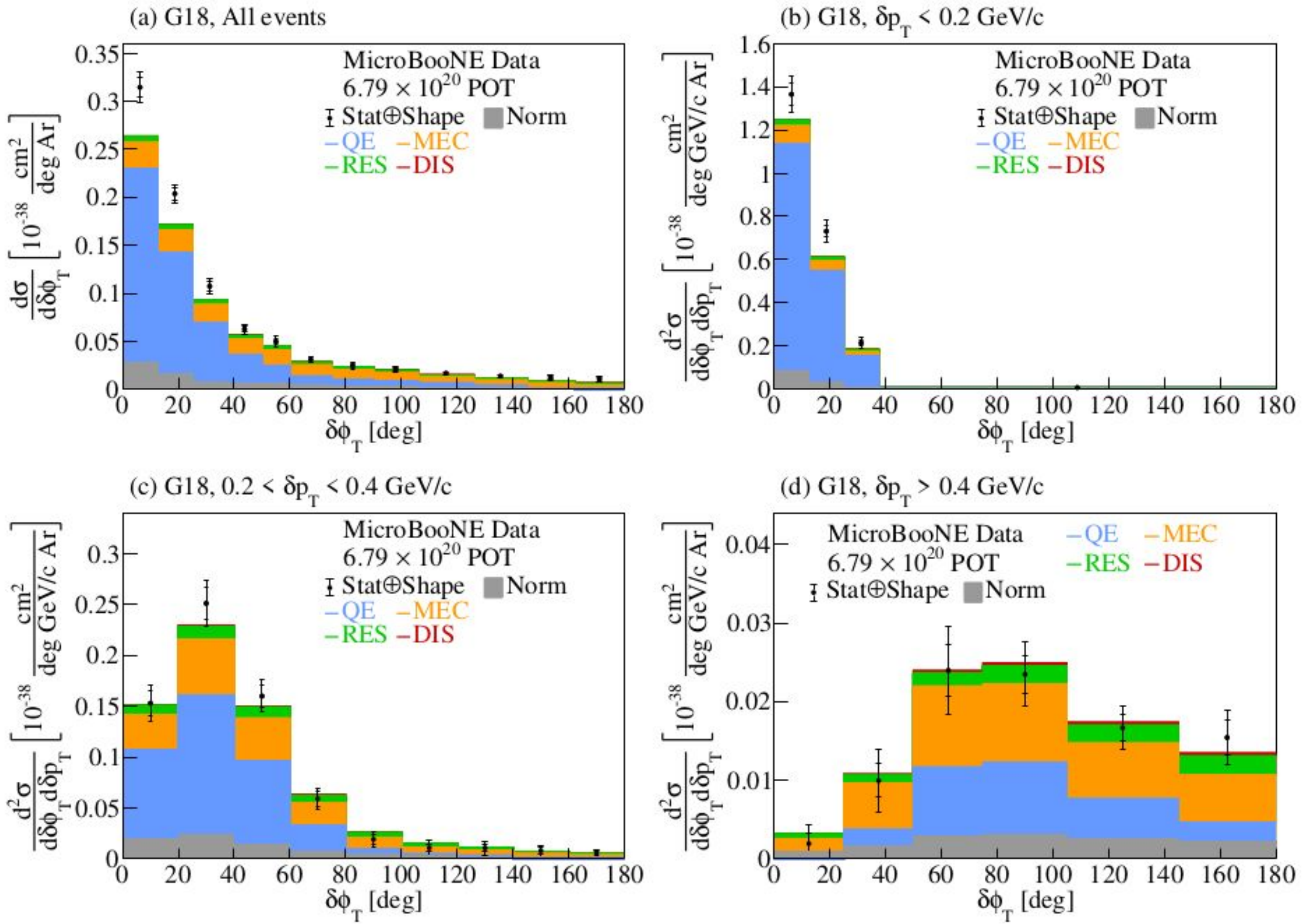

(a) G18, All events
MicroBooNE Data
6.79 × 10^20 POT
Stat⊕Shape
Norm
QE
MEC
RES
DIS
δφ_T [deg]
dσ/dδφ_T [10^-38 cm^2/deg Ar]
(b) G18, δp_T < 0.2 GeV/c
d^2σ/dδφ_T dδp_T [10^-38 cm^2/deg GeV/c Ar]
(c) G18, 0.2 < δp_T < 0.4 GeV/c
(d) G18, δp_T > 0.4 GeV/c

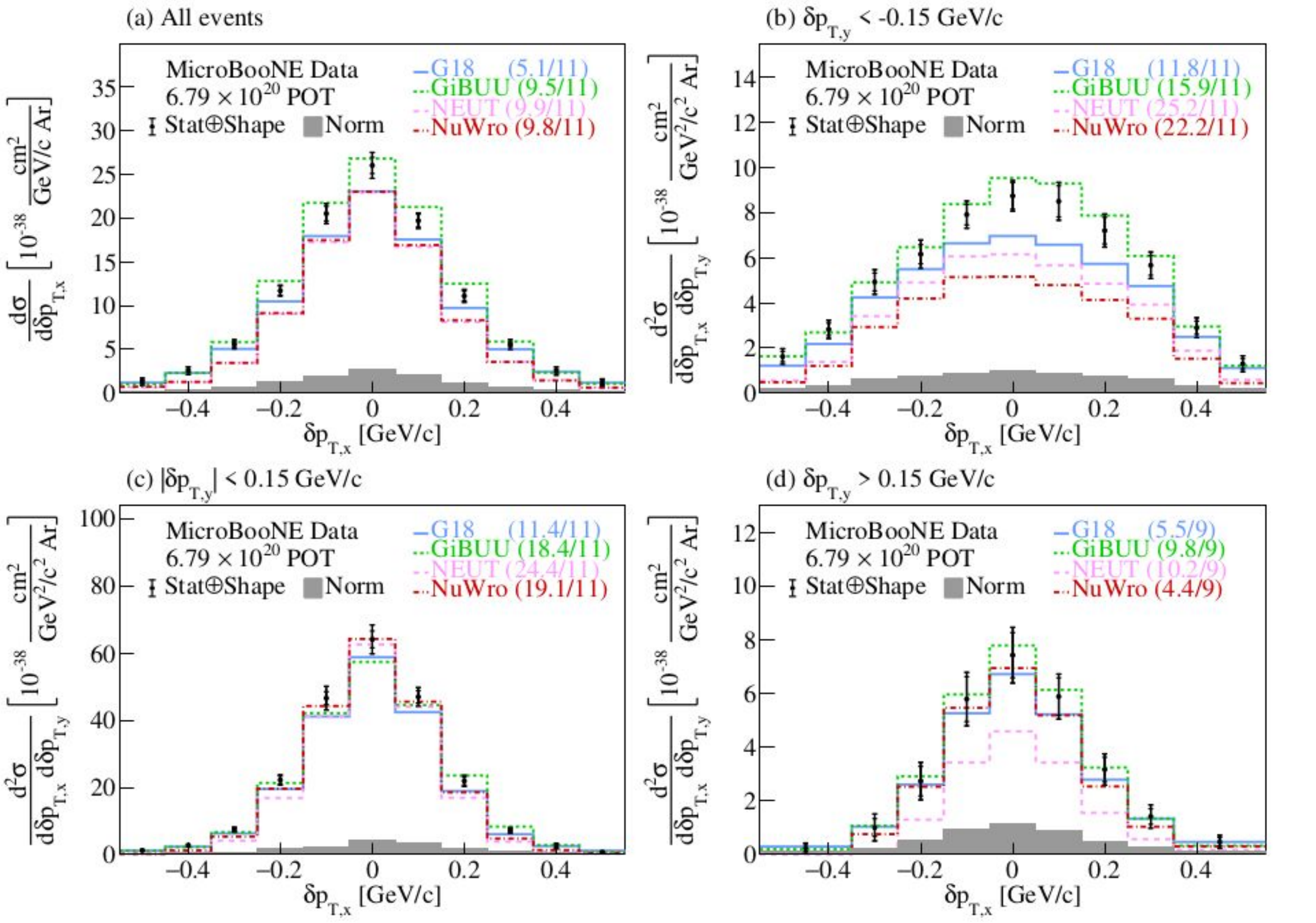
(a) All events
MicroBooNE Data
6.79 × 10^20 POT
Stat⊕Shape
Norm
G18 (5.1/11)
GiBUU (9.5/11)
NEUT (9.9/11)
NuWro (9.8/11)
(b) δp_T,y < -0.15 GeV/c
G18 (11.8/11)
GiBUU (15.9/11)
NEUT (25.2/11)
NuWro (22.2/11)
(c) |δp_T,y| < 0.15 GeV/c
G18 (11.4/11)
GiBUU (18.4/11)
NEUT (24.4/11)
NuWro (19.1/11)
(d) δp_T,y > 0.15 GeV/c
G18 (5.5/9)
GiBUU (9.8/9)
NEUT (10.2/9)
NuWro (4.4/9)
δp_T,x [GeV/c]
dσ/dδp_T,x [10^-38 cm^2/(GeV/c Ar)]
d^2σ/(dδp_T,x dδp_T,y) [10^-38 cm^2/(GeV^2/c^2 Ar)]

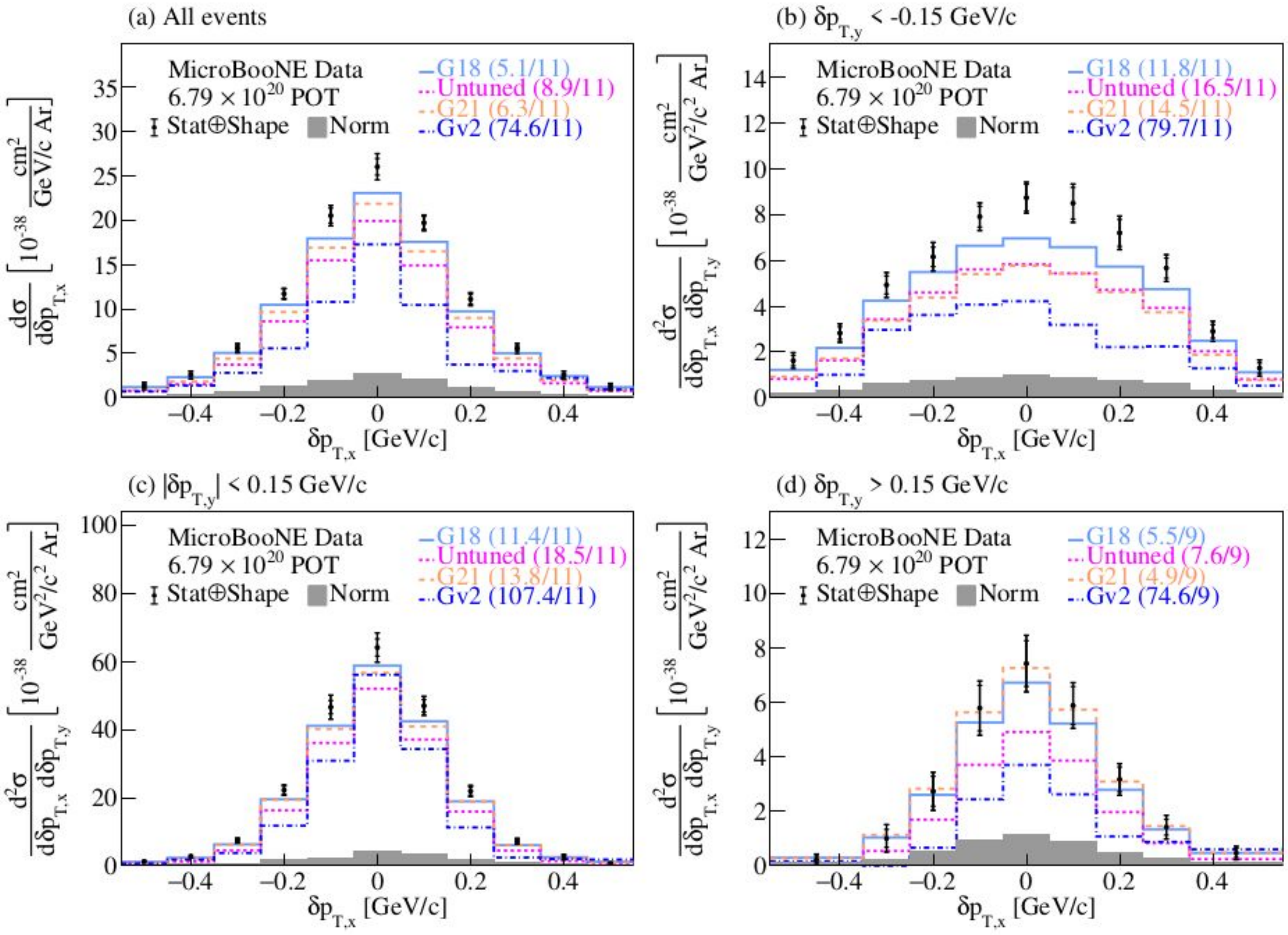
(a) All events
MicroBooNE Data
6.79 × 10^20 POT
Stat⊕Shape
Norm
G18 (5.1/11)
Untuned (8.9/11)
G21 (6.3/11)
Gv2 (74.6/11)
(b) δp_T,y < -0.15 GeV/c
G18 (11.8/11)
Untuned (16.5/11)
G21 (14.5/11)
Gv2 (79.7/11)
(c) |δp_T,y| < 0.15 GeV/c
G18 (11.4/11)
Untuned (18.5/11)
G21 (13.8/11)
Gv2 (107.4/11)
(d) δp_T,y > 0.15 GeV/c
G18 (5.5/9)
Untuned (7.6/9)
G21 (4.9/9)
Gv2 (74.6/9)
δp_T,x [GeV/c]
dσ/dδp_T,x [10^-38 cm²/GeV/c Ar]
d²σ/dδp_T,x dδp_T,y [10^-38 cm²/GeV²/c² Ar]

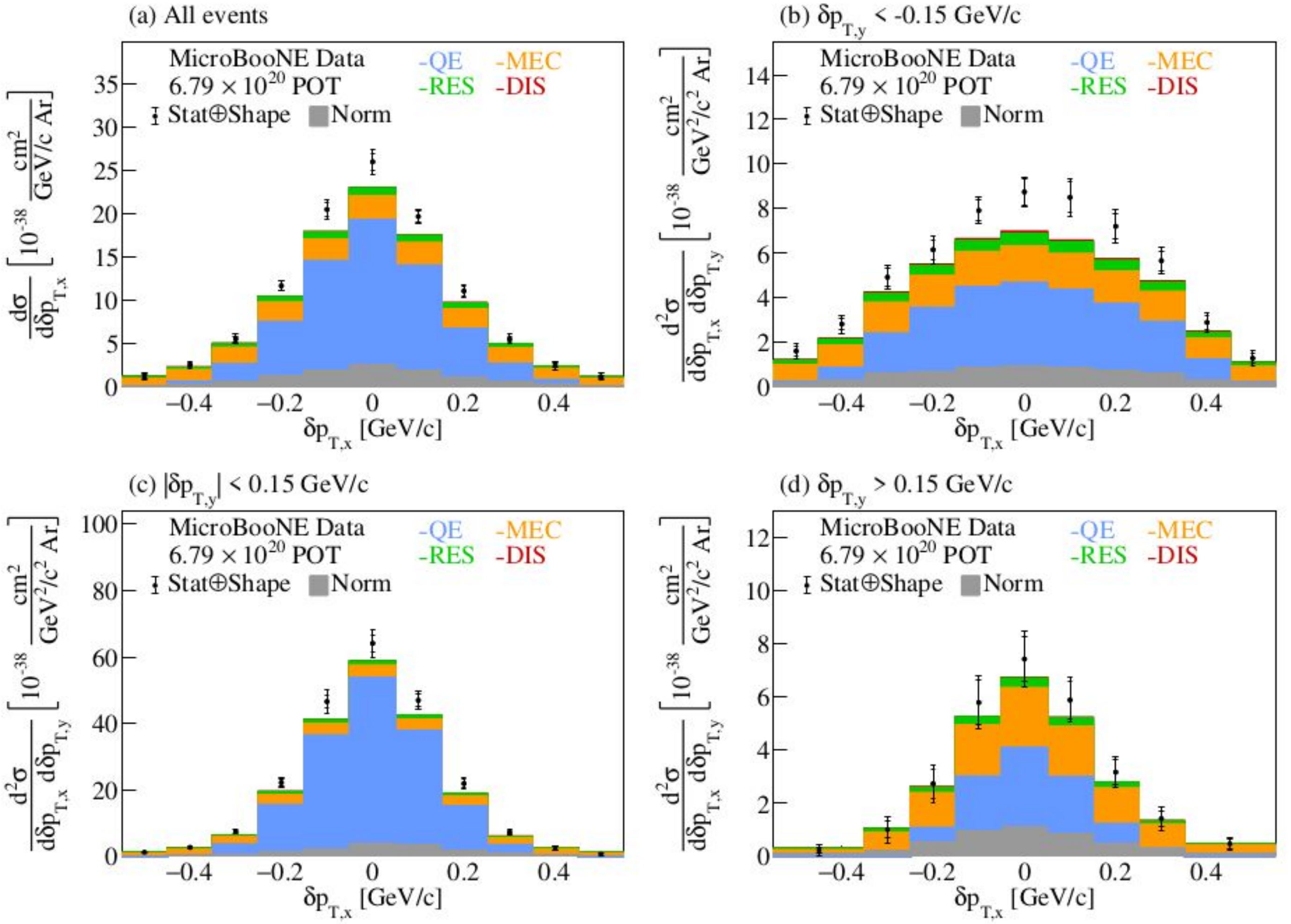

(a) All events
(b) $\delta p_{T,y}$ < -0.15 GeV/c
(c) $|\delta p_{T,y}|$ < 0.15 GeV/c
(d) $\delta p_{T,y}$ > 0.15 GeV/c
MicroBooNE Data
6.79×10^{20} POT
Stat⊕Shape
Norm
-QE
-MEC
-RES
-DIS
$\frac{d\sigma}{d\delta p_{T,x}}$ $\left[10^{-38} \frac{cm^2}{GeV/c\ Ar}\right]$
$\frac{d^2\sigma}{d\delta p_{T,x}\, d\delta p_{T,y}}$ $\left[10^{-38} \frac{cm^2}{GeV^2/c^2\ Ar}\right]$
$\delta p_{T,x}$ [GeV/c]

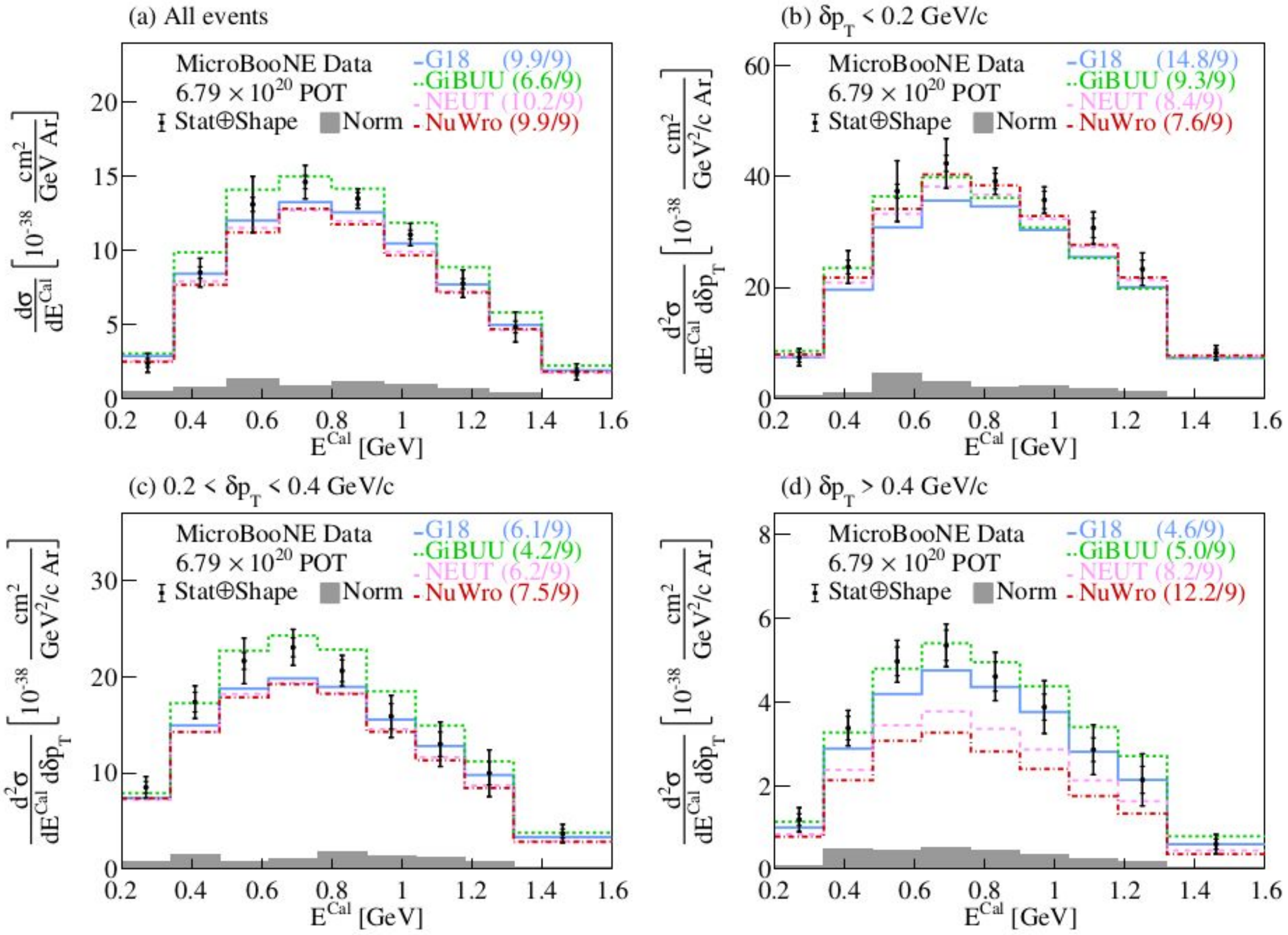

(a) All events
(b) δp_T < 0.2 GeV/c
(c) 0.2 < δp_T < 0.4 GeV/c
(d) δp_T > 0.4 GeV/c
MicroBooNE Data
6.79 × 10^20 POT
Stat⊕Shape
Norm
G18 (9.9/9)
GiBUU (6.6/9)
NEUT (10.2/9)
NuWro (9.9/9)
G18 (14.8/9)
GiBUU (9.3/9)
NEUT (8.4/9)
NuWro (7.6/9)
G18 (6.1/9)
GiBUU (4.2/9)
NEUT (6.2/9)
NuWro (7.5/9)
G18 (4.6/9)
GiBUU (5.0/9)
NEUT (8.2/9)
NuWro (12.2/9)
dσ/dE^Cal [10^-38 cm²/GeV Ar]
d²σ/dE^Cal dδp_T [10^-38 cm²/GeV²/c Ar]
E^Cal [GeV]

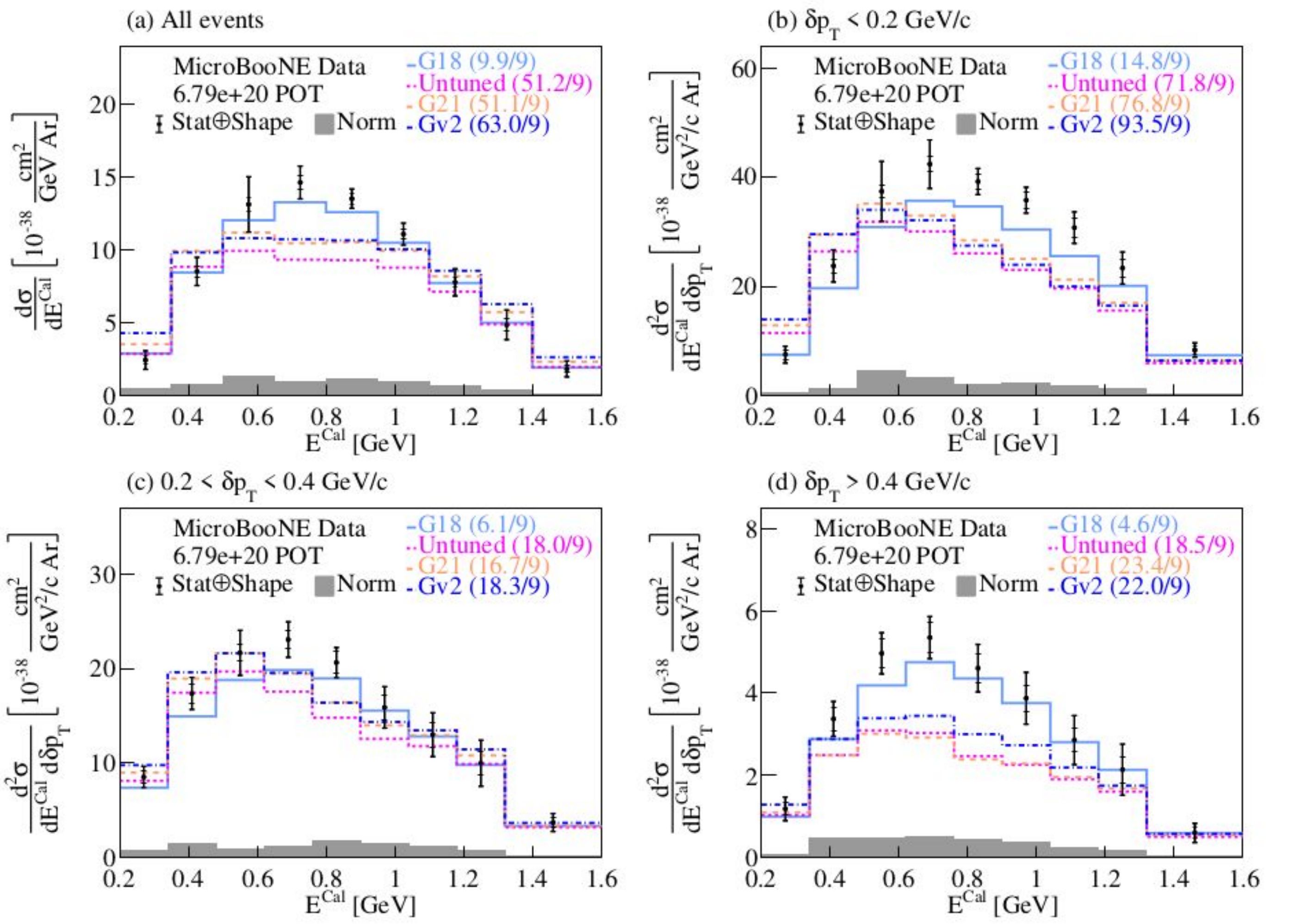

(a) All events
MicroBooNE Data
6.79e+20 POT
Stat⊕Shape
Norm
G18 (9.9/9)
Untuned (51.2/9)
G21 (51.1/9)
Gv2 (63.0/9)
$\frac{d\sigma}{dE^{Cal}} \left[10^{-38} \frac{cm^2}{GeV\ Ar}\right]$
E^{Cal} [GeV]
(b) δp_T < 0.2 GeV/c
MicroBooNE Data
6.79e+20 POT
Stat⊕Shape
Norm
G18 (14.8/9)
Untuned (71.8/9)
G21 (76.8/9)
Gv2 (93.5/9)
$\frac{d^2\sigma}{dE^{Cal} d\delta p_T} \left[10^{-38} \frac{cm^2}{GeV^2/c\ Ar}\right]$
E^{Cal} [GeV]
(c) 0.2 < δp_T < 0.4 GeV/c
MicroBooNE Data
6.79e+20 POT
Stat⊕Shape
Norm
G18 (6.1/9)
Untuned (18.0/9)
G21 (16.7/9)
Gv2 (18.3/9)
$\frac{d^2\sigma}{dE^{Cal} d\delta p_T} \left[10^{-38} \frac{cm^2}{GeV^2/c\ Ar}\right]$
E^{Cal} [GeV]
(d) δp_T > 0.4 GeV/c
MicroBooNE Data
6.79e+20 POT
Stat⊕Shape
Norm
G18 (4.6/9)
Untuned (18.5/9)
G21 (23.4/9)
Gv2 (22.0/9)
$\frac{d^2\sigma}{dE^{Cal} d\delta p_T} \left[10^{-38} \frac{cm^2}{GeV^2/c\ Ar}\right]$
E^{Cal} [GeV]

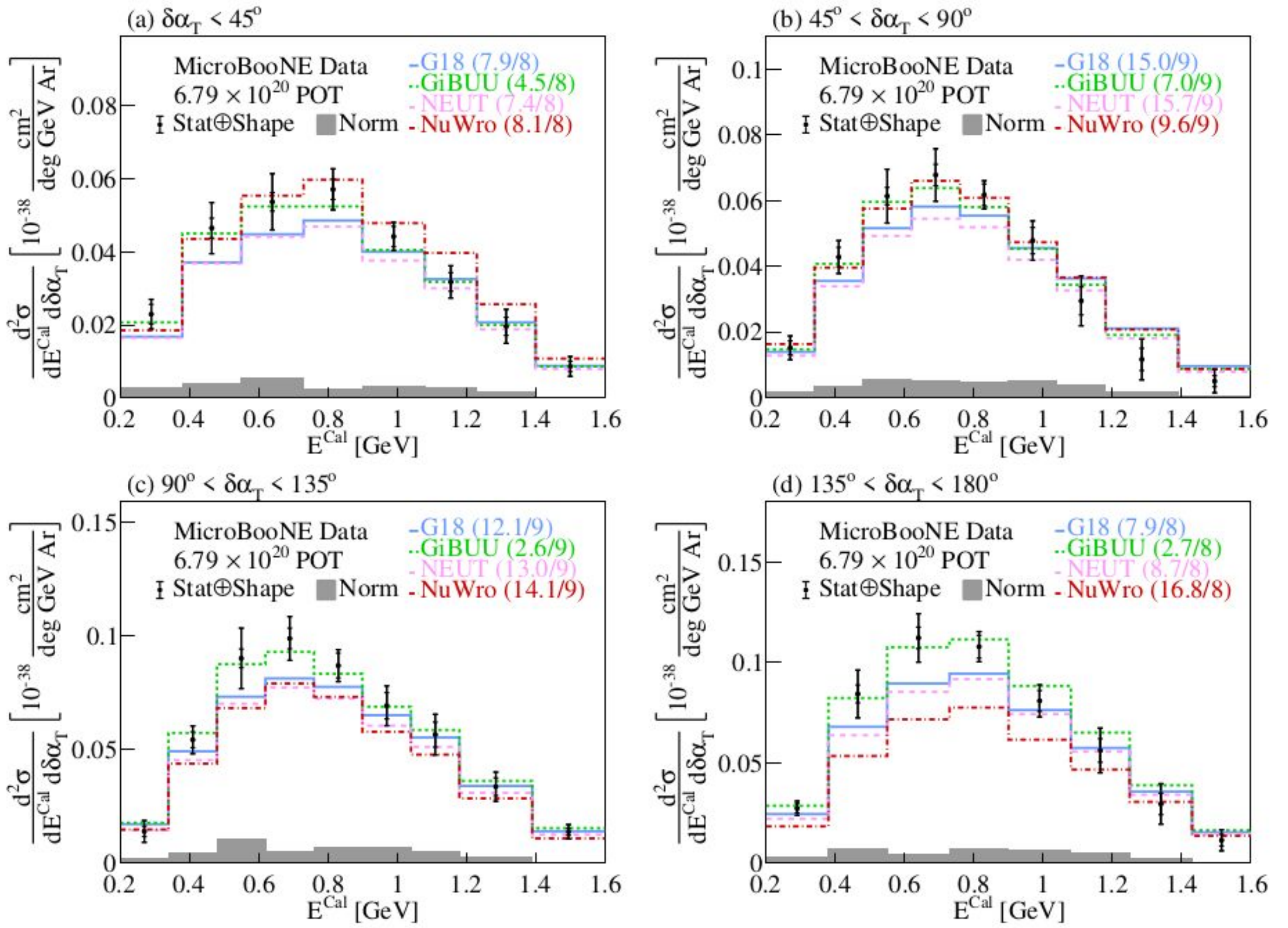

(a) δα_T < 45°
MicroBooNE Data
6.79 × 10^20 POT
Stat⊕Shape
Norm
G18 (7.9/8)
GiBUU (4.5/8)
NEUT (7.4/8)
NuWro (8.1/8)
(b) 45° < δα_T < 90°
G18 (15.0/9)
GiBUU (7.0/9)
NEUT (15.7/9)
NuWro (9.6/9)
(c) 90° < δα_T < 135°
G18 (12.1/9)
GiBUU (2.6/9)
NEUT (13.0/9)
NuWro (14.1/9)
(d) 135° < δα_T < 180°
G18 (7.9/8)
GiBUU (2.7/8)
NEUT (8.7/8)
NuWro (16.8/8)
d²σ/dE^Cal dδα_T [10^-38 cm²/deg GeV Ar]
E^Cal [GeV]

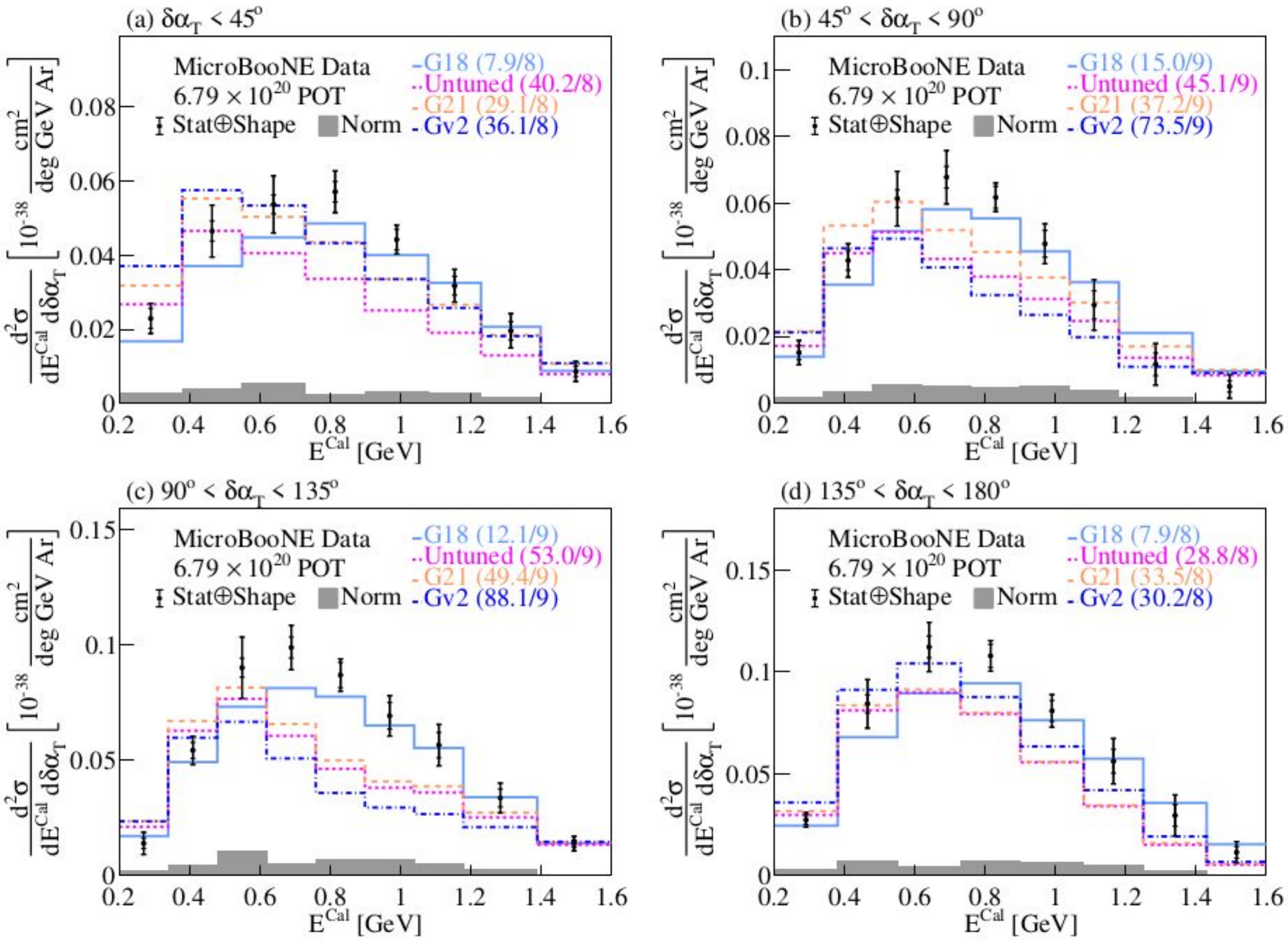

(a) δα_T < 45°
MicroBooNE Data
6.79 × 10^20 POT
Stat⊕Shape
Norm
G18 (7.9/8)
Untuned (40.2/8)
G21 (29.1/8)
Gv2 (36.1/8)
(b) 45° < δα_T < 90°
MicroBooNE Data
6.79 × 10^20 POT
Stat⊕Shape
Norm
G18 (15.0/9)
Untuned (45.1/9)
G21 (37.2/9)
Gv2 (73.5/9)
(c) 90° < δα_T < 135°
MicroBooNE Data
6.79 × 10^20 POT
Stat⊕Shape
Norm
G18 (12.1/9)
Untuned (53.0/9)
G21 (49.4/9)
Gv2 (88.1/9)
(d) 135° < δα_T < 180°
MicroBooNE Data
6.79 × 10^20 POT
Stat⊕Shape
Norm
G18 (7.9/8)
Untuned (28.8/8)
G21 (33.5/8)
Gv2 (30.2/8)
d²σ / dE^Cal dδα_T [10^-38 cm² / deg GeV Ar]
E^Cal [GeV]

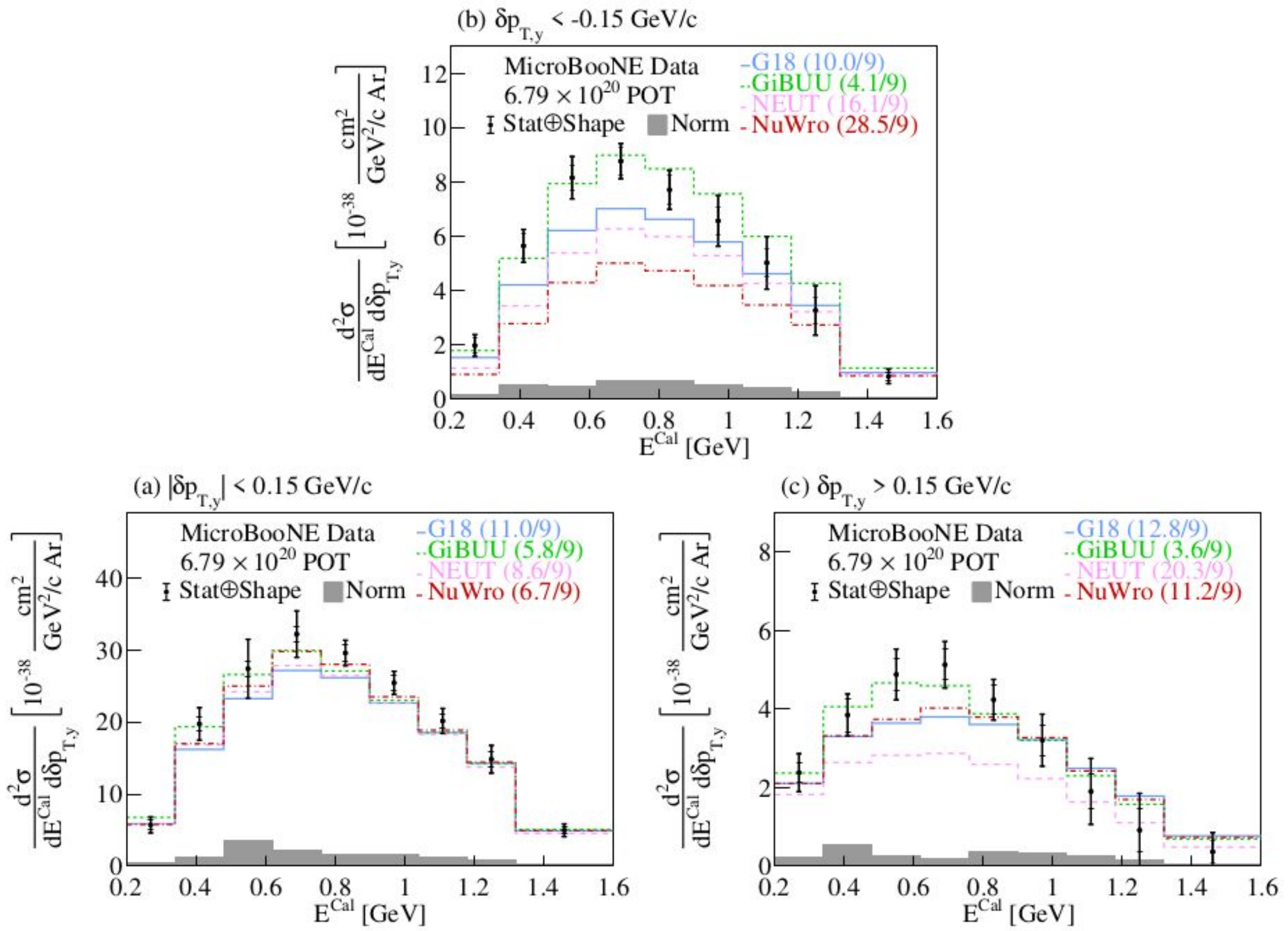
(b) $\delta p_{T,y}$ < -0.15 GeV/c
MicroBooNE Data
6.79×10^{20} POT
Stat⊕Shape
Norm
G18 (10.0/9)
GiBUU (4.1/9)
NEUT (16.1/9)
NuWro (28.5/9)
(a) $|\delta p_{T,y}|$ < 0.15 GeV/c
MicroBooNE Data
6.79×10^{20} POT
Stat⊕Shape
Norm
G18 (11.0/9)
GiBUU (5.8/9)
NEUT (8.6/9)
NuWro (6.7/9)
(c) $\delta p_{T,y}$ > 0.15 GeV/c
MicroBooNE Data
6.79×10^{20} POT
Stat⊕Shape
Norm
G18 (12.8/9)
GiBUU (3.6/9)
NEUT (20.3/9)
NuWro (11.2/9)
$\frac{d^2\sigma}{dE^{Cal}\, d\delta p_{T,y}} \left[10^{-38} \frac{cm^2}{GeV^2/c\ Ar}\right]$
E^{Cal} [GeV]

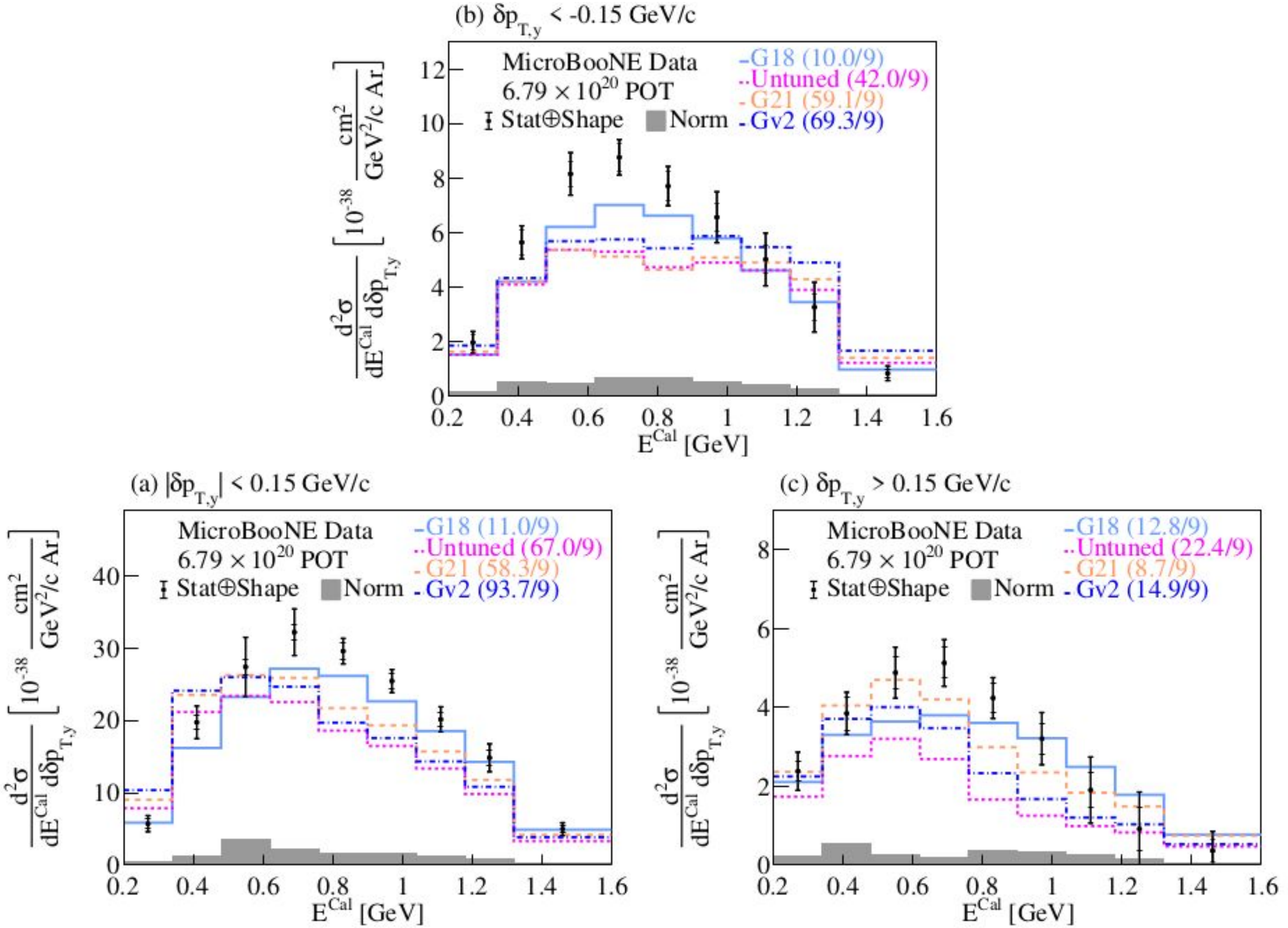

(b) $\delta p_{T,y}$ < -0.15 GeV/c
MicroBooNE Data
6.79 × 10^20 POT
Stat⊕Shape
Norm
G18 (10.0/9)
Untuned (42.0/9)
G21 (59.1/9)
Gv2 (69.3/9)
(a) $|\delta p_{T,y}|$ < 0.15 GeV/c
G18 (11.0/9)
Untuned (67.0/9)
G21 (58.3/9)
Gv2 (93.7/9)
(c) $\delta p_{T,y}$ > 0.15 GeV/c
G18 (12.8/9)
Untuned (22.4/9)
G21 (8.7/9)
Gv2 (14.9/9)
$\frac{d^2\sigma}{dE^{Cal}\, d\delta p_{T,y}}$ $\left[10^{-38} \frac{cm^2}{GeV^2/c\ Ar}\right]$
E^{Cal} [GeV]

Calorimetric Energy

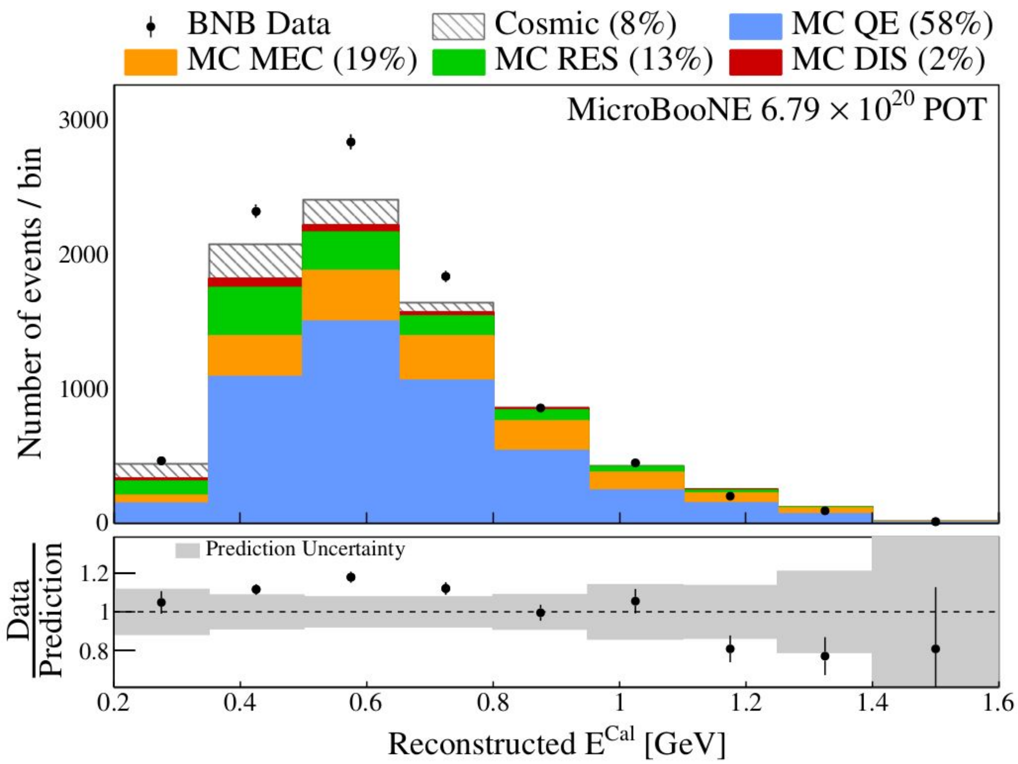

$$E^{Cal} = E_\mu + T_p + BE$$

- E_μ = muon energy
- T_p = proton kinetic energy
- BE = 40 MeV binding energy
- Peak at ~0.7 GeV

arXiv:2301.03700

Calorimetric Energy Cross Section

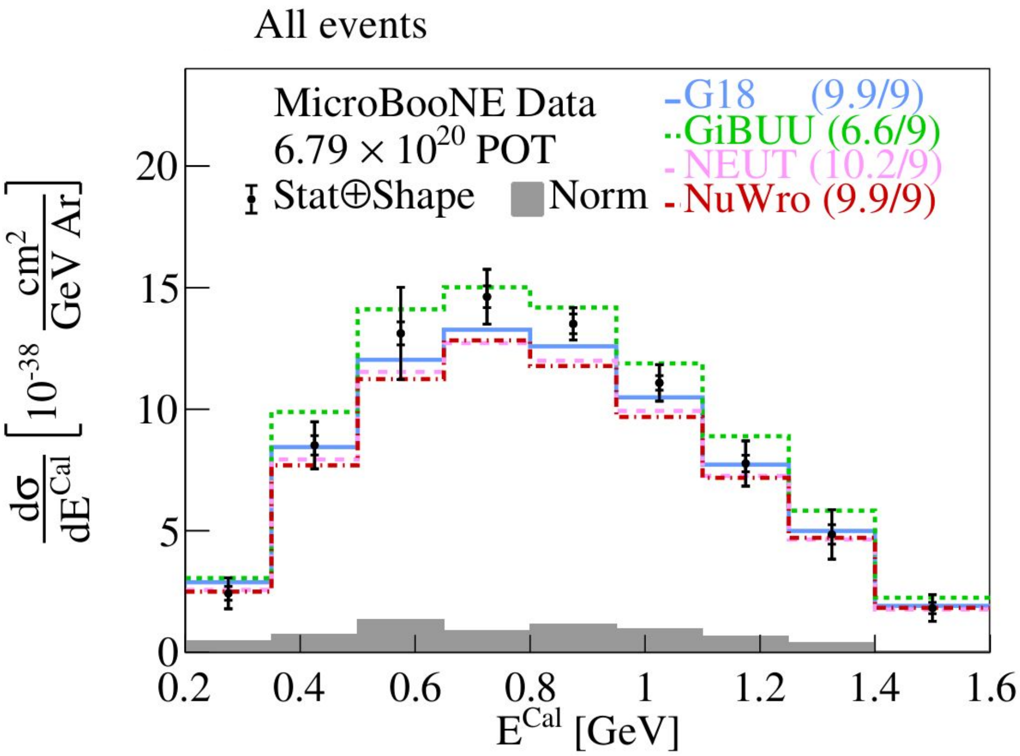

$$E^{Cal} = E_\mu + T_p + BE$$

- E_μ = muon energy
- T_p = proton kinetic energy
- BE = 40 MeV binding energy
- All generators yield good agreement

arXiv:2301.03700

NEUT = NEUT v5.4.0, NuWro = NuWro 19.02.2

High Statistics→Into the Multiverse!

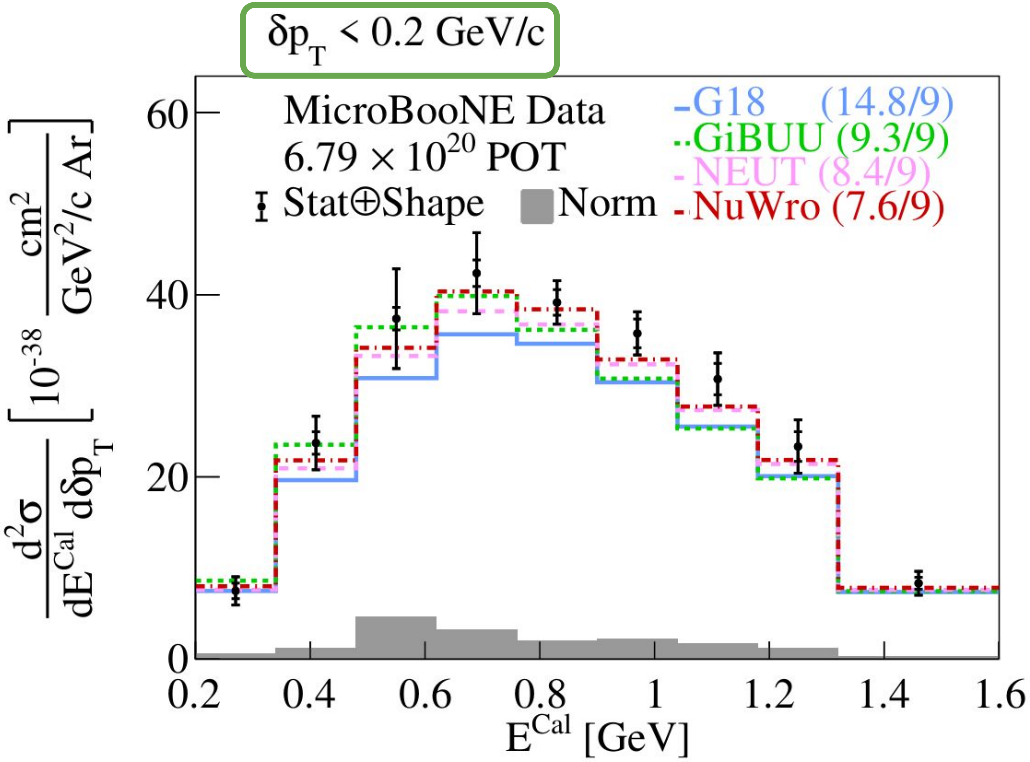

- QE dominated region
- All generators yield good agreement

NEUT = NEUT v5.4.0, NuWro = NuWro 19.02.2

arXiv:2301.03700

High Statistics→Into the Multiverse!

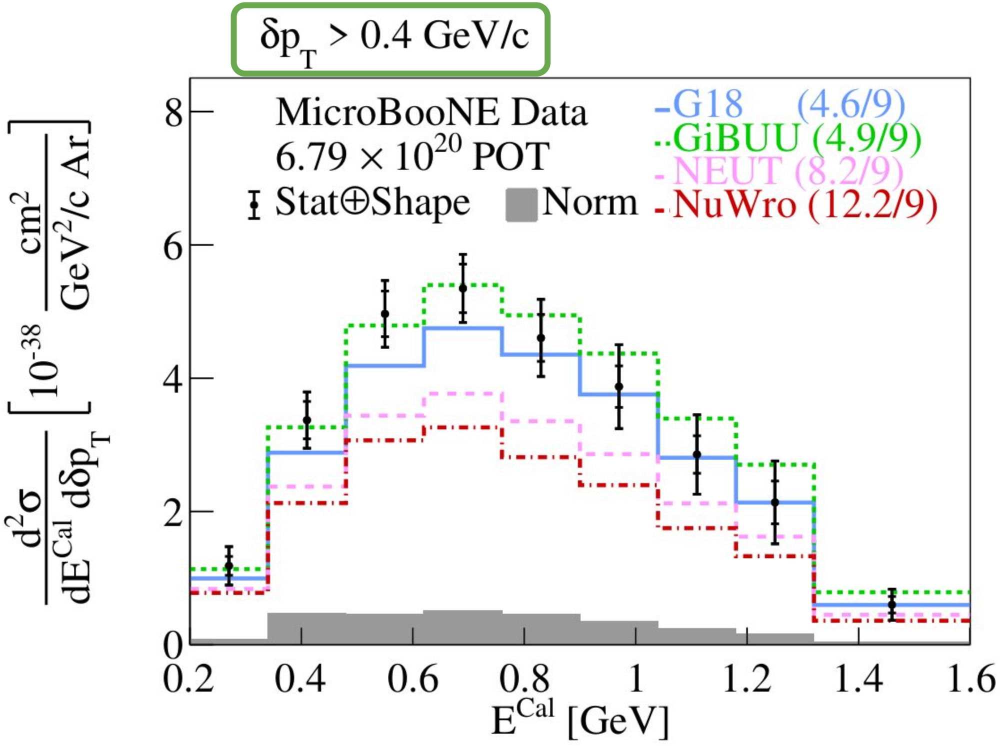

- MEC/RES dominated region
- Similar shapes
- Normalization differences
- Still reasonable χ^2!

arXiv:2301.03700

NEUT = NEUT v5.4.0, NuWro = NuWro 19.02.2

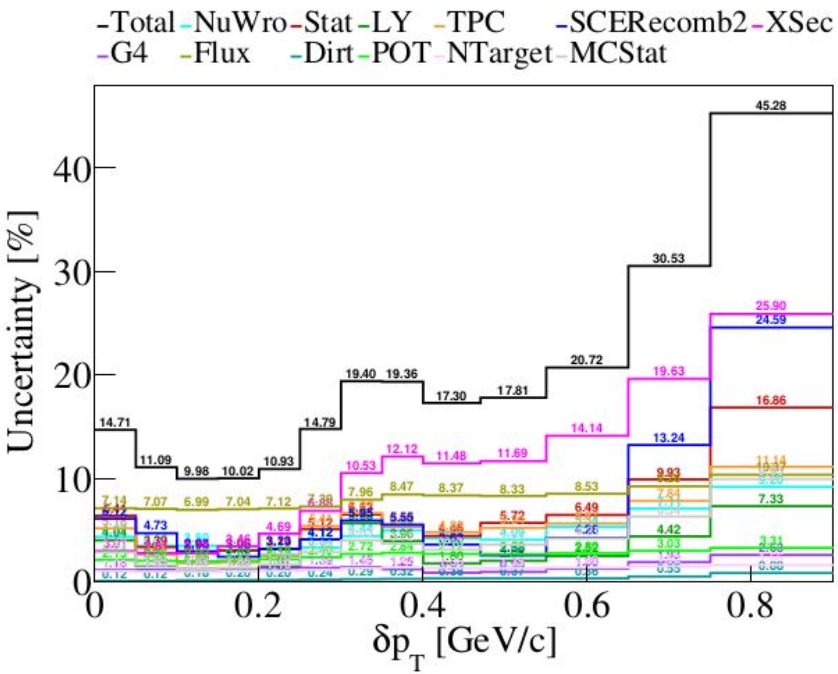

-Total -NuWro -Stat -LY -TPC -SCERecomb2 -XSec
-G4 -Flux -Dirt -POT -NTarget -MCStat
Uncertainty [%]
δp_T [GeV/c]

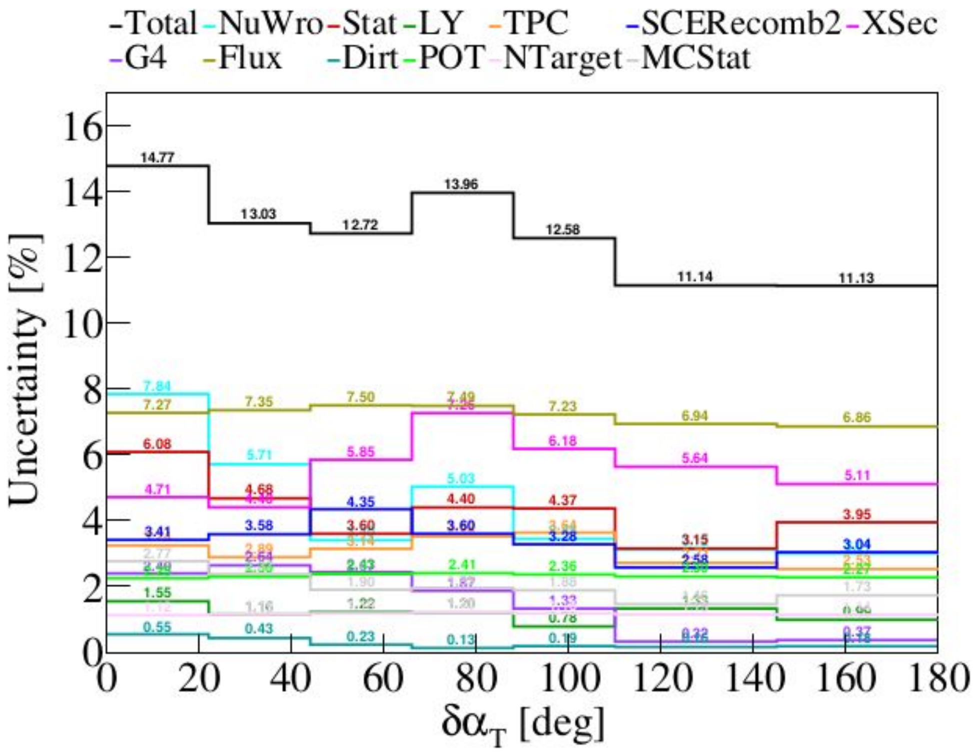

-Total -NuWro -Stat -LY -TPC -SCERecomb2 -XSec
-G4 -Flux -Dirt -POT -NTarget -MCStat
Uncertainty [%]
$\delta\alpha_T$ [deg]

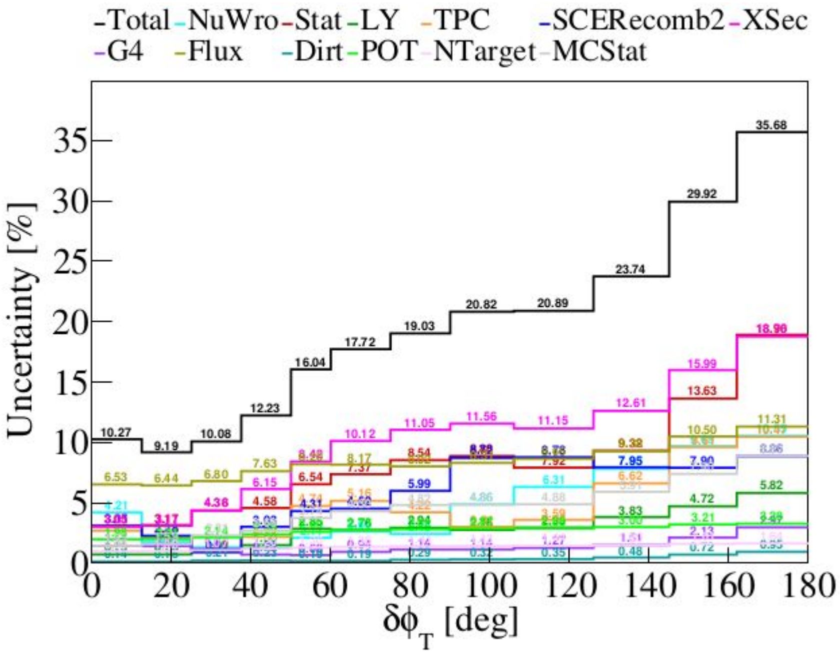
Total
NuWro
Stat
LY
TPC
SCERecomb2
XSec
G4
Flux
Dirt
POT
NTarget
MCStat
Uncertainty [%]
$\delta\phi_T$ [deg]

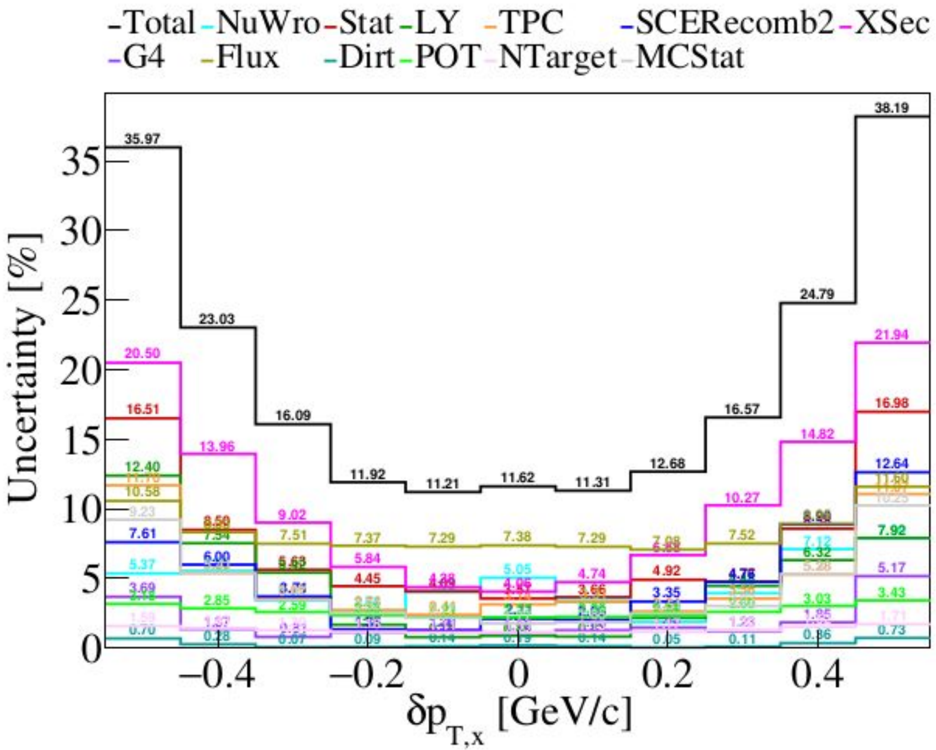
Total
NuWro
Stat
LY
TPC
SCERecomb2
XSec
G4
Flux
Dirt
POT
NTarget
MCStat
Uncertainty [%]
$\delta p_{T,x}$ [GeV/c]

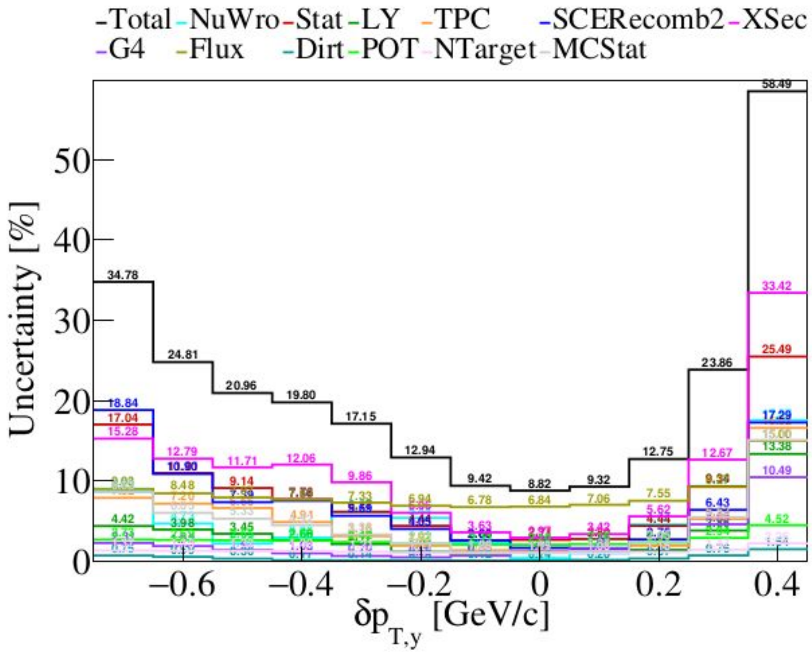
Total NuWro Stat LY TPC SCERecomb2 XSec
G4 Flux Dirt POT NTarget MCStat
Uncertainty [%]
δp_T,y [GeV/c]

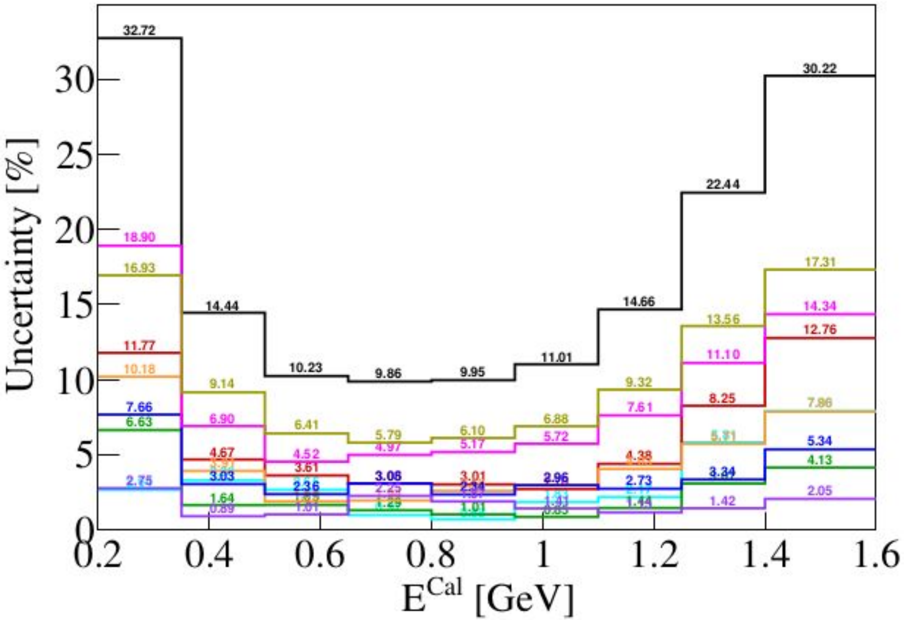
Uncertainty [%]
E^Cal [GeV]

Parameter	Description	CV	1σ Uncertainty	Contributing Uncertainty (%)
Quasi-Elastic Parameters				
`MaCCQE`	CCQE axial mass	1.10 GeV	±0.1 GeV	0.038
`RPA CCQE`	Strength of the RPA correction	0.151	±0.4	2.094
`MaNCEL`	Axial mass for NCEL	0.961242 GeV	±25%	0.348
`EtaNCEL`	Empirical parameter used to account for sea quark contribution to NCEL form factor	0.12	±30%	0.010
`AxFFCCQEshape`	Parametrisation of the nucleon axial form factor	Dipole	z-expansion	0.022
`VecFFCCQEshape`	Parametrisation of the nucleon vector form factors	BBA07	Dipole	0.051
MEC Parameters				
`NormCCMEC`	Energy-independent normalization for CCMEC	1.66	±0.5	1.832
`NormNCMEC`	Energy-independent normalization for NCMEC	1	±20%	0.129
`FracPNCCMEC`	Fraction of initial nucleon pairs that are pn (0 = Valencia)	0	±20%	0.041
`FracDeltaCCMEC`	Relative contribution of Δ diagrams to total MEC cross section (0 = Valencia)	0	±30%	0.124
`XSecShape CCMEC`	Changes shape of differential cross section	1.0	0.0	2.273
`DecayAngMEC`	Changes angular distribution of nucleon cluster	Isotropic	$\cos^2\vartheta$ in rest frame	0.693
Resonant Parameters				
`MaCCRES`	CCRES axial mass	1.120 GeV	±0.2	0.986
`MvCCRES`	Shape-only CCRES axial mass	0.840 GeV	±0.1	0.775
`MaNCRES`	NCRES axial mass	1.120 GeV	±0.2	0.969
`MvNCRES`	NCRES vector mass.	0.840 GeV	±0.1	0.395
`ThetaDelta2Npi`	Interpolates angular distribution for $\Delta \to N + \pi$	Rein-Sehgal	Isotropic	1.533
`ThetaDelta2NRad`	Interpolates angular distribution for $\Delta \to N + \gamma$	Rein-Sehgal	$\cos^2\vartheta$	0.016

Parameter	Description	CV	1σ Uncertainty	Contributing Uncertainty (%)
Non-Resonant Parameters				
NonRESBGvpNC1pi	Non-resonant background normalization for νp NC1π	0.1	± 0.5	0.041
NonRESBGvpNC2pi	Non-resonant background normalization for νp NC2π	1	± 0.5	0.096
NonRESBGvnNC1pi	Non-resonant background normalization for νn NC1π	0.3	± 0.5	0.390
NonRESBGvnNC2pi	Non-resonant background normalization for νn NC2π	1	± 0.5	0.022
NonRESBGvbarpNC1pi	Non-resonant background normalization for $\bar{\nu} p$ NC1π	0.3	± 0.5	0.010
NonRESBGvbarpNC2pi	Non-resonant background normalization for $\bar{\nu} p$ NC2π	1	± 0.5	0.010
NonRESBGvbarnNC1pi	Non-resonant background normalization for $\bar{\nu} n$ NC1π	0.1	± 0.5	0.010
NonRESBGvbarnNC2pi	Non-resonant background normalization for $\bar{\nu} n$ NC2π	1	± 0.5	0.010
NonRESBGvpCC1pi	Non-resonant background normalization for νp CC1π	0.007713	± 0.5	0.014
NonRESBGvpCC2pi	Non-resonant background normalization for νp CC2π	0.787999	± 0.5	0.059
NonRESBGvnCC1pi	Non-resonant background normalization for νn CC1π	0.127858	± 0.5	0.217
NonRESBGvnCC2pi	Non-resonant background normalization for νn CC2π	2.11523	± 0.5	0.079
NonRESBGvbarpCC1pi	Non-resonant background normalization for $\bar{\nu} p$ CC1π	0.127858	± 0.5	0.013
NonRESBGvbarpCC2pi	Non-resonant background normalization for $\bar{\nu} p$ CC2π	2.11523	± 0.5	0.010
NonRESBGvbarnCC1pi	Non-resonant background normalization for $\bar{\nu} n$ CC1π	0.007713	± 0.5	0.010
NonRESBGvbarnCC2pi	Non-resonant background normalization for $\bar{\nu} n$ CC2π	0.787999	± 0.5	0.010
AhtBY	A_{HT} higher-twist parameter in the Bodek-Yang model scaling variable ξ_w	0.538	± 0.25	0.010
BhtBY	BHT higher-twist parameter in the Bodek-Yang model scaling variable ξ_w	0.305	± 0.25	0.010
CV1uBY	CV1u valence GRV98 PDF correction parameter in the Bodek-Yang model	0.291	± 0.3	0.010
CV2uBY	CV2u valence GRV98 PDF correction parameter in the Bodek-Yang model	0.189	± 0.4	0.010

Hadronisation Parameters				
AGKYxF1pi	Hadronization parameter, applicable to true DIS interactions only	-0.385	±0.2	0.108
AGKYpT1pi	Hadronization parameter, applicable to true DIS interactions only	1/6.625	±0.03	0.034
Final State Interaction Parameters				
$\mathtt{MFP}_\pi$	π mean free path	0	±0.2	0.032
$\mathtt{MFP}_\mathrm{N}$	Nucleon mean free path	0	±0.2	1.212
$\mathtt{FrCEx}_\pi$	Fractional cross section for π charge exchange	0	±0.5	0.159
$\mathtt{FrInel}_\pi$	Fractional cross section for π inelastic scattering	0	±0.4	0.133
$\mathtt{FrAbs}_\pi$	Fractional cross section for π absorption	0	±0.3	0.906
$\mathtt{FrCEx}_\mathrm{N}$	Fractional cross section for nucleon charge exchange	0	±0.2	0.953
$\mathtt{FrInel}_\mathrm{N}$	Fractional cross section for nucleon inelastic scattering	0	±0.5	0.289
$\mathtt{FrAbs}_\mathrm{N}$	Fractional cross section for nucleon absorption	0	±0.4	0.906
Delta Resonant Decay Parameters				
RDecBR1gamma	Normalization for $\Delta \rightarrow \gamma$ decays	Nominal BR	±0.5	0.042
RDecBR1eta	Normalization for $\Delta \rightarrow \eta$ decays	Nominal BR	±0.5	0.513
Coherent Parameters				
NormCCCOH	Scaling factor for CCCOH π production total cross section	Nominal	100% increase	0.027
NormNCCOH	Scaling factor for NCCOH π production total cross section	Nominal	100% increase	0.016

Variation	Description
Wire Mod x position	Wire modification of x position
Wire Mod (y,z) position	Wire modification of (y,z) position
Wire Mod θ_{XZ}	Wire modification of angle in XZ plane
Wire Mod θ_{YZ}	Wire modification of angle in YZ plane
Light Yield Attenuation	Attenuation of LY response in detector over time
Light Yield Down	Turn down the light yield in the detector by 25%
Light Yield Rayleigh	Increase Rayleigh scattering length from 60 cm to 90 cm
Recombination	Reduce value of β' in the Modified Box Model
SCE	Use an alternative Space Charge Map

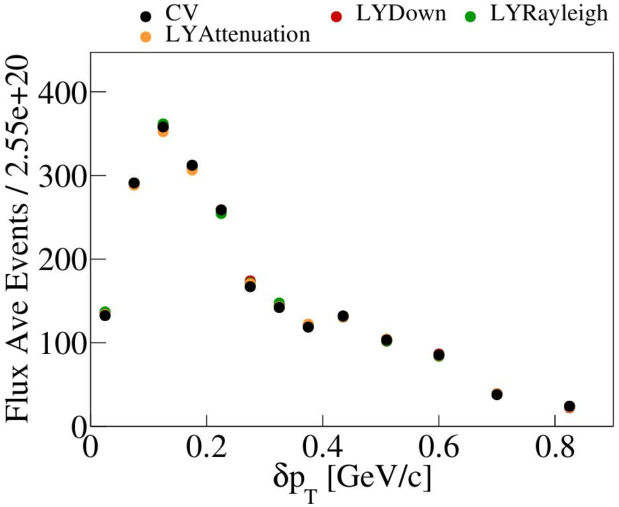

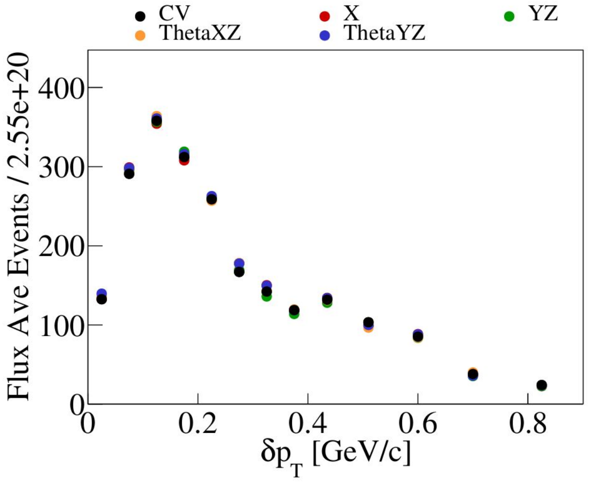

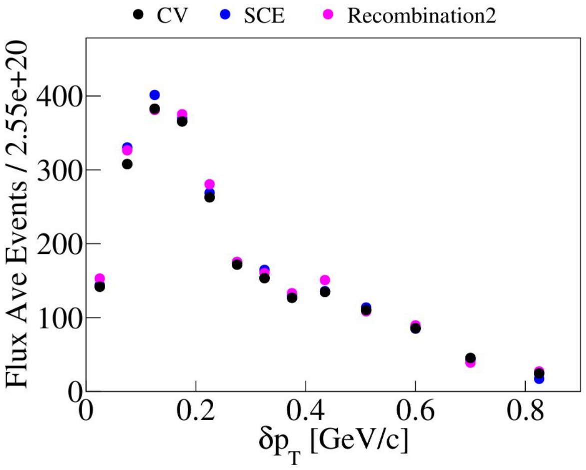

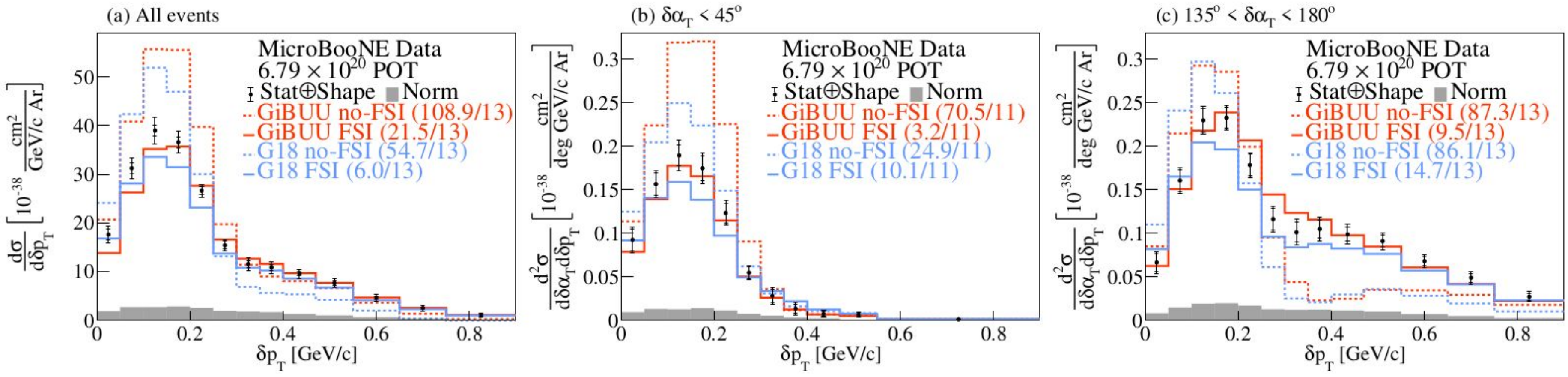

FIG. 1. The flux-integrated (a) single- and (b-c) double- (in $\delta\alpha_T$ bins) differential CC1p0π cross sections as a function of the transverse missing momentum δp_T. Inner and outer error bars show the statistical and total (statistical and shape systematic) uncertainty at the 1σ, or 68%, confidence level. The gray band shows the separate normalization systematic uncertainty. Colored lines show the results of theoretical cross section calculations with (solid line) and without (dashed line) FSI based on the GENIE (blue) and GiBUU (orange) event generators.

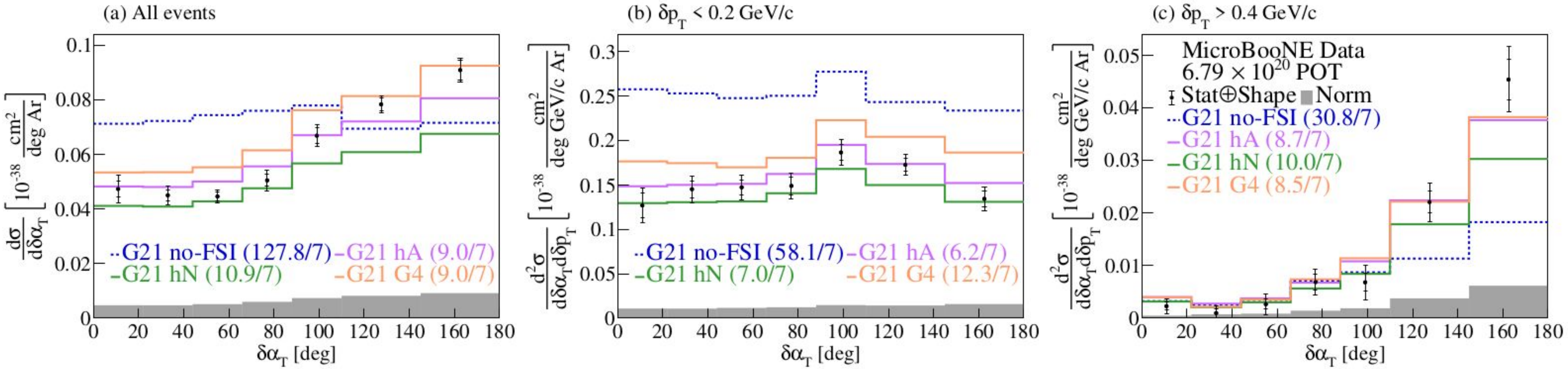

FIG. 2. The flux-integrated (a) single- and (b-c) double- (in δp_T bins) differential CC1p0π cross sections as a function of the angle $\delta\alpha_T$. Inner and outer error bars show the statistical and total (statistical and shape systematic) uncertainty at the 1σ, or 68%, confidence level. The gray band shows the separate normalization systematic uncertainty. Colored lines show the results of theoretical cross section calculations with a number of FSI-modeling choices based on the GENIE event generator.

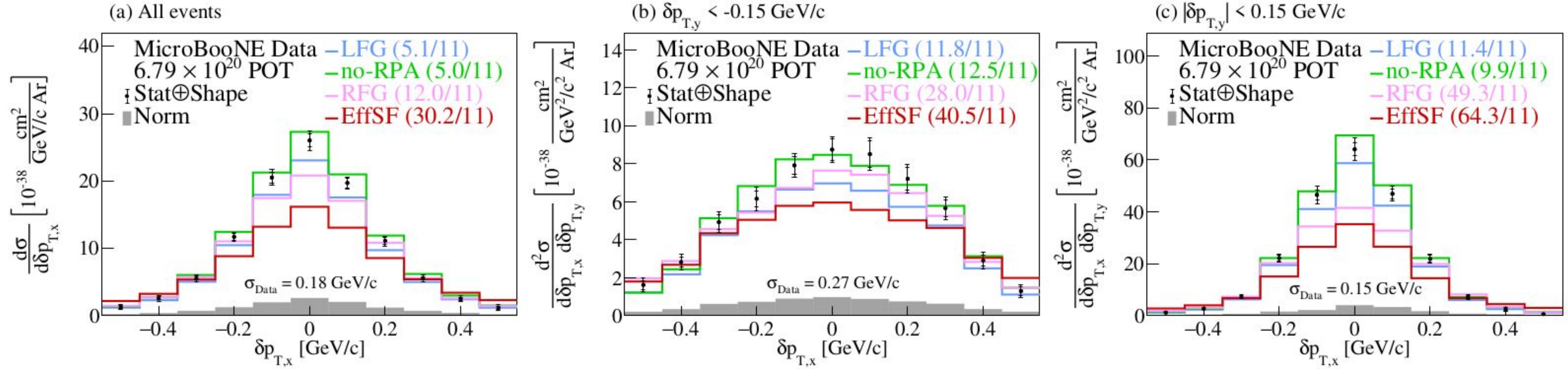

FIG. 3. The flux-integrated (a) single- and (b-c) double- (in $\delta p_{T,y}$ bins) differential CC1p0π cross sections as a function of the transverse three-momentum transfer component, $\delta p_{T,x}$. Inner and outer error bars show the statistical and total (statistical and shape systematic) uncertainty at the 1σ, or 68%, confidence level. The gray band shows the separate normalization systematic uncertainty. Colored lines show the results of theoretical cross section calculations with a number of event generators. The standard deviation (σ_{Data}) of a Gaussian fit to the data is shown on each panel.

High Statistics→Into the Multiverse!

QE-dominated region

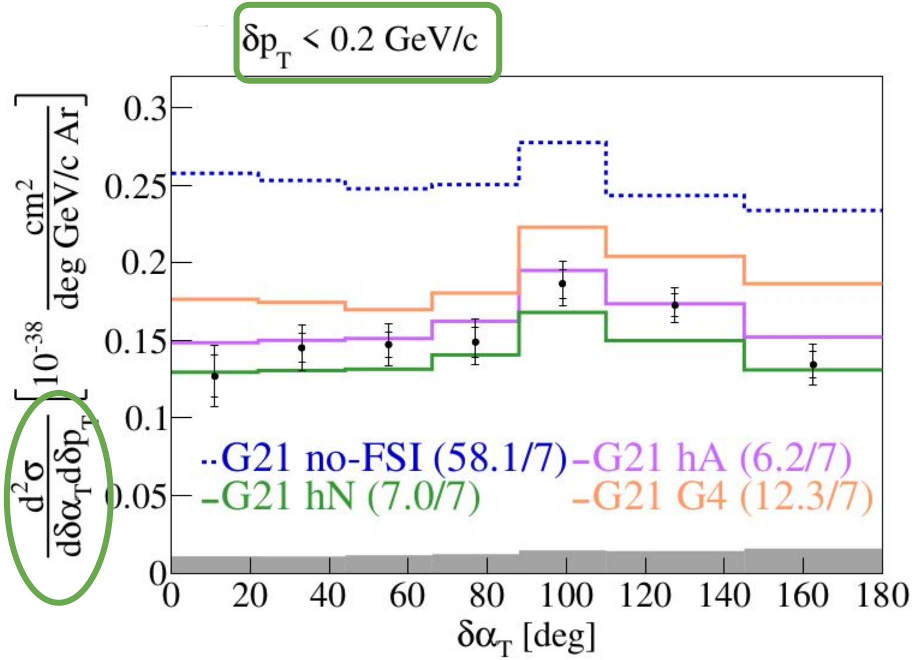

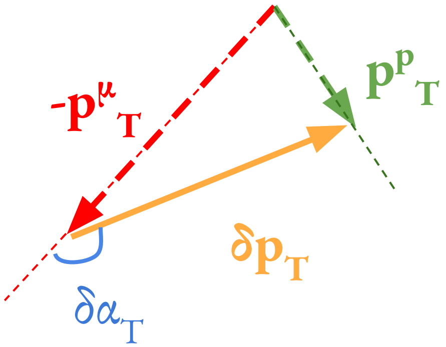

- Flat distribution indicative of absence of proton FSI
- Shape and normalization differences across FSI models

G21 = GENIE v3.0.6 G21_11b_00_000

SuSAv2 QE & MEC*, hA/hN/G4 = FSI modeling options

Phys. Rev. Lett. 131, 101802 (2023)

* Phys. Rev. D 101, 033003 (2020)

Transverse Orientation $\delta\alpha_T$ Cross Section

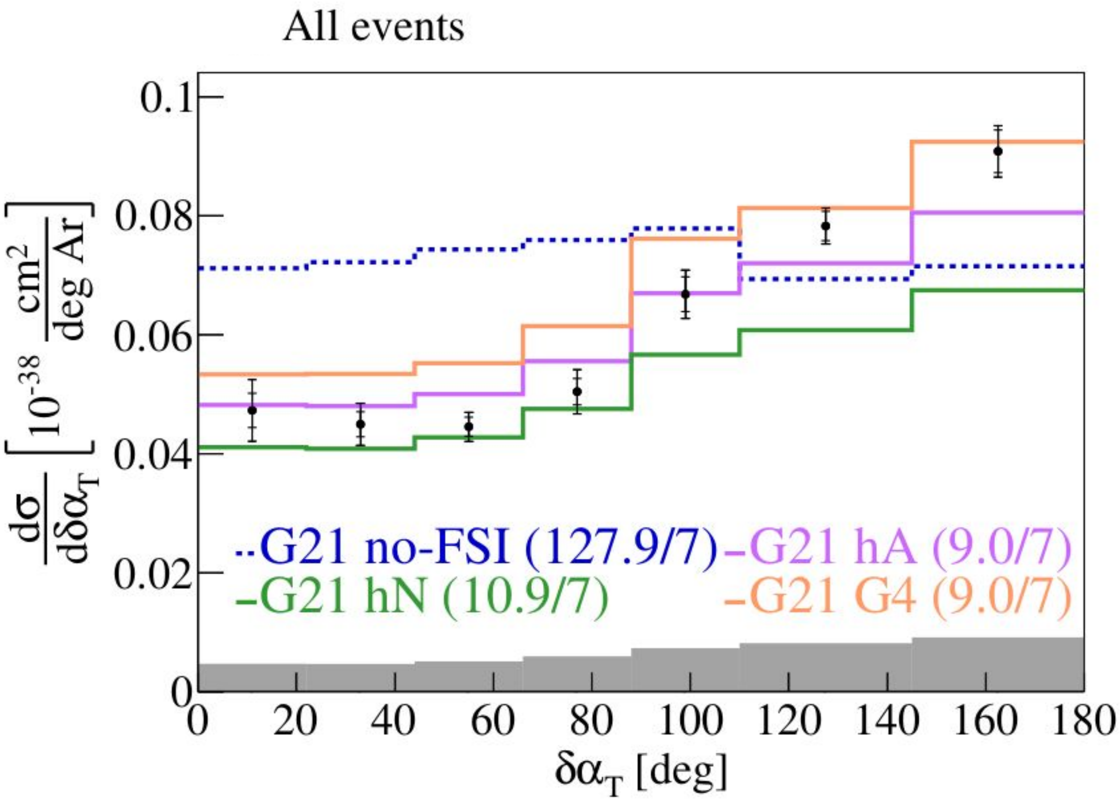

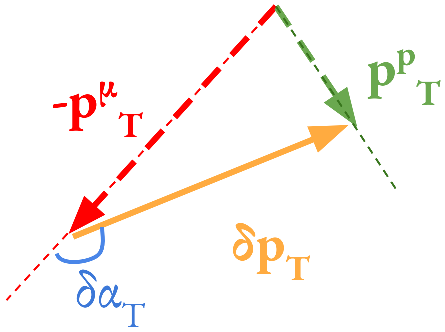

- First neutrino-argon differential cross section in $\delta\alpha_T$
- Sensitive to proton FSI modeling
- Data favors FSI addition
- Shape differences observed

G21 = GENIE v3.0.6 G21_11b_00_000
SuSAv2 QE & MEC*, hA/hN/G4 = FSI modeling options

arXiv:2301.03706
* Phys. Rev. D 101, 033003 (2020)

High Statistics→Into the Multiverse!

- **Extension to 2D** for the first time on argon
- Probe regions with greater model discrimination power

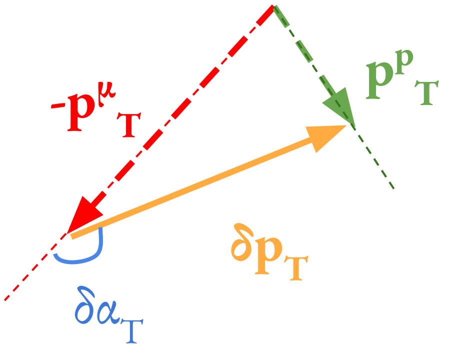

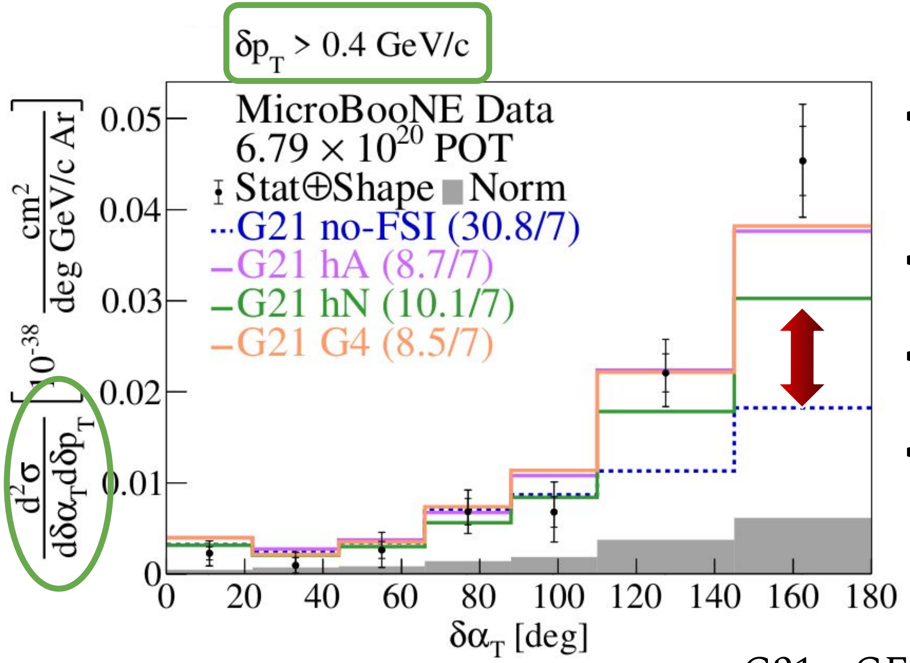

- Primarily contributions from MEC/RES & QE events undergoing FSI
- More assymmetric behavior compared to 1D result
- No-FSI contribution lower than FSI ones
- High $\delta\alpha_T$ & high δp_T part of phase-space ideal to test FSI / multinucleon effect sensitivity

G21 = GENIE v3.0.6 G21_11b_00_000
SuSAv2 QE & MEC*, hA/hN/G4 = FSI modeling options

arXiv:2301.03706
* Phys. Rev. D 101, 033003 (2020)

VI. MODELING CONFIGURATIONS

The nominal MC neutrino interaction prediction (G18) uses the local Fermi gas (LFG) model [50], the Nieves CCQE scattering prescription [51] which includes Coulomb corrections for the outgoing muon [52] and random phase approximation (RPA) corrections [53]. Additionally, it uses the Nieves MEC model [54], the KLN-BS RES [55–58] and Berger-Sehgal coherent (COH) [59] scattering models, the hA2018 FSI model [60], and MicroBooNE-specific tuning of model parameters [38].

Our results are also compared to a number of alternative event generators. GiBUU 2021 (GiBUU) uses similar models, but they are implemented in a coherent way by solving the Boltzmann-Uehling-Uhlenbeck transport equation [61]. The modeling includes the LFG model [50], a standard CCQE expression [62], an empirical MEC model and a dedicated spin dependent resonance amplitude calculation following the MAID analysis [61]. The DIS model is from PYTHIA [63]. GiBUU's FSI treatment propagates the hadrons through the residual nucleus in a nuclear potential which is consistent with the initial state. NuWro v19.02.2 (NuWro) uses the LFG model [50], the Llewellyn Smith model for QE events [64], the Nieves model for MEC events [65], the Adler-Rarita-Schwinger formalism to calculate the Δ resonance explicitly [58], the BS COH [59] scattering model and an intranuclear cascade model for FSI [65]. NEUT v5.4.0 (NEUT) uses the LFG model [50], the Nieves CCQE scattering prescription [51], the Nieves MEC model [54], the BS RES [55–58] and BS COH [59] scattering models, and FSI with Oset medium corrections for pions [35, 36].

In addition to the alternative event generators, our results are compared to a number of different GENIE configurations. These include an older version, GENIE v2.12.10 (Gv2) [35, 36], which uses the Bodek-Ritchie Fermi Gas model, the Llewellyn Smith CCQE scattering prescription [64], the empirical MEC model [66], a Rein-Sehgal RES and COH scattering model [67], and a data driven FSI model denoted as "hA" [68]. Another model, "Untuned", uses the GENIE v3.0.6 G18_10a_02_11a configuration without additional MicroBooNE-specific tuning. Finally, the newly added theory-driven GENIE v3.2.0 G21_11b_00_000 configuration (G21) is shown. This includes the SuSAv2 prediction for the QE and MEC scattering parts [69] and the hN2018 FSI model [70]. The modeling options for RES, DIS, and COH interactions are the same as for G18.

To quantify the data-simulation agreement, the χ^2/bins ratio data comparison for each generator is shown on all the figures and is calculated by taking into account the total covariance matrix. Ratios close to unity are indicative of a sufficiently accurate modeling performance. Theoretical uncertainties on the models themselves are not included.

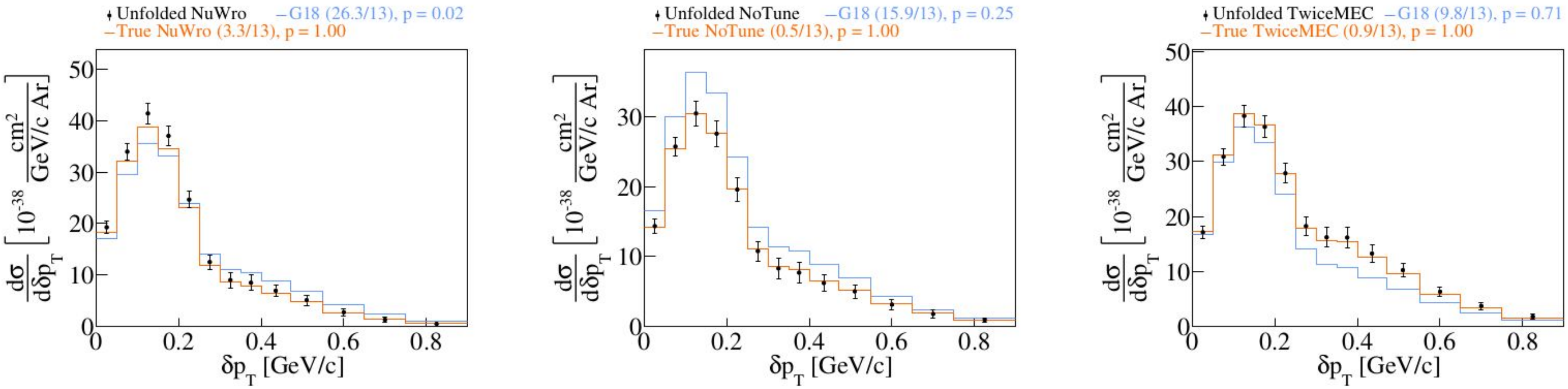

FIG. 1. Fake data studies for δp_T using (left) NuWro, (center) GENIE without the MicroBooNE tune (NoTune), and (right) twice the weights for MEC events (TwiceMEC) as fake data samples.

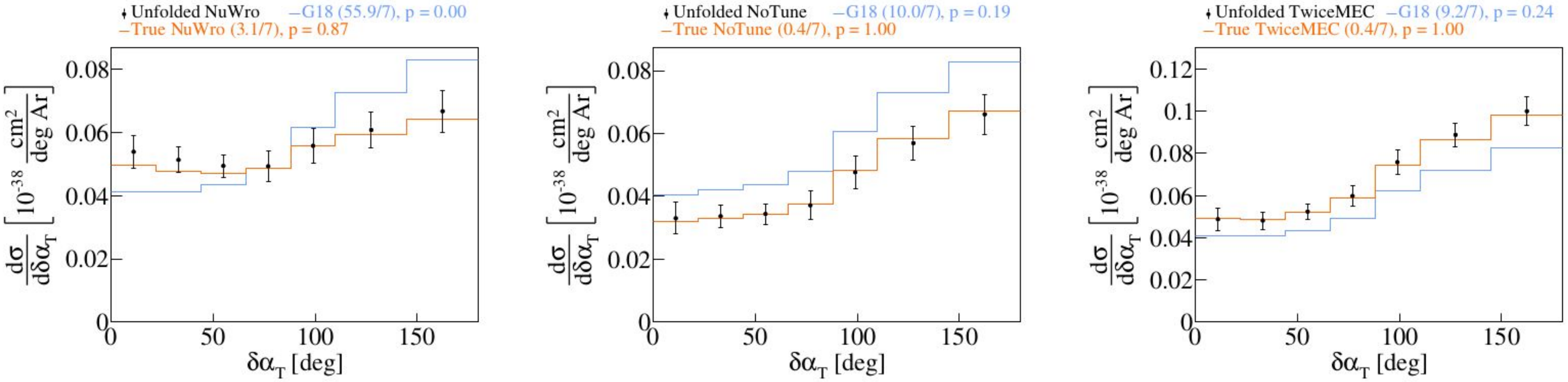

FIG. 2. Fake data studies for $\delta\alpha_T$ using (left) NuWro, (center) GENIE without the MicroBooNE tune (NoTune), and (right) twice the weights for MEC events (TwiceMEC) as fake data samples.

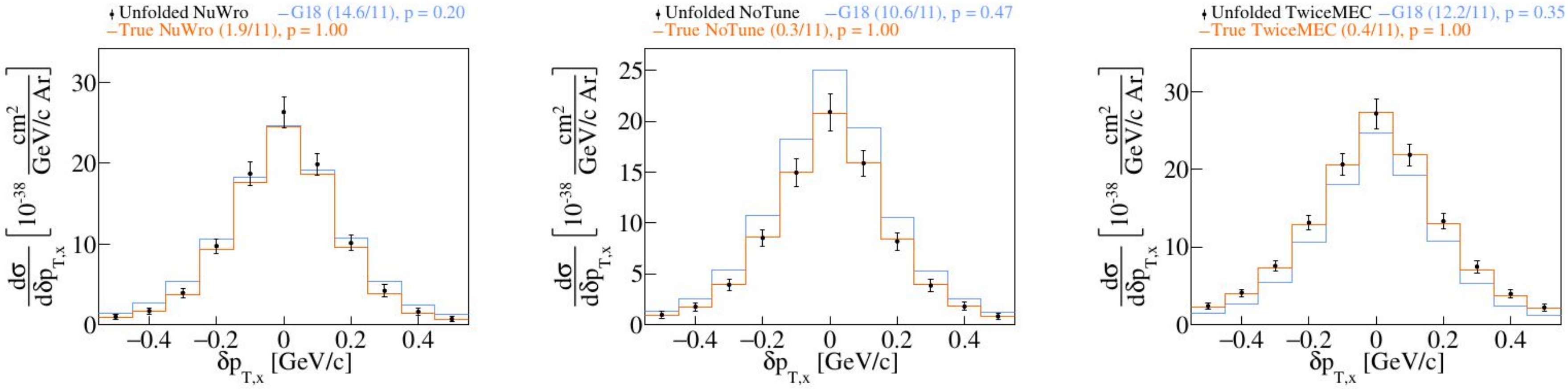

FIG. 3. Fake data studies for $\delta p_{T,x}$ using (left) NuWro, (center) GENIE without the MicroBooNE tune (NoTune), and (right) twice the weights for MEC events (TwiceMEC) as fake data samples.

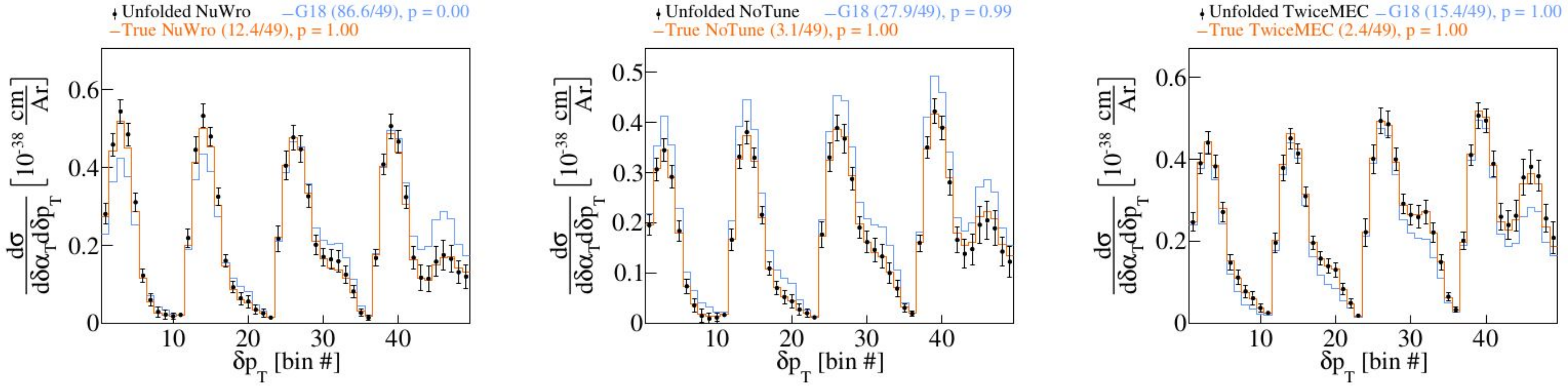

FIG. 4. Fake data studies for δp_T in $\delta\alpha_T$ bins using (left) NuWro, (center) GENIE without the MicroBooNE tune (NoTune), and (right) twice the weights for MEC events (TwiceMEC) as fake data samples.

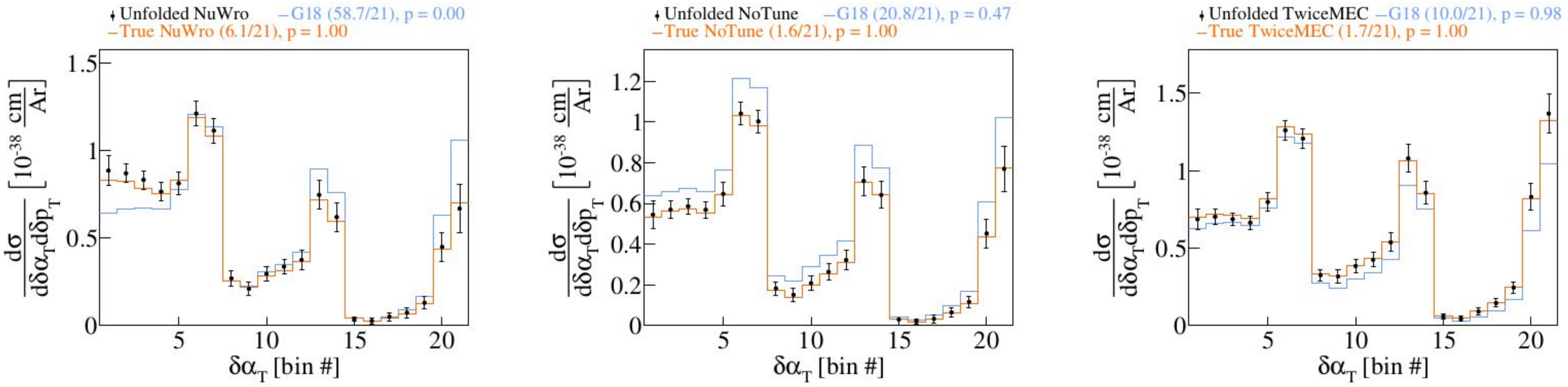

FIG. 5. Fake data studies for $\delta\alpha_T$ in δp_T bins using (left) NuWro, (center) GENIE without the MicroBooNE tune (NoTune), and (right) twice the weights for MEC events (TwiceMEC) as fake data samples.

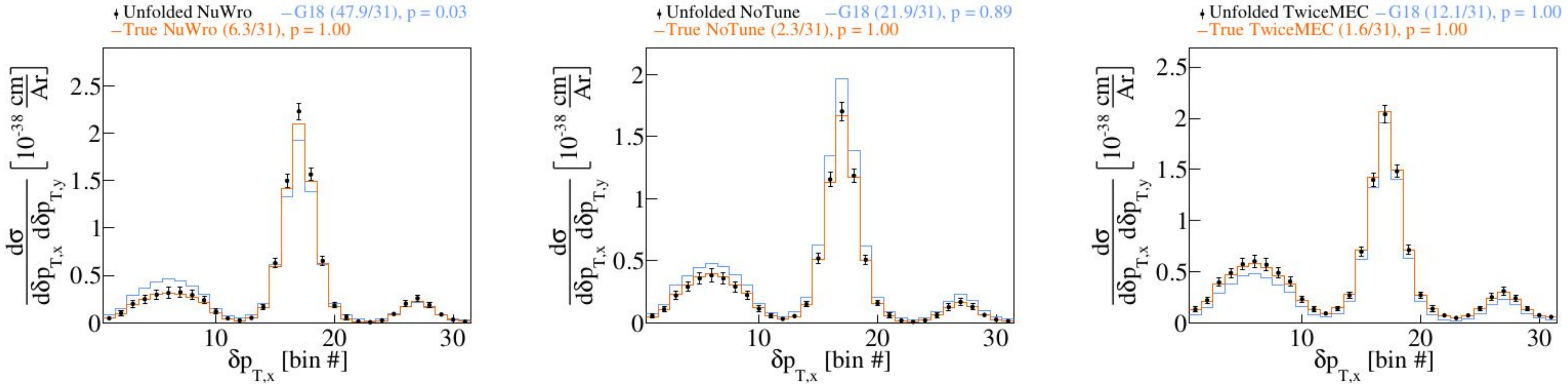

FIG. 6. Fake data studies for $\delta p_{T,x}$ in $\delta p_{T,y}$ bins using (left) NuWro, (center) GENIE without the MicroBooNE tune (NoTune), and (right) twice the weights for MEC events (TwiceMEC) as fake data samples.

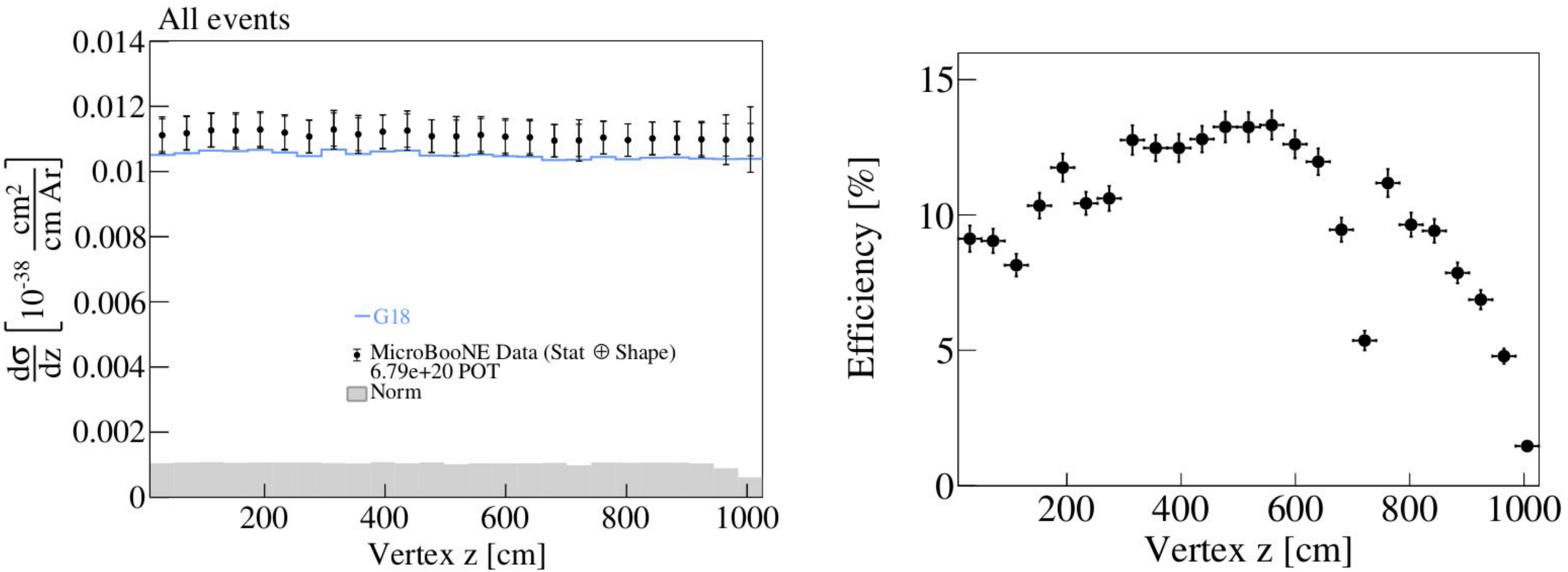

FIG. 7. (Left) extracted cross section as a function of the vertex z distribution. (Right) vertex z efficiency function.

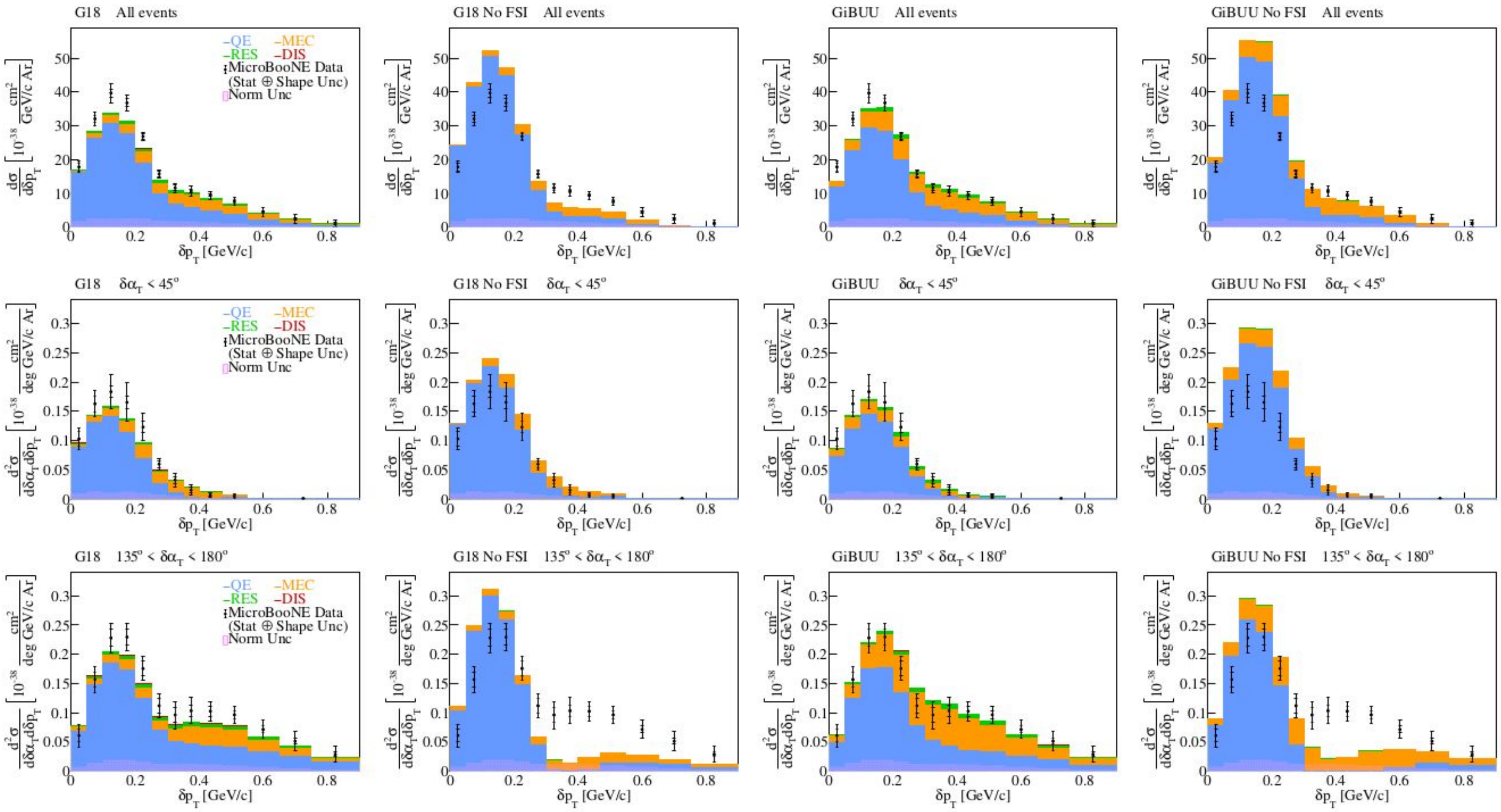

FIG. 8. Cross section interaction breakdown for (top) all the selected events, (middle) events with $\delta\alpha_T < 45^{o}$, and (bottom) events with $135^{o} < \delta\alpha_T < 180^{o}$. The breakdown is shown for (first column) the G18 configuration with FSI effects, (second column) the G18 configuration without FSI effects, (third column) GiB with FSI effects, and (forth column) GiB without FSI effects.

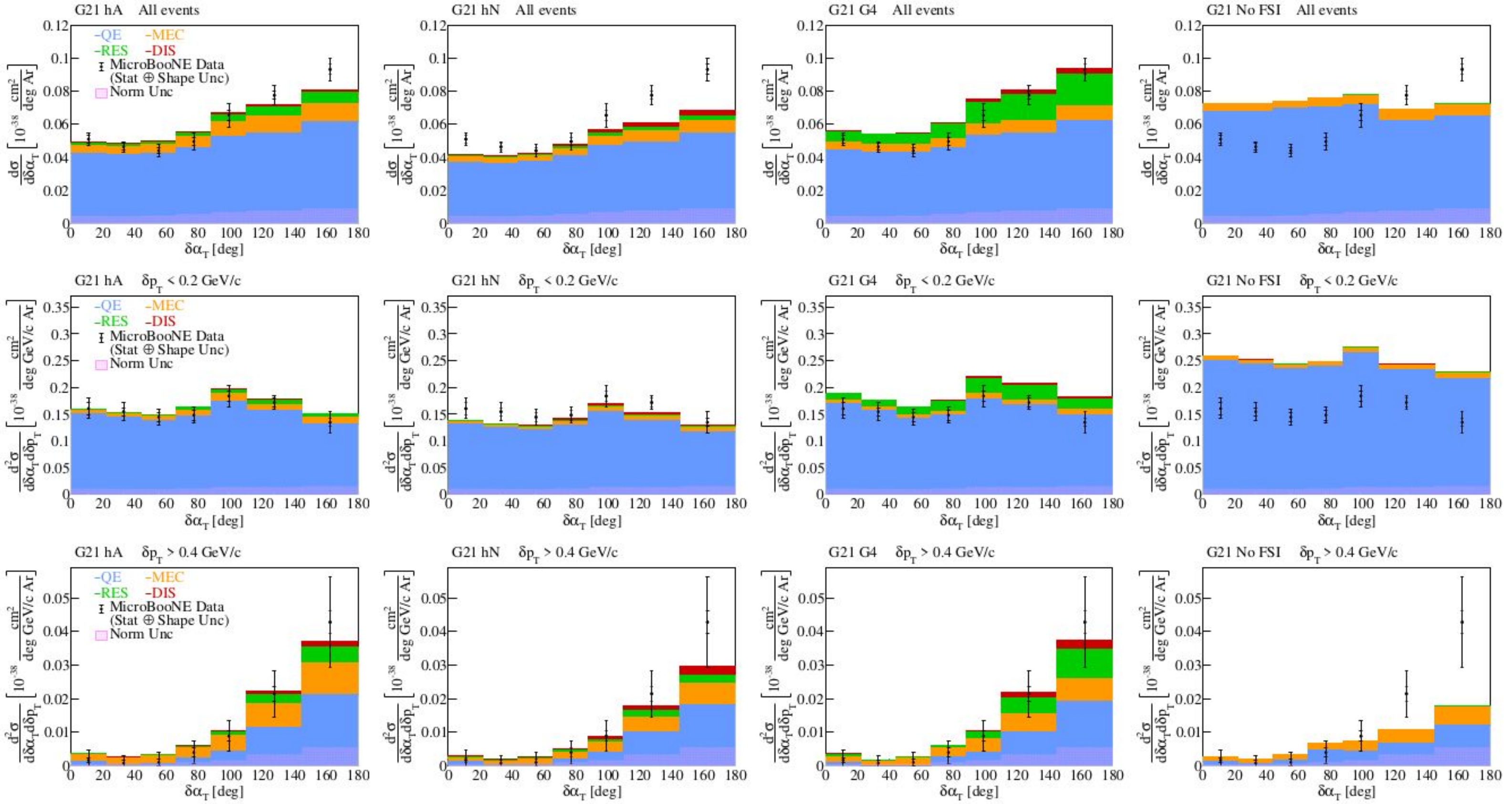

FIG. 9. Cross section interaction breakdown for (top) all the selected events, (middle) events with $\delta p_T < 0.2\,\mathrm{GeV/c}$, and (bottom) events with $\delta p_T > 0.4\,\mathrm{GeV/c}$. The breakdown is shown for (first column) the G21 hA configuration with the hA2018 FSI model, (second column) the G21 hN configuration with the hN FSI model, (third column) the G21 G4 configuration with the G4 FSI model, and (forth column) the G21 No FSI configuration without FSI effects.

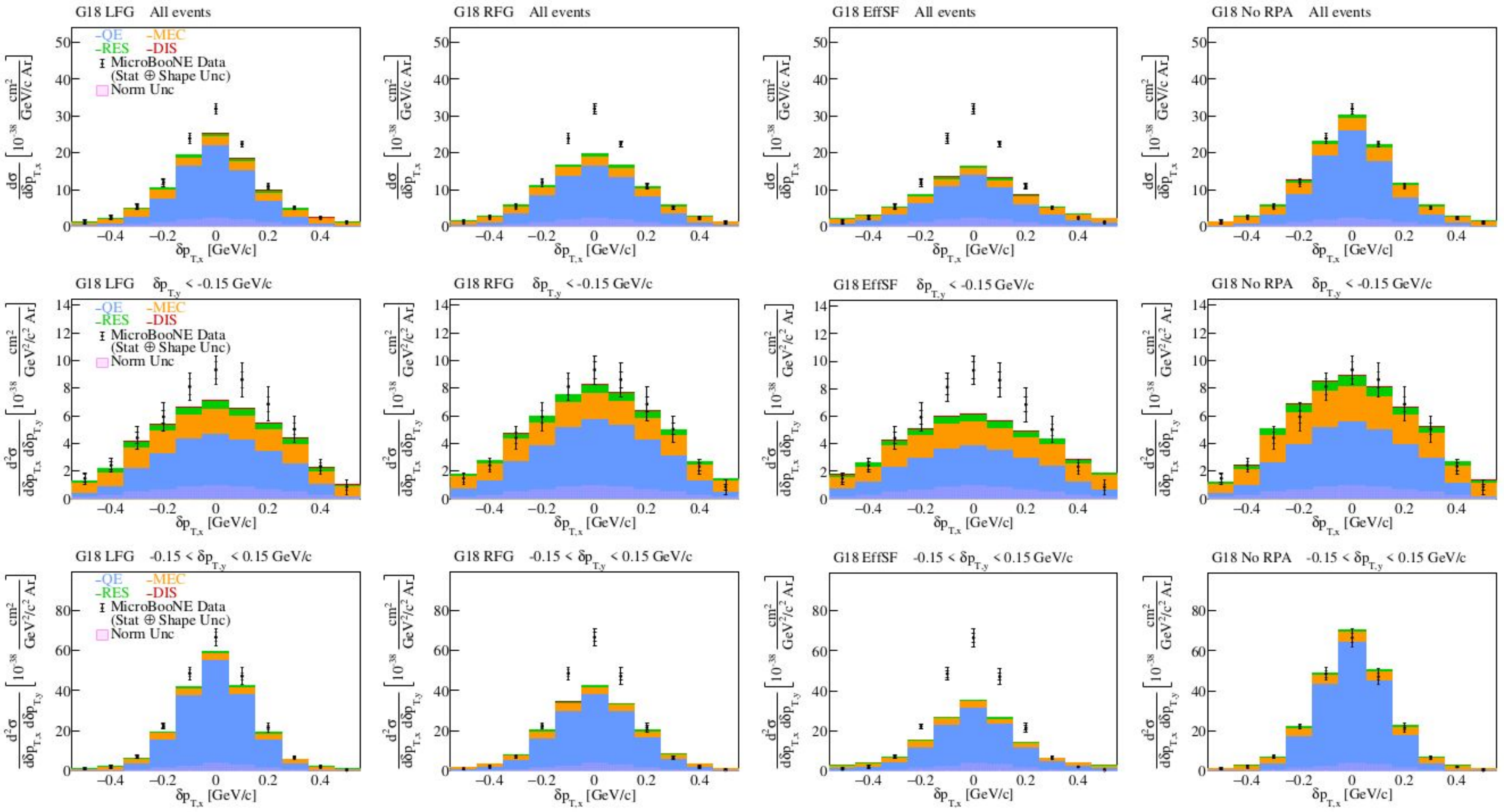

FIG. 10. Cross section interaction breakdown for (top) all the selected events, (middle) events with $\delta p_{T,y} < -0.15\,\mathrm{GeV/c}$, and (bottom) events with $-0.15 < \delta p_{T,y} < 0.15\,\mathrm{GeV/c}$. The breakdown is shown for (first column) the G18 LFG configuration, (second column) the G18 RFG configuration, (third column) the G18 EffSF configuration, and (forth column) the G18 No RPA configuration.

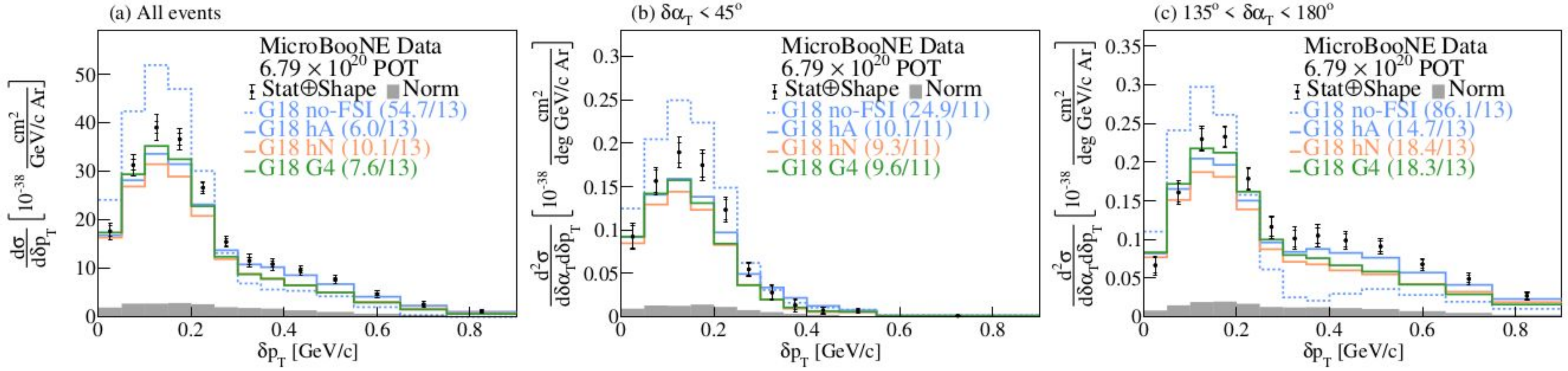

FIG. 11. The flux-integrated (a) single- and (b-c) double- (in $\delta\alpha_T$ bins) differential CC1p0π cross sections as a function of the transverse missing momentum, δp_T. Inner and outer error bars show the statistical and total (statistical and shape systematic) uncertainty at the 1σ, or 68%, confidence level. The gray band shows the separate normalization systematic uncertainty. Colored lines show the results of theoretical cross section calculations with a number of `G21` FSI modeling variations.

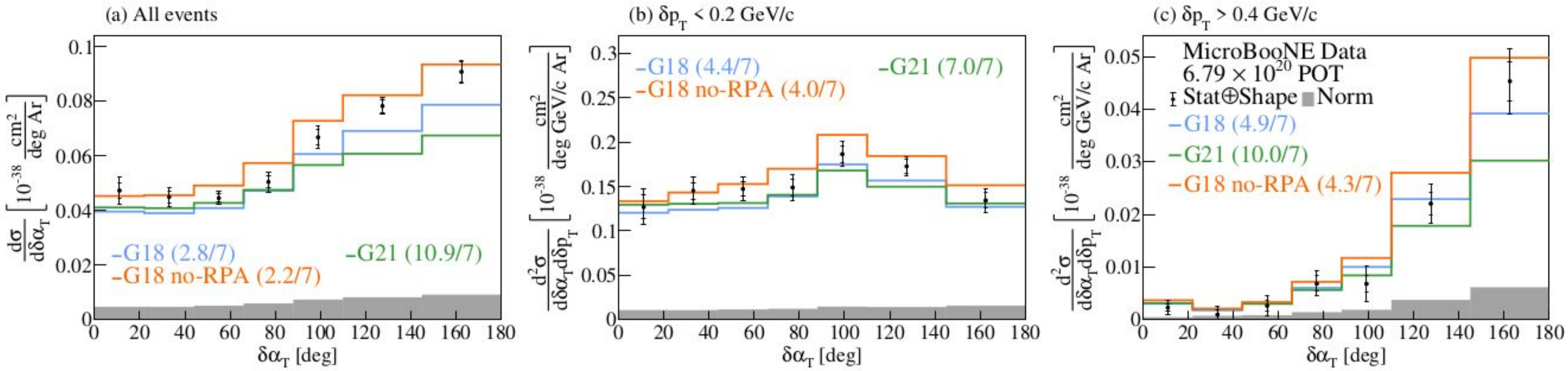

FIG. 12. The flux-integrated (a) single- and (b-c) double- (in δp_T bins) differential CC1p0π cross sections as a function of the angle $\delta\alpha_T$. Inner and outer error bars show the statistical and total (statistical and shape systematic) uncertainty at the 1σ, or 68%, confidence level. The gray band shows the separate normalization systematic uncertainty. Colored lines show the results of theoretical cross section calculations with a number of QE-modeling choices based on the GENIE event generator.

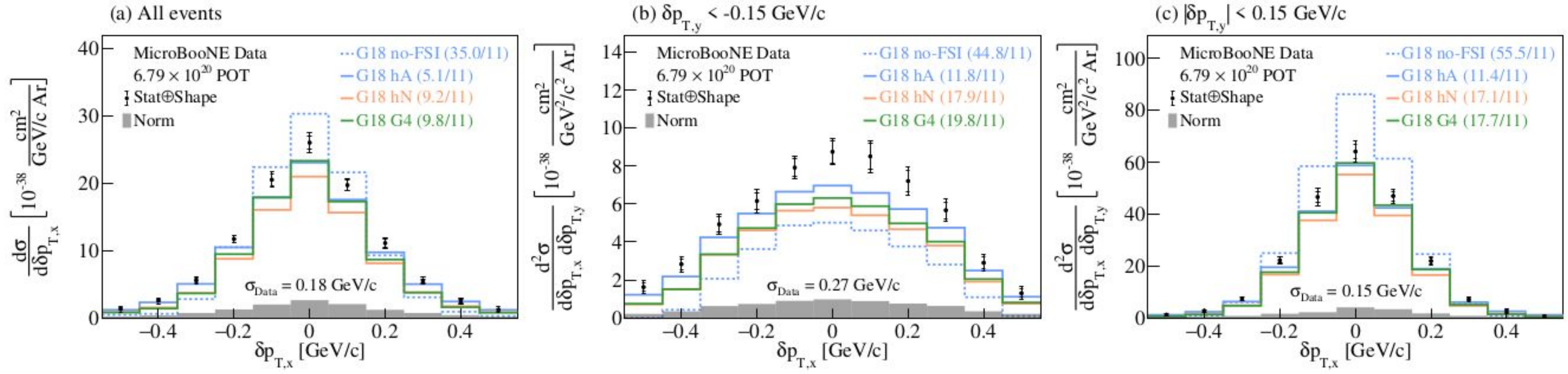

FIG. 13. The flux-integrated (a) single- and (b-c) double- (in $\delta p_{T,y}$ bins) differential CC1p0π cross sections as a function of the transverse three-momentum transfer component, $\delta p_{T,x}$. Inner and outer error bars show the statistical and total (statistical and shape systematic) uncertainty at the 1σ, or 68%, confidence level. The gray band shows the separate normalization systematic uncertainty. Colored lines show the results of theoretical cross section calculations with a number of `G18` FSI modeling variations. The standard deviation ($\sigma_{\rm Data}$) of a Gaussian fit to the data is shown on each panel.

Transverse Component $\delta p_{T,x}$

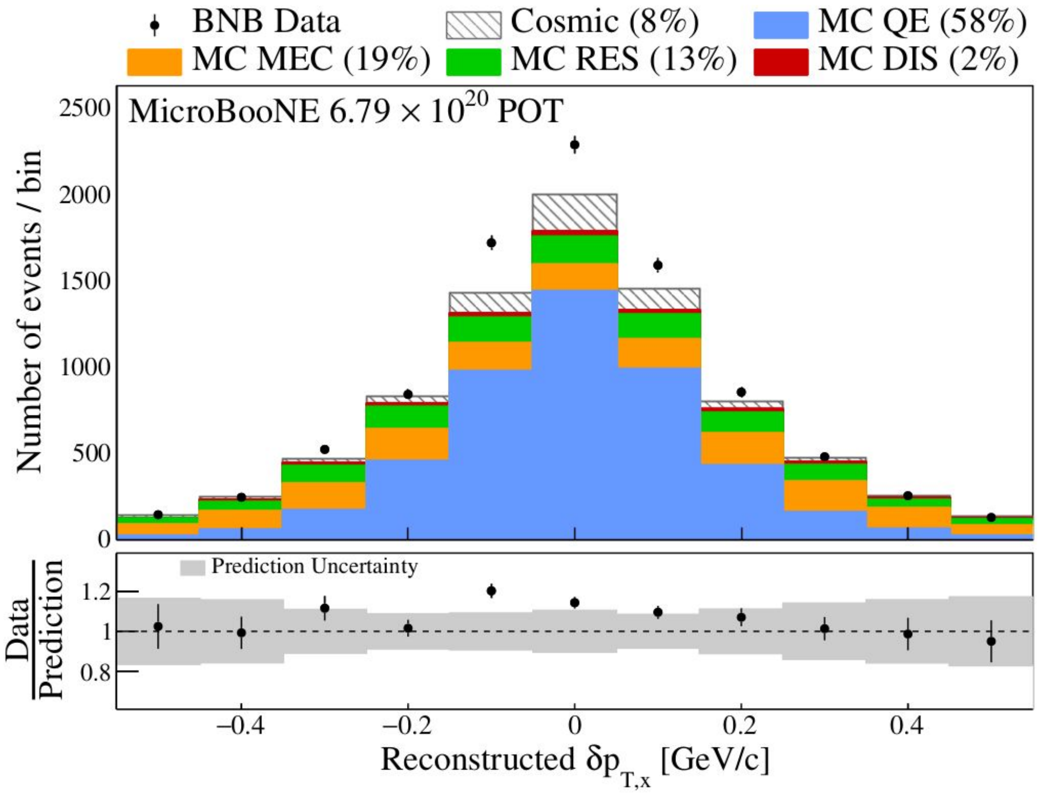

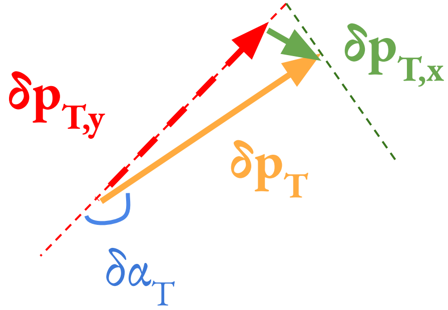

$$\delta p_{T,x} = \delta p_T \bullet \sin\delta\alpha_T$$

- Symmetric around 0 GeV/c
- **QE** dominance in central region
- **MEC**/**RES** events primarily in the tail

arXiv:2301.03700

Transverse Component $\delta p_{T,x}$ Cross Section

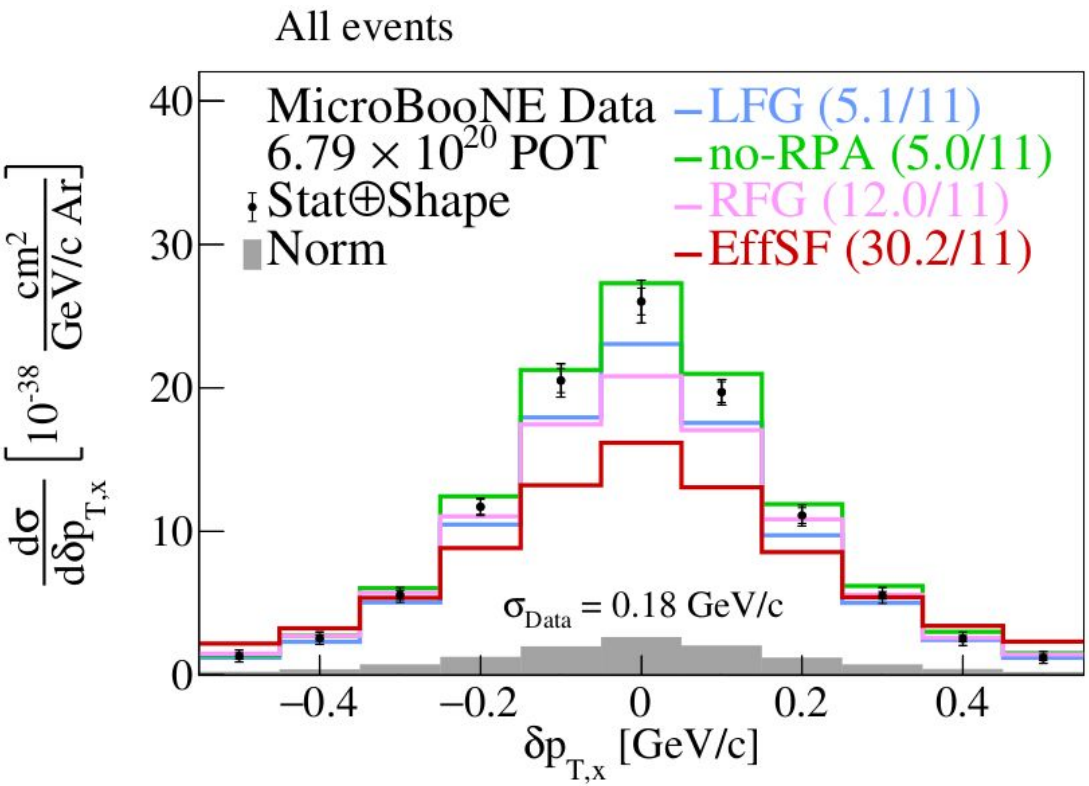

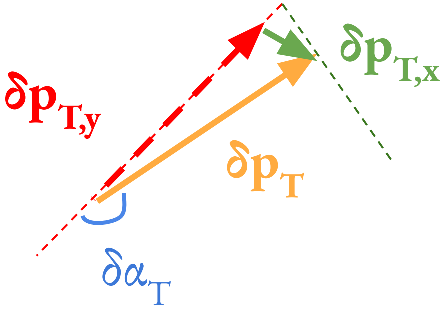

$$\delta p_{T,x} = \delta p_T \cdot \sin\delta\alpha_T$$

- G18 LFG = GENIE v3.0.6 G18_10a_02_11a (G18) + uB Tune with local Fermi gas
- G18 no-RPA = G18 w/o RPA effects
- G18 RFG = G18 with relativistic Fermi gas (RFG)
- G18 EffSF = G18 with spectral function (EffSF)

arXiv:2301.03706

Longitudinal Component $\delta p_{T,y}$

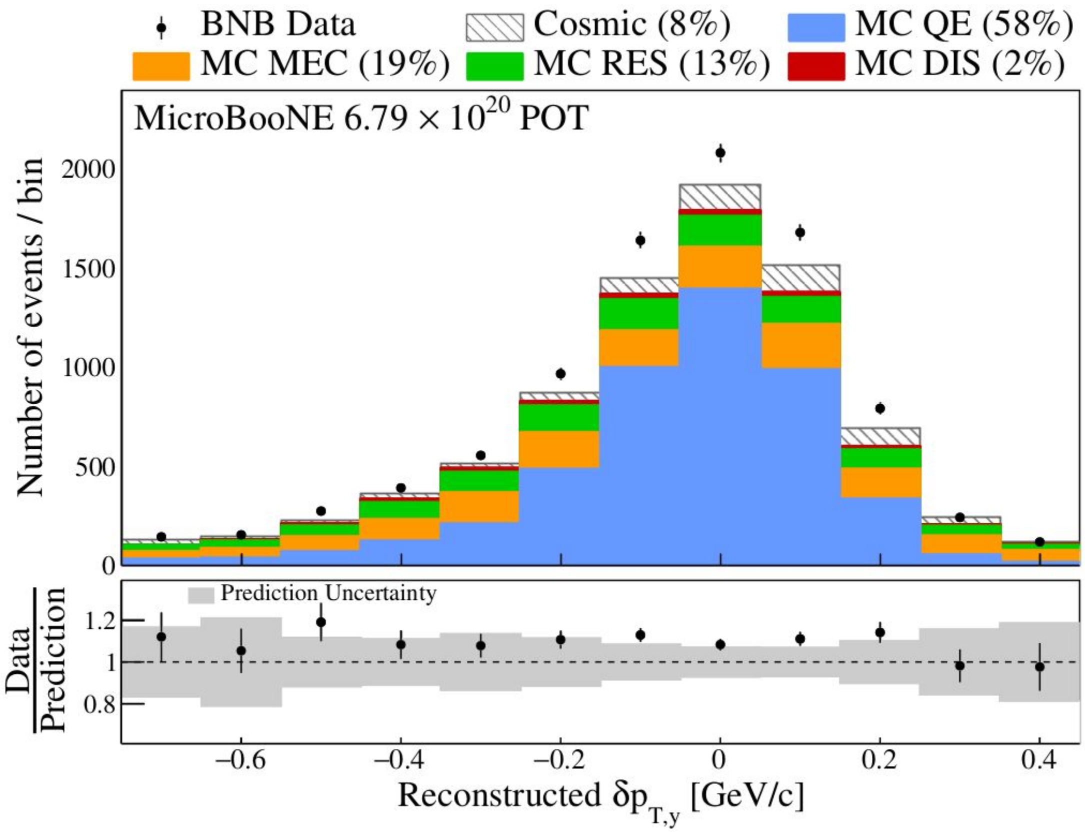

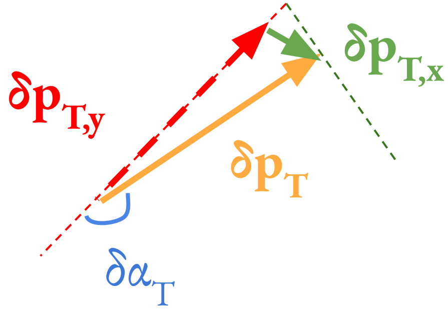

$$\delta p_{T,y} = \delta p_T \bullet \cos\delta\alpha_T$$

- Asymmetric due to $\delta\alpha_T$ enhancement at ~180°
- **QE** dominance in central region
- Spread of tail sensitive to FSI strength & **MEC**/**RES**

arXiv:2301.03700

High Statistics→Into the Multiverse!

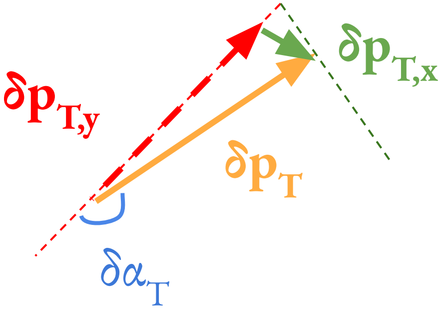

- First neutrino-argon differential cross section in TKI variables
- Sensitive to initial nucleon motion & proton FSI modeling

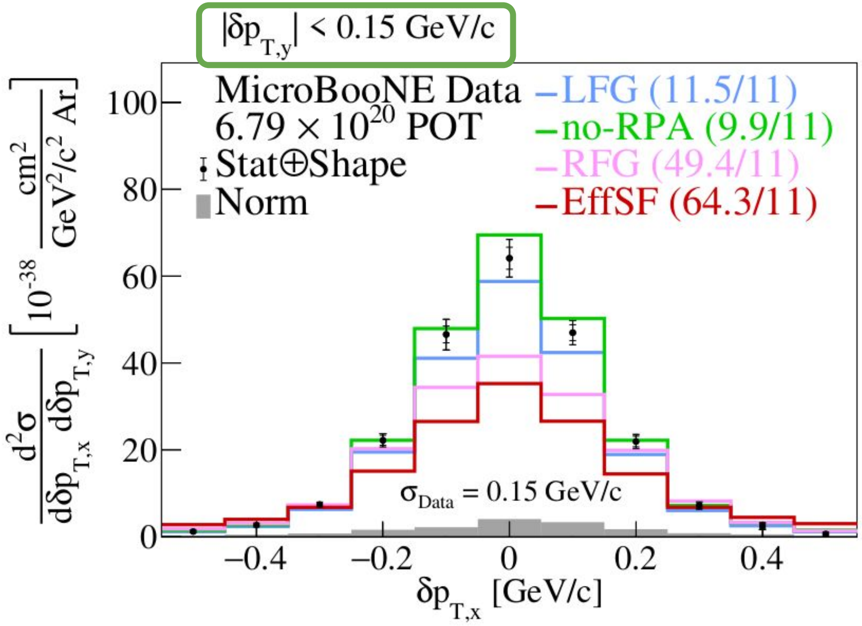

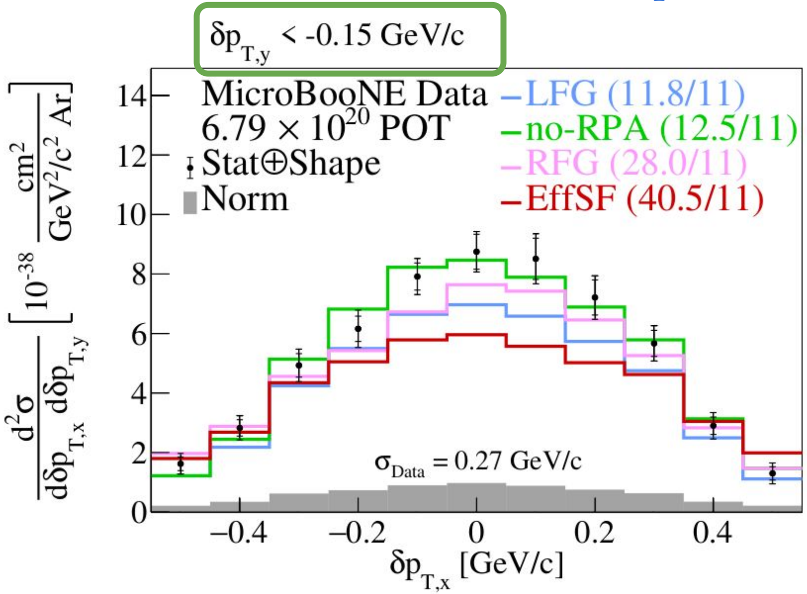

arXiv:2301.03706

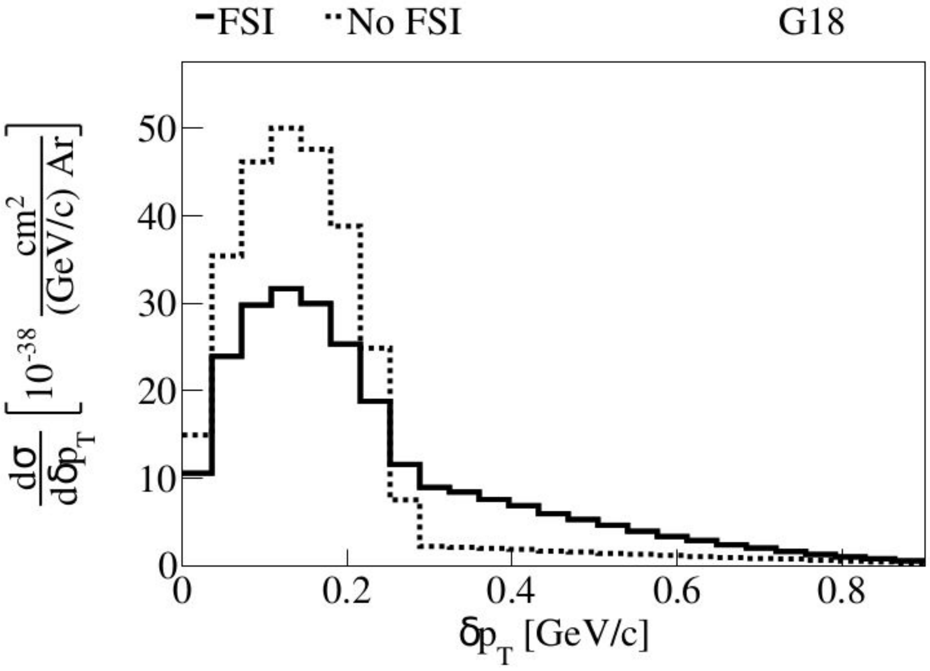
FSI
No FSI
G18
$\frac{d\sigma}{d\delta p_T}\left[10^{-38}\frac{cm^2}{(GeV/c)\ Ar}\right]$
δp_T [GeV/c]

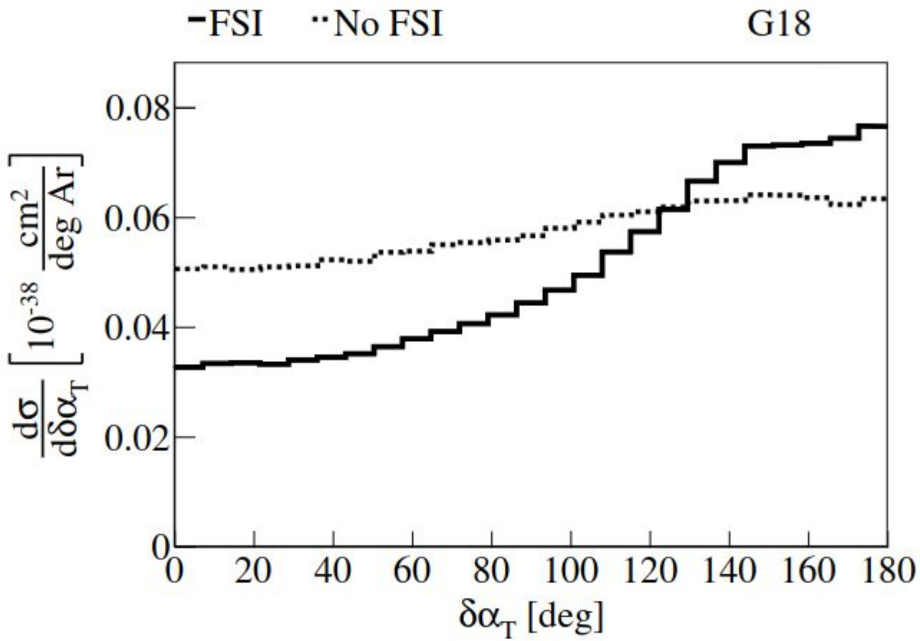
FSI
No FSI
G18
$\frac{d\sigma}{d\delta\alpha_T}\left[10^{-38}\frac{cm^2}{deg\ Ar}\right]$
$\delta\alpha_T$ [deg]

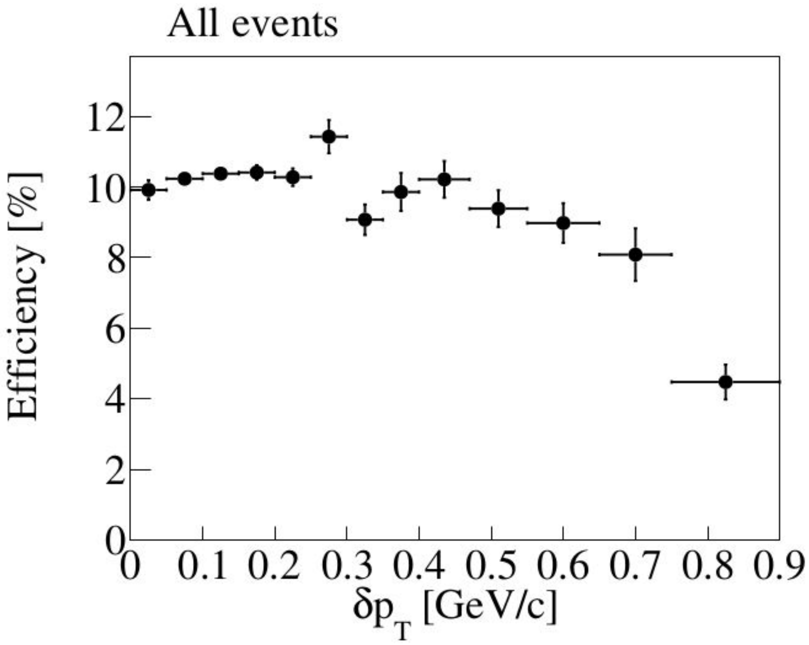
All events
Efficiency [%]
0
2
4
6
8
10
12
0
0.1
0.2
0.3
0.4
0.5
0.6
0.7
0.8
0.9
δp_T [GeV/c]

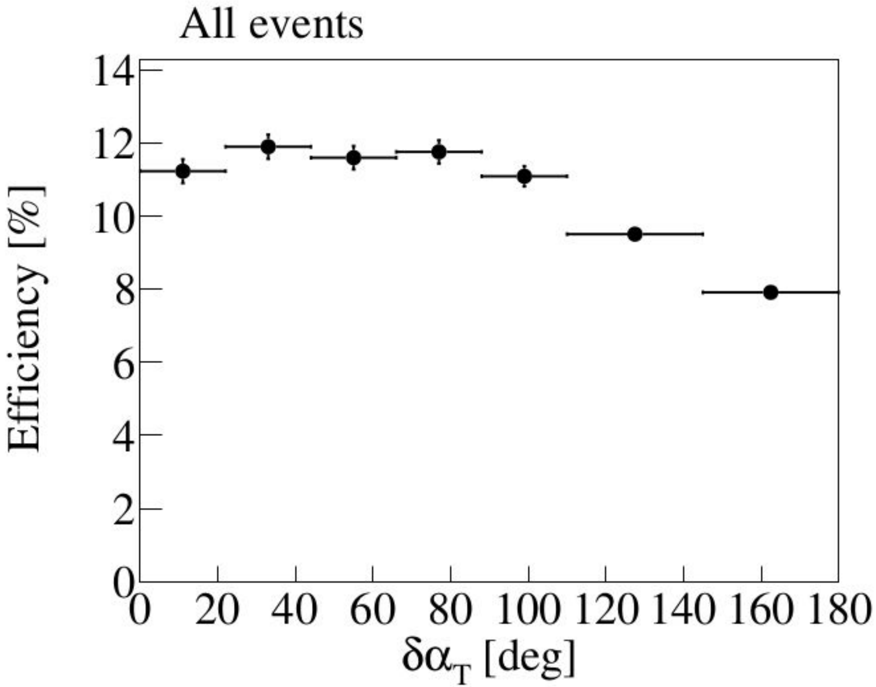
All events
Efficiency [%]
0
2
4
6
8
10
12
14
0
20
40
60
80
100
120
140
160
180
$\delta\alpha_T$ [deg]

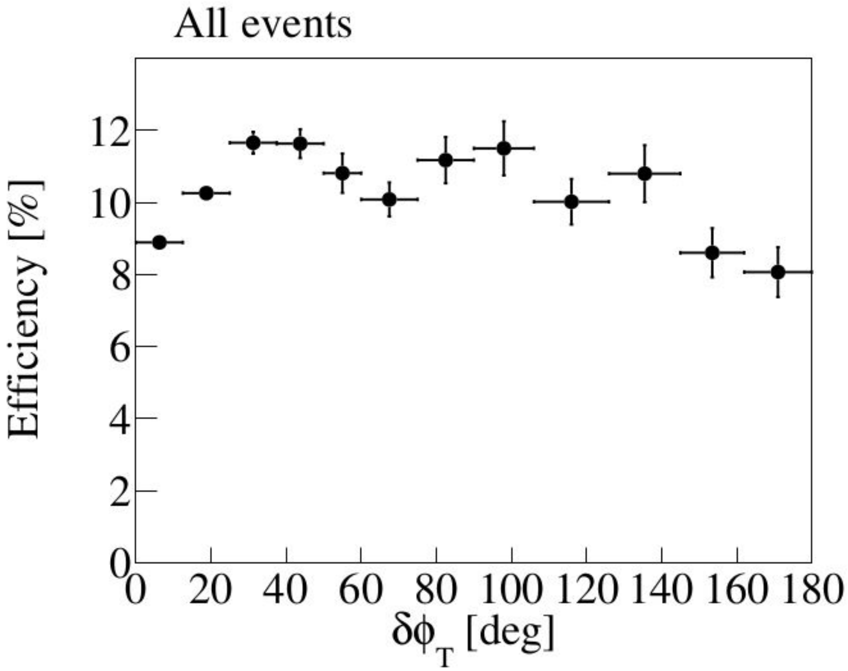
All events
Efficiency [%]
0
2
4
6
8
10
12
0 20 40 60 80 100 120 140 160 180
δφ_T [deg]

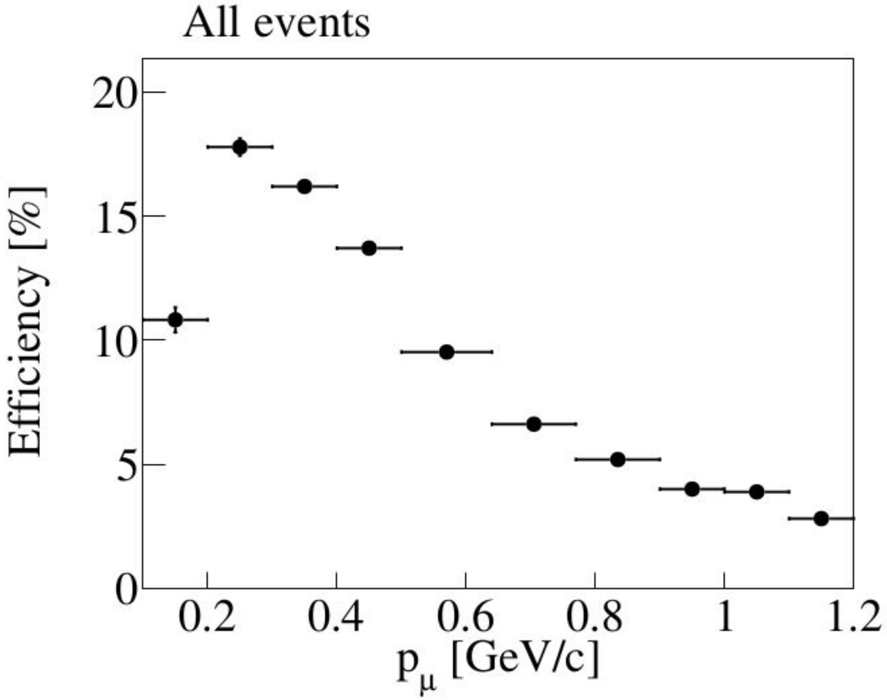
All events
Efficiency [%]
20
15
10
5
0
0.2
0.4
0.6
0.8
1
1.2
p_μ [GeV/c]

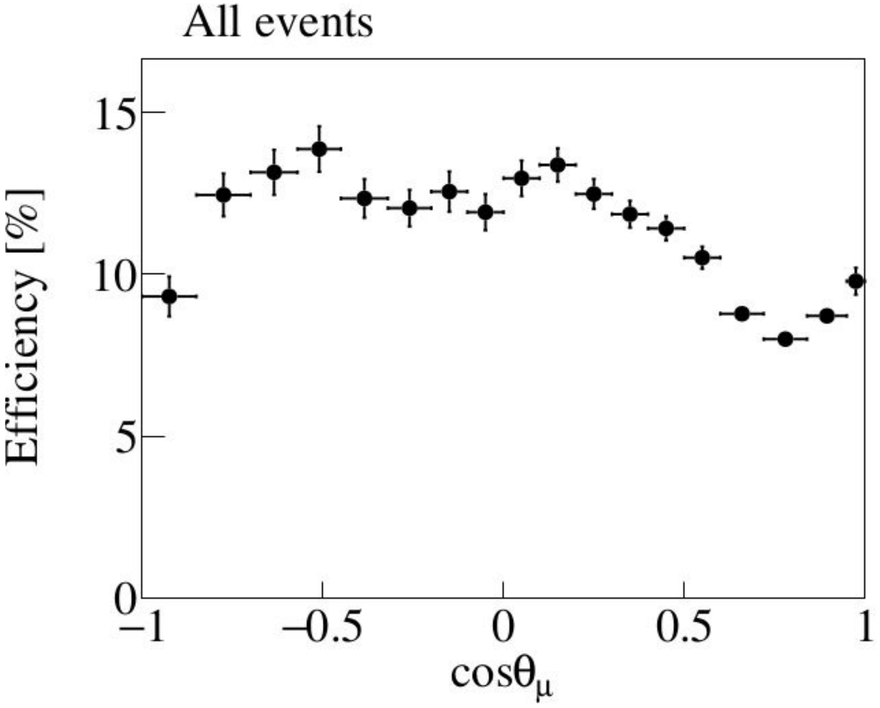
All events
Efficiency [%]
15
10
5
0
–1
–0.5
0
0.5
1
cosθ_μ

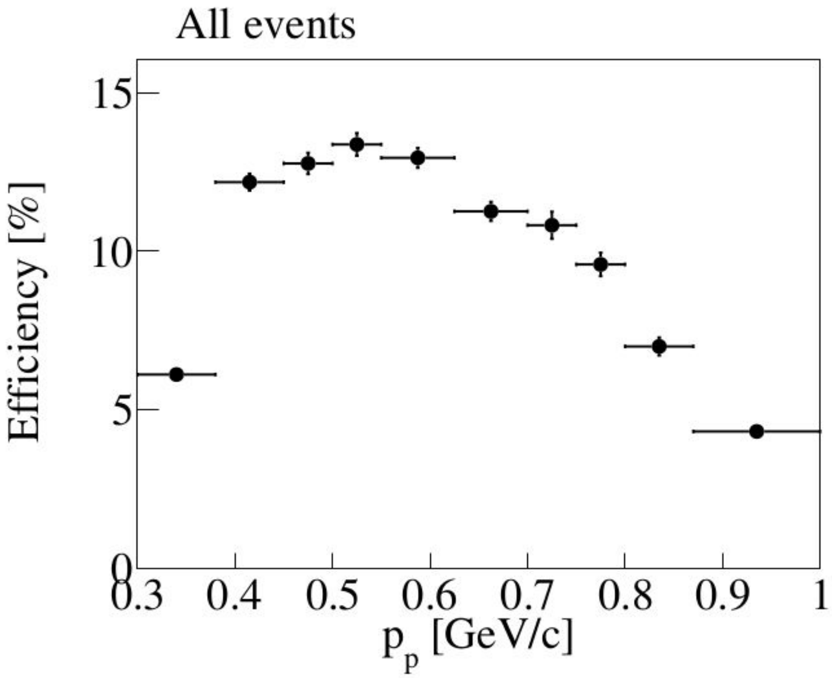
All events
Efficiency [%]
15
10
5
0
0.3
0.4
0.5
0.6
0.7
0.8
0.9
1
p_p [GeV/c]

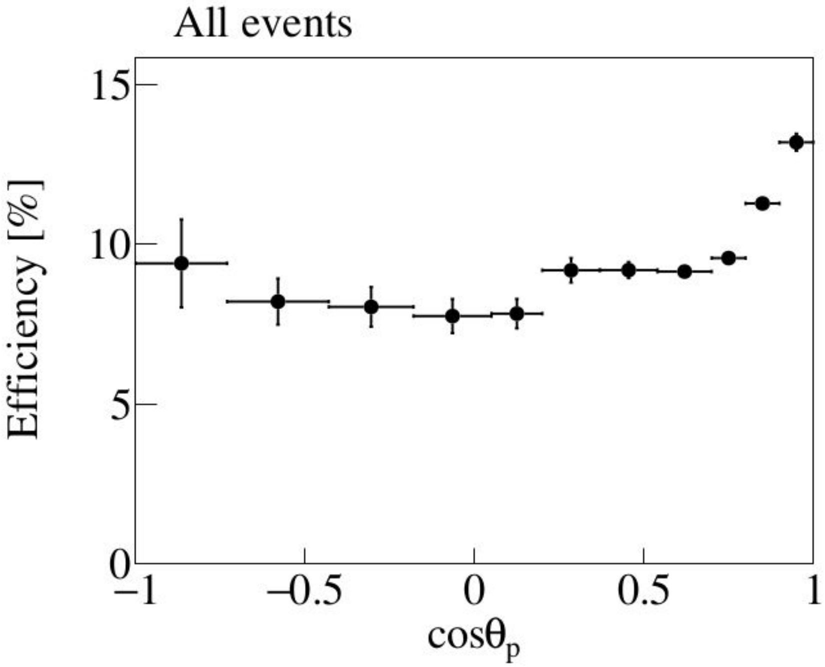
All events
Efficiency [%]
15
10
5
0
−1
−0.5
0
0.5
1
$\cos\theta_p$

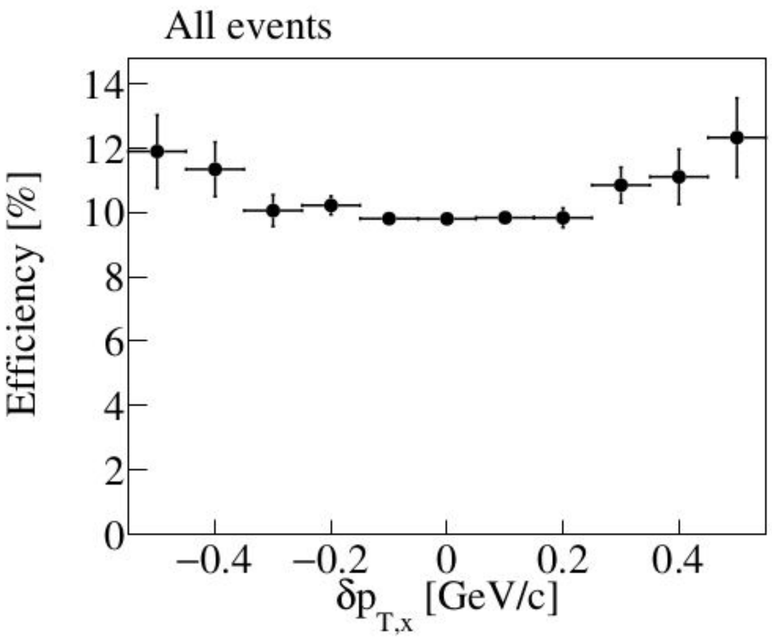
All events
Efficiency [%]
14
12
10
8
6
4
2
0
−0.4
−0.2
0
0.2
0.4
$\delta p_{T,x}$ [GeV/c]

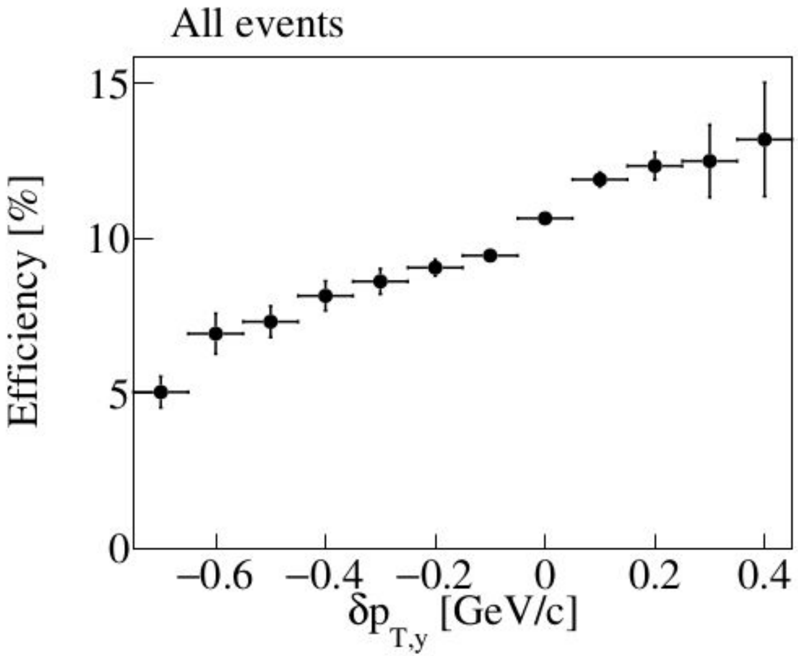
All events
Efficiency [%]
15
10
5
0
−0.6
−0.4
−0.2
0
0.2
0.4
$\delta p_{T,y}$ [GeV/c]

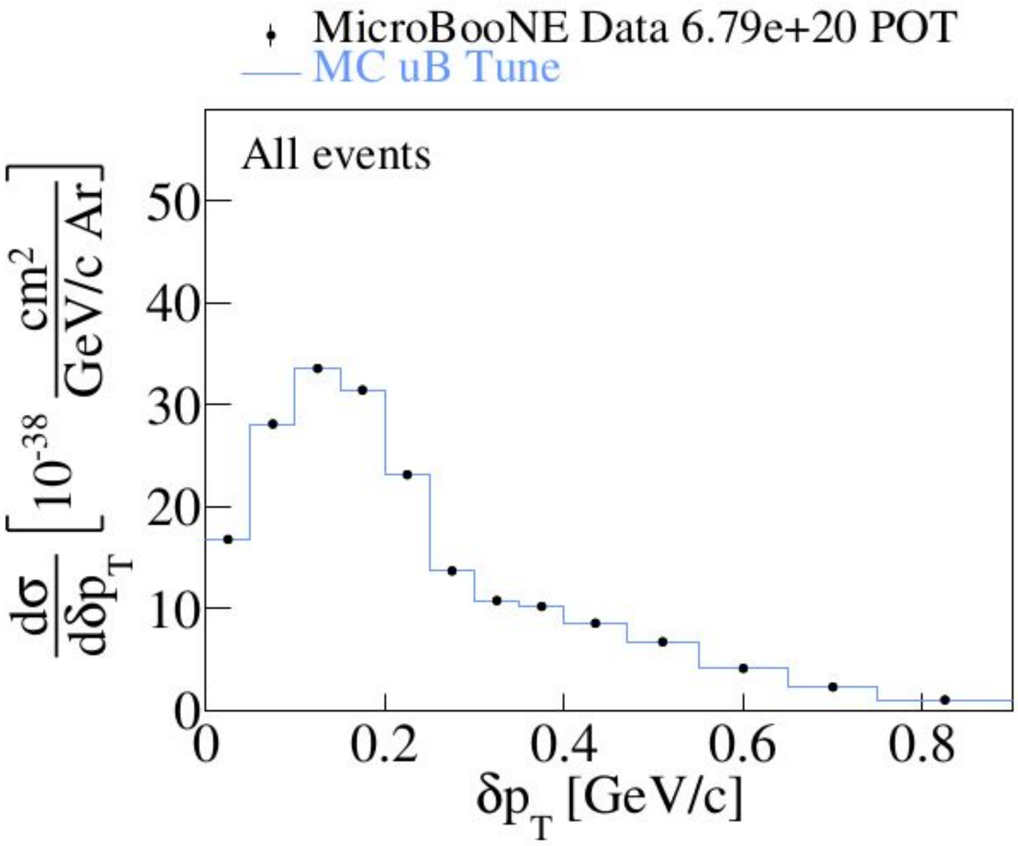

Figure 56: Closure test for δp_T.

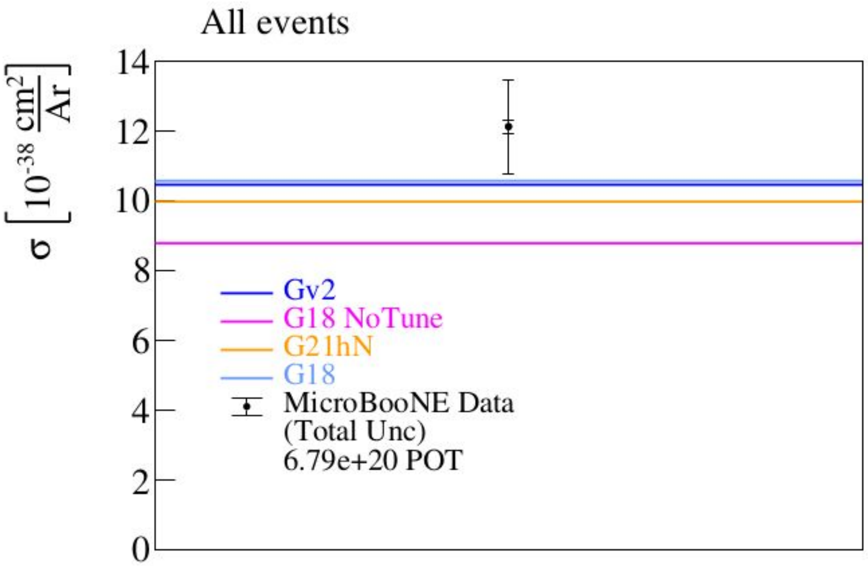
All events
$\sigma \left[10^{-38} \frac{cm^2}{Ar}\right]$
14
12
10
8
6
4
2
0
Gv2
G18 NoTune
G21hN
G18
MicroBooNE Data
(Total Unc)
6.79e+20 POT

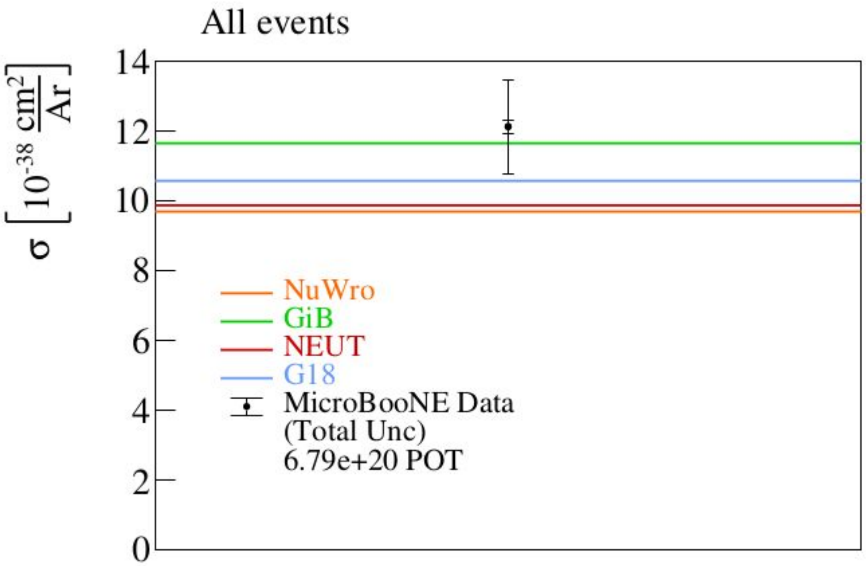
All events
$\sigma \left[10^{-38} \frac{cm^2}{Ar}\right]$
14
12
10
8
6
4
2
0
NuWro
GiB
NEUT
G18
MicroBooNE Data
(Total Unc)
6.79e+20 POT

Generalized Kinematic Imbalance (GKI)

Straightforward extension to 3D by considering longitudinal component of missing moment
However, an assumption on the incoming energy has to be made
First attempt in Phys. Rev. C 95, 065501 (2017) using CCQE interactions off a bound stationary neutron

Leveraging calorimetric energy estimator definition

$$E_{\mathrm{cal}} = E_\mu + K_p + B$$

to obtain the longitudinal component of missing momentum

$$p_L = p_L^\mu + p_L^p - E_{\mathrm{cal}}$$

and the energy transfer vector

$$\vec{q} = E_{\mathrm{cal}}\hat{z} - \vec{p}_\mu$$

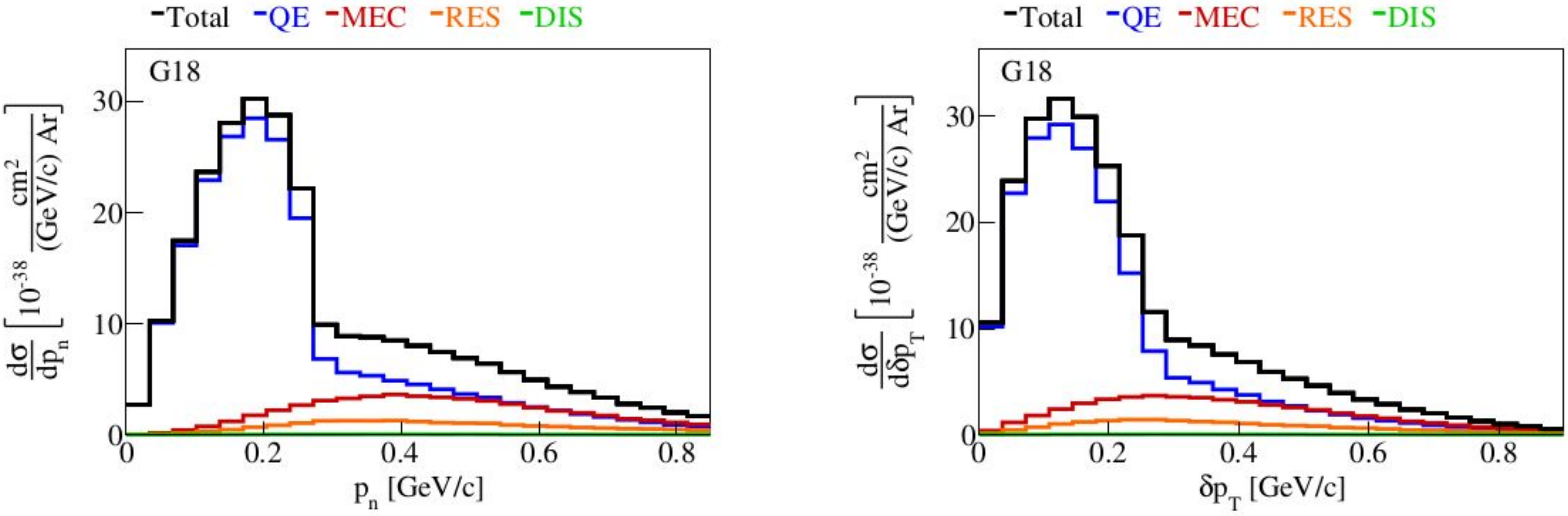
Total
QE
MEC
RES
DIS
G18
$\frac{d\sigma}{dp_n}$ $\left[10^{-38} \frac{cm^2}{(GeV/c)\ Ar}\right]$
p_n [GeV/c]
G18
$\frac{d\sigma}{d\delta p_T}$ $\left[10^{-38} \frac{cm^2}{(GeV/c)\ Ar}\right]$
δp_T [GeV/c]

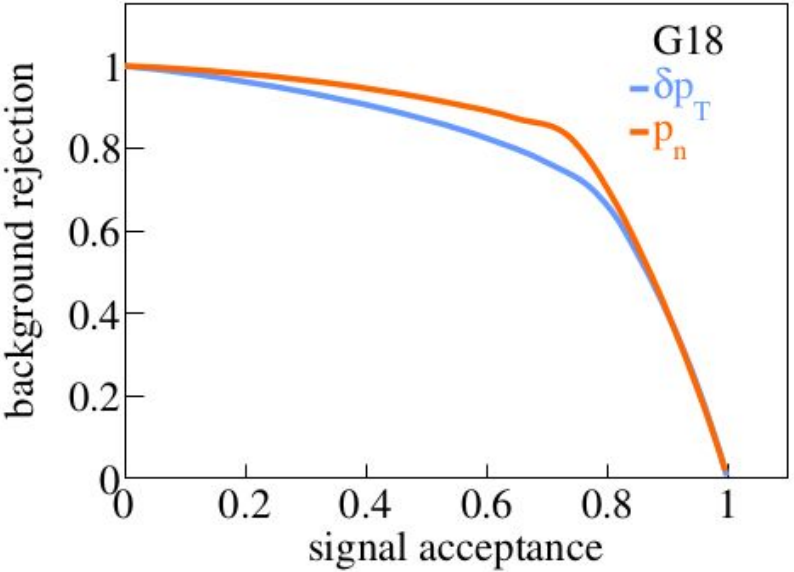
G18
δp_T
p_n
background rejection
signal acceptance
0
0.2
0.4
0.6
0.8
1

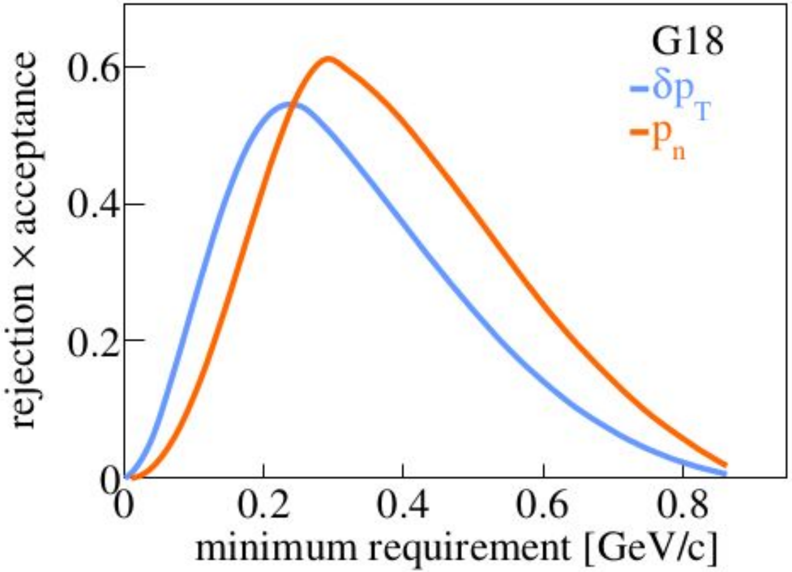
G18
δp_T
p_n
rejection × acceptance
minimum requirement [GeV/c]
0
0.2
0.4
0.6
0.8

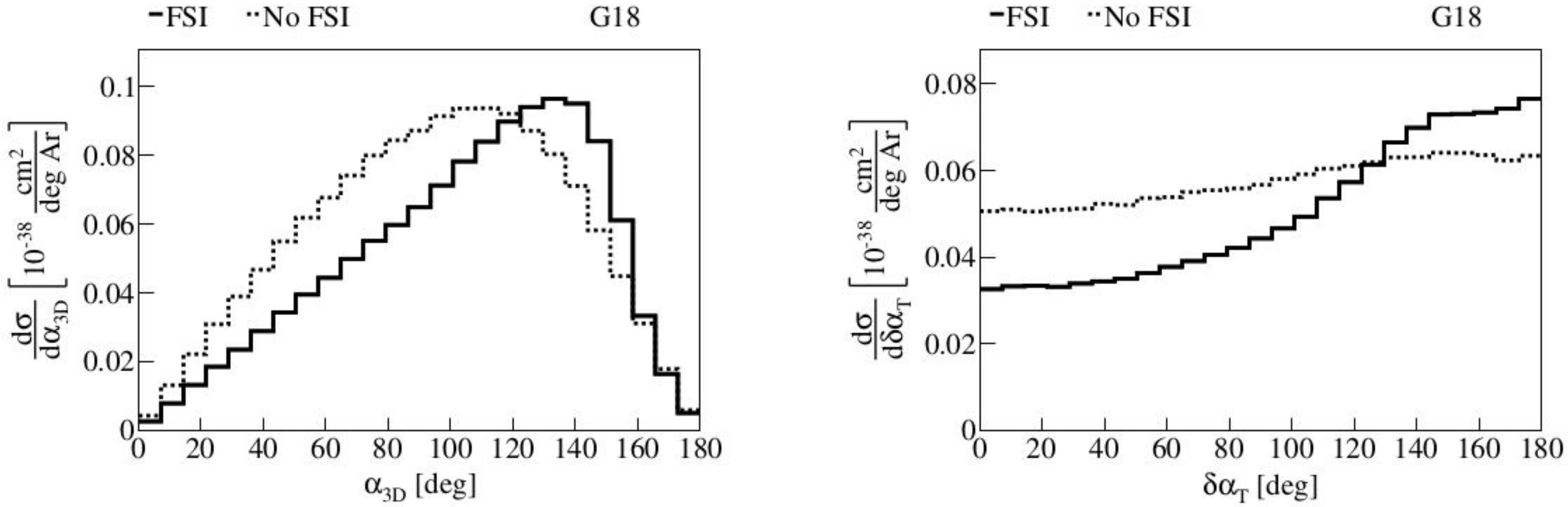

FSI
No FSI
G18
0.1
0.08
0.06
0.04
0.02
0
20
40
60
80
100
120
140
160
180
α_{3D} [deg]
$\frac{d\sigma}{d\alpha_{3D}}$ $\left[10^{-38}\ \frac{cm^2}{deg\ Ar}\right]$
FSI
No FSI
G18
0.08
0.06
0.04
0.02
0
20
40
60
80
100
120
140
160
180
$\delta\alpha_T$ [deg]
$\frac{d\sigma}{d\delta\alpha_T}$ $\left[10^{-38}\ \frac{cm^2}{deg\ Ar}\right]$

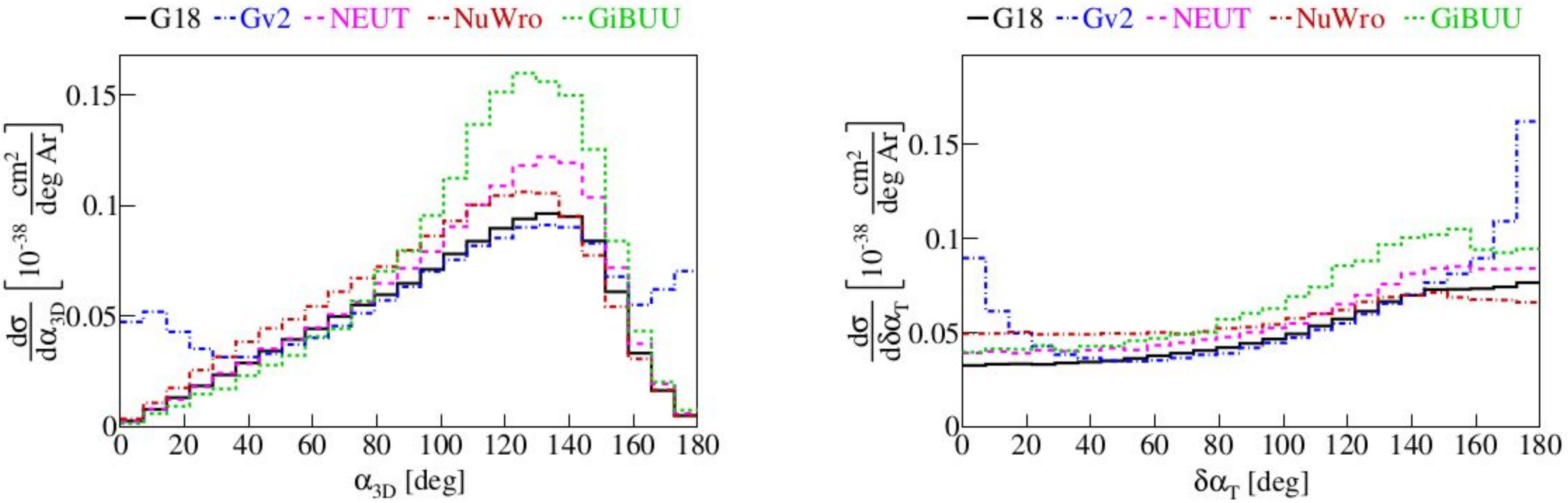

G18
Gv2
NEUT
NuWro
GiBUU
$\frac{d\sigma}{d\alpha_{3D}}$ $\left[10^{-38}\ \frac{cm^2}{deg\ Ar}\right]$
0
0.05
0.1
0.15
0
20
40
60
80
100
120
140
160
180
α_{3D} [deg]
G18
Gv2
NEUT
NuWro
GiBUU
$\frac{d\sigma}{d\delta\alpha_T}$ $\left[10^{-38}\ \frac{cm^2}{deg\ Ar}\right]$
0
0.05
0.1
0.15
0
20
40
60
80
100
120
140
160
180
$\delta\alpha_T$ [deg]

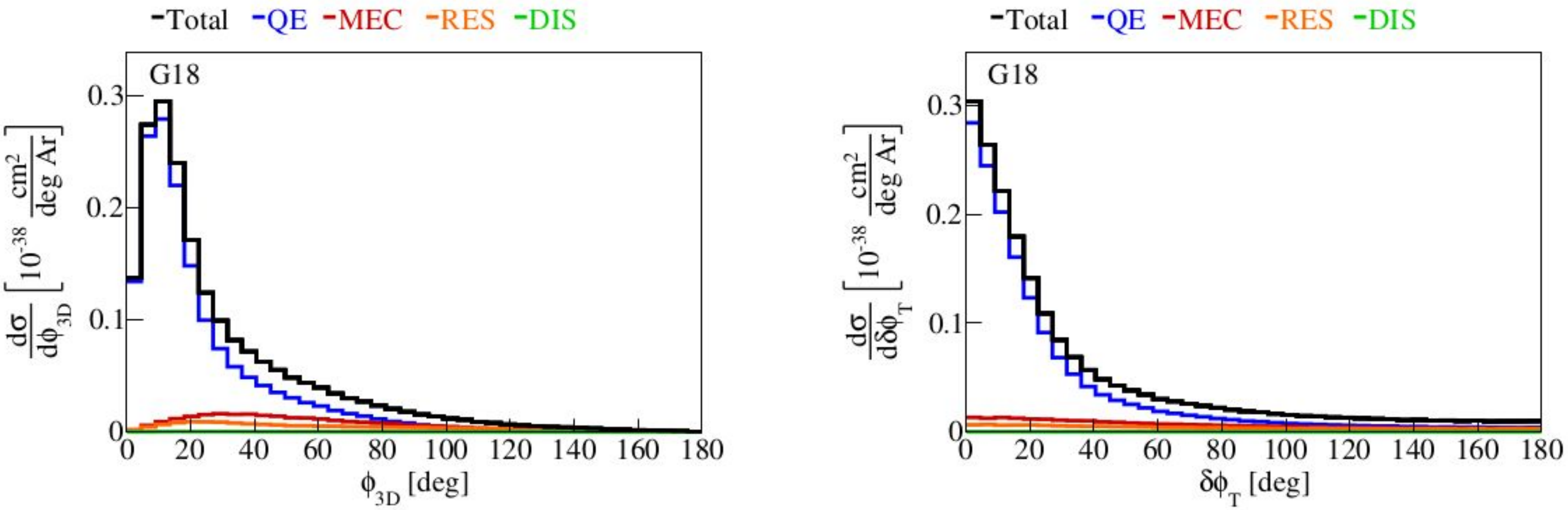

Total
QE
MEC
RES
DIS
G18
$\frac{d\sigma}{d\phi_{3D}}\left[10^{-38}\frac{cm^2}{deg\ Ar}\right]$
ϕ_{3D} [deg]
Total
QE
MEC
RES
DIS
G18
$\frac{d\sigma}{d\delta\phi_T}\left[10^{-38}\frac{cm^2}{deg\ Ar}\right]$
$\delta\phi_T$ [deg]

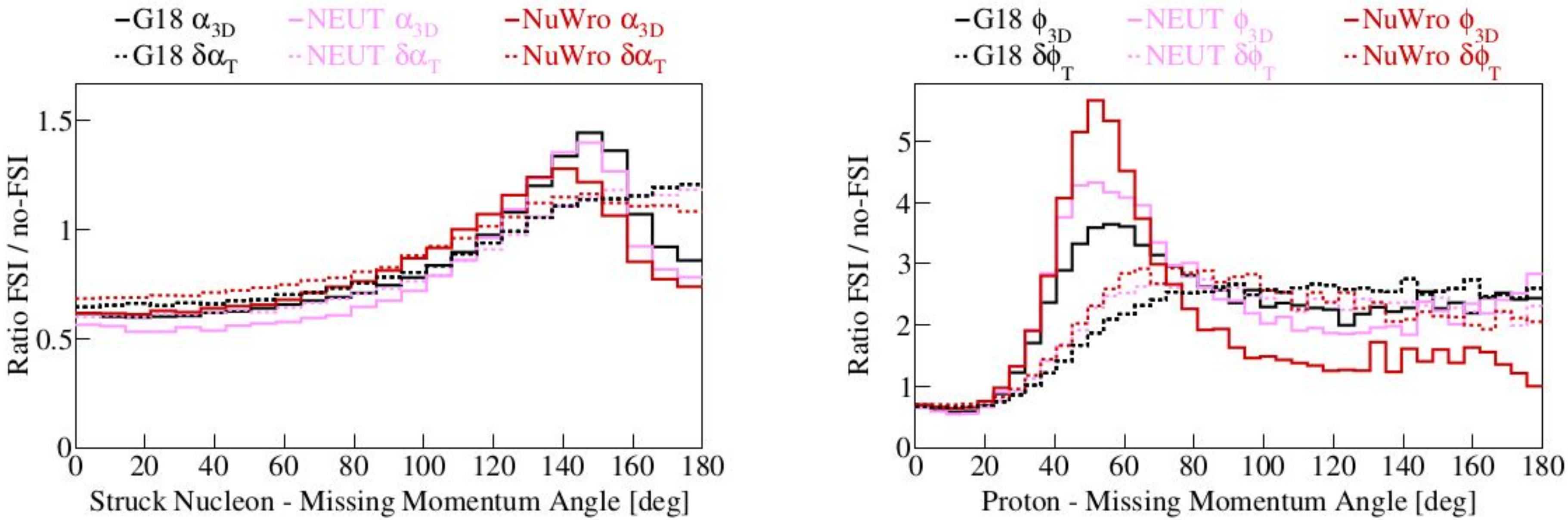

G18 α_{3D}
G18 $\delta\alpha_T$
NEUT α_{3D}
NEUT $\delta\alpha_T$
NuWro α_{3D}
NuWro $\delta\alpha_T$
Ratio FSI / no-FSI
Struck Nucleon - Missing Momentum Angle [deg]
G18 ϕ_{3D}
G18 $\delta\phi_T$
NEUT ϕ_{3D}
NEUT $\delta\phi_T$
NuWro ϕ_{3D}
NuWro $\delta\phi_T$
Ratio FSI / no-FSI
Proton - Missing Momentum Angle [deg]

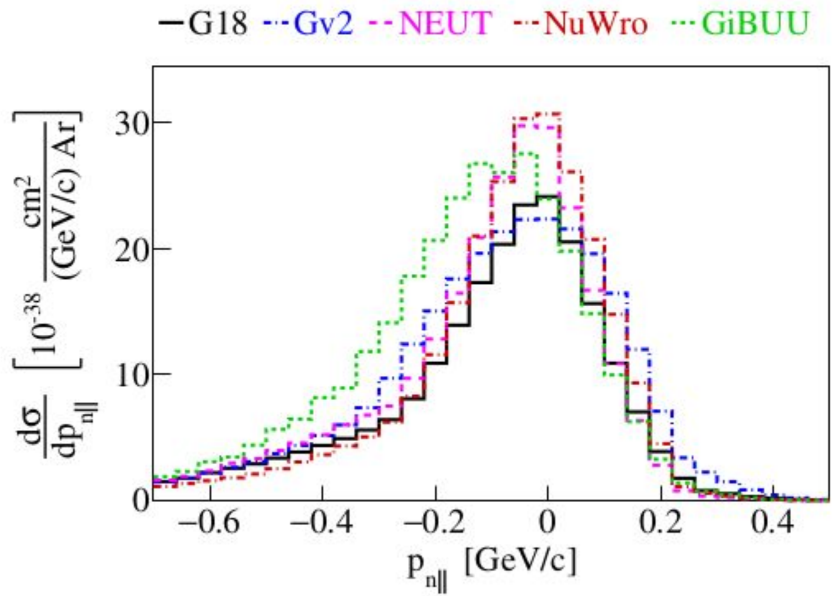

G18 Gv2 NEUT NuWro GiBUU
$\frac{d\sigma}{dp_{n\parallel}}$ $\left[10^{-38} \frac{cm^2}{(GeV/c)\ Ar}\right]$
0
10
20
30
−0.6
−0.4
−0.2
0
0.2
0.4
$p_{n\parallel}$ [GeV/c]

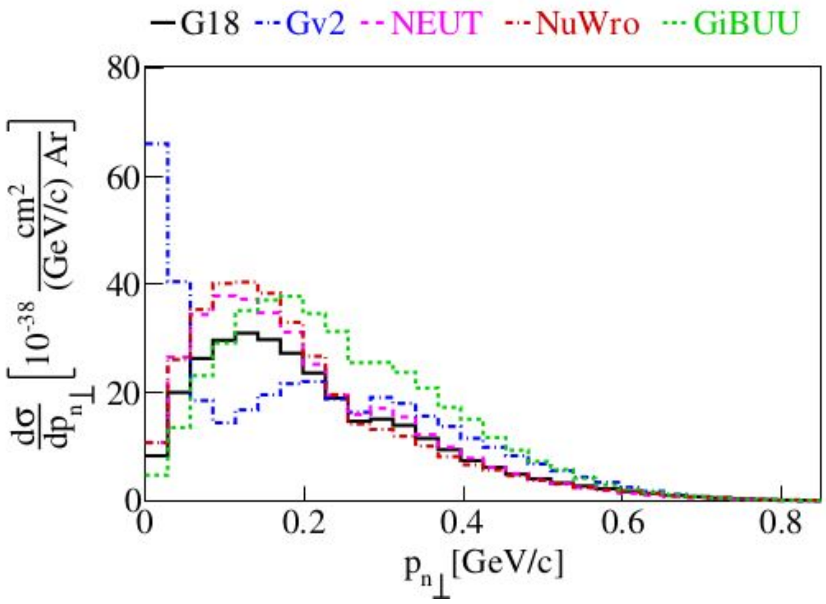

G18 Gv2 NEUT NuWro GiBUU
$\frac{d\sigma}{dp_{n\perp}}$ $\left[10^{-38} \frac{cm^2}{(GeV/c)\ Ar}\right]$
0
20
40
60
80
0
0.2
0.4
0.6
0.8
$p_{n\perp}$ [GeV/c]

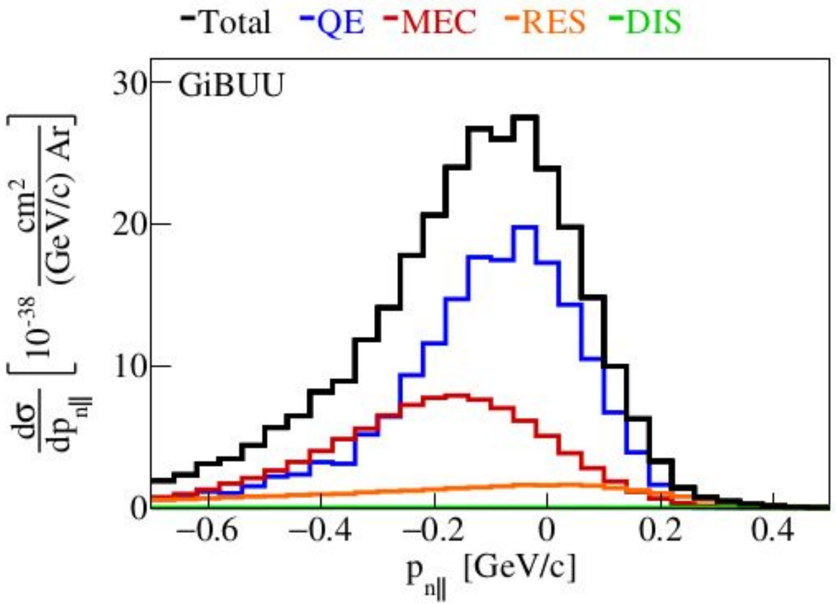

Total
QE
MEC
RES
DIS
GiBUU
$\frac{d\sigma}{dp_{n\parallel}}$ $\left[10^{-38} \frac{cm^2}{(GeV/c)\ Ar}\right]$
30
20
10
0
−0.6
−0.4
−0.2
0
0.2
0.4
$p_{n\parallel}$ [GeV/c]

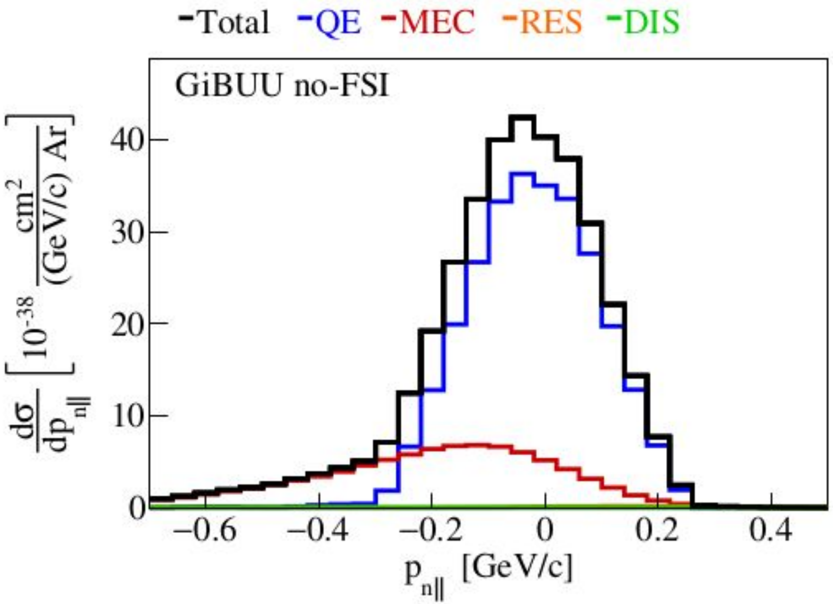

Total
QE
MEC
RES
DIS
GiBUU no-FSI
$\frac{d\sigma}{dp_{n\parallel}}$ $\left[10^{-38} \frac{cm^2}{(GeV/c)\ Ar}\right]$
40
30
20
10
0
−0.6
−0.4
−0.2
0
0.2
0.4
$p_{n\parallel}$ [GeV/c]

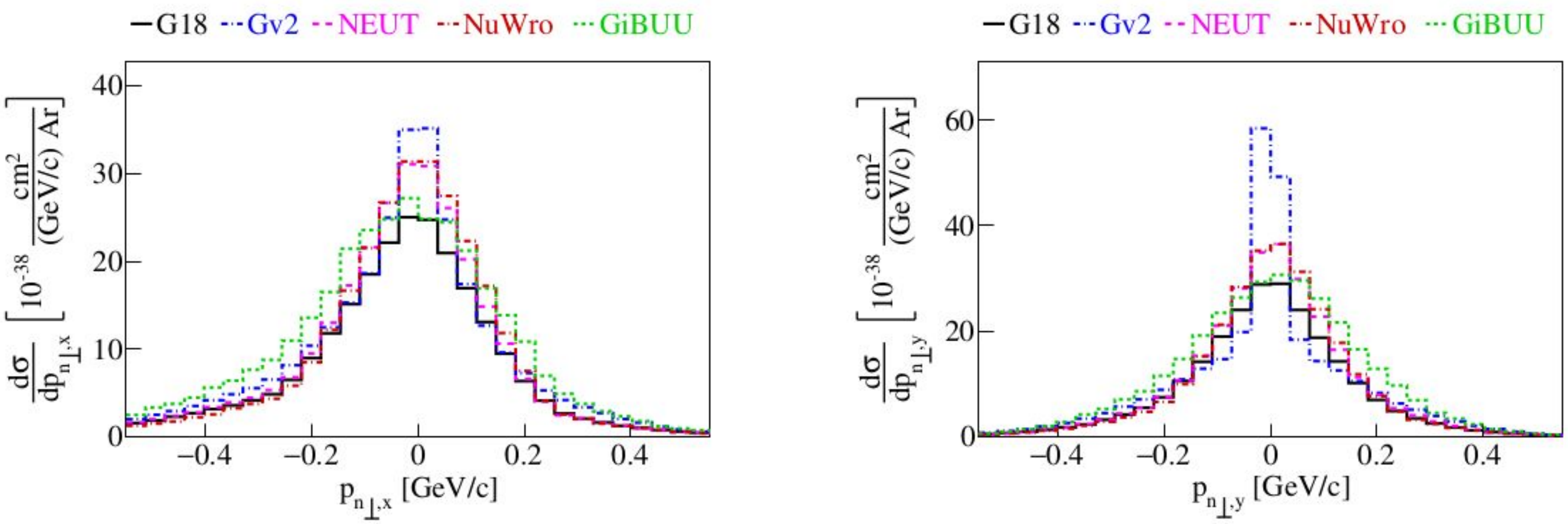

G18 Gv2 NEUT NuWro GiBUU
$\frac{d\sigma}{dp_{n\perp,x}}$ $\left[10^{-38}\frac{cm^2}{(GeV/c)\ Ar}\right]$
$p_{n\perp,x}$ [GeV/c]
G18 Gv2 NEUT NuWro GiBUU
$\frac{d\sigma}{dp_{n\perp,y}}$ $\left[10^{-38}\frac{cm^2}{(GeV/c)\ Ar}\right]$
$p_{n\perp,y}$ [GeV/c]

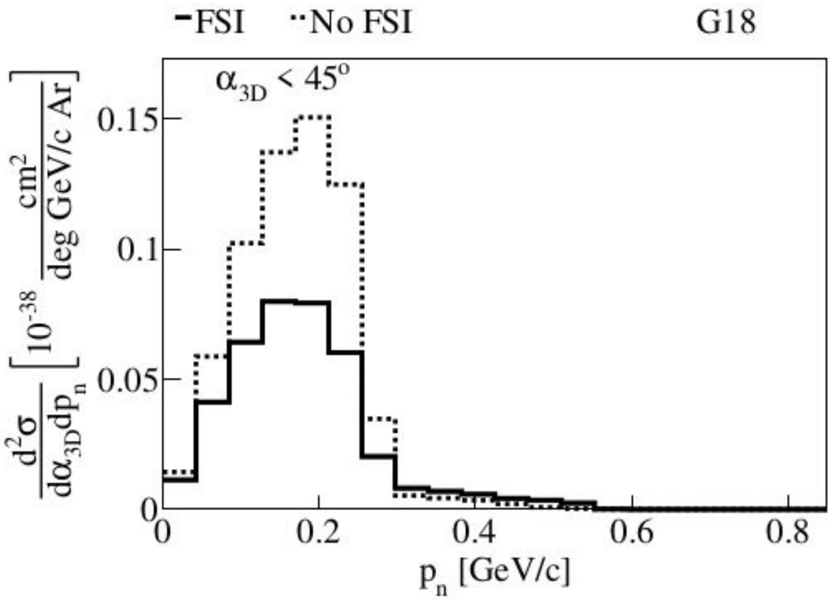

FSI
No FSI
G18
α_{3D} < 45°
$\frac{d^2\sigma}{d\alpha_{3D}dp_n}$ $\left[10^{-38} \frac{cm^2}{deg\ GeV/c\ Ar}\right]$
0
0.05
0.1
0.15
0
0.2
0.4
0.6
0.8
p_n [GeV/c]

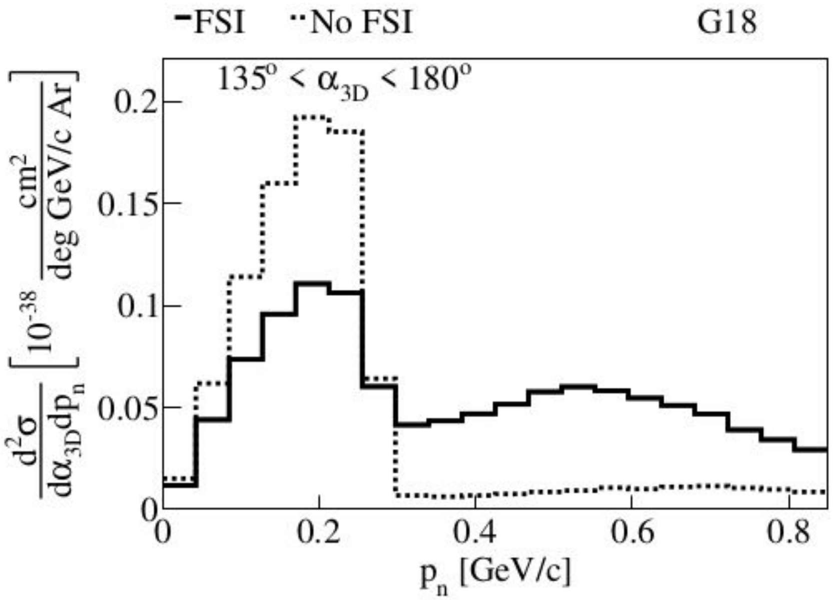

FSI
No FSI
G18
135° < α_{3D} < 180°
$\frac{d^2\sigma}{d\alpha_{3D}dp_n}$ $\left[10^{-38} \frac{cm^2}{deg\ GeV/c\ Ar}\right]$
0
0.05
0.1
0.15
0.2
0
0.2
0.4
0.6
0.8
p_n [GeV/c]

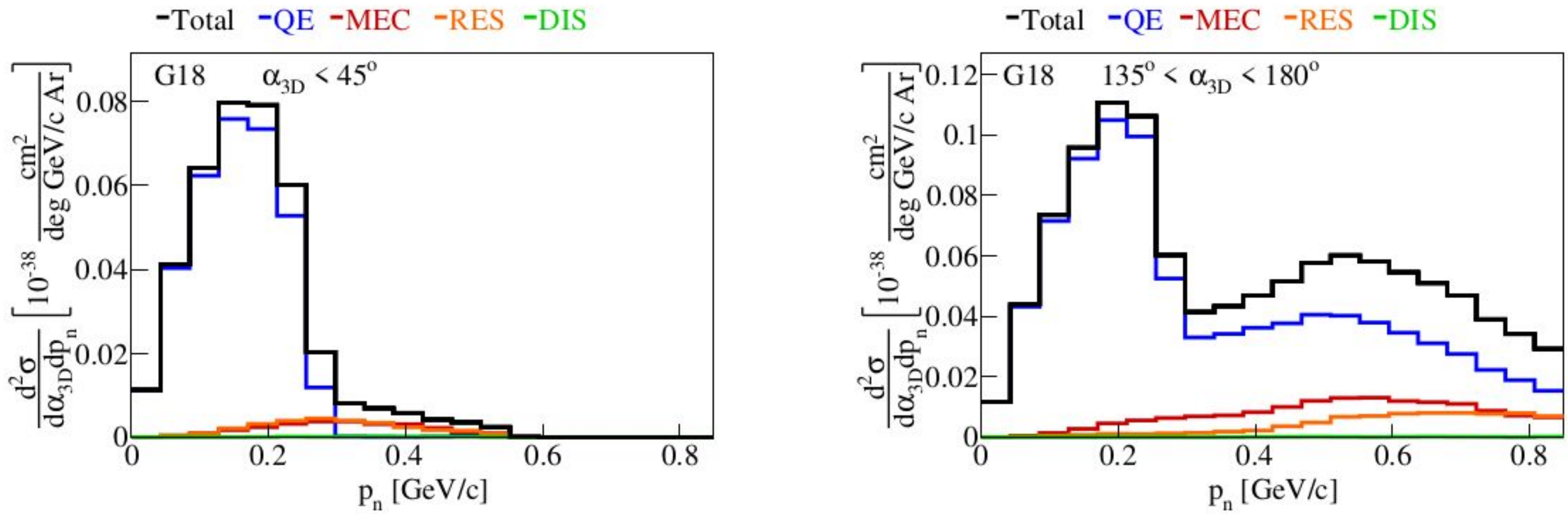

Total
QE
MEC
RES
DIS
G18
$\alpha_{3D} < 45^o$
$\frac{d^2\sigma}{d\alpha_{3D}dp_n} \left[10^{-38} \frac{cm^2}{deg\ GeV/c\ Ar}\right]$
0
0.02
0.04
0.06
0.08
0.2
0.4
0.6
0.8
p_n [GeV/c]
Total
QE
MEC
RES
DIS
G18
$135^o < \alpha_{3D} < 180^o$
$\frac{d^2\sigma}{d\alpha_{3D}dp_n} \left[10^{-38} \frac{cm^2}{deg\ GeV/c\ Ar}\right]$
0
0.02
0.04
0.06
0.08
0.1
0.12
0.2
0.4
0.6
0.8
p_n [GeV/c]

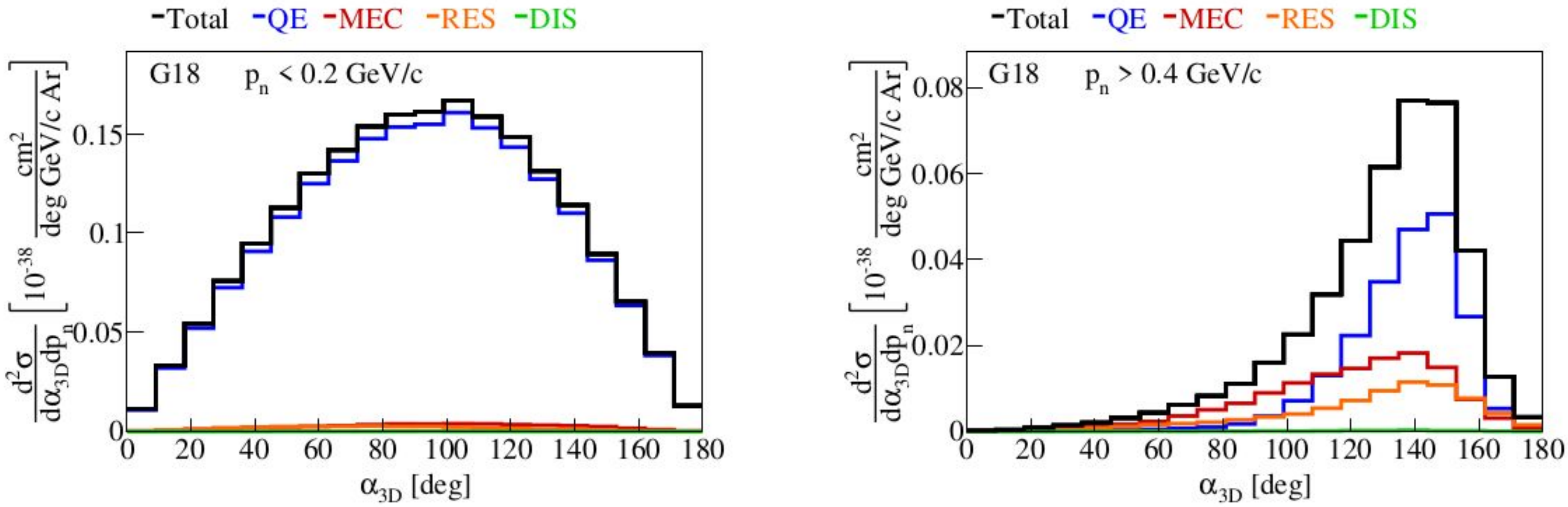

Total
QE
MEC
RES
DIS
G18
p_n < 0.2 GeV/c
$\frac{d^2\sigma}{d\alpha_{3D}dp_n}$ $\left[10^{-38} \frac{cm^2}{deg\ GeV/c\ Ar}\right]$
α_{3D} [deg]
G18
p_n > 0.4 GeV/c

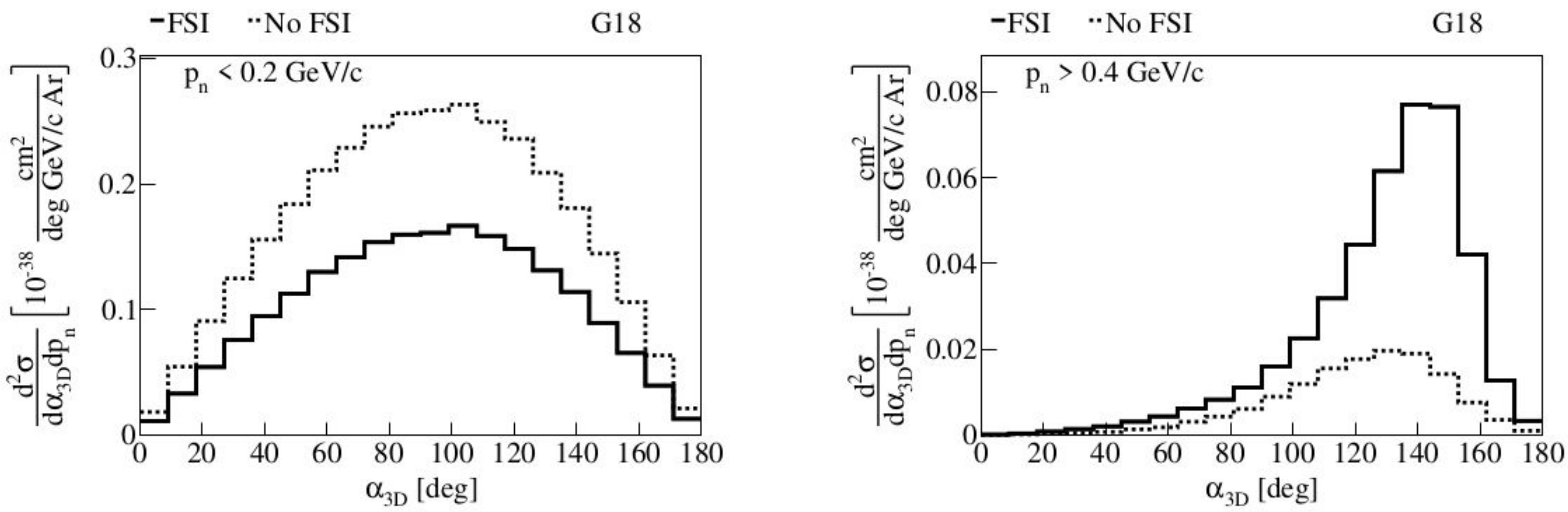

FSI
No FSI
G18
$p_n < 0.2$ GeV/c
$\frac{d^2\sigma}{d\alpha_{3D}dp_n}$ $\left[10^{-38} \frac{cm^2}{deg\ GeV/c\ Ar}\right]$
α_{3D} [deg]
FSI
No FSI
G18
$p_n > 0.4$ GeV/c
$\frac{d^2\sigma}{d\alpha_{3D}dp_n}$ $\left[10^{-38} \frac{cm^2}{deg\ GeV/c\ Ar}\right]$
α_{3D} [deg]

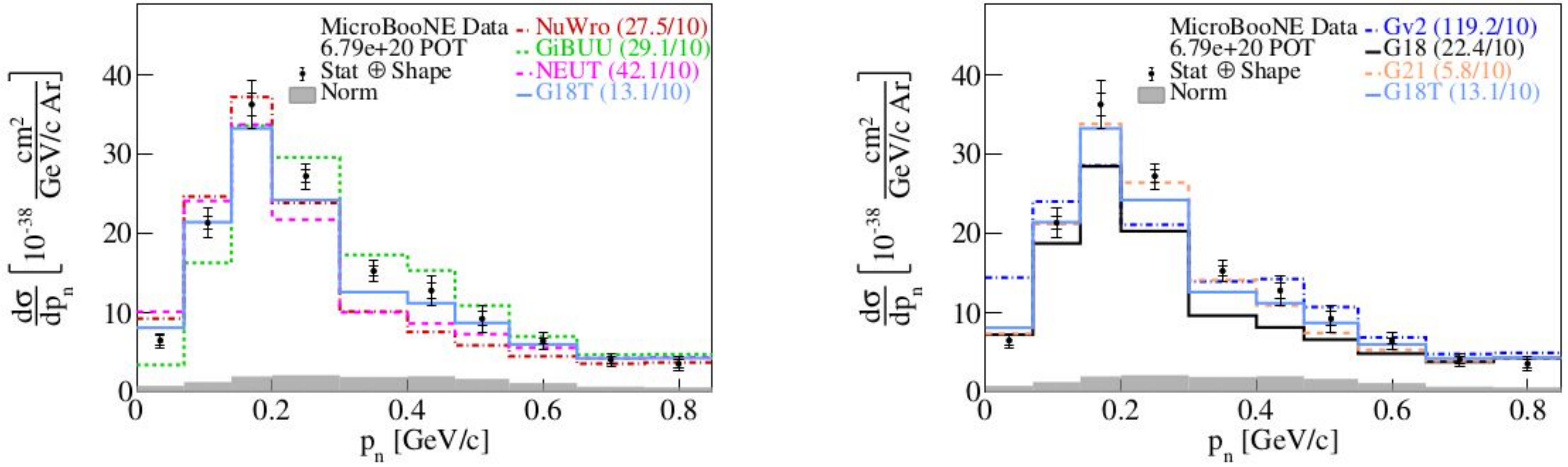

MicroBooNE Data
6.79e+20 POT
Stat ⊕ Shape
Norm
NuWro (27.5/10)
GiBUU (29.1/10)
NEUT (42.1/10)
G18T (13.1/10)
$\frac{d\sigma}{dp_n}$ $\left[10^{-38} \frac{cm^2}{GeV/c\ Ar}\right]$
p_n [GeV/c]
MicroBooNE Data
6.79e+20 POT
Stat ⊕ Shape
Norm
Gv2 (119.2/10)
G18 (22.4/10)
G21 (5.8/10)
G18T (13.1/10)
$\frac{d\sigma}{dp_n}$ $\left[10^{-38} \frac{cm^2}{GeV/c\ Ar}\right]$
p_n [GeV/c]

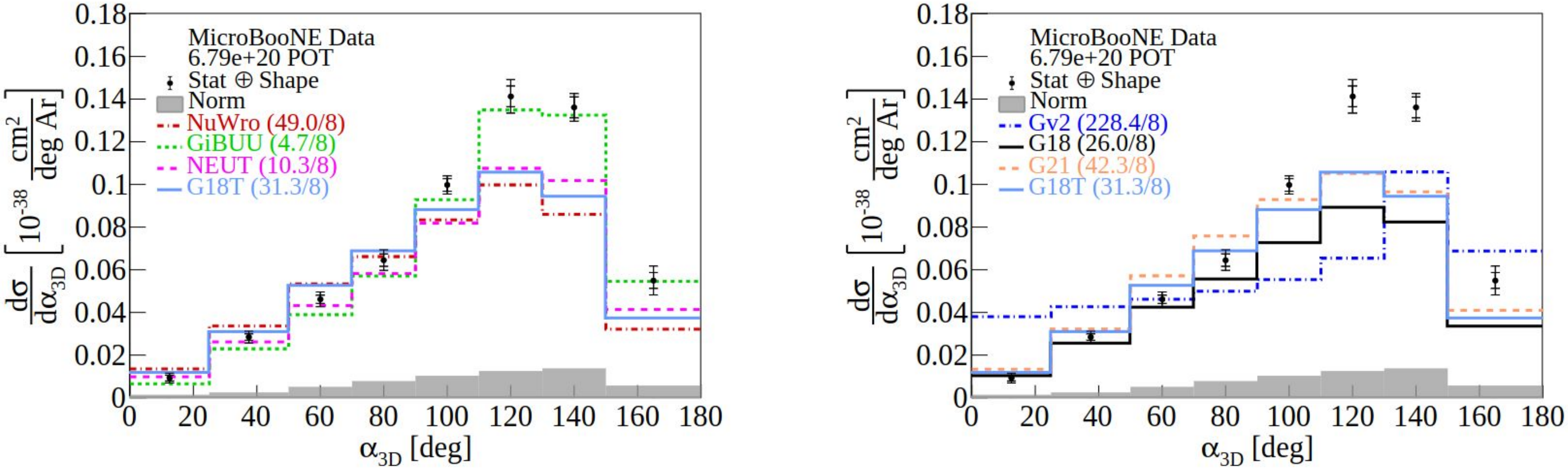
MicroBooNE Data
6.79e+20 POT
Stat ⊕ Shape
Norm
NuWro (49.0/8)
GiBUU (4.7/8)
NEUT (10.3/8)
G18T (31.3/8)
Gv2 (228.4/8)
G18 (26.0/8)
G21 (42.3/8)
$\frac{d\sigma}{d\alpha_{3D}}$ $\left[10^{-38} \frac{cm^2}{deg\ Ar}\right]$
α_{3D} [deg]

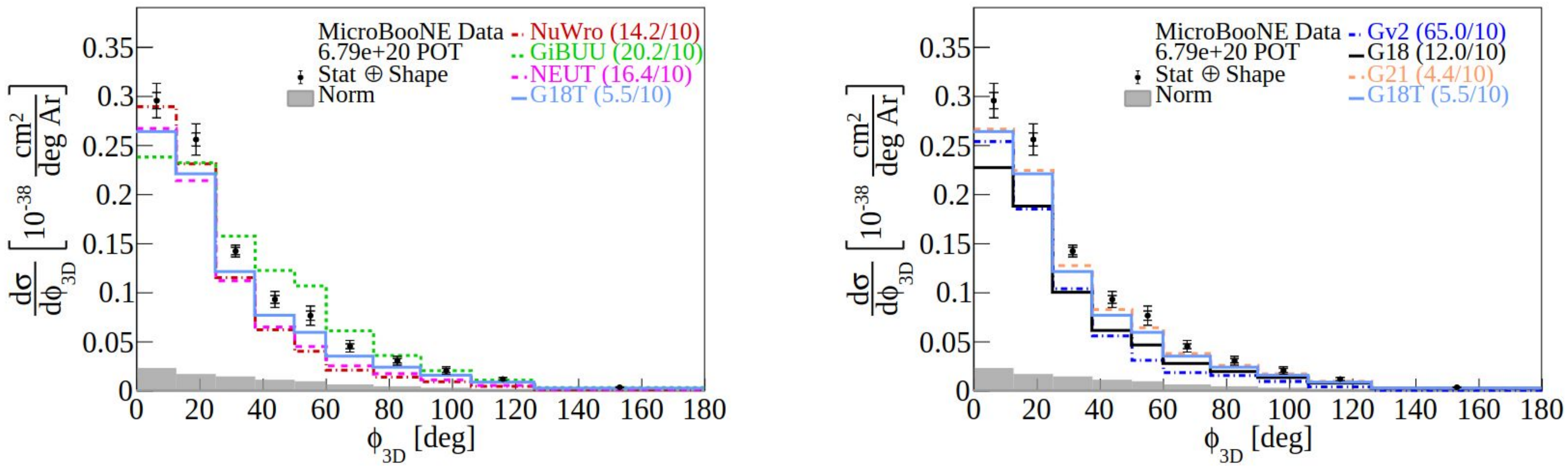
MicroBooNE Data
6.79e+20 POT
Stat ⊕ Shape
Norm
NuWro (14.2/10)
GiBUU (20.2/10)
NEUT (16.4/10)
G18T (5.5/10)
Gv2 (65.0/10)
G18 (12.0/10)
G21 (4.4/10)
$\frac{d\sigma}{d\phi_{3D}} \left[10^{-38} \frac{cm^2}{deg\ Ar}\right]$
ϕ_{3D} [deg]

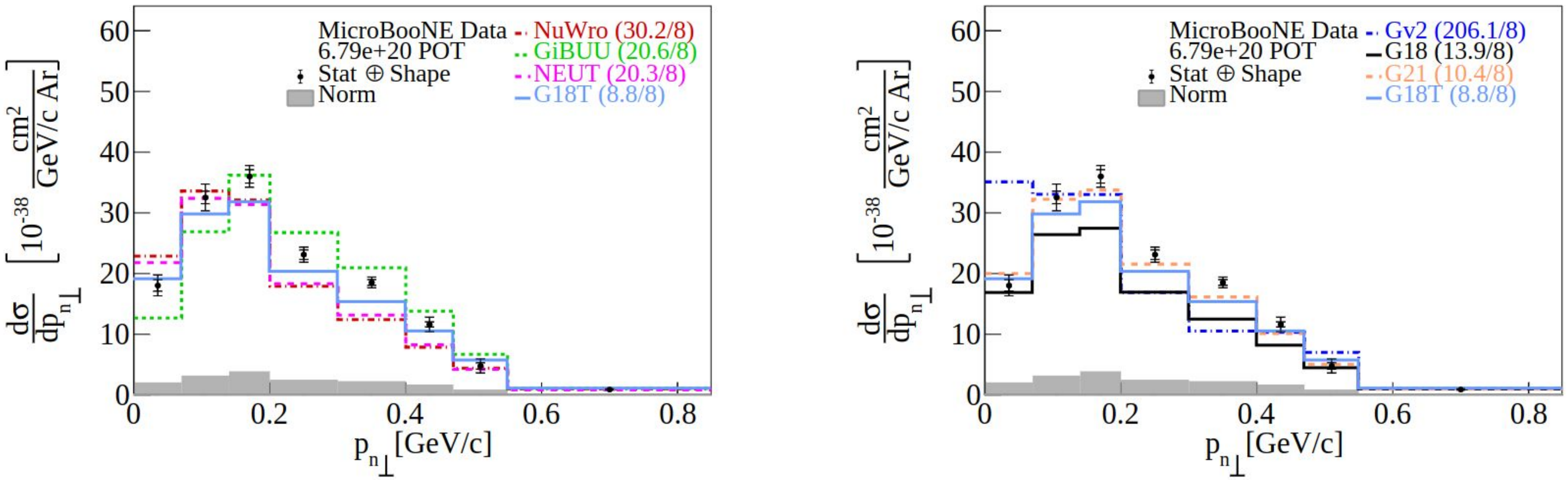

MicroBooNE Data
6.79e+20 POT
Stat ⊕ Shape
Norm
NuWro (30.2/8)
GiBUU (20.6/8)
NEUT (20.3/8)
G18T (8.8/8)
Gv2 (206.1/8)
G18 (13.9/8)
G21 (10.4/8)
G18T (8.8/8)
$\frac{d\sigma}{dp_{n\perp}}$ $\left[10^{-38} \frac{cm^2}{GeV/c\ Ar}\right]$
$p_{n\perp}$ [GeV/c]

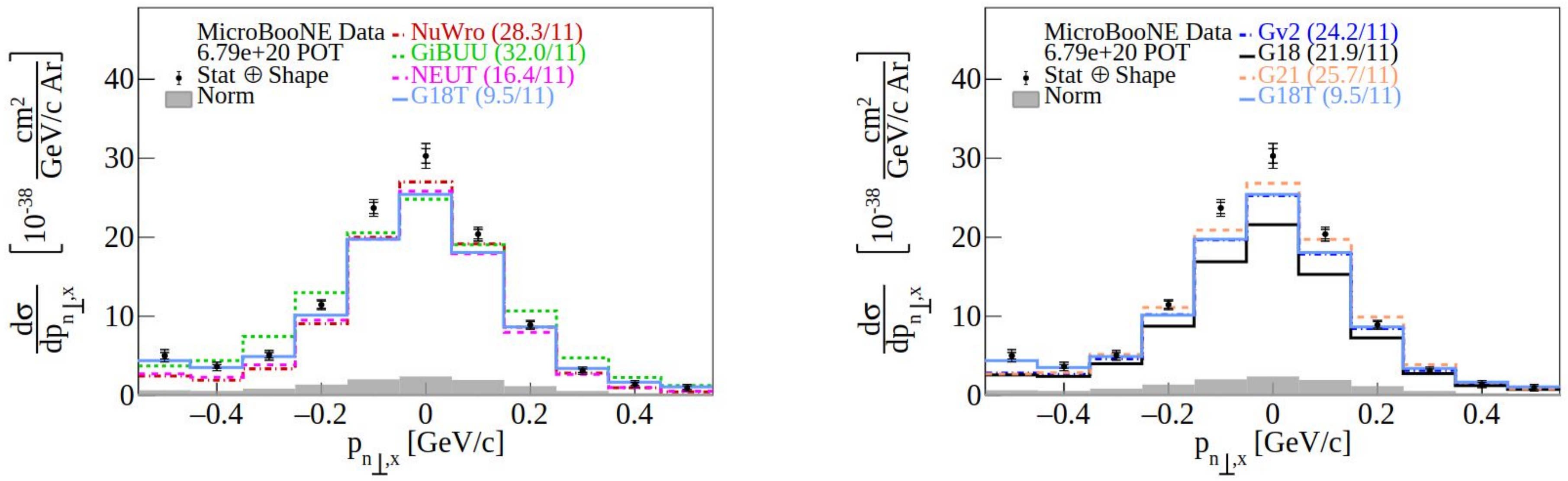
MicroBooNE Data
6.79e+20 POT
Stat ⊕ Shape
Norm
NuWro (28.3/11)
GiBUU (32.0/11)
NEUT (16.4/11)
G18T (9.5/11)
Gv2 (24.2/11)
G18 (21.9/11)
G21 (25.7/11)
$\frac{d\sigma}{dp_{n\perp,x}}$ $\left[10^{-38} \frac{cm^2}{GeV/c\ Ar}\right]$
$p_{n\perp,x}$ [GeV/c]

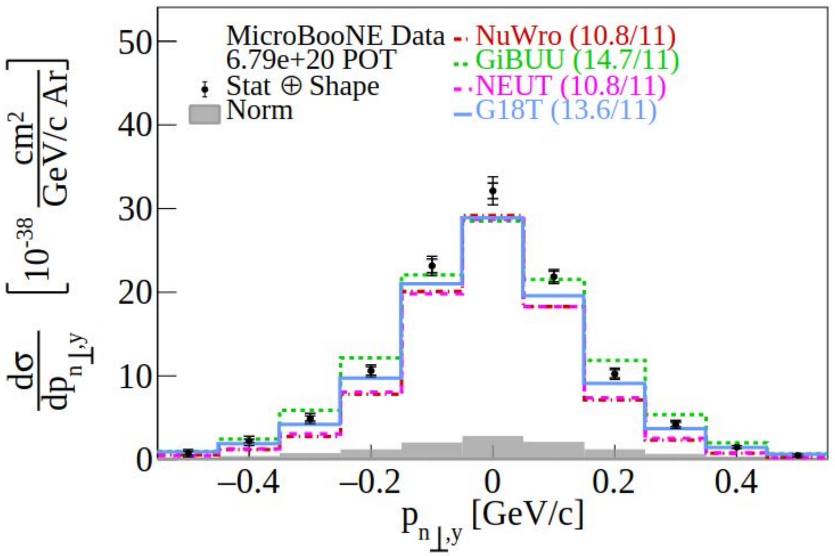

MicroBooNE Data
6.79e+20 POT
Stat ⊕ Shape
Norm
NuWro (10.8/11)
GiBUU (14.7/11)
NEUT (10.8/11)
G18T (13.6/11)
$\frac{d\sigma}{dp_{n\perp,y}}$ $\left[10^{-38} \frac{cm^2}{GeV/c\ Ar}\right]$
$p_{n\perp,y}$ [GeV/c]

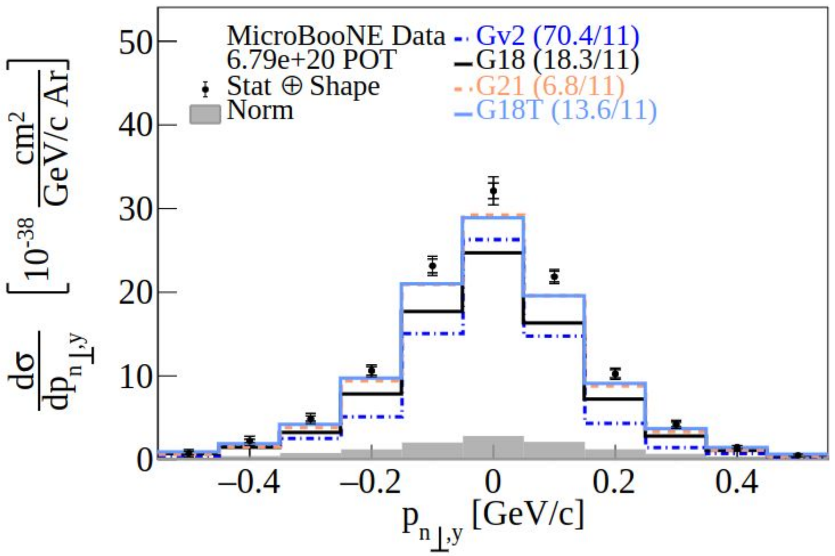

MicroBooNE Data
6.79e+20 POT
Stat ⊕ Shape
Norm
Gv2 (70.4/11)
G18 (18.3/11)
G21 (6.8/11)
G18T (13.6/11)
$\frac{d\sigma}{dp_{n\perp,y}}$ $\left[10^{-38} \frac{cm^2}{GeV/c\ Ar}\right]$
$p_{n\perp,y}$ [GeV/c]

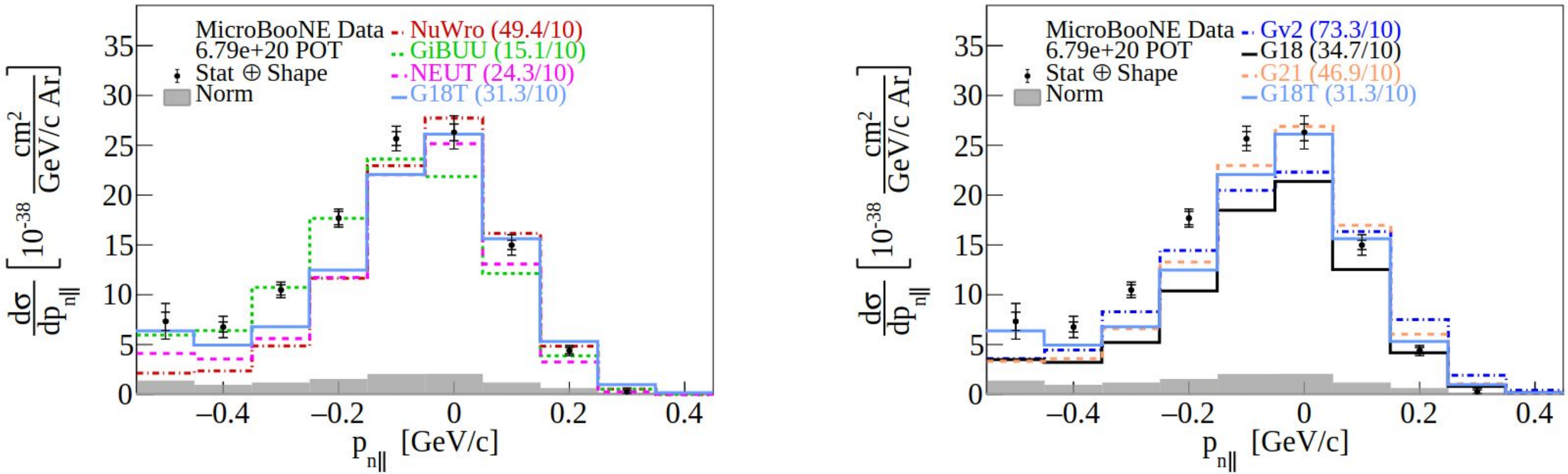
MicroBooNE Data
6.79e+20 POT
Stat ⊕ Shape
Norm
NuWro (49.4/10)
GiBUU (15.1/10)
NEUT (24.3/10)
G18T (31.3/10)
Gv2 (73.3/10)
G18 (34.7/10)
G21 (46.9/10)
G18T (31.3/10)
$\frac{d\sigma}{dp_{n\|}}$ $\left[10^{-38}\frac{cm^2}{GeV/c\ Ar}\right]$
$p_{n\|}$ [GeV/c]

Into the GKI multiverse!

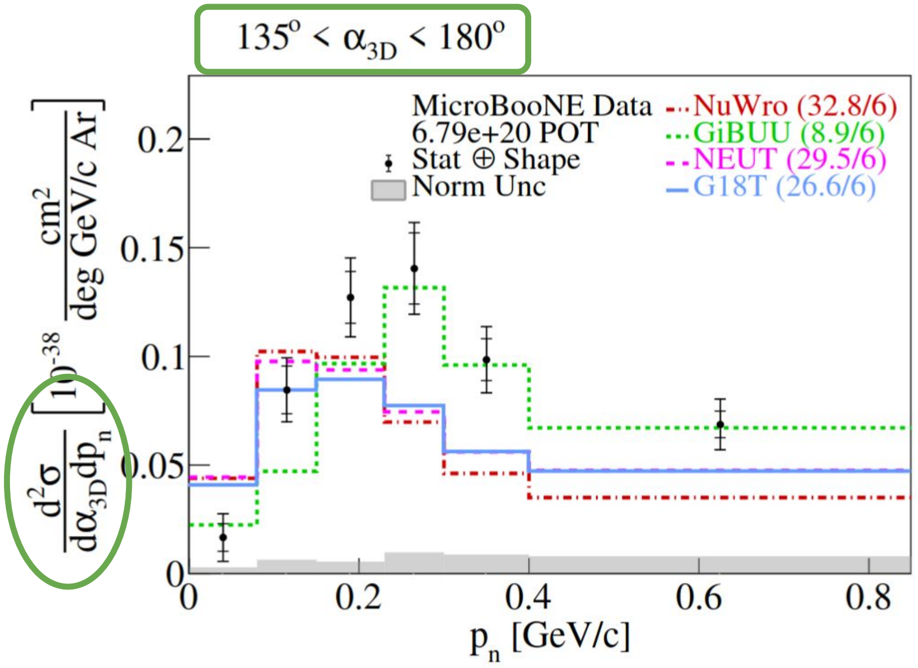

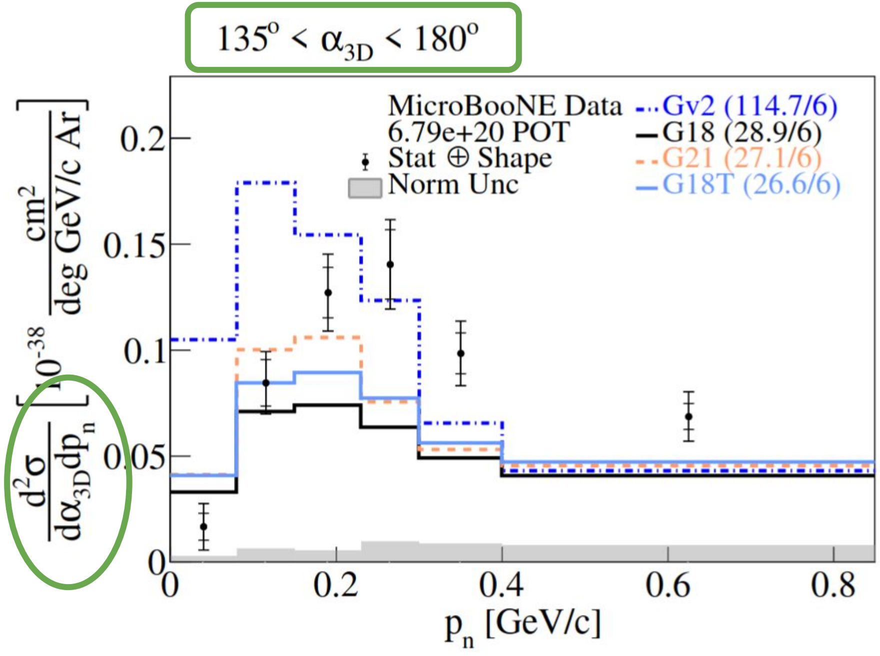

- Extended tail to higher values
- FSI-dominated region

- GiBUU shift to the right, yet lowest χ^2
- Gv2 yields worst agreement
- Other generators yield comparable ratios

arXiv:2310.06082

Into the GKI multiverse!

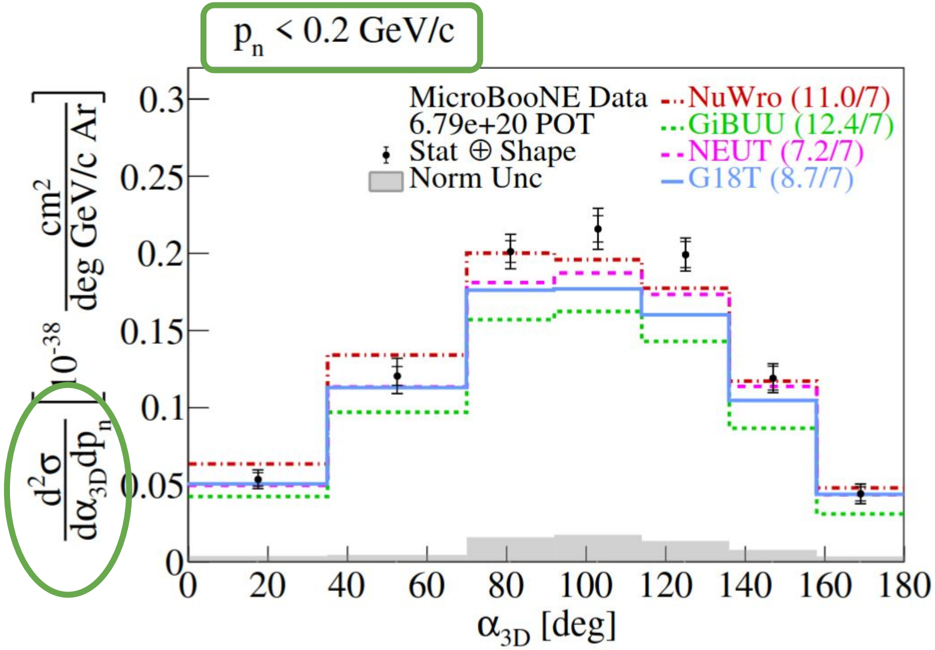

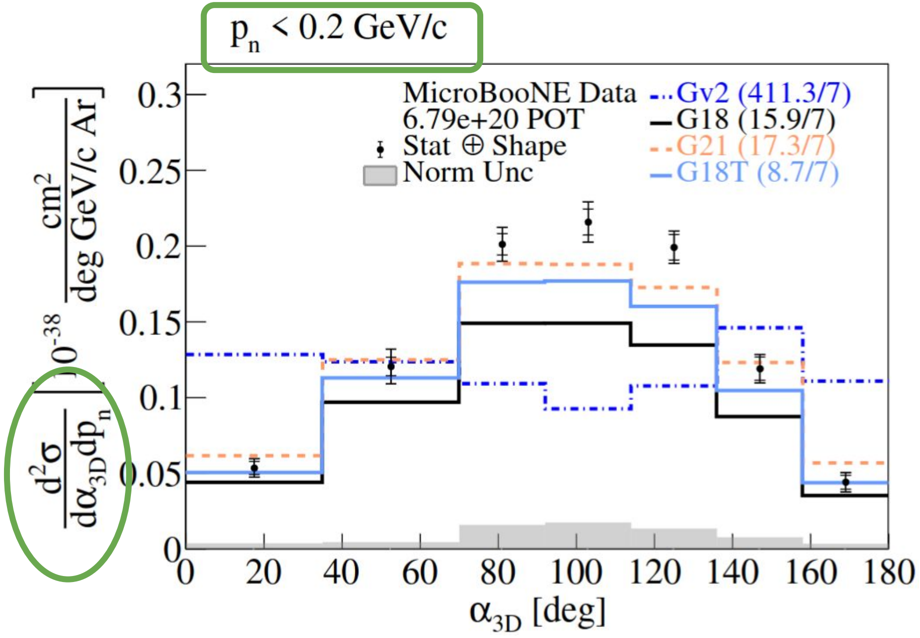

- QE-dominated region
- Most generators result in comparable results

- Gv2 yields worst agreement
- G18T results in good agreement

arXiv:2310.06082

Why electrons?

- Common vector current
- Identical nuclear effects

- Monoenergetic beams
- High statistics
  - Precision measurements

Any model must work for electrons,
or it won't work for neutrinos !

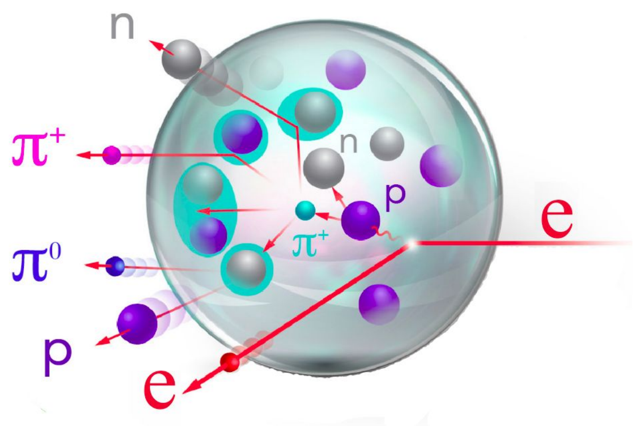

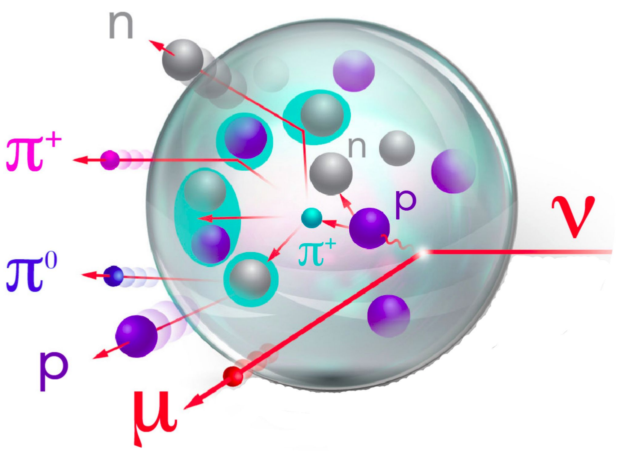

Similar ν & e Distributions

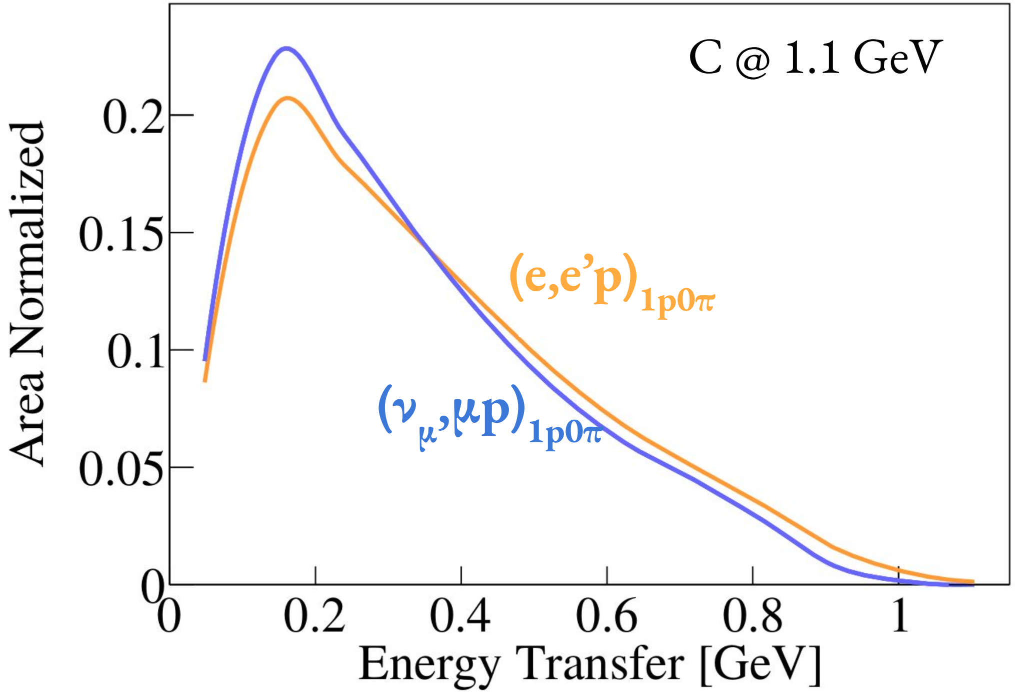

Accounting for propagator mass (γ vs W) via Q^4 scaling of the electron side

Phys. Rev. D 103, 113003 (2021)

Jefferson Laboratory

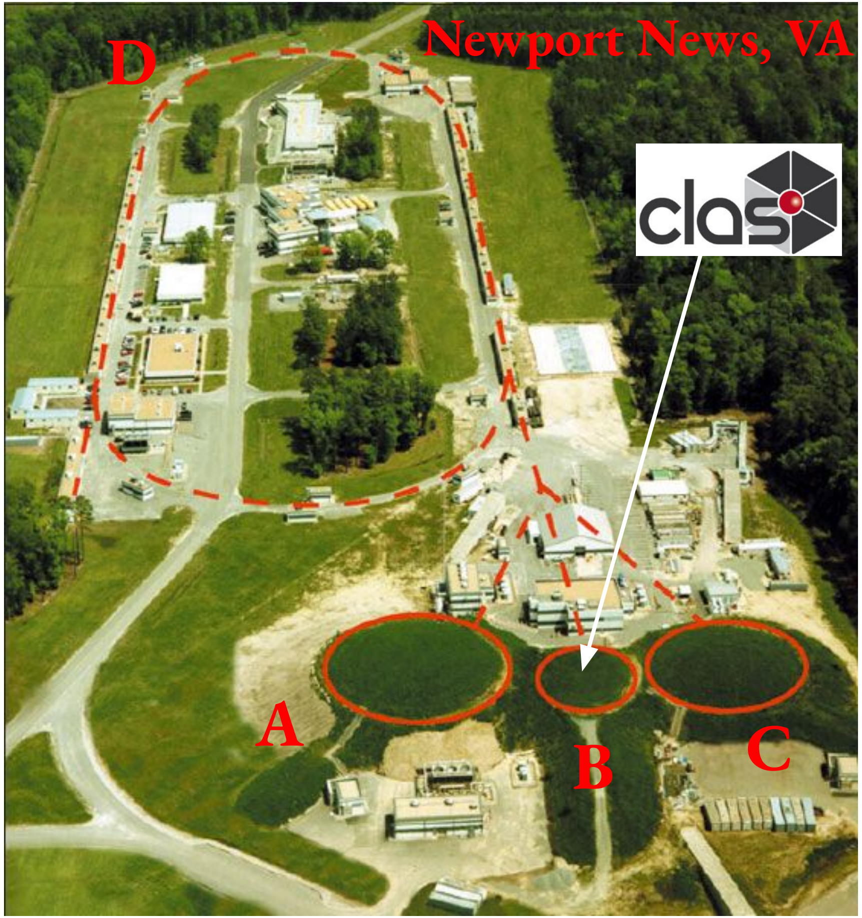

- Electron beam accelerator facility
- Energies up to 12 GeV
- Using Hall B & CLAS detector

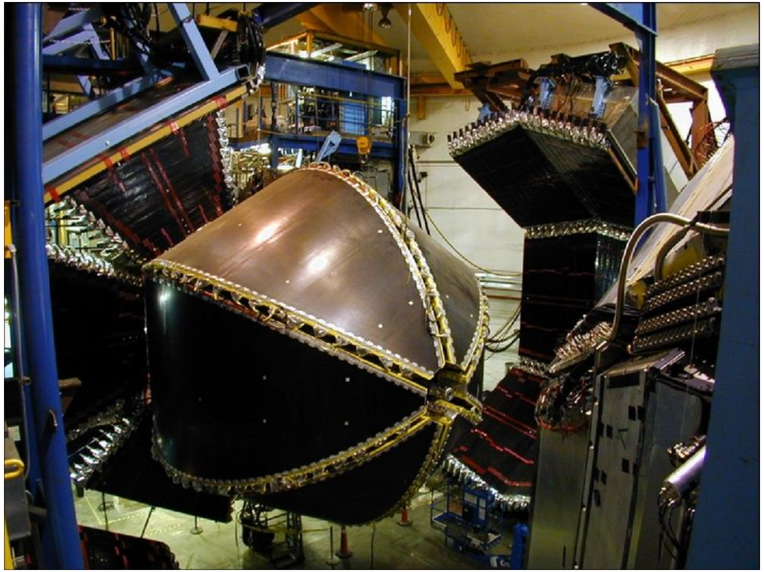

e4ν Data-Mining With CLAS

- Charged particle threshold similar to ν tracking detectors
- ~50% of "4π" coverage

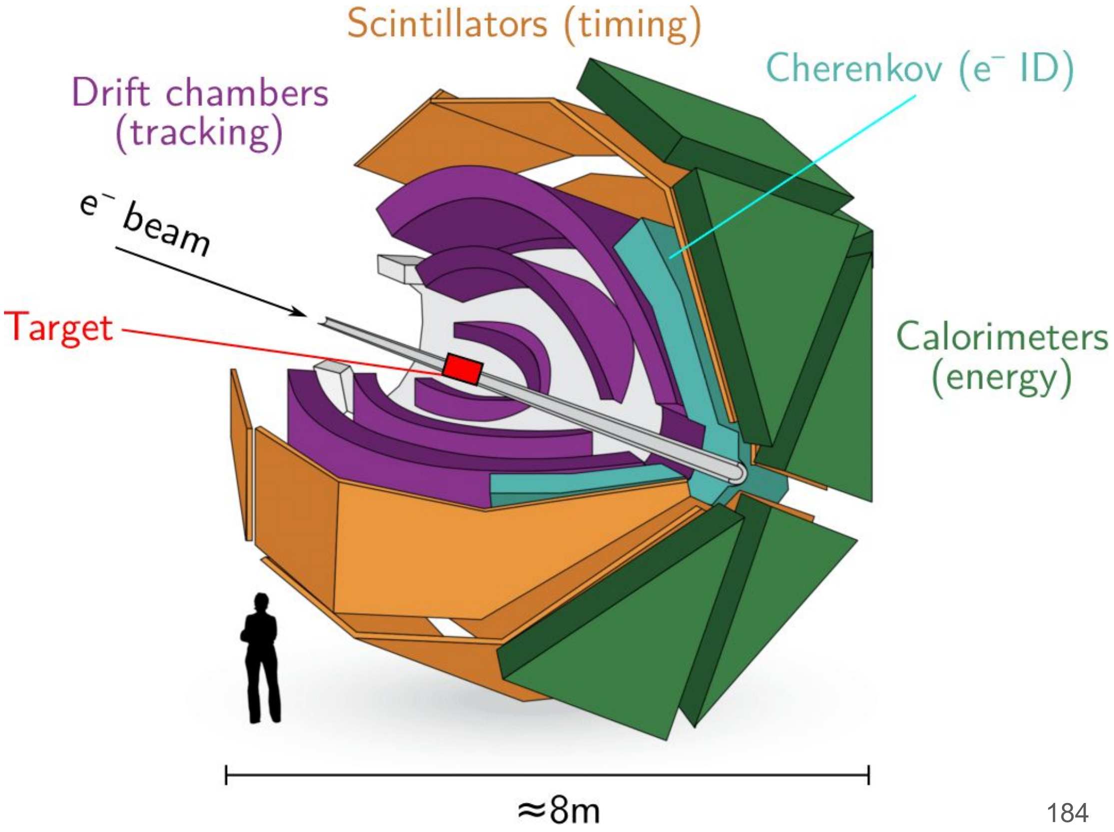

e4ν Data-Mining With CLAS

- Charged particle threshold similar to ν tracking detectors
- ~50% of "4π" coverage
- Energies: 1, 2 & 4 GeV
- Targets: ^{4}He, ^{12}C, ^{56}Fe

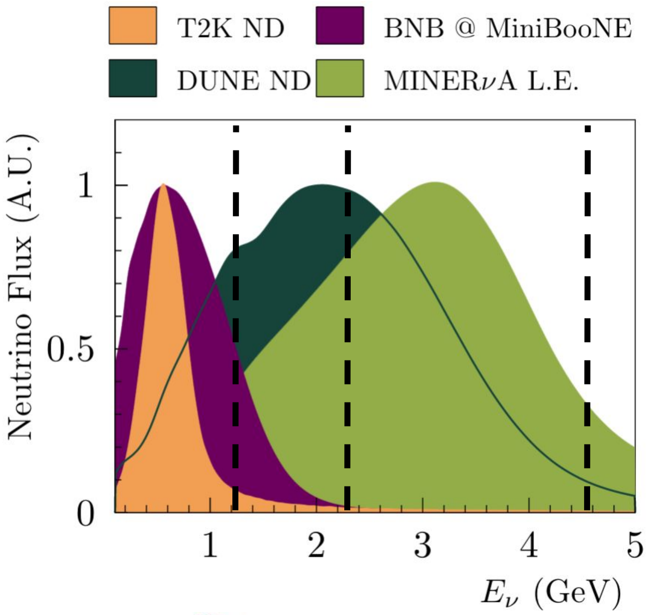

H_2O

CH

Ar

Playing The QE-like Neutrino Game

μBooNE

- 1 proton (> 300 MeV/c)
- No $\pi^{\pm}$ (> 70 MeV/c)

Phys. Rev. Lett. 125, 201803 (2020)
arXiv:2301.03706
arXiv:2301.03700

e4ν

- 1 proton (> 300 MeV/c)
- No $\pi^{\pm}$ (> 150 MeV/c)
- Scale by $\sigma_{\nu N} / \sigma_{eN} \propto Q^4$

Nature 599, 565–570 (2021)

- Study energy reconstruction
- Test against GENIE event generator

QE Energy Reconstruction

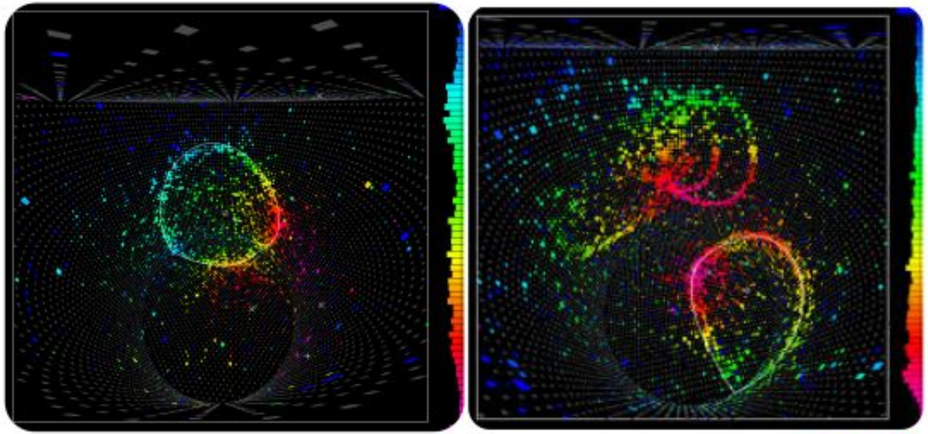

Cherenkov detectors
Assuming QE interaction
Using lepton kinematics

$$E_{QE} = \frac{2M\epsilon + 2ME_l - m_l^2}{2(M - E_l + |k_l|\cos\theta_l)}$$

QE Energy Reconstruction

C @ 1.16 GeV

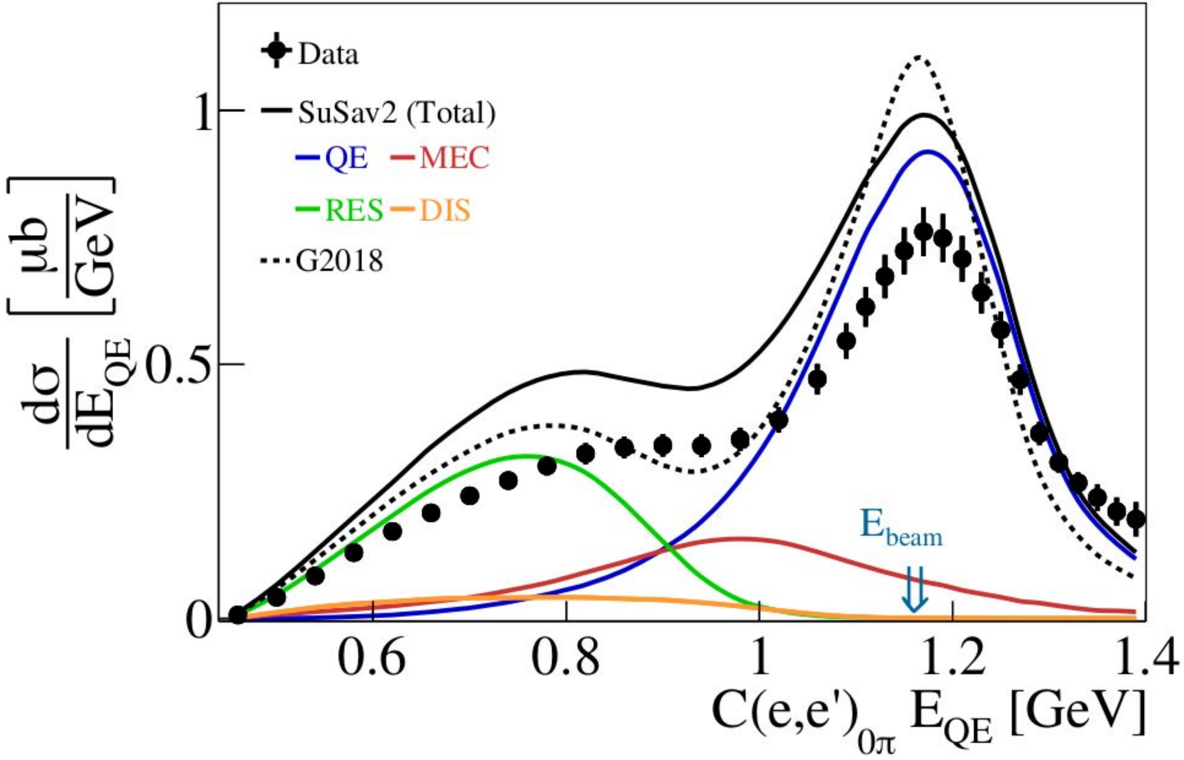

- Relevant for T2K
- Overestimation of QE peak & RES tail

$$E_{QE} = \frac{2M\epsilon + 2ME_l - m_l^2}{2\,(M - E_l + |k_l|\cos\theta_l)}$$

Nature 599, 565–570 (2021)

Calorimetric Energy Reconstruction

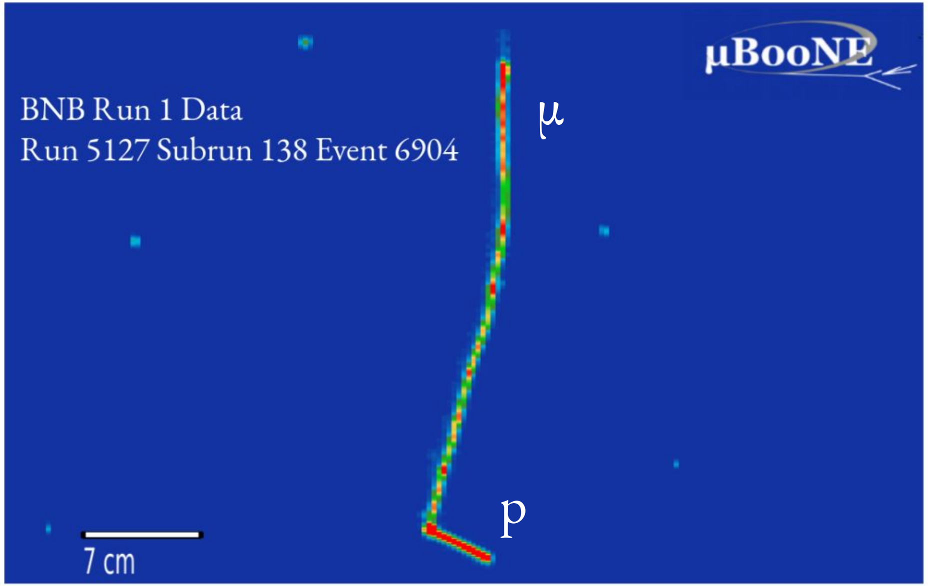

Tracking detectors
Calorimetric sum
Using all detected particles

$$E_{cal} = E_l + T_p + \epsilon_B$$

Calorimetric Energy Reconstruction

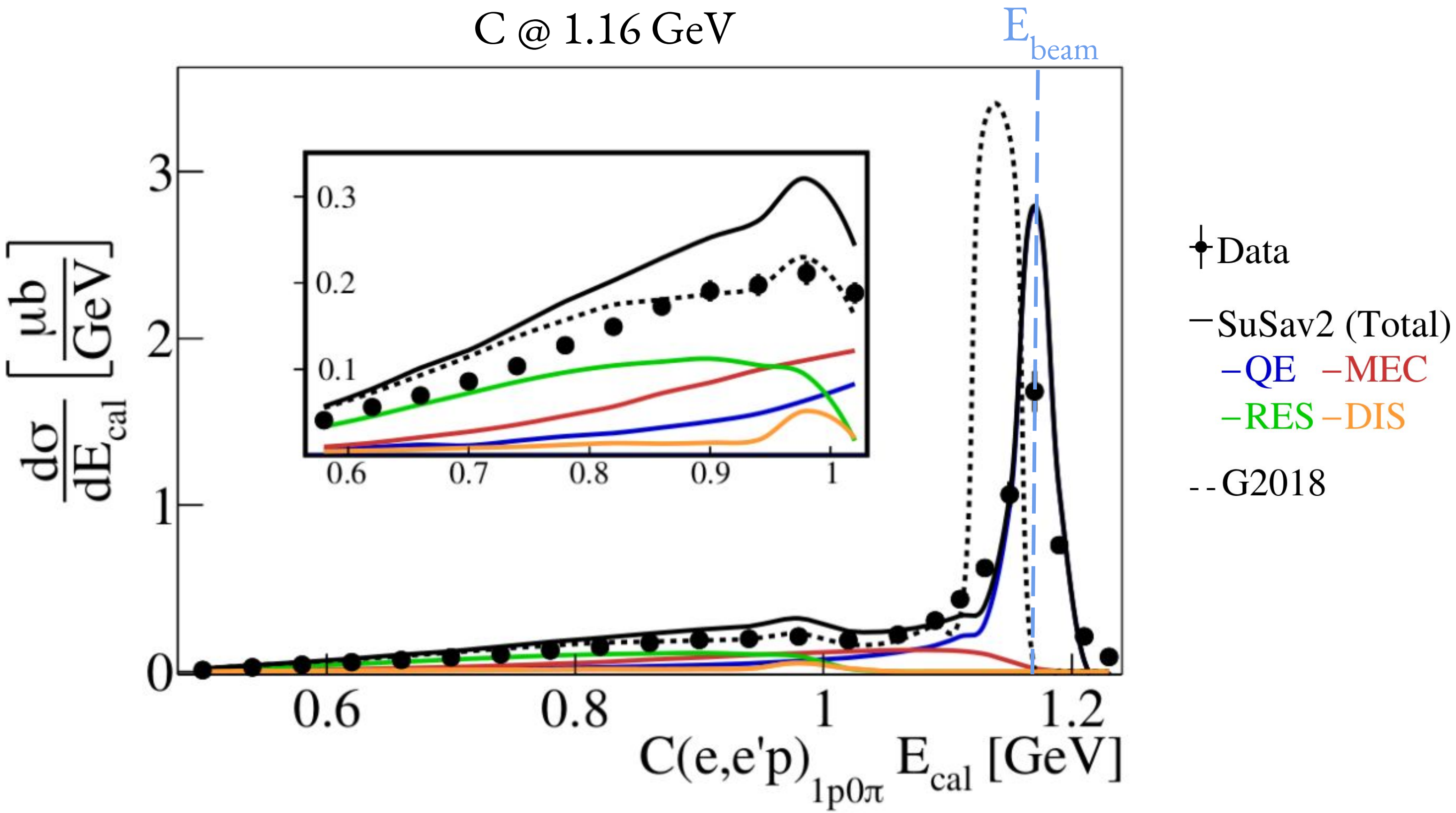

$$E_{cal} = E_l + T_p + \epsilon$$

Nature 599, 565–570 (2021)

E_{cal} Nucleus & Energy Dependence

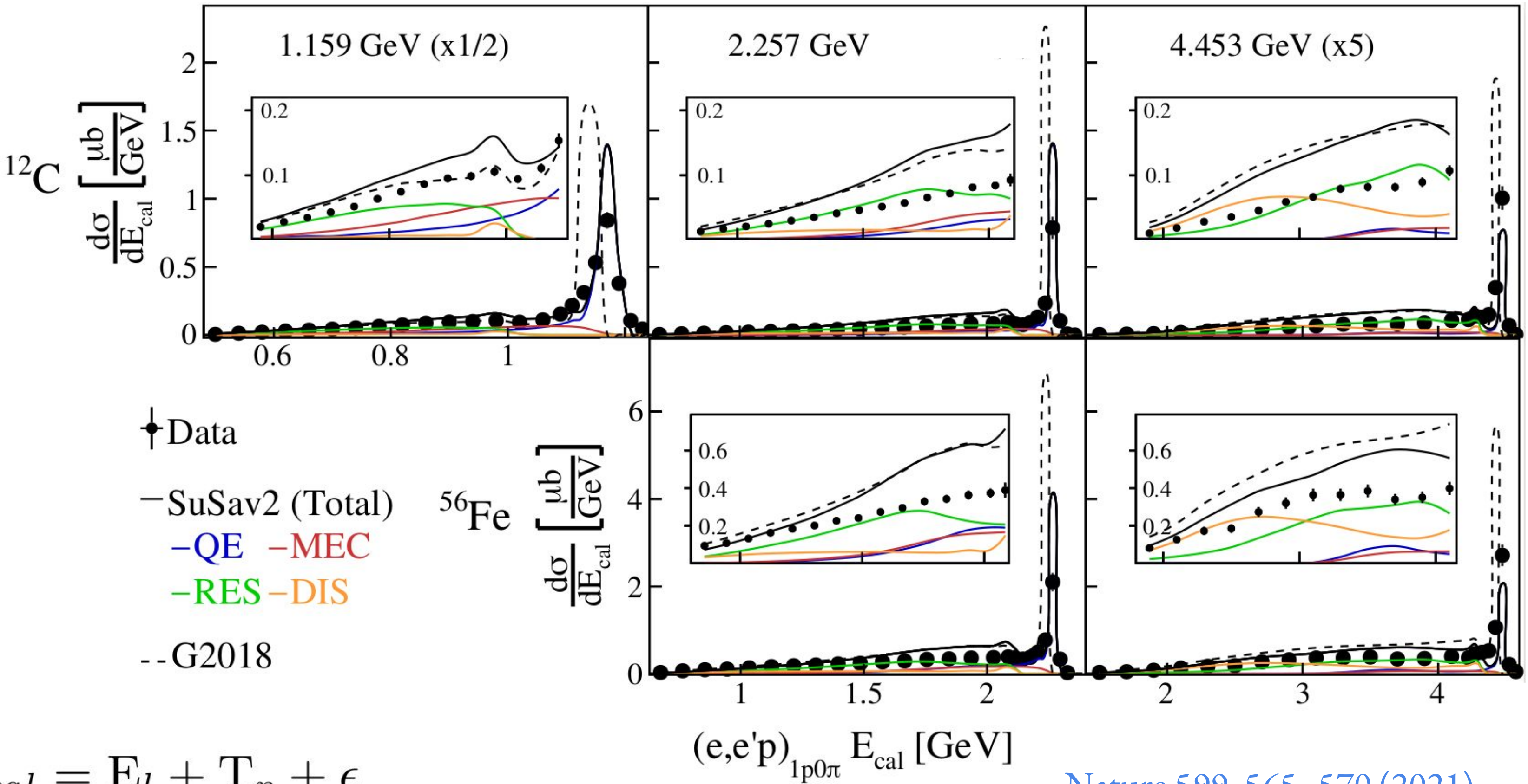

$$E_{cal} = E_l + T_p + \epsilon$$

Nature 599, 565–570 (2021)

Nucleus & Energy Dependence

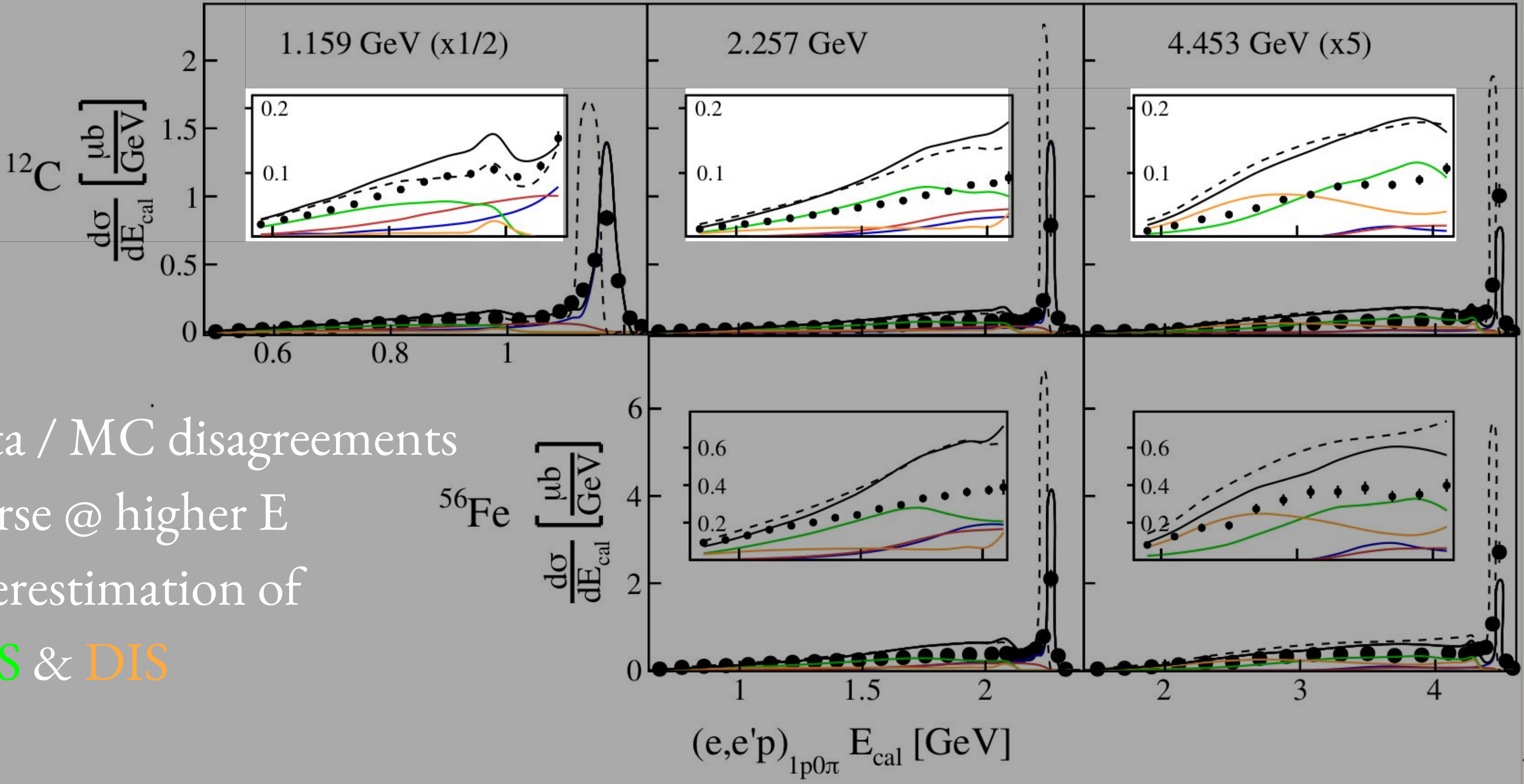

- Data / MC disagreements
- Worse @ higher E
- Overestimation of RES & DIS

Nucleus & Energy Dependence

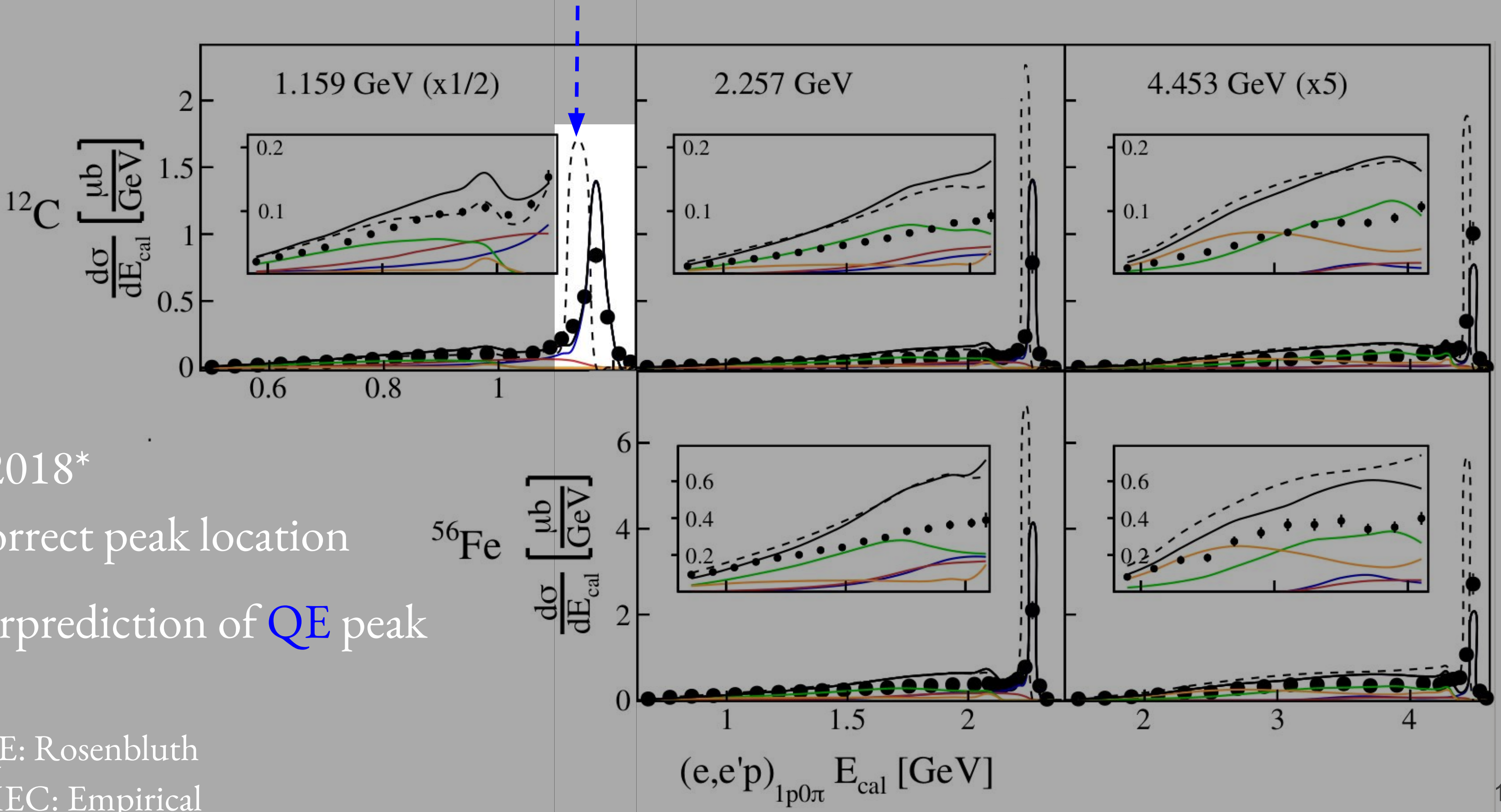

--- G2018*

- Incorrect peak location
- Overprediction of QE peak

* EMQE: Rosenbluth
EMMEC: Empirical

Nucleus & Energy Dependence

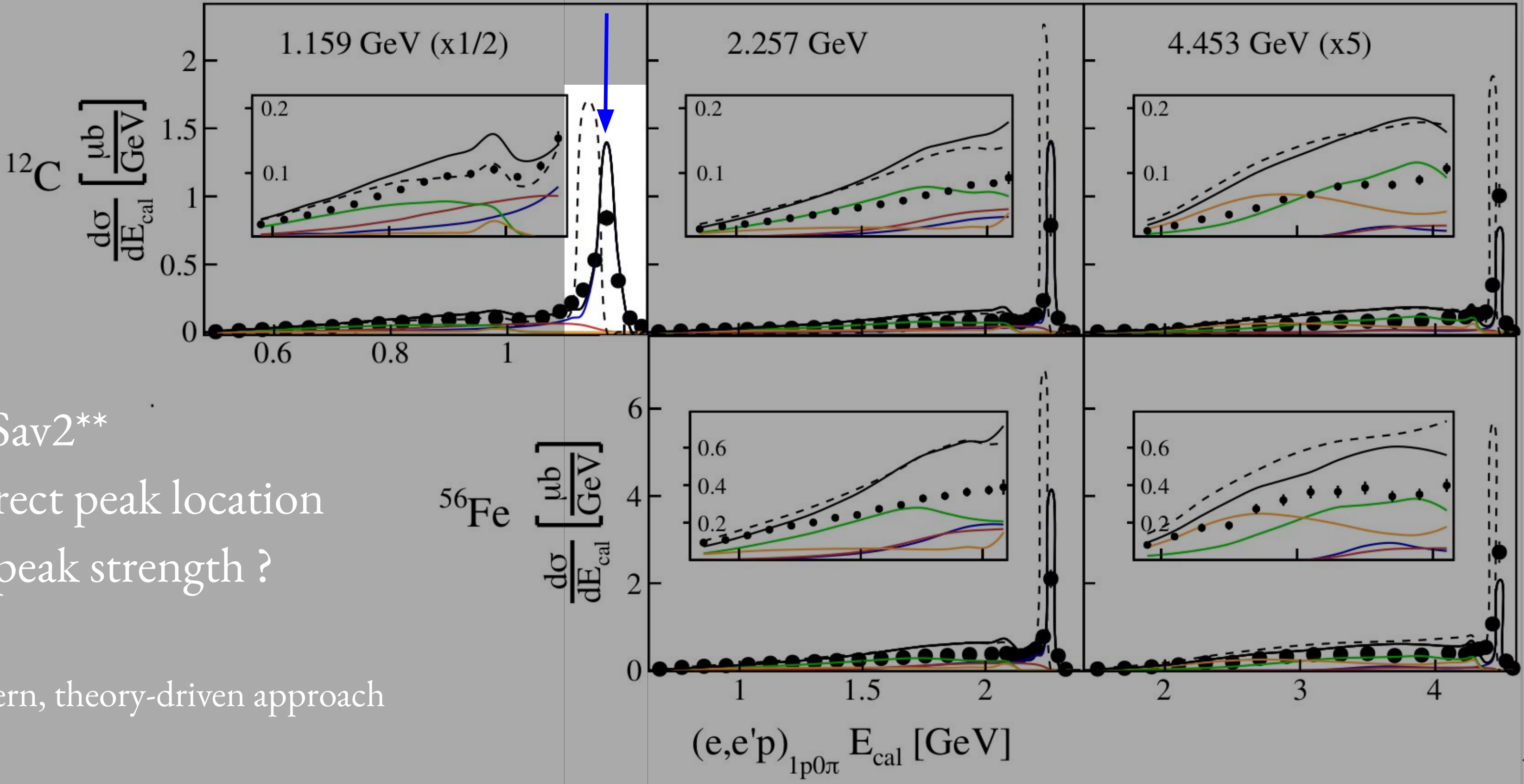

– SuSav2**

- Correct peak location
- QE peak strength ?

** Modern, theory-driven approach

Transverse Momentum

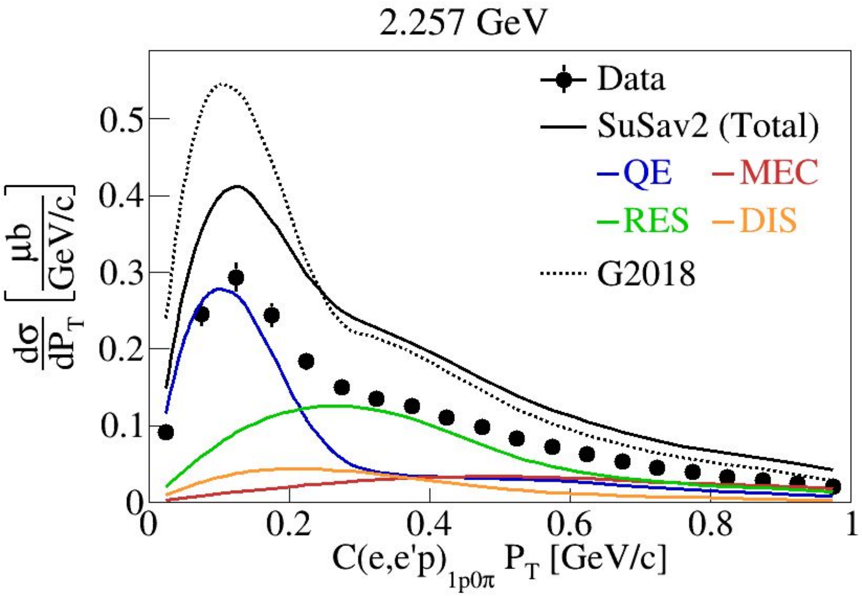

Nature 599, 565–570 (2021)

$$P_T = |\,\mathbf{P_T}^{e'} + \mathbf{P_T}^{p}\,|$$

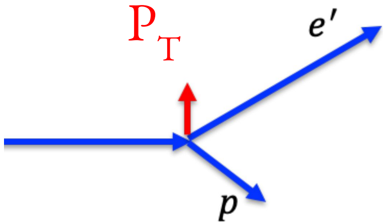

- P_T sensitivity to nuclear effects (fermi motion, final-state interactions, ...)
- Overestimation of QE peak & RES tail

Energy Reconstruction In P_T Slices

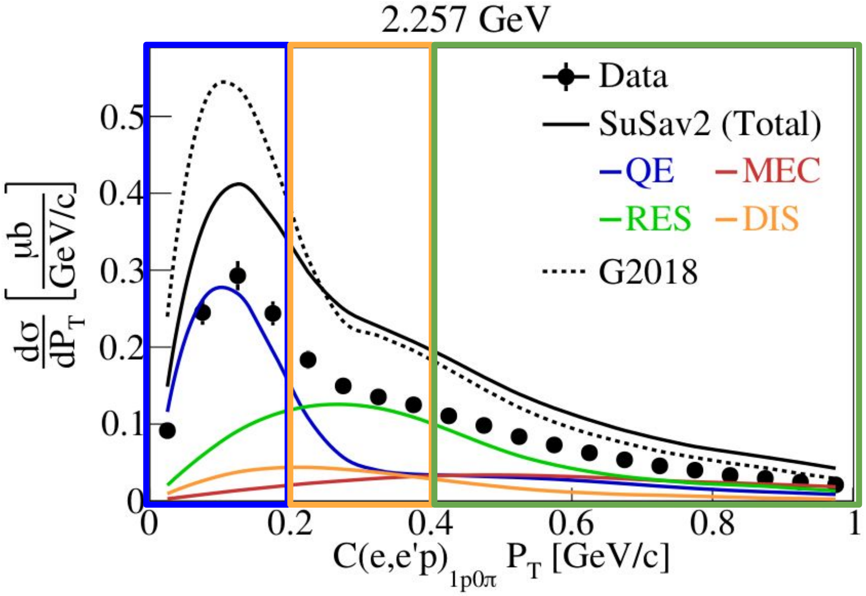

Nature 599, 565–570 (2021)

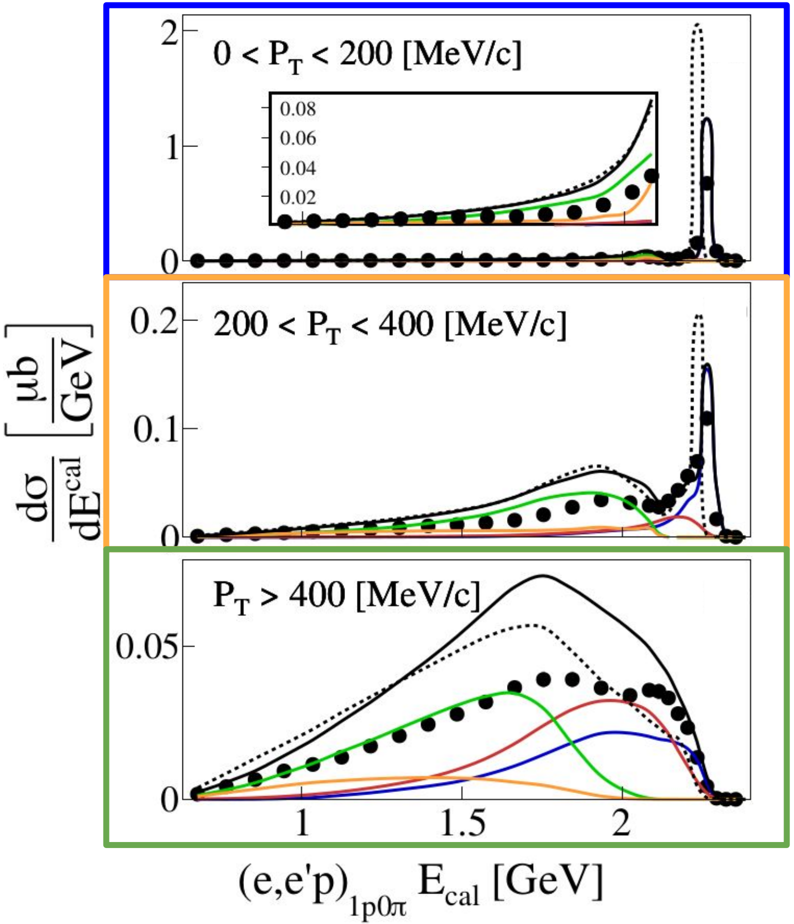

Example: Benchmarking New Generators & Kinematic Variables!

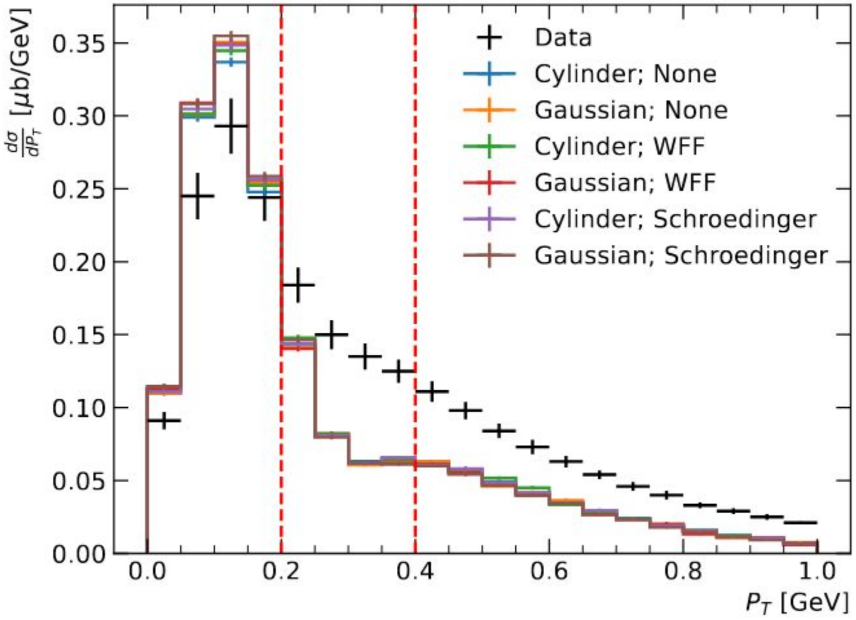

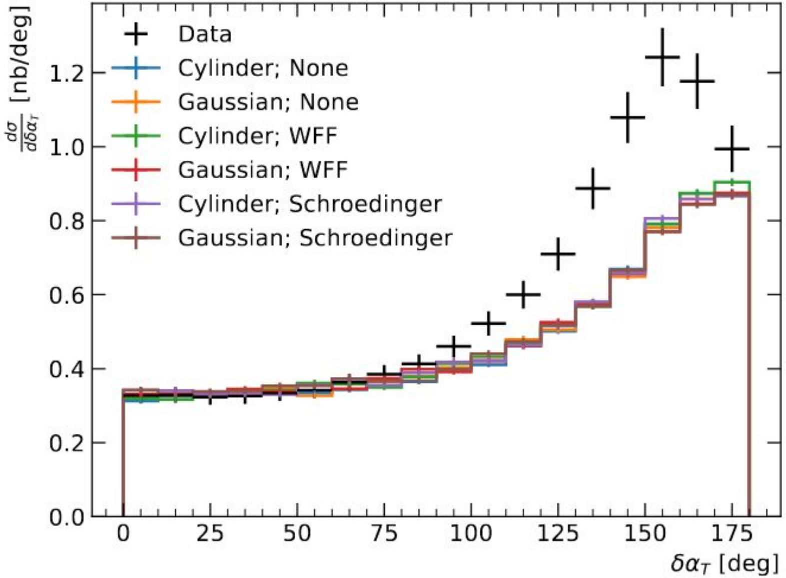

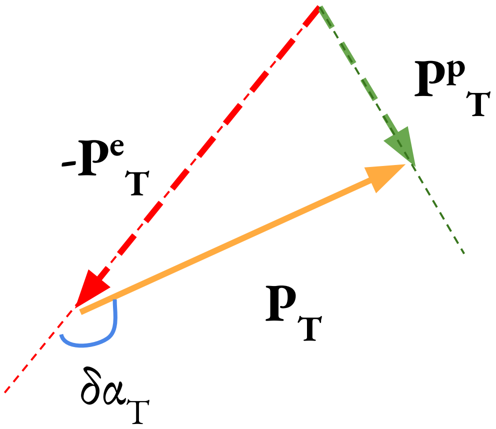

- $\delta\alpha_T$ sensitivity to final-state interactions

First step: only QE & FSI
ACHILLES arXiv: 2205.06378

Example: 2D Kinematic Imbalance

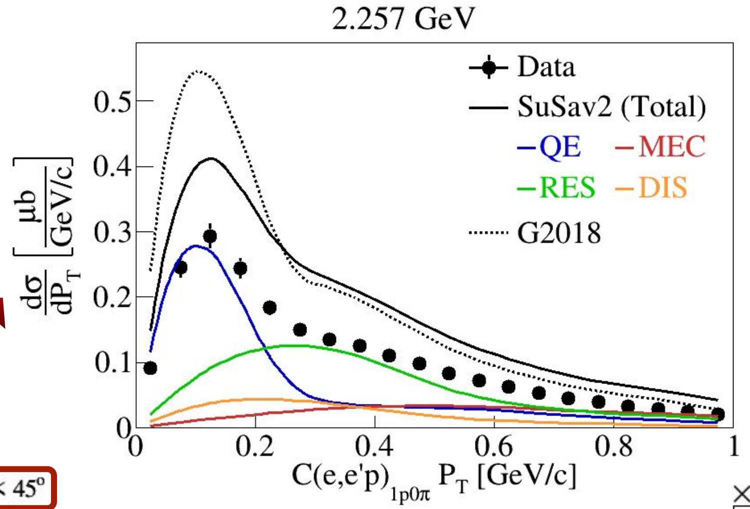

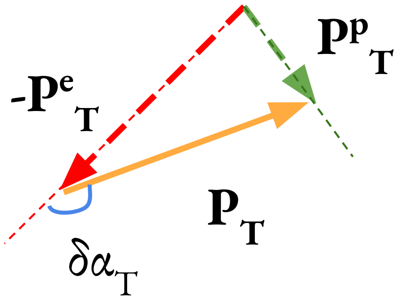

Low $\delta\alpha_T$

High $\delta\alpha_T$

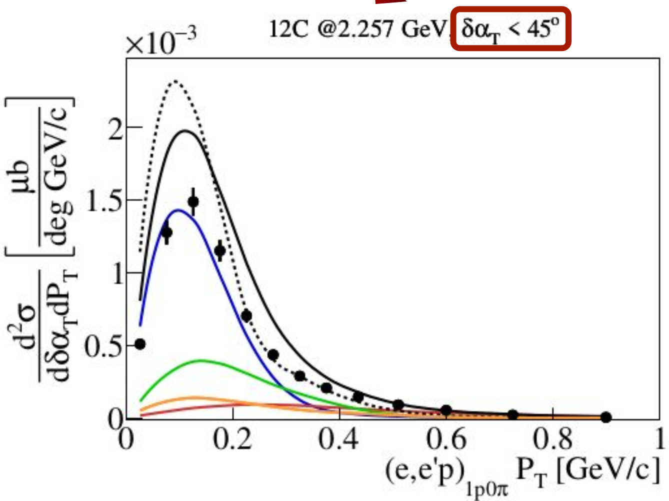

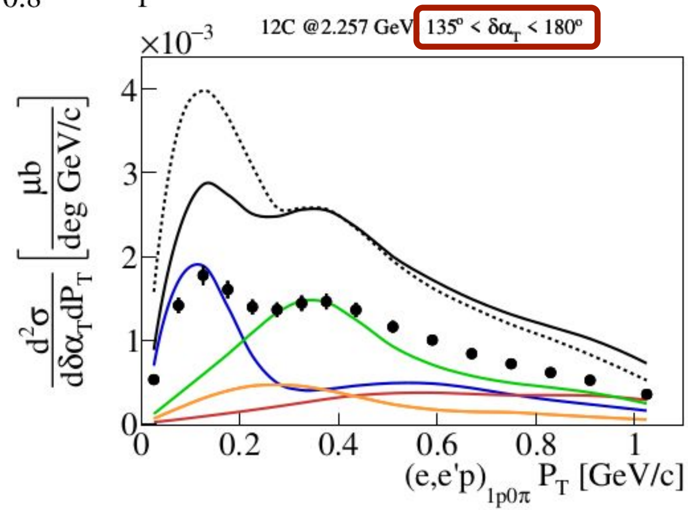

Example: 2D Kinematic Imbalance

Low $\delta\alpha_T$
QE-enhanced region
Sensitive to ground-state modeling

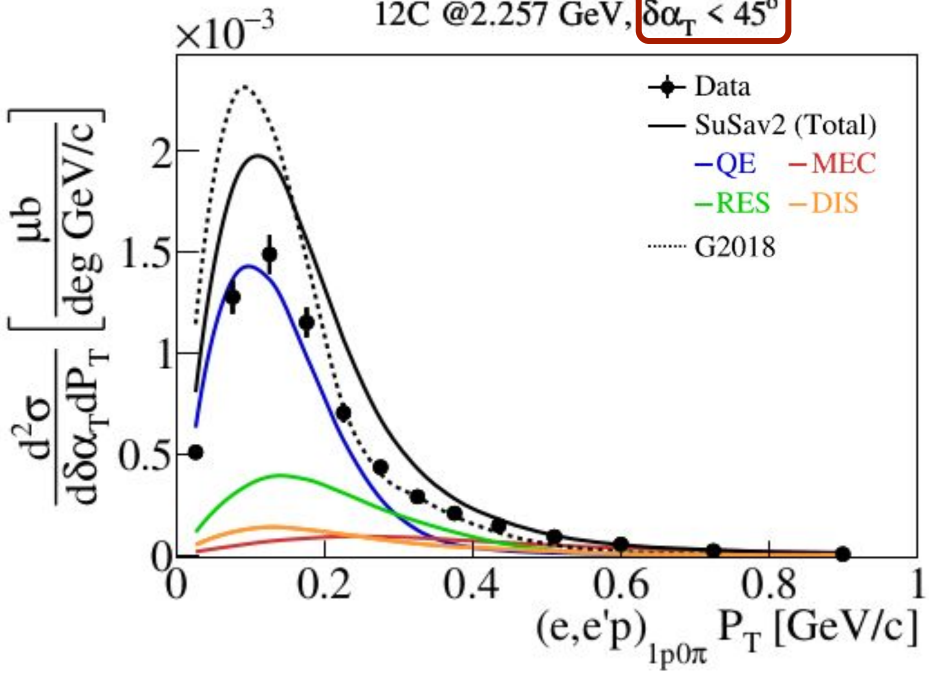

High $\delta\alpha_T$
Large non-QE contributions
Strong final-state interaction effects

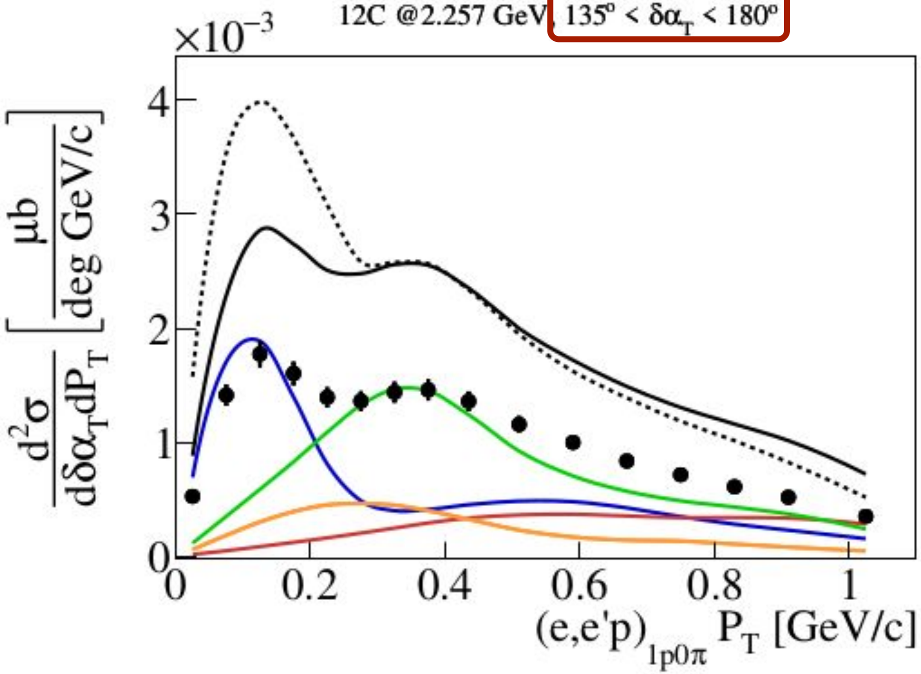

Example: 2D Kinematic Imbalance

Low $\delta\alpha_T$
QE-enhanced region
Sensitive to ground-state modeling

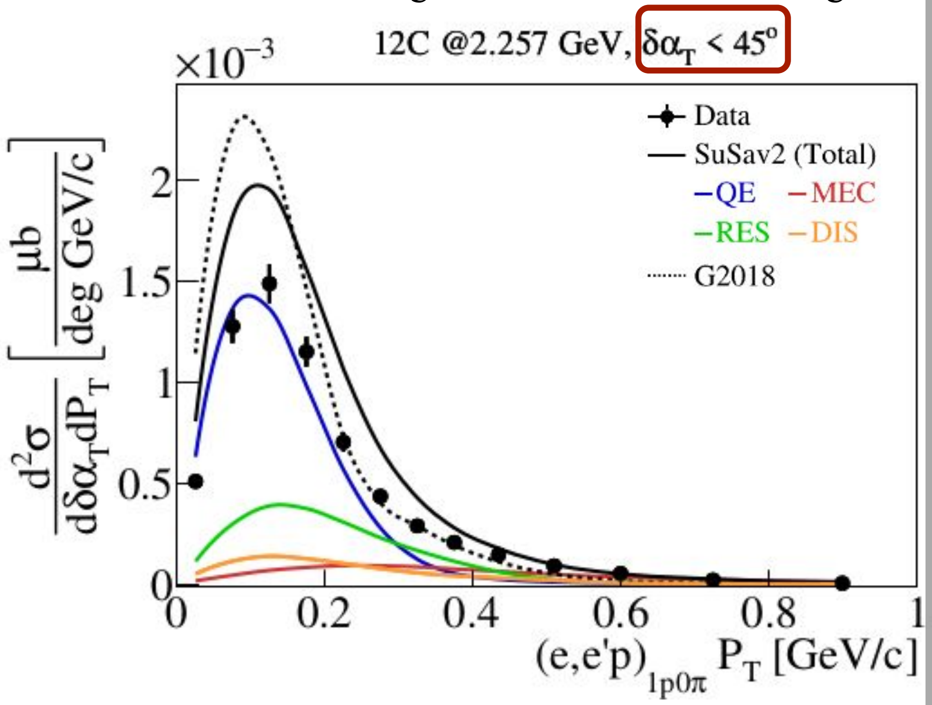

High $\delta\alpha_T$
Large non-QE contributions
Strong final-state interaction effects

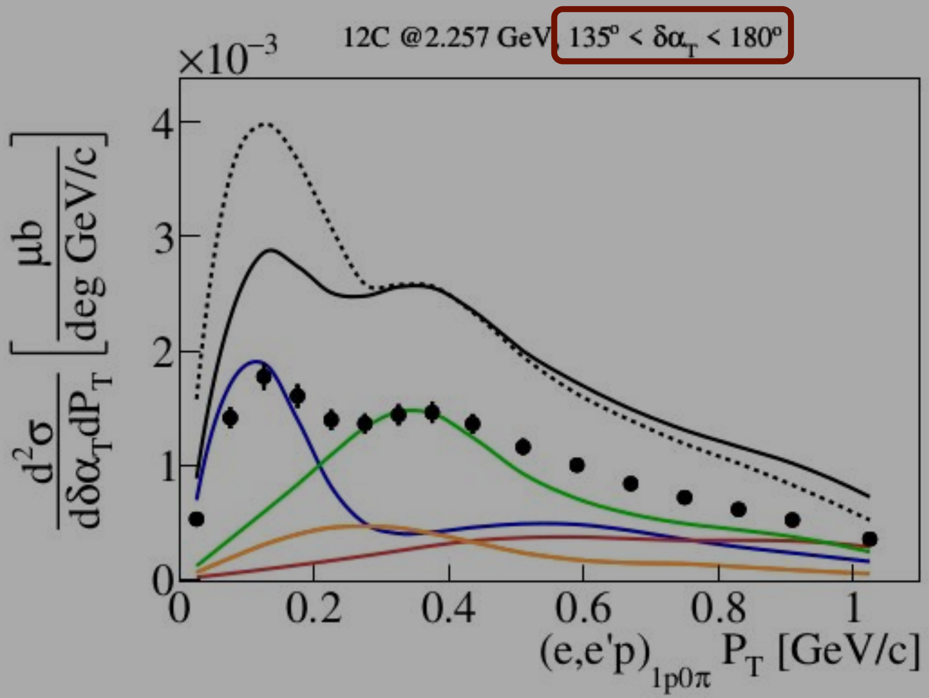

Example: 2D Kinematic Imbalance

Low $\delta\alpha_T$
QE-enhanced region
Sensitive to ground-state modeling

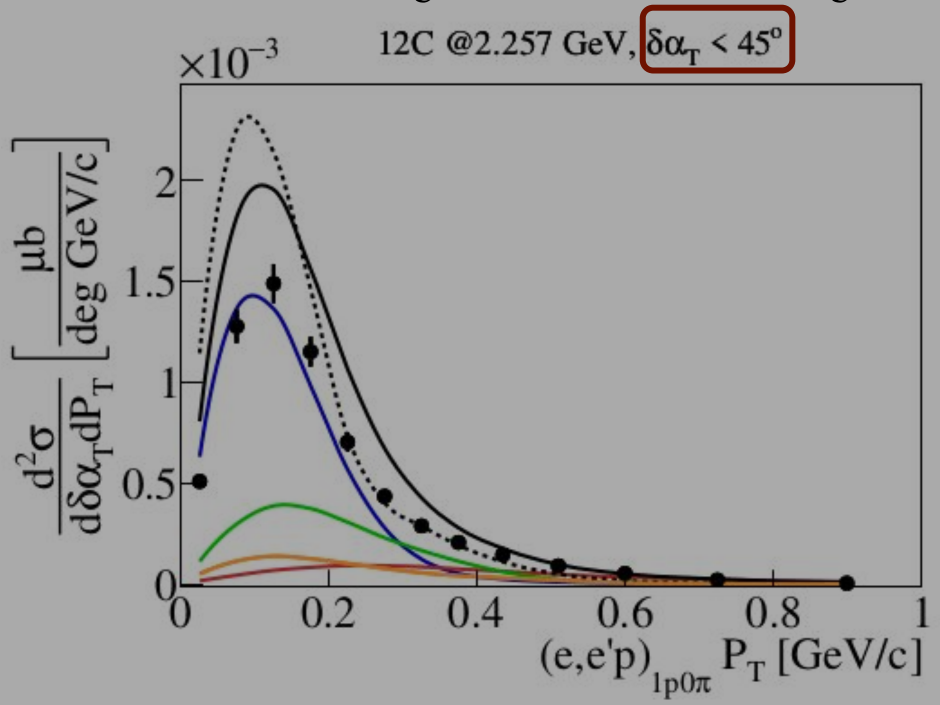

High $\delta\alpha_T$
Large non-QE contributions
Strong final-state interaction effects

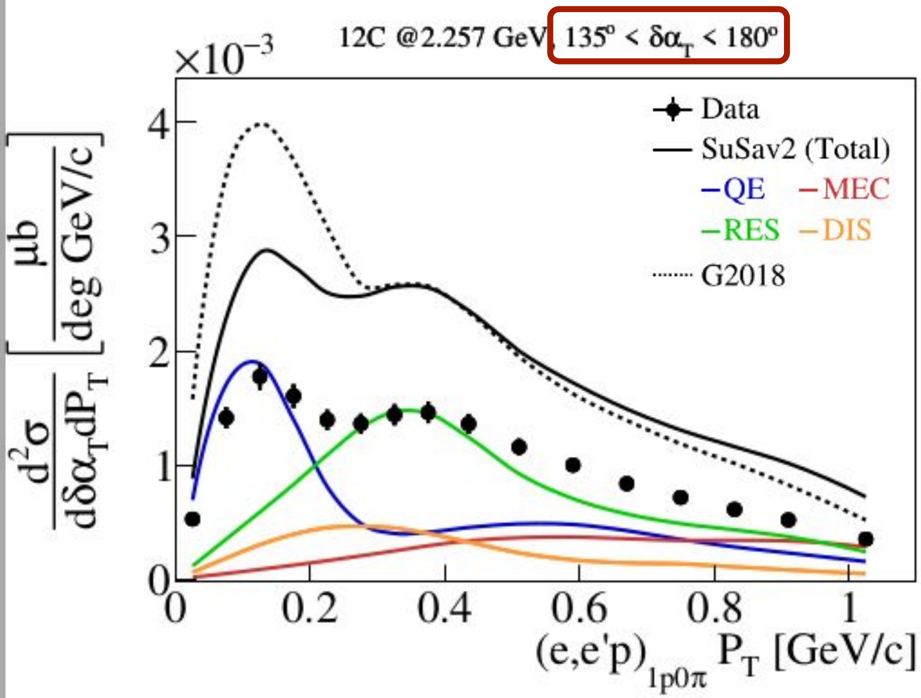

Next Steps

- Even more differential! Into the 3D multiverse
  Taking advantage of massive statistics
- More nuclear sensitivity variables
  Help decide what to tune
- 1p1π exclusive cross sections

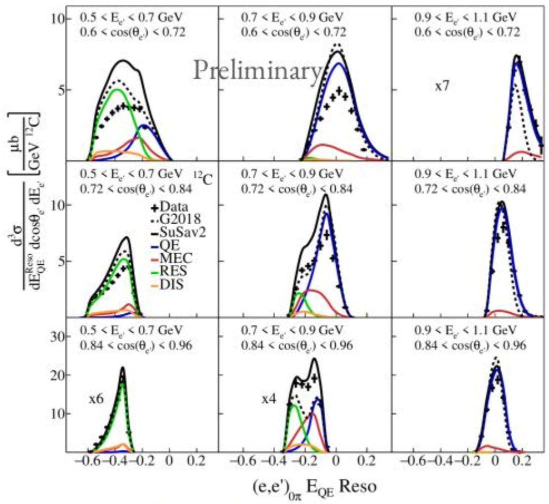

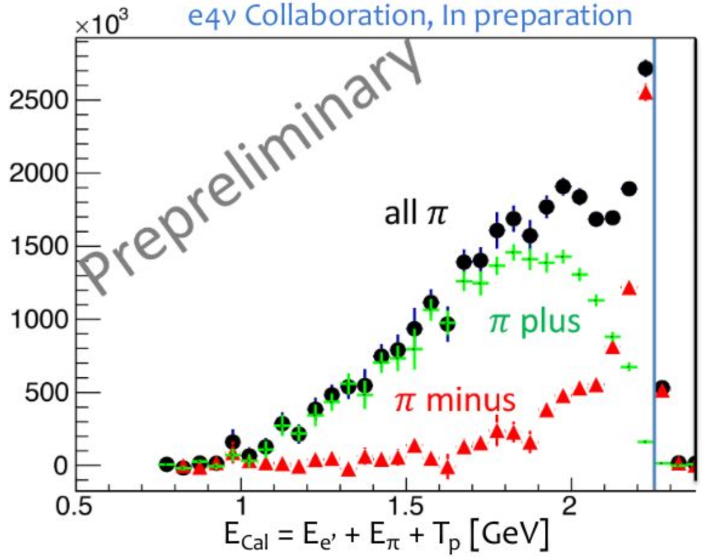

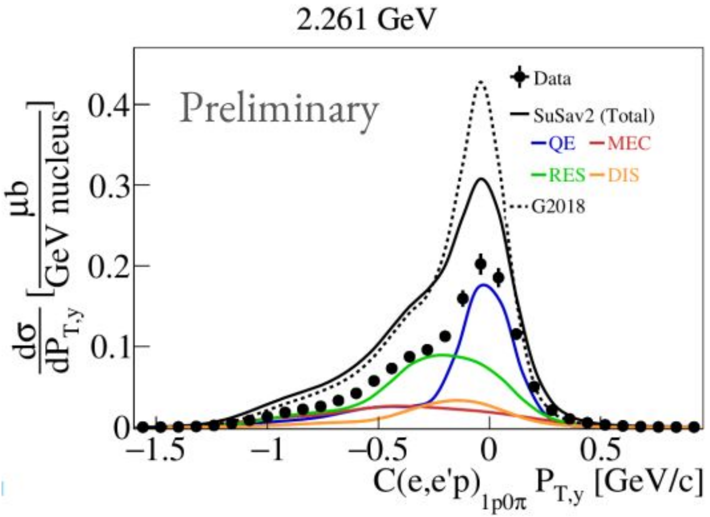

Next Steps

- More with CLAS6

❑ Proton transparency studies
  - Observable that summarizes strength of intranuclear rescattering
  - Measurement study
    $$T = N_{prot}^{detected} / N_{prot}^{PWIA}$$
  - Test event generator FSI models in GENIE across multiple nuclear targets
  - Testing dependency of transparency calculations on PWIA normalization

Phys. Rev. D **104**, 053006 (2021)

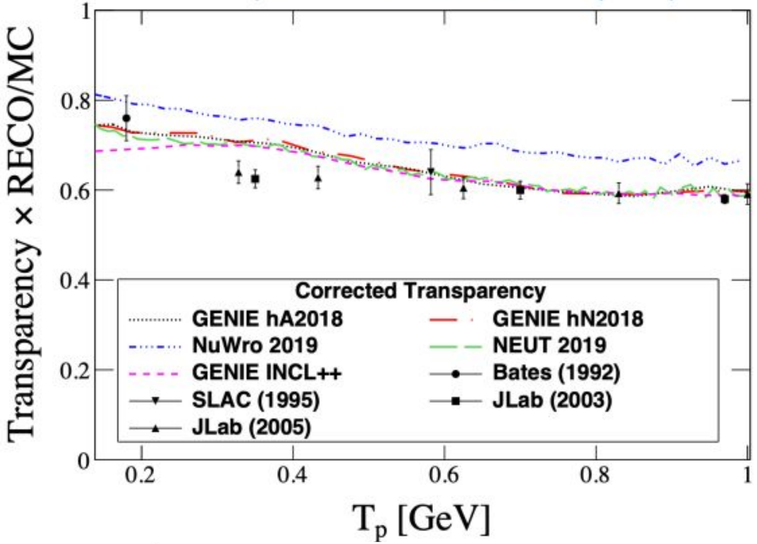

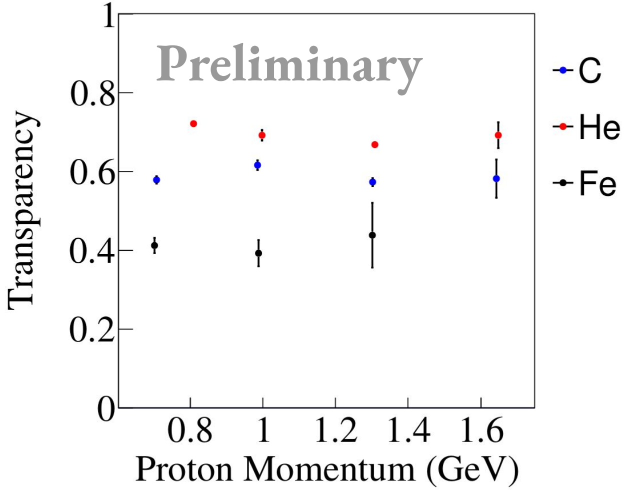

Next Steps

- More with CLAS6
  - ❑ Prepare suite of cross sections in same variables as neutrinos for first e-GENIE tune
    - Compare with neutrino CC0π tune

- e4ν data already being used to validate event generators

2206.11050 [hep-ph]

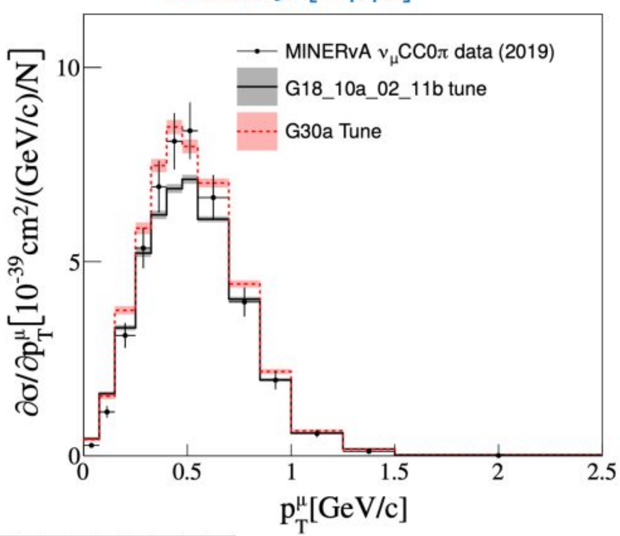

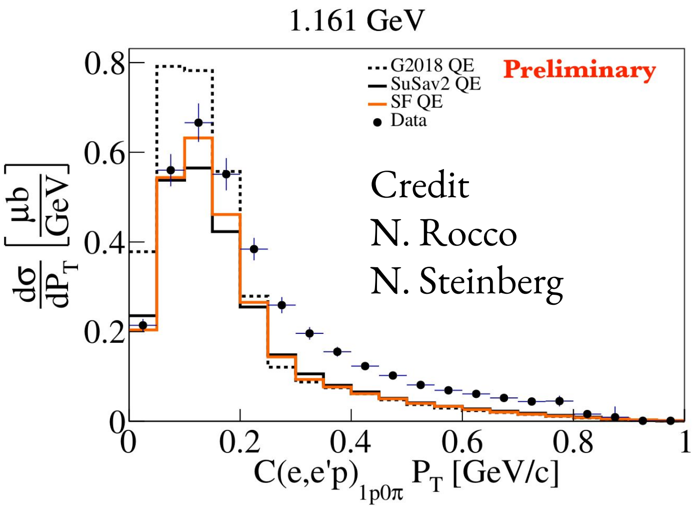

Credit
N. Rocco
N. Steinberg

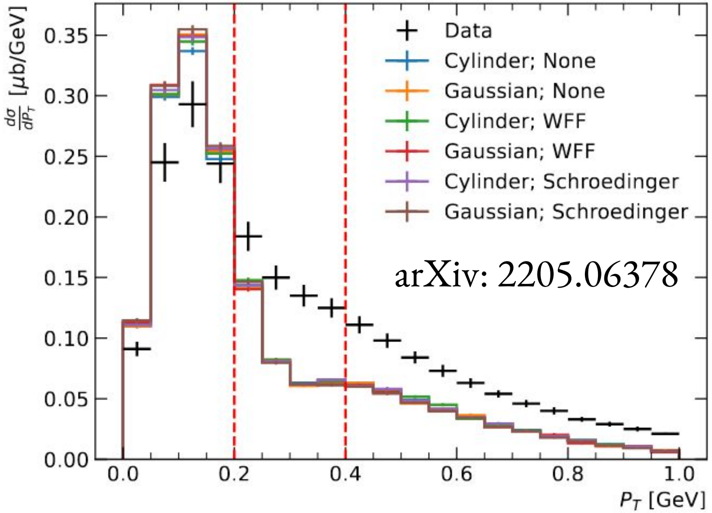

arXiv: 2205.06378

Next Steps

- New data with CLAS12
  Targets: ^{4}He, ^{12}C, **^{40}Ar**, ^{120}Sn
- 2 - 6 GeV beam energies
- More phase-space coverage ($\theta_e > 5^o$)
- Neutrons!

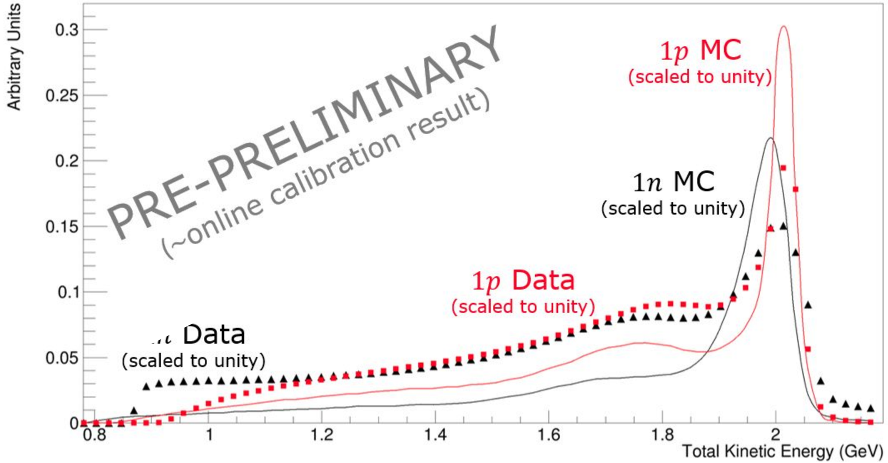

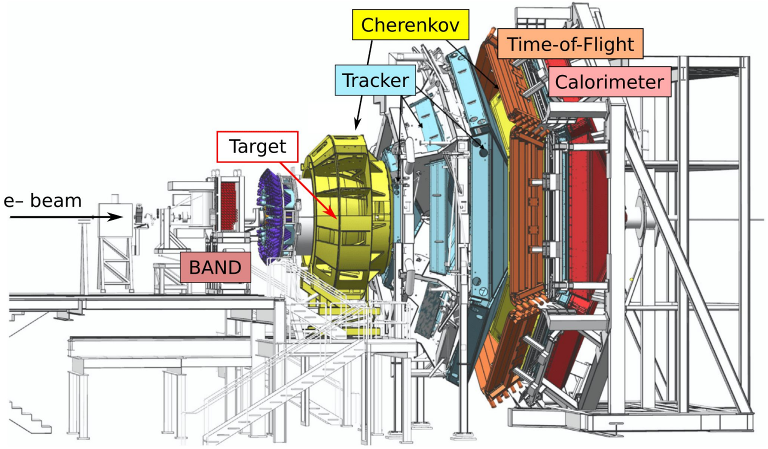

Why electrons?

- Common vector current
- Identical nuclear effects

- Monoenergetic beams
- High statistics
  - Precision measurements

Any model must work for electrons,
or it won't work for neutrinos !

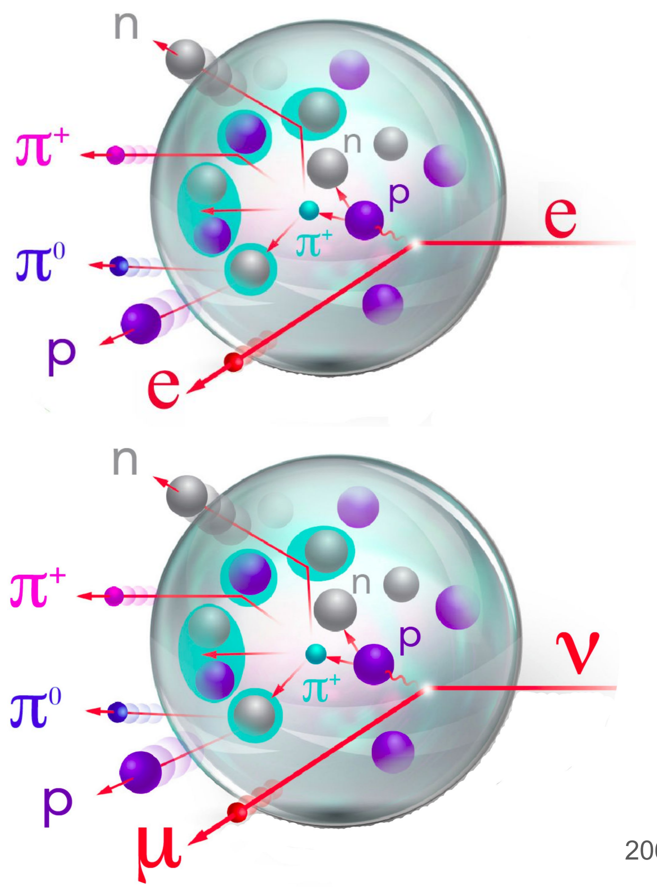

Similar ν & e Distributions

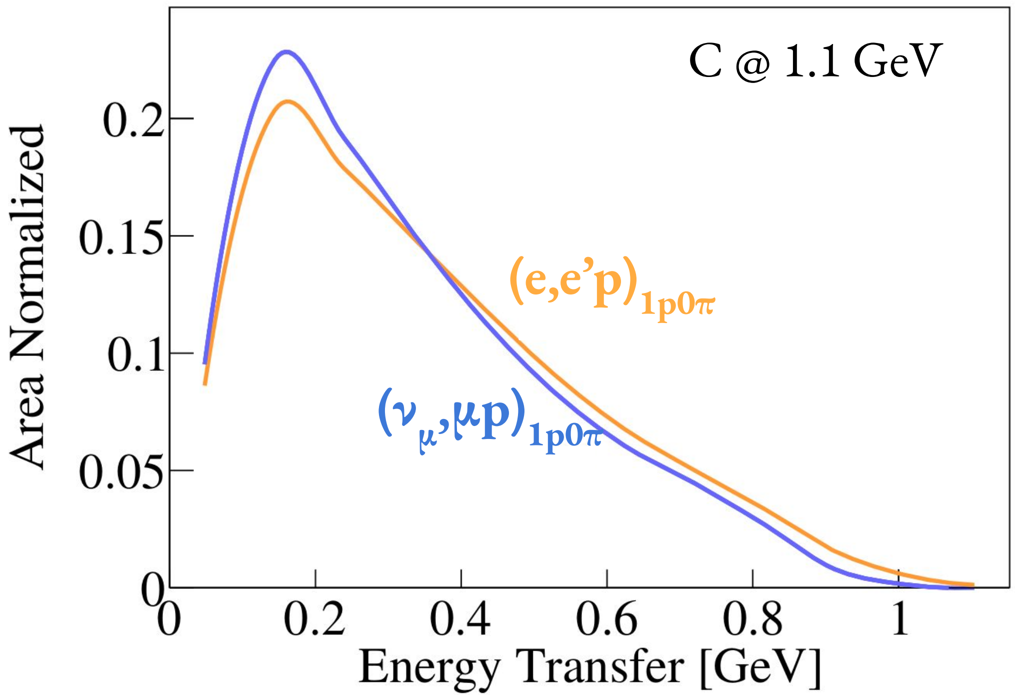

Accounting for propagator mass (γ vs W) via Q^4 scaling of the electron side

Phys. Rev. D 103, 113003 (2021)

Jefferson Laboratory

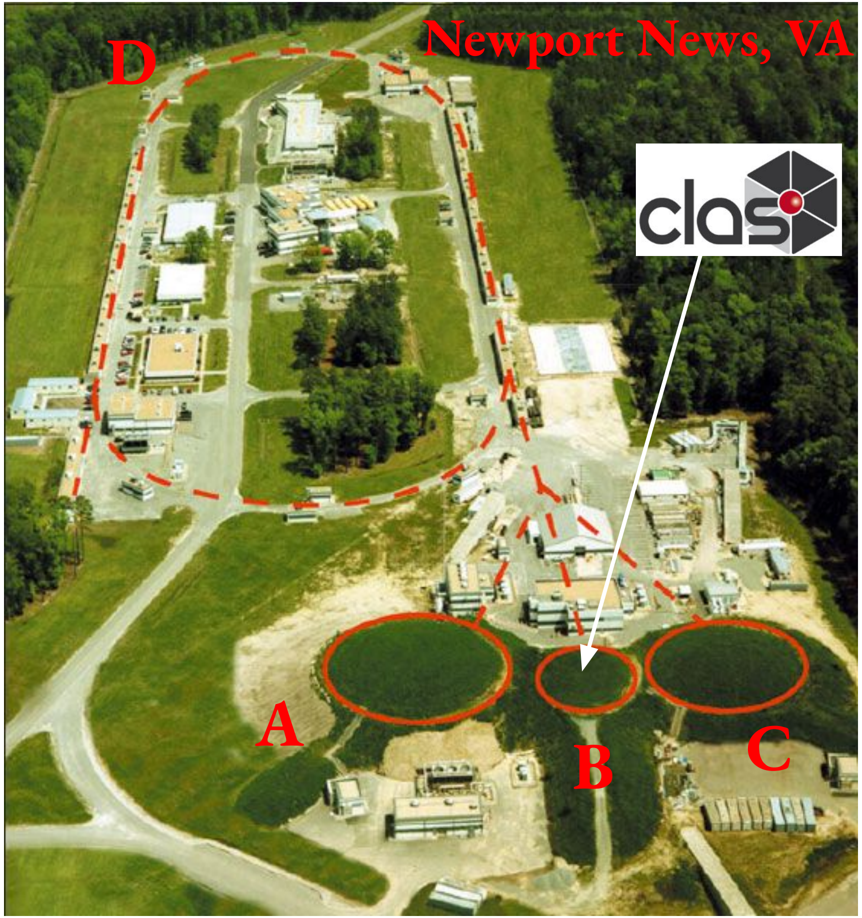

- Electron beam accelerator facility
- Energies up to 12 GeV
- Using Hall B & CLAS detector

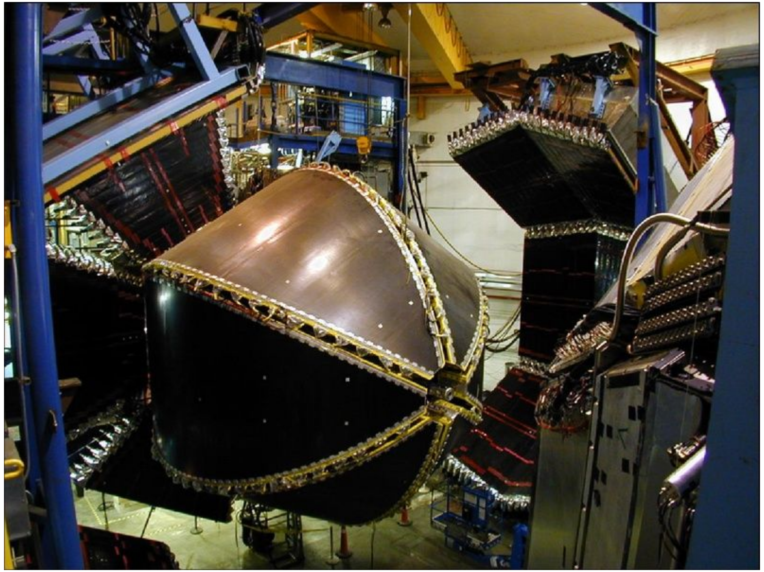

e4ν Data-Mining With CLAS

- Charged particle threshold similar to ν tracking detectors
- ~50% of "4π" coverage

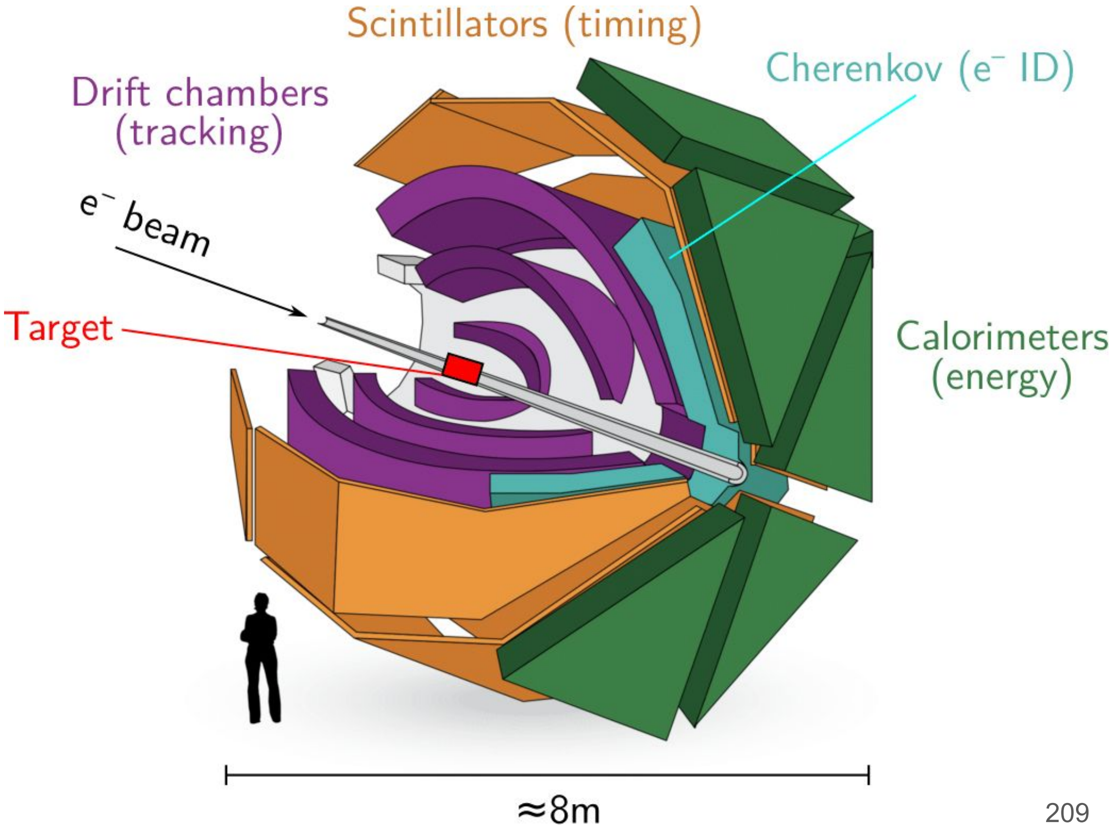

e4ν Data-Mining With CLAS

- Charged particle threshold similar to ν tracking detectors
- ~50% of "4π" coverage
- Energies: 1, 2 & 4 GeV
- Targets: ^{4}He, ^{12}C, ^{56}Fe

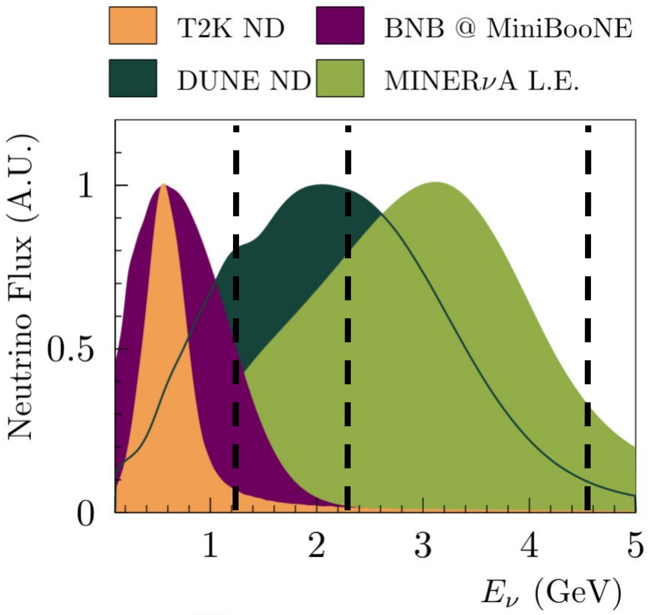

T2K — H_2O
NOvA, MINERvA — CH
SBN Program, DUNE — Ar

Playing The QE-like Neutrino Game

- 1 proton (> 300 MeV/c)
- No $\pi^{\pm}$ (> 70 MeV/c)

Phys. Rev. Lett. 125, 201803 (2020)
arXiv:2301.03706
arXiv:2301.03700

- 1 proton (> 300 MeV/c)
- No $\pi^{\pm}$ (> 150 MeV/c)
- Scale by $\sigma_{\nu N} / \sigma_{eN} \propto Q^4$

Nature 599, 565–570 (2021)

- Study energy reconstruction
- Test against GENIE event generator

QE Energy Reconstruction

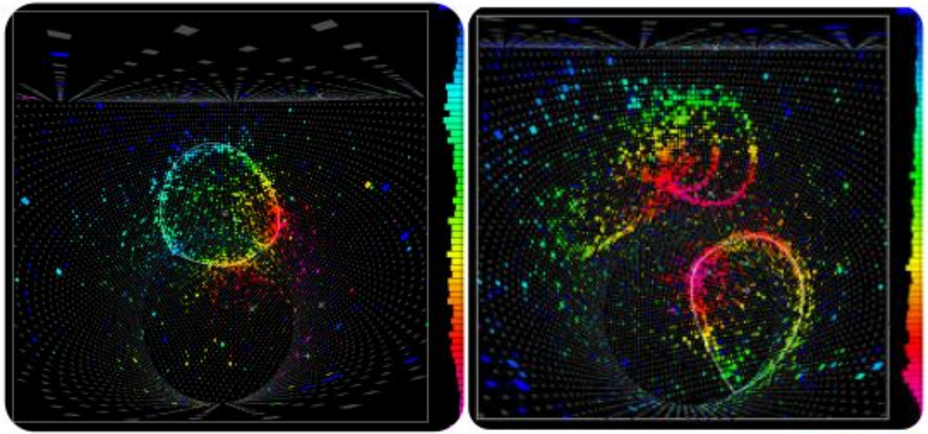

Cherenkov detectors
Assuming QE interaction
Using lepton kinematics

$$E_{QE} = \frac{2M\epsilon + 2ME_l - m_l^2}{2\left(M - E_l + |k_l|\cos\theta_l\right)}$$

QE Energy Reconstruction

C @ 1.16 GeV

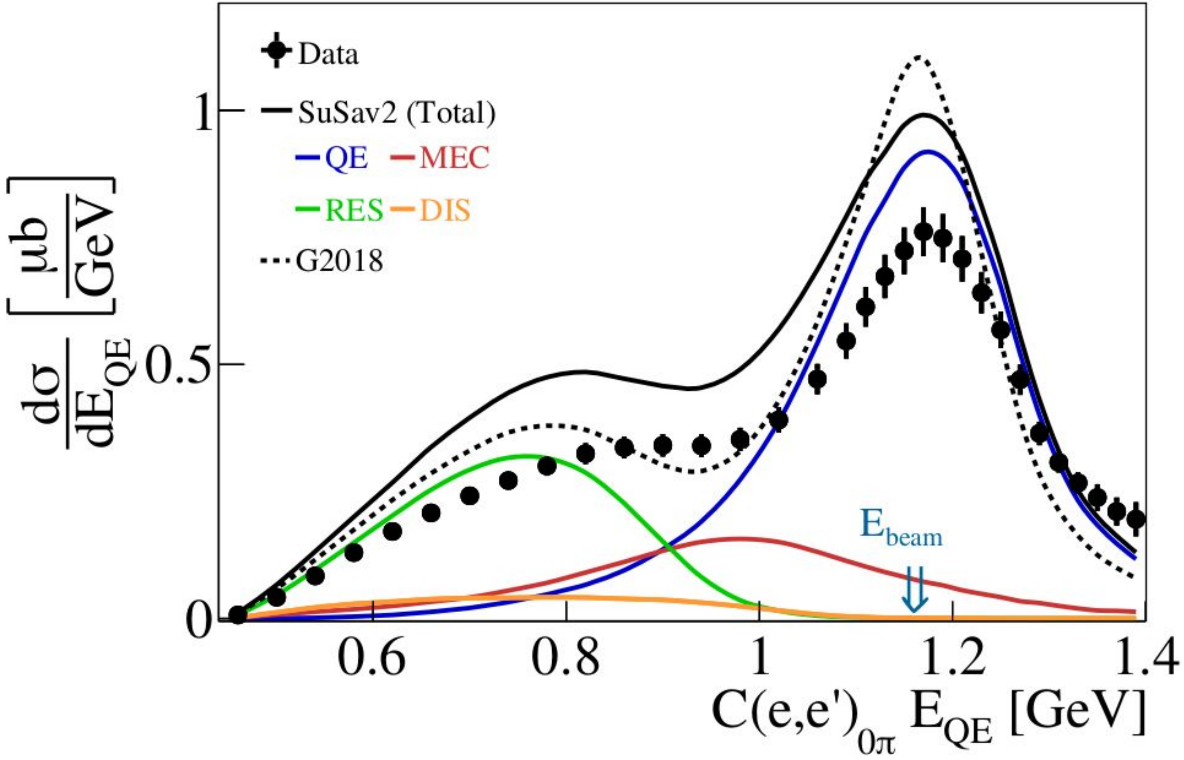

- Relevant for T2K
- Overestimation of QE peak & RES tail

$$E_{QE} = \frac{2M\epsilon + 2ME_l - m_l^2}{2\,(M - E_l + |k_l|\cos\theta_l)}$$

Nature 599, 565–570 (2021)

Calorimetric Energy Reconstruction

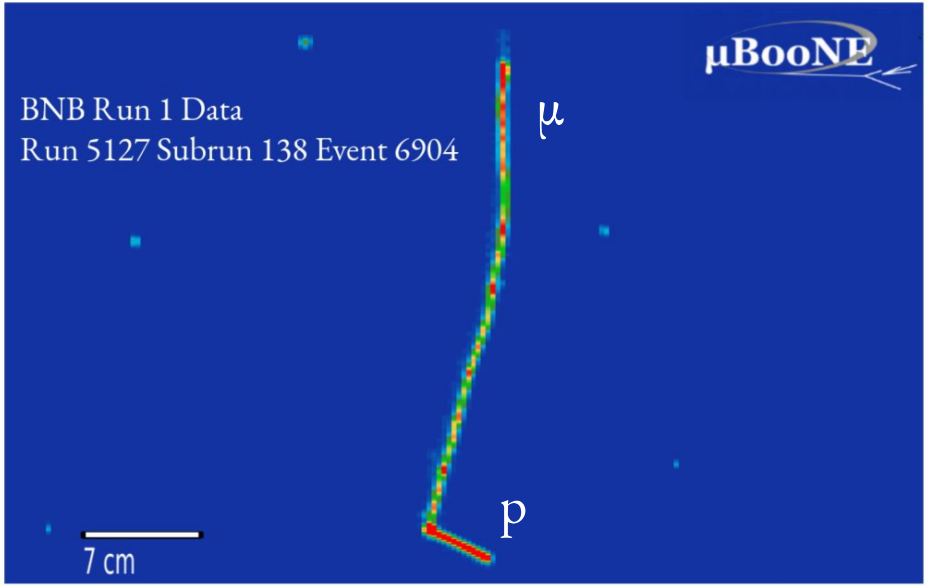

Tracking detectors
Calorimetric sum
Using all detected particles

$$\mathrm{E}_{cal} = \mathrm{E}_l + \mathrm{T}_p + \epsilon_{\mathrm{B}}$$

Calorimetric Energy Reconstruction

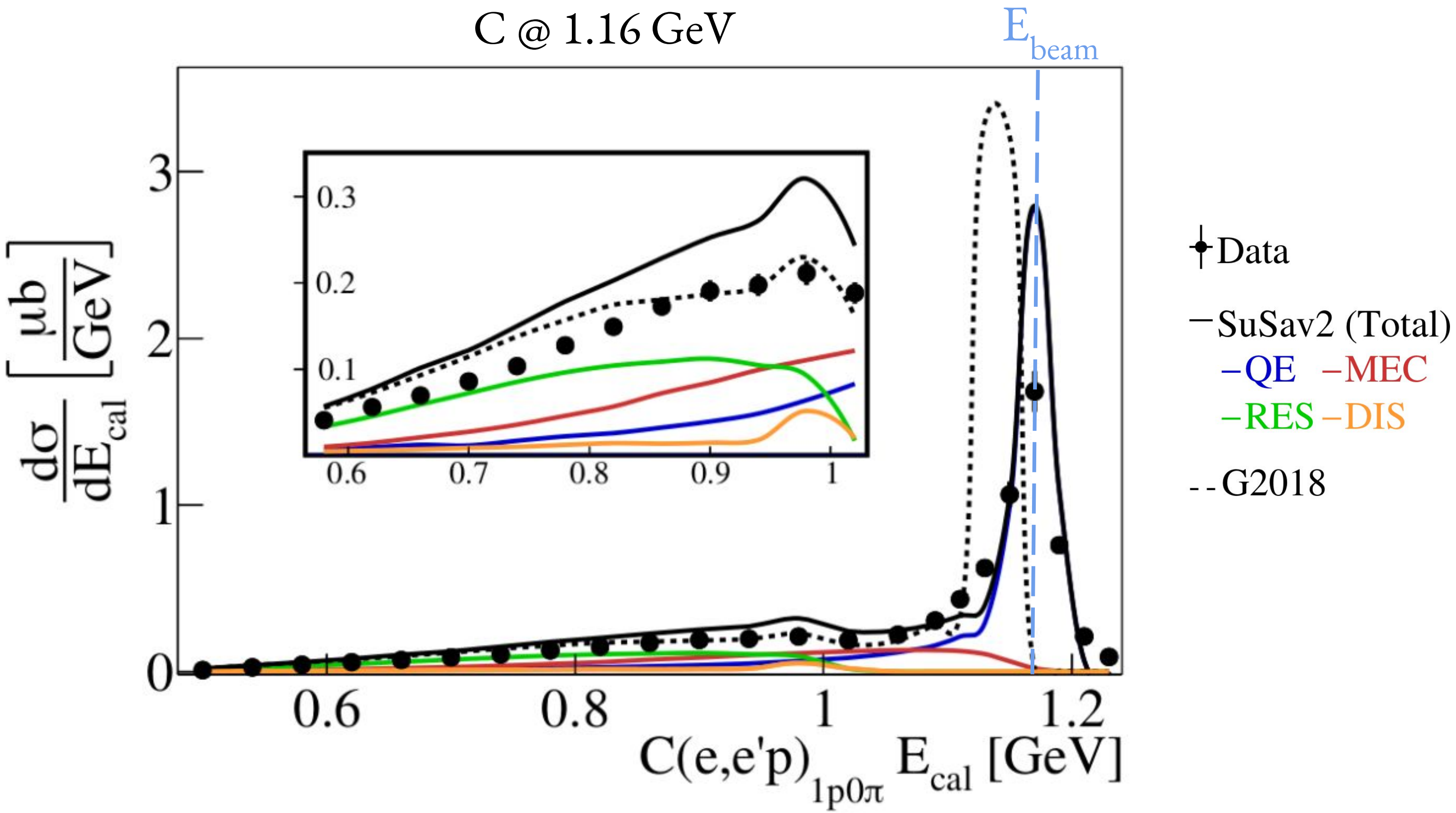

$E_{cal} = E_l + T_p + \epsilon$

Nature 599, 565–570 (2021)

E_{cal} Nucleus & Energy Dependence

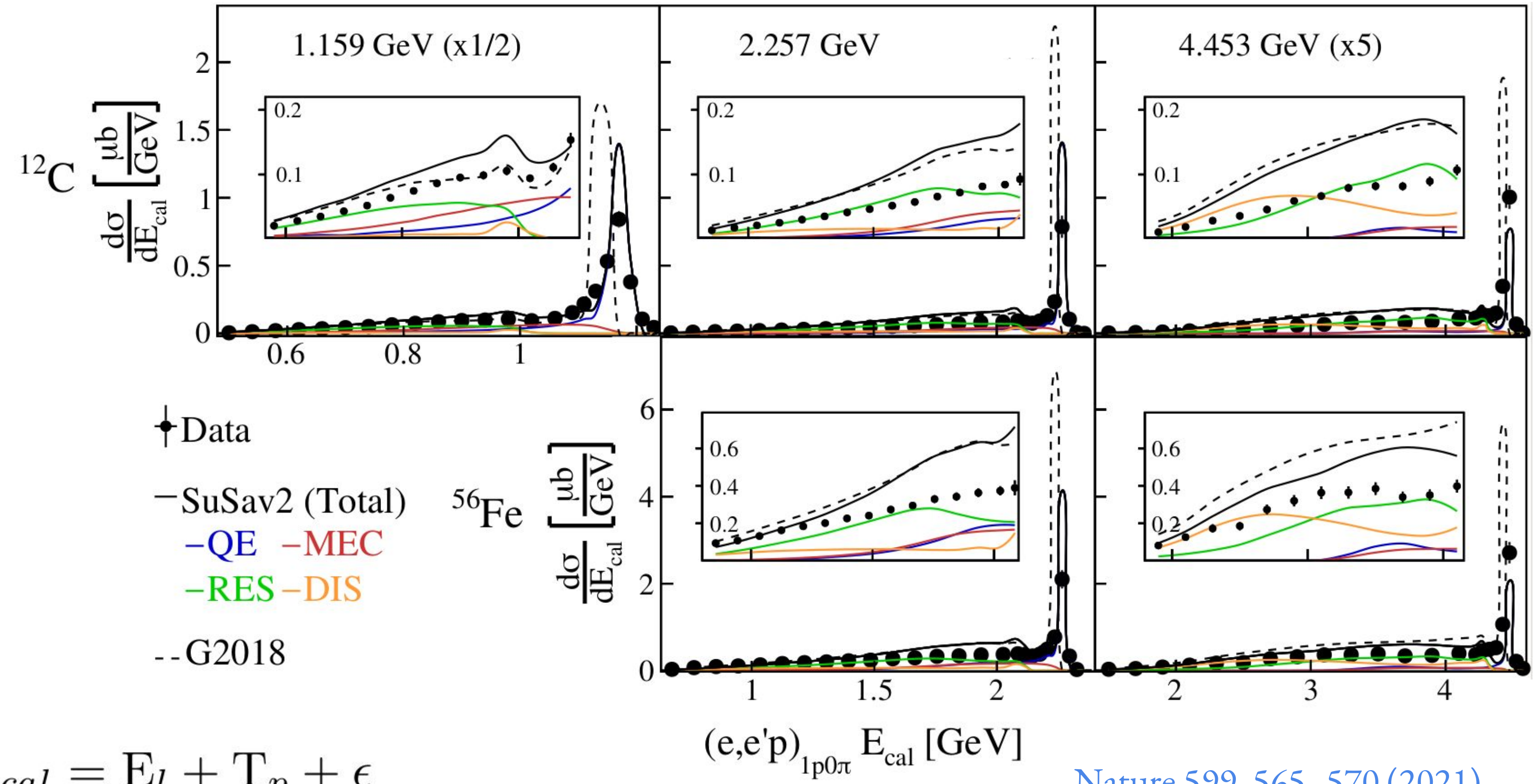

$$E_{cal} = E_l + T_p + \epsilon$$

Nature 599, 565–570 (2021)

Nucleus & Energy Dependence

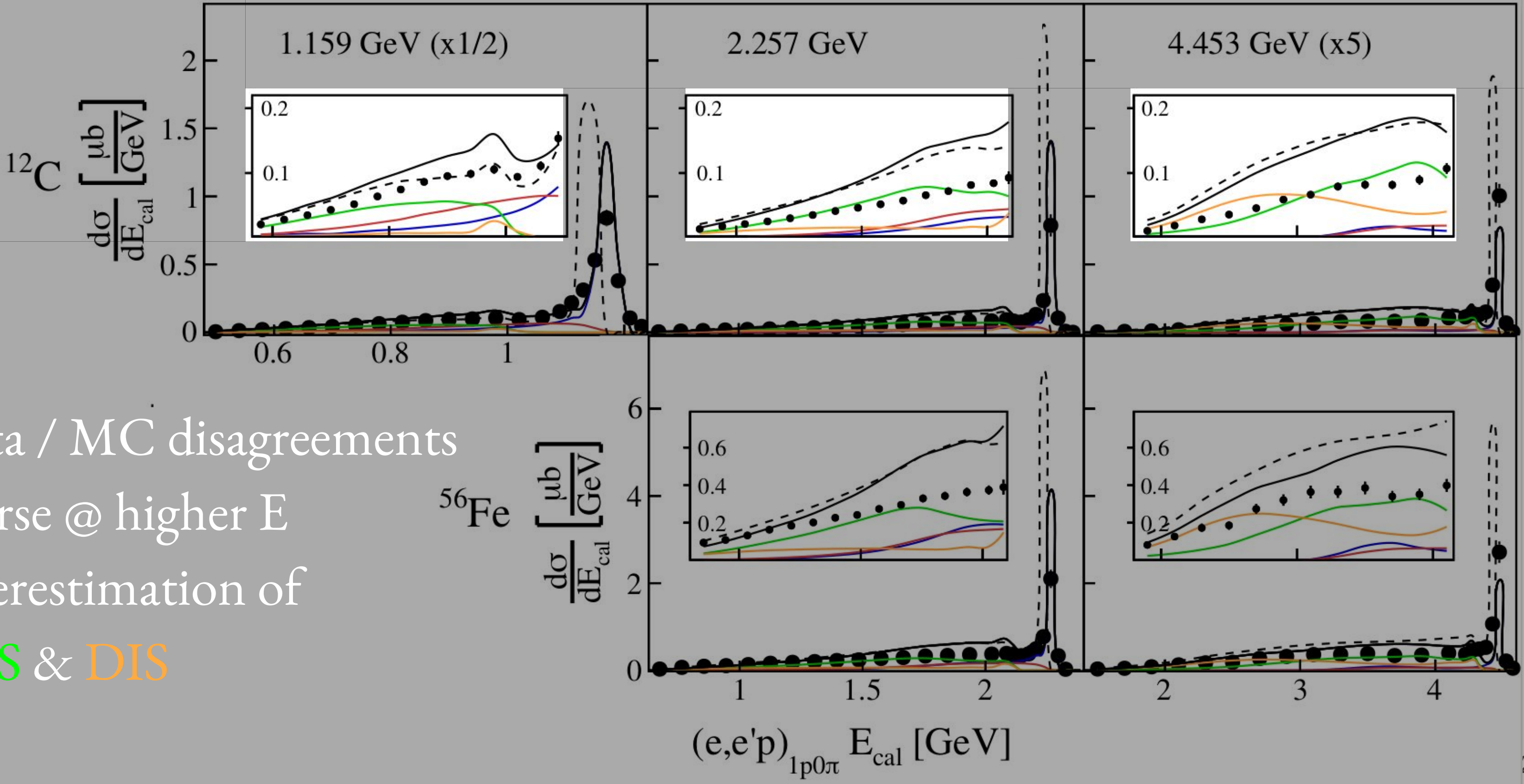

- Data / MC disagreements
- Worse @ higher E
- Overestimation of RES & DIS

Nucleus & Energy Dependence

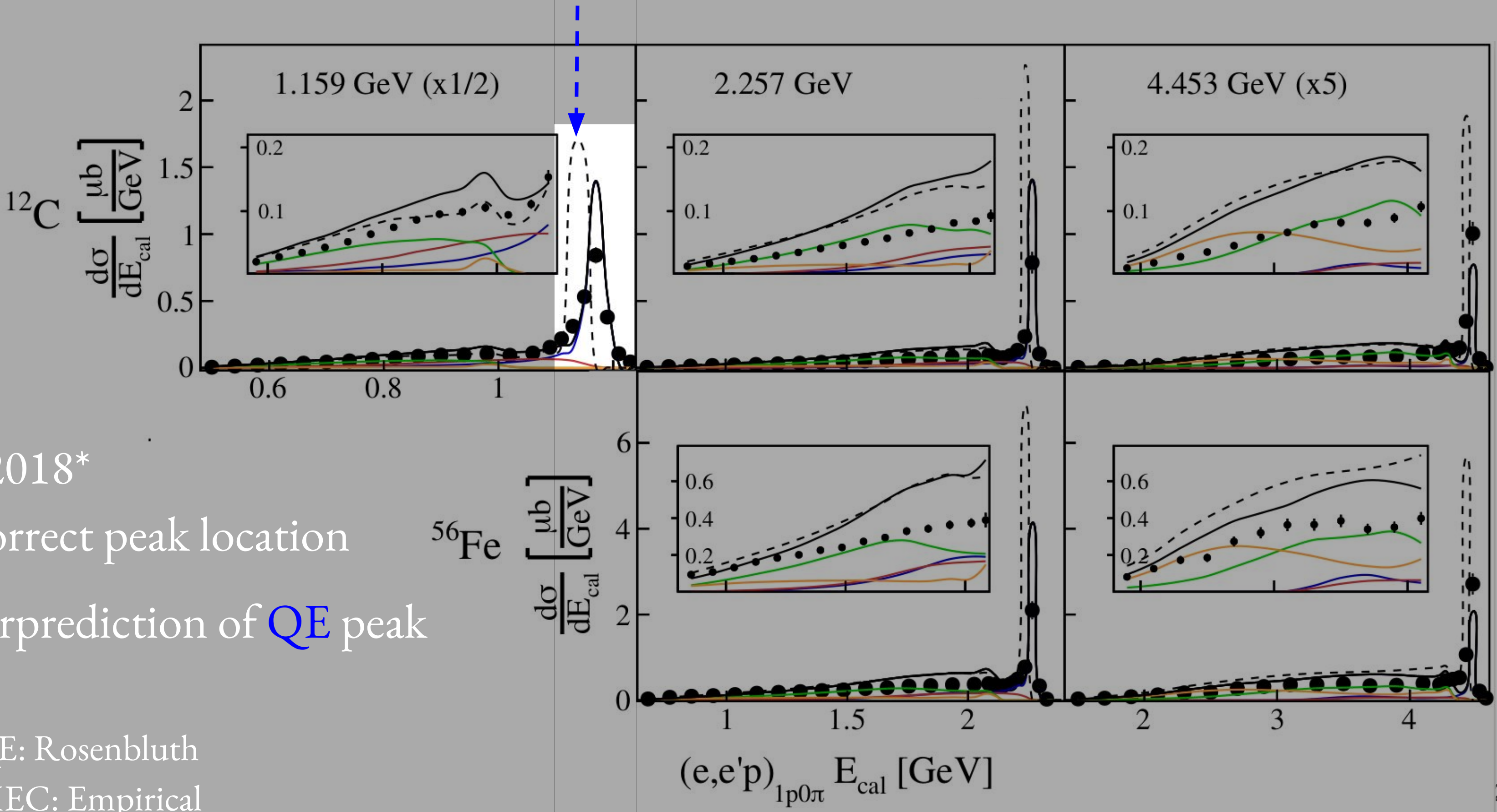

--- G2018*

- Incorrect peak location
- Overprediction of QE peak

* EMQE: Rosenbluth
EMMEC: Empirical

Nucleus & Energy Dependence

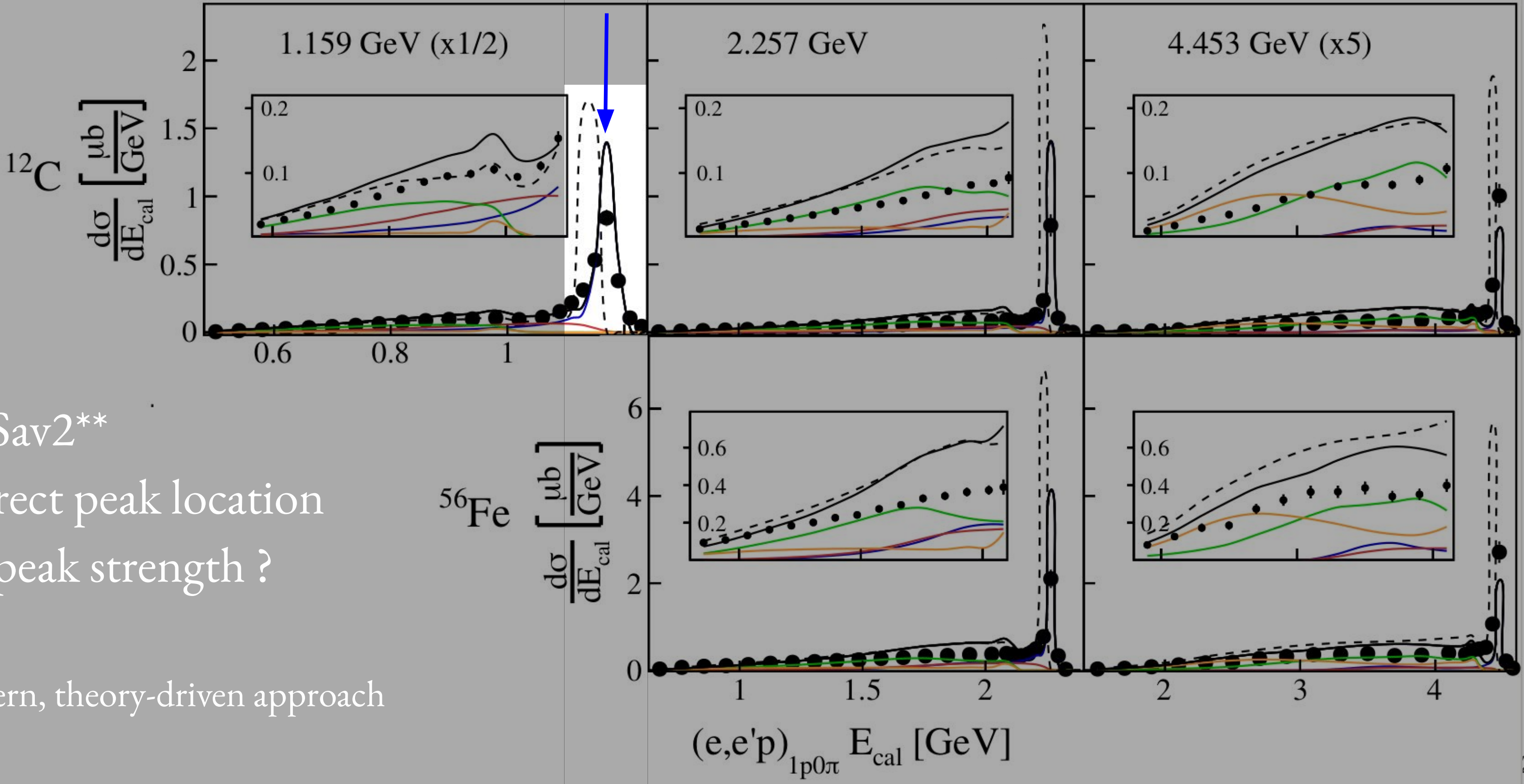

– SuSav2**

- Correct peak location
- QE peak strength ?

** Modern, theory-driven approach

Transverse Momentum

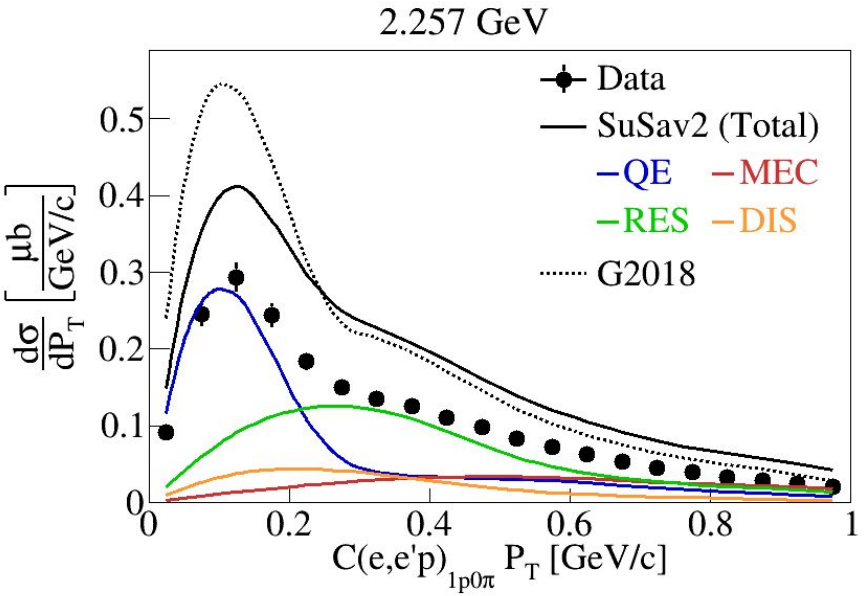

Nature 599, 565–570 (2021)

$$P_T = |\,\mathbf{P_T}^{e'} + \mathbf{P_T}^{p}\,|$$

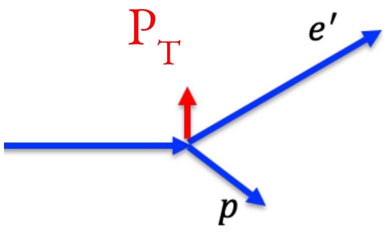

- P_T sensitivity to nuclear effects (fermi motion, final-state interactions, ...)
- Overestimation of QE peak & RES tail

Energy Reconstruction In P_T Slices

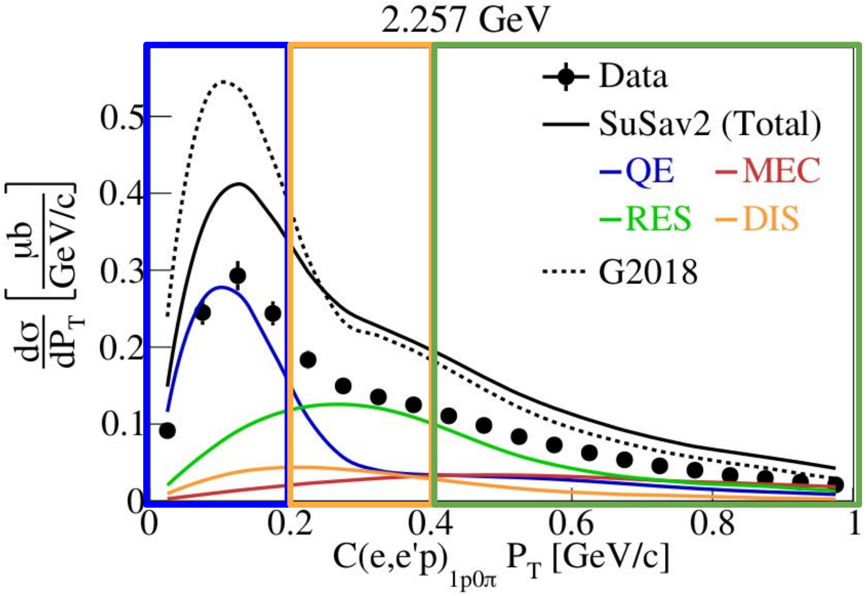

Nature 599, 565–570 (2021)

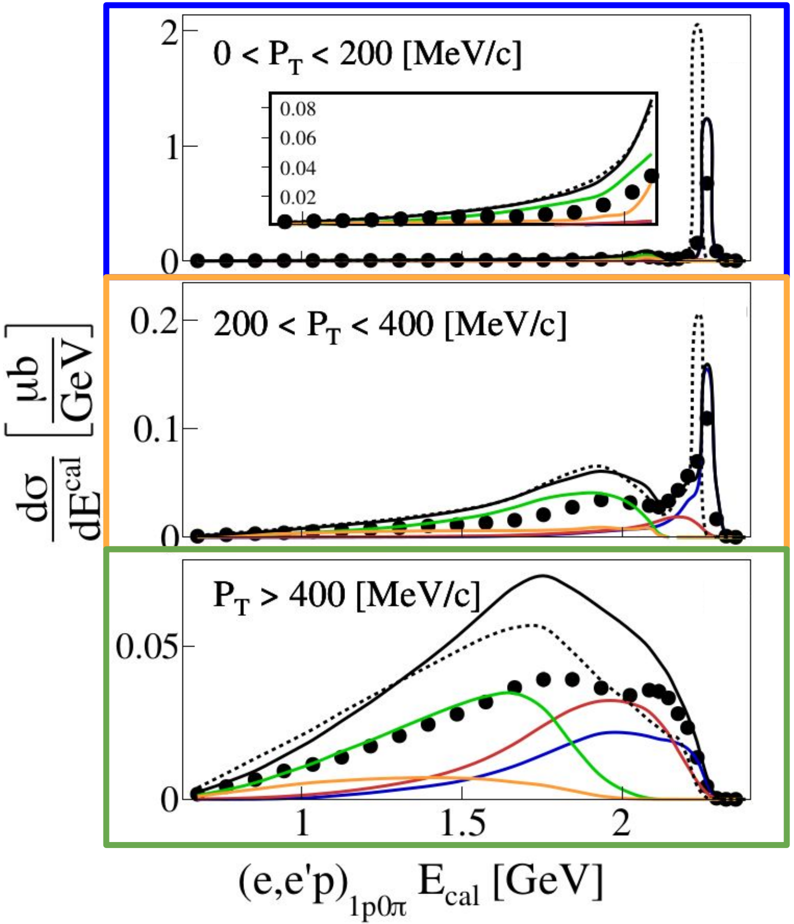

Example: Benchmarking New Generators & Kinematic Variables!

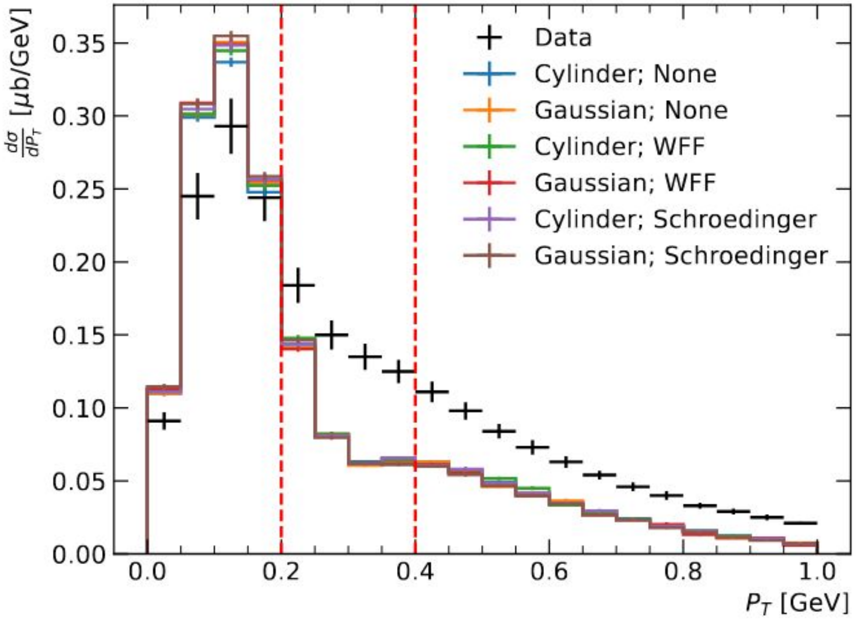

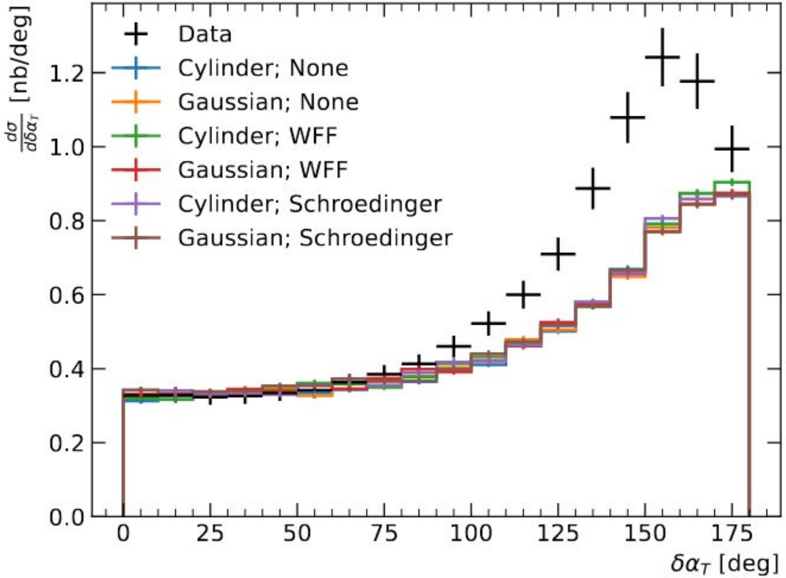

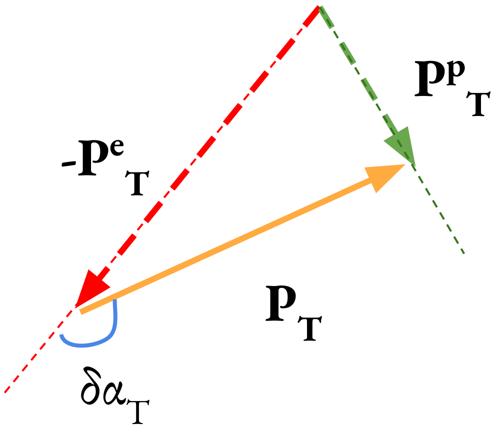

- $\delta\alpha_T$ sensitivity to final-state interactions

First step: only QE & FSI
ACHILLES arXiv: 2205.06378

Example: 2D Kinematic Imbalance

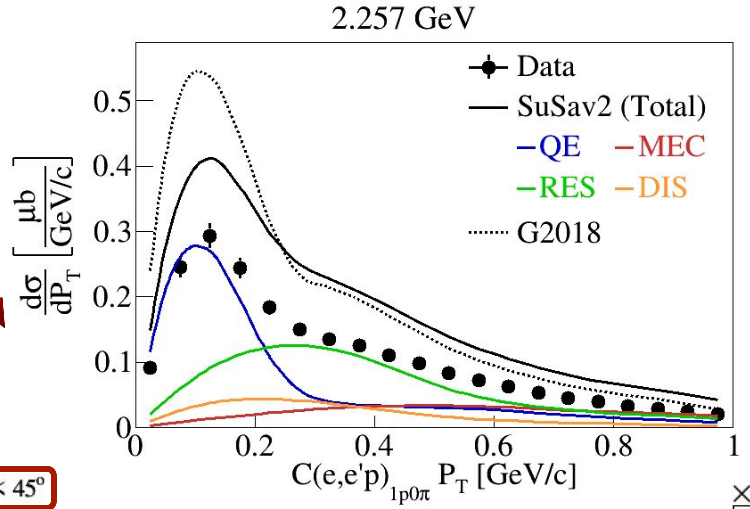

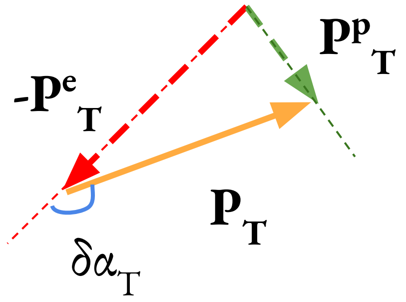

Low $\delta\alpha_T$

High $\delta\alpha_T$

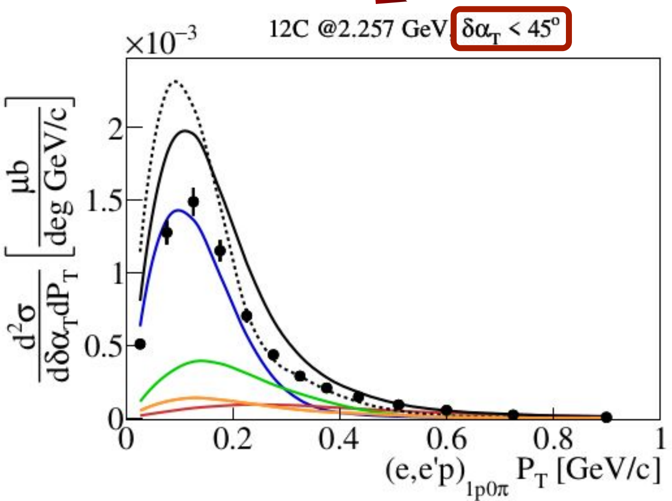

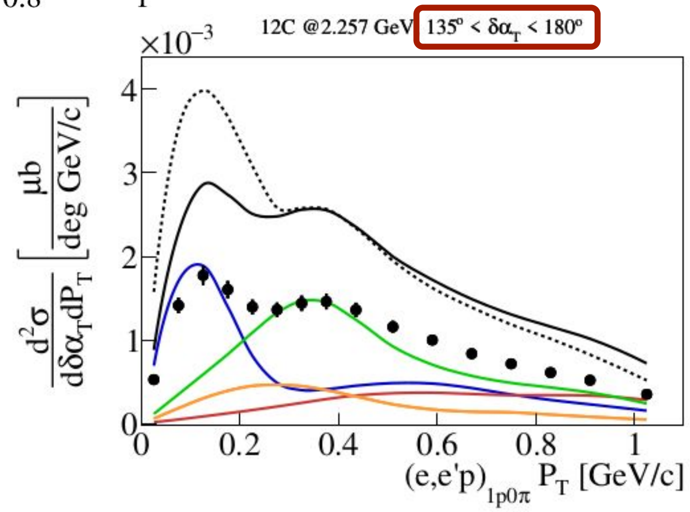

Example: 2D Kinematic Imbalance

Low $\delta\alpha_T$
QE-enhanced region
Sensitive to ground-state modeling

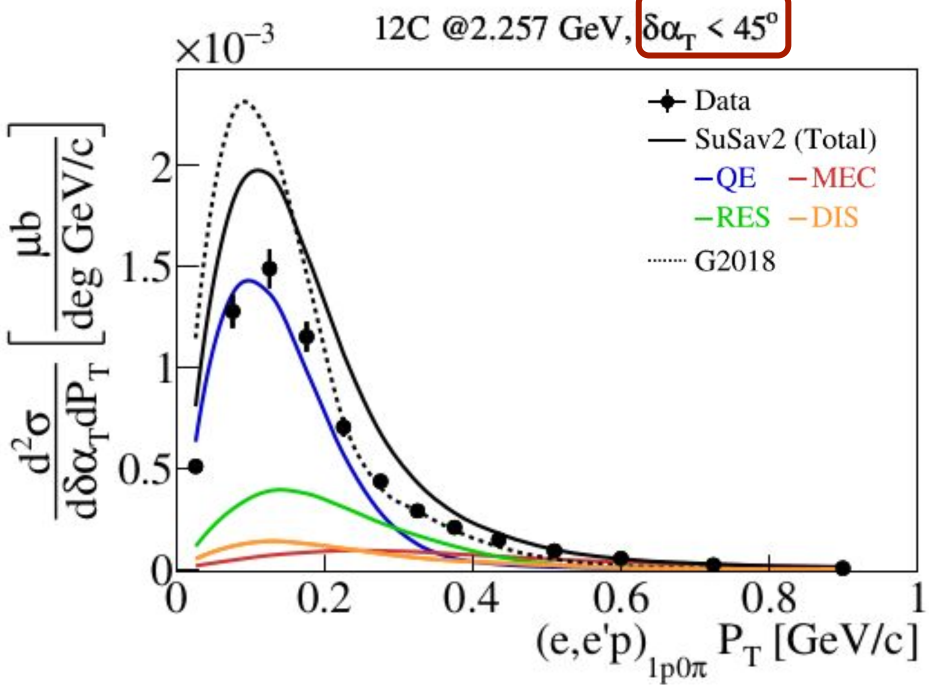

High $\delta\alpha_T$
Large non-QE contributions
Strong final-state interaction effects

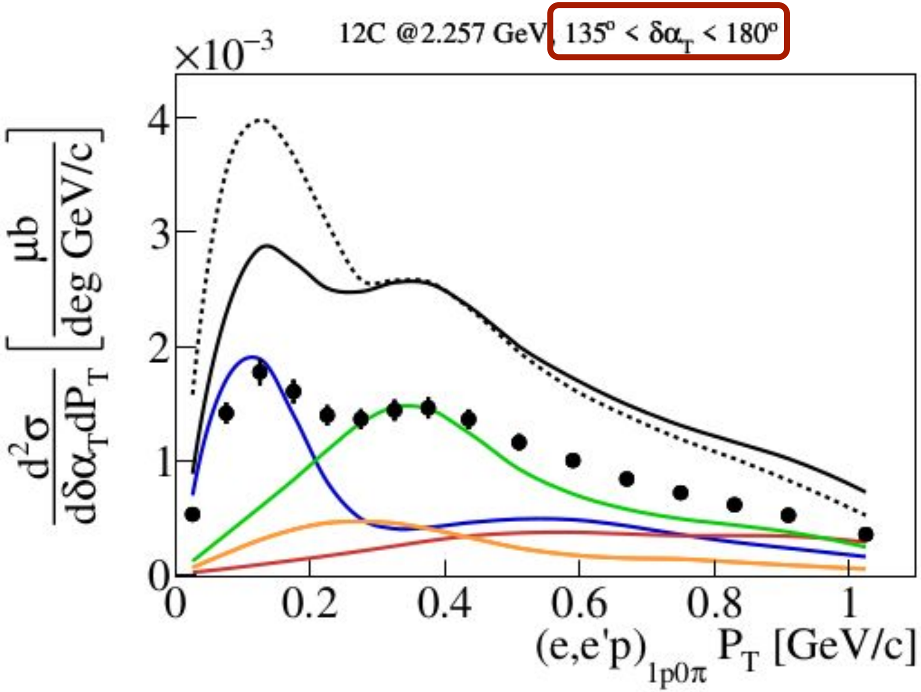

Example: 2D Kinematic Imbalance

Low $\delta\alpha_T$
QE-enhanced region
Sensitive to ground-state modeling

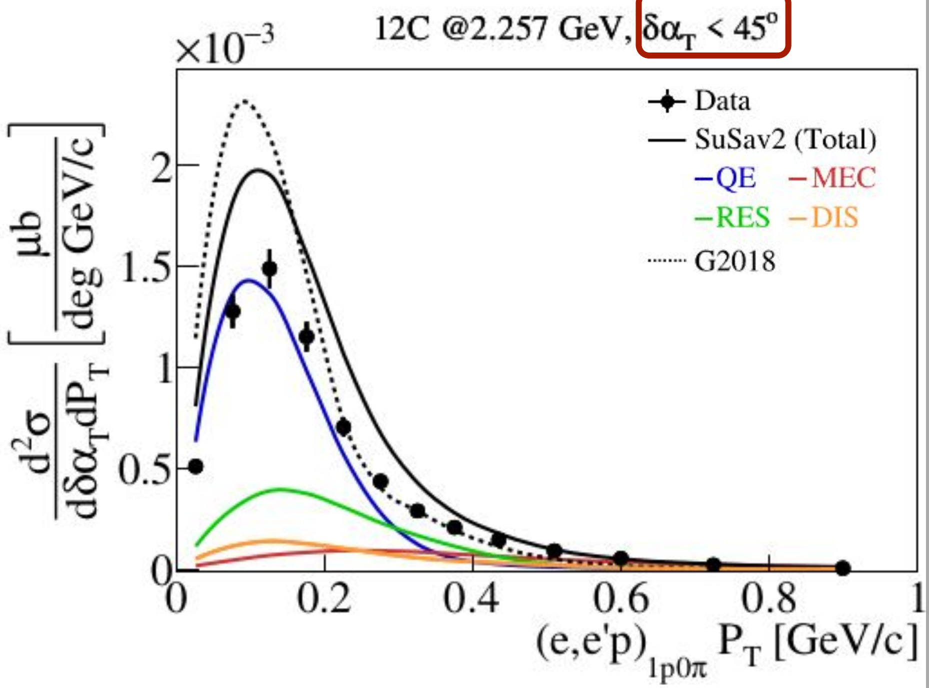

High $\delta\alpha_T$
Large non-QE contributions
Strong final-state interaction effects

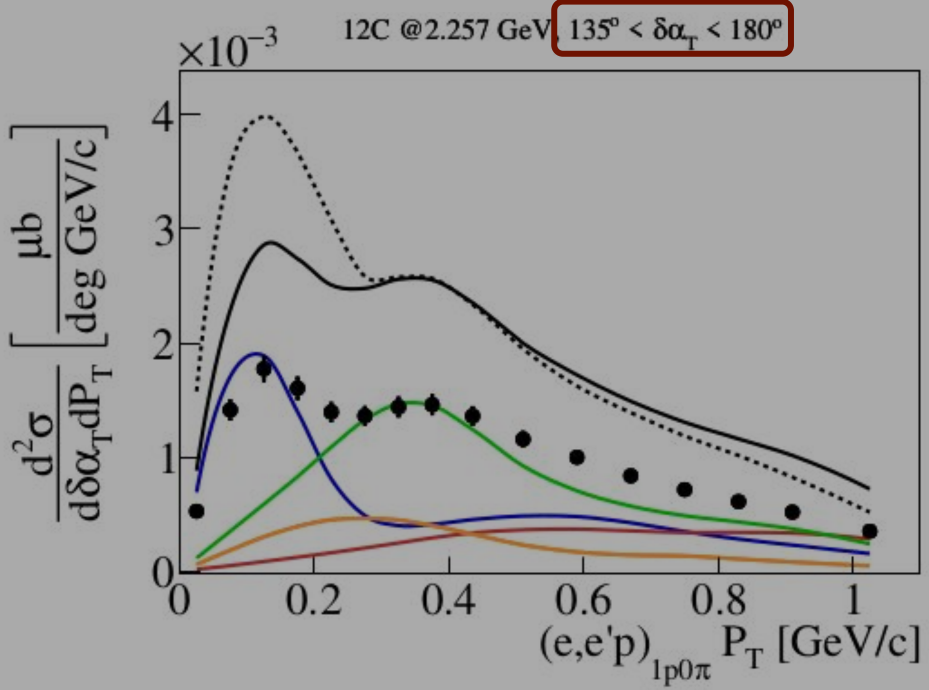

Example: 2D Kinematic Imbalance

Low $\delta\alpha_T$
QE-enhanced region
Sensitive to ground-state modeling

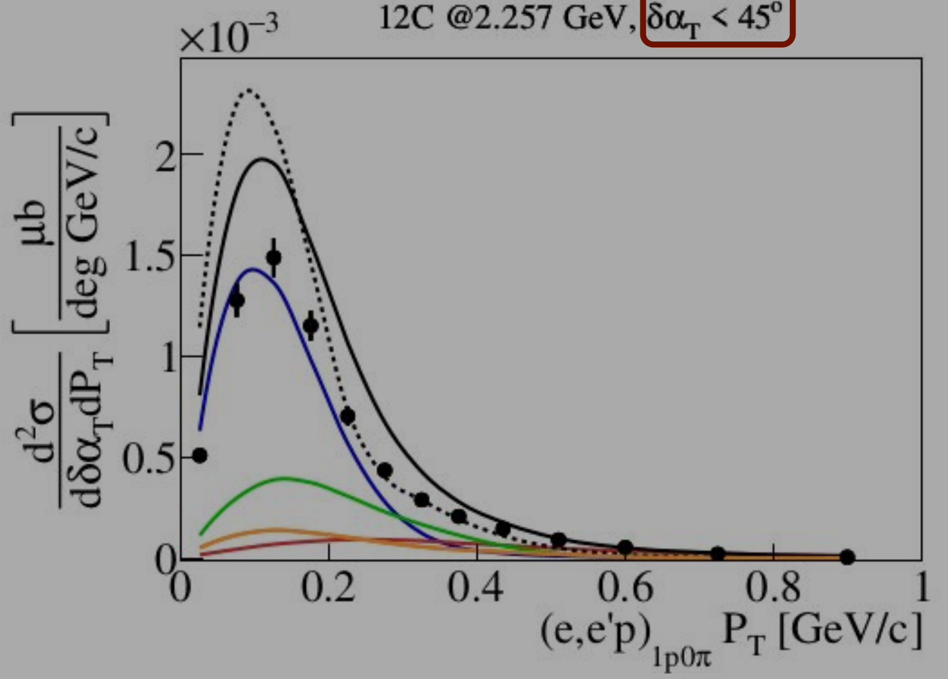

High $\delta\alpha_T$
Large non-QE contributions
Strong final-state interaction effects

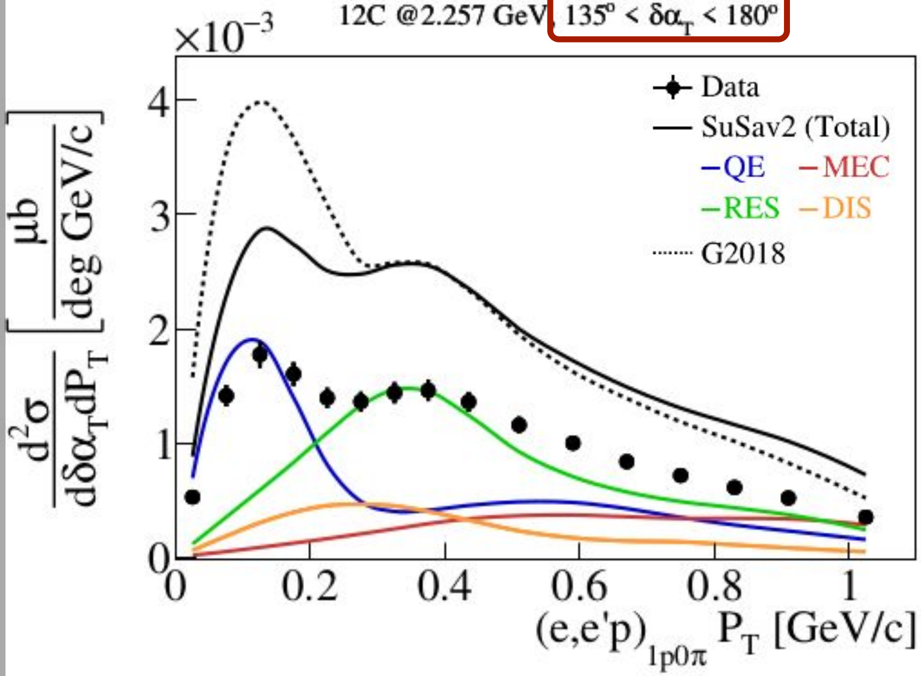

Next Steps

- Even more differential! Into the 3D multiverse
  Taking advantage of massive statistics
- More nuclear sensitivity variables
  Help decide what to tune
- 1p1π exclusive cross sections

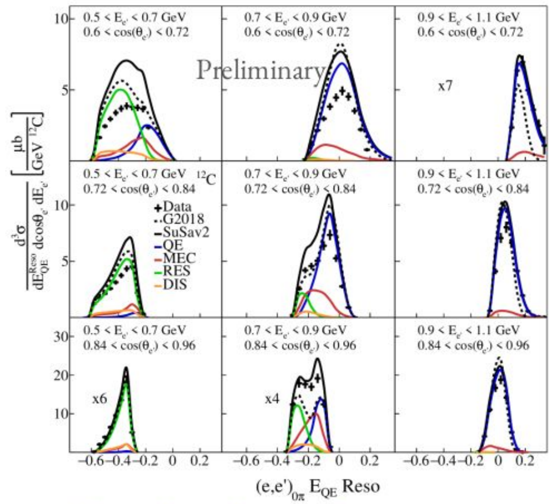

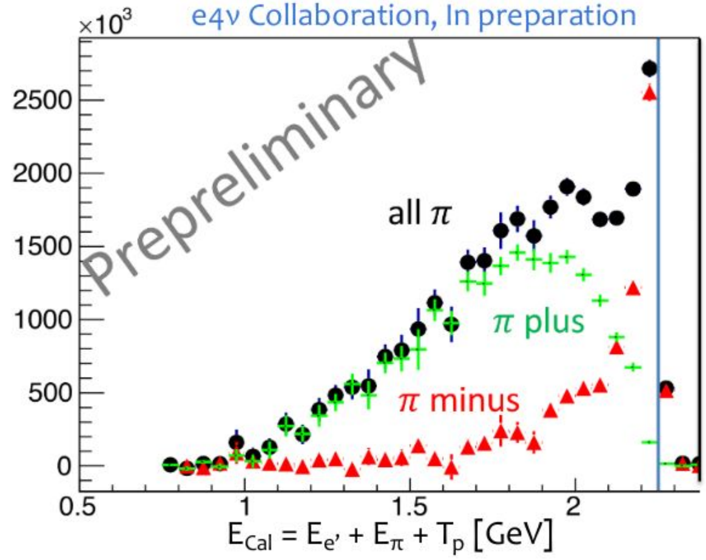

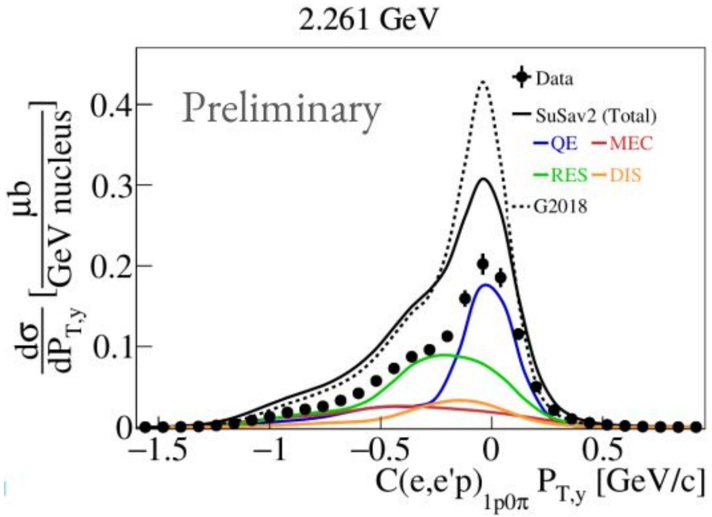

Next Steps

- More with CLAS6

❑ Proton transparency studies
  - Observable that summarizes strength of intranuclear rescattering
  - Measurement study
    $$T = N_{prot}^{detected} / N_{prot}^{PWIA}$$
  - Test event generator FSI models in GENIE across multiple nuclear targets
  - Testing dependency of transparency calculations on PWIA normalization

Phys. Rev. D **104**, 053006 (2021)

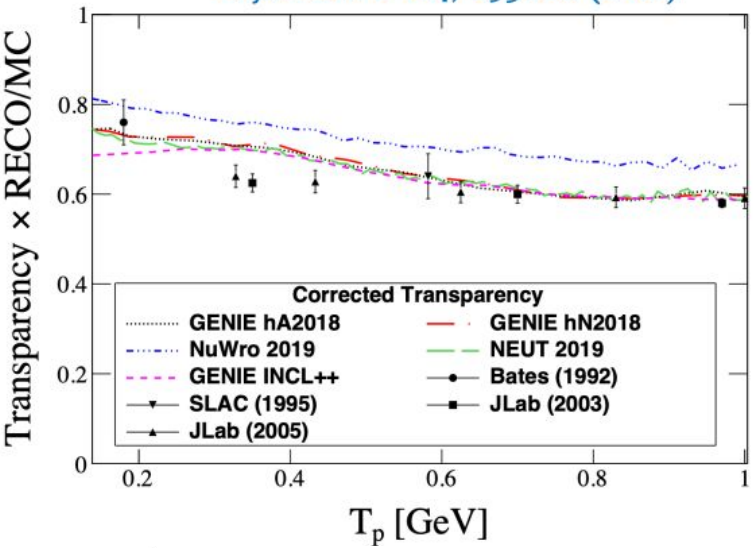

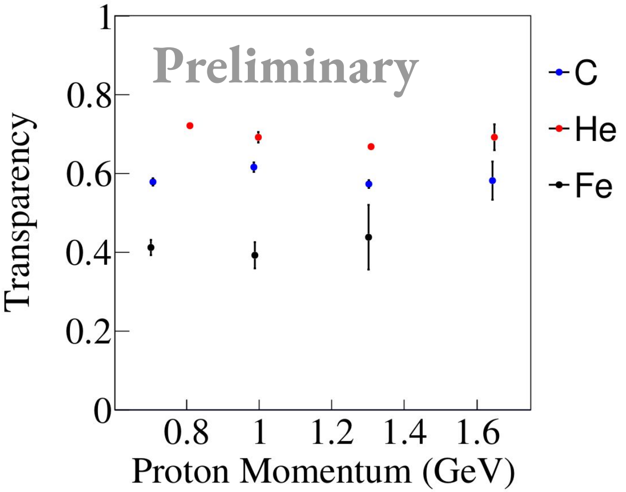

Next Steps

- More with CLAS6

❑ Prepare suite of cross sections in same variables as neutrinos for first e-GENIE tune
  - Compare with neutrino CC0π tune

- e4ν data already being used to validate event generators

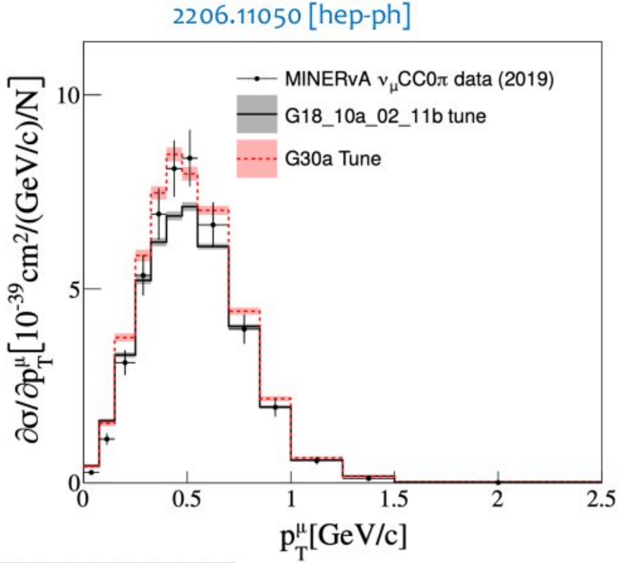

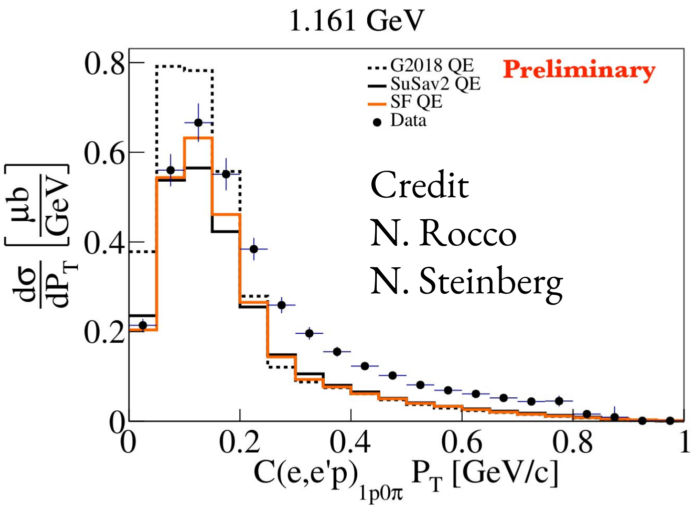

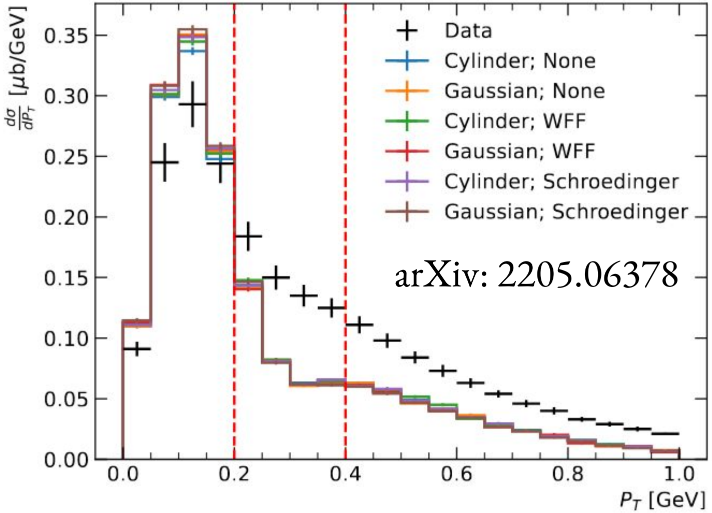

Next Steps

- New data with CLAS12
  Targets: ^{4}He, ^{12}C, **^{40}Ar**, ^{120}Sn
- 2 - 6 GeV beam energies
- More phase-space coverage ($\theta_e > 5^o$)
- Neutrons!

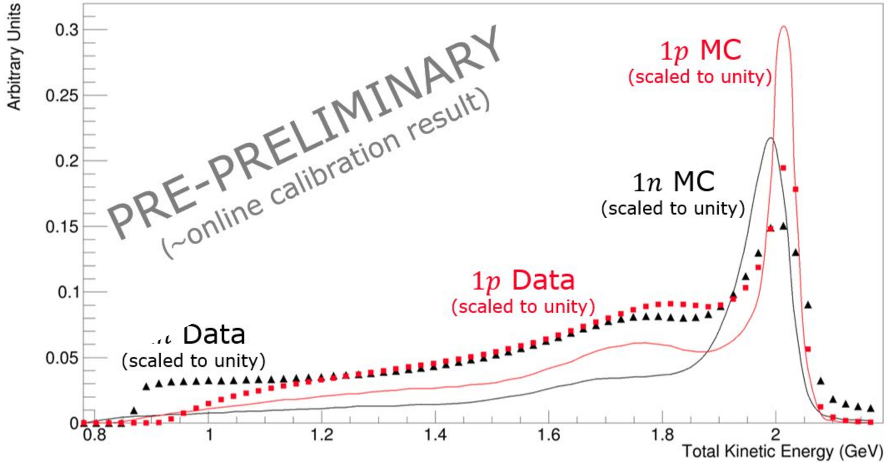

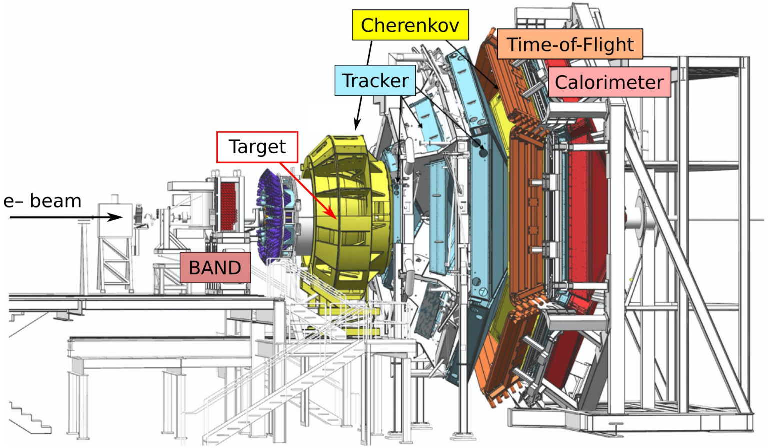

Mismodelling Impact On Mixing Parameters

Charged current cross sections obtained using GENIE for the DUNE near detector (left) and far detector (right) oscillated fluxes

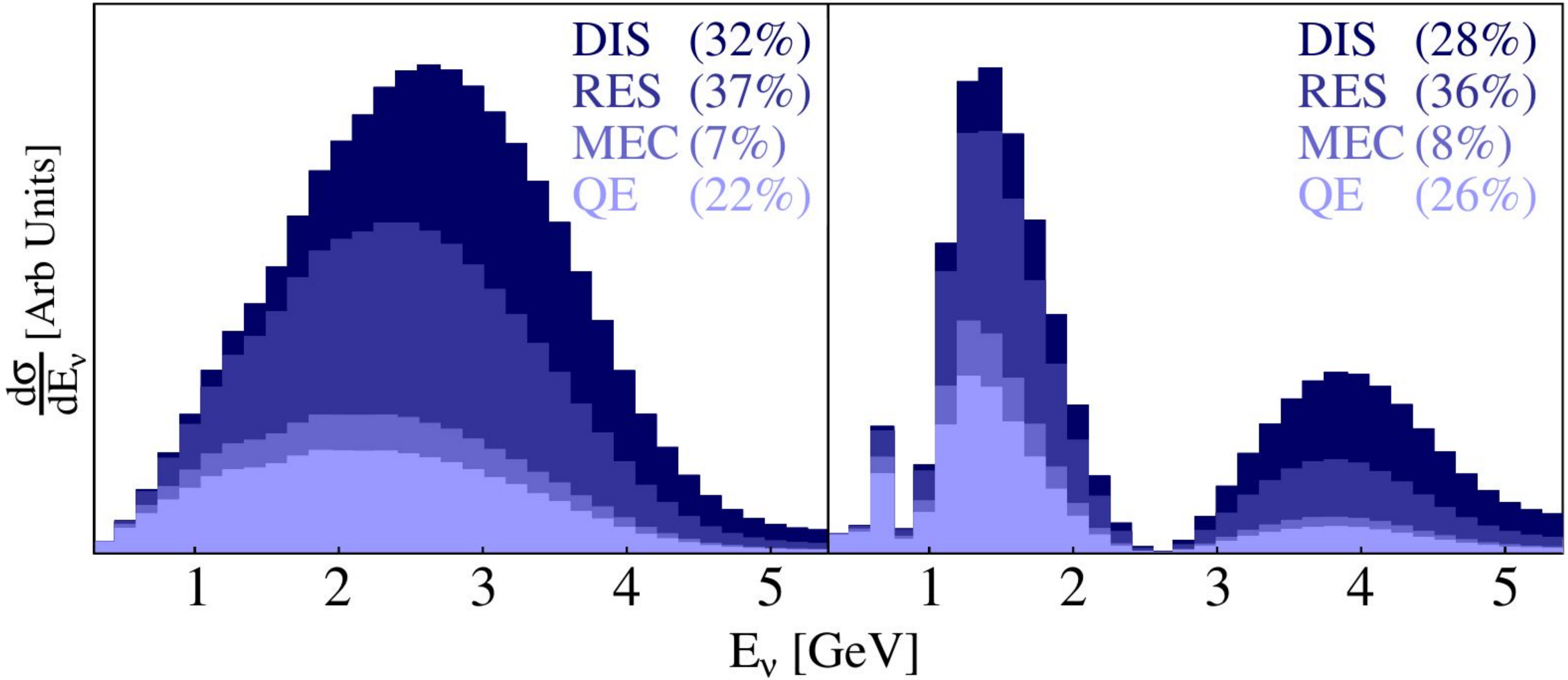

Phys. Rev. D 103, 113003 (2021)

Issues Identified & Fixed In G2018

(e,e') ^{12}C with G2018

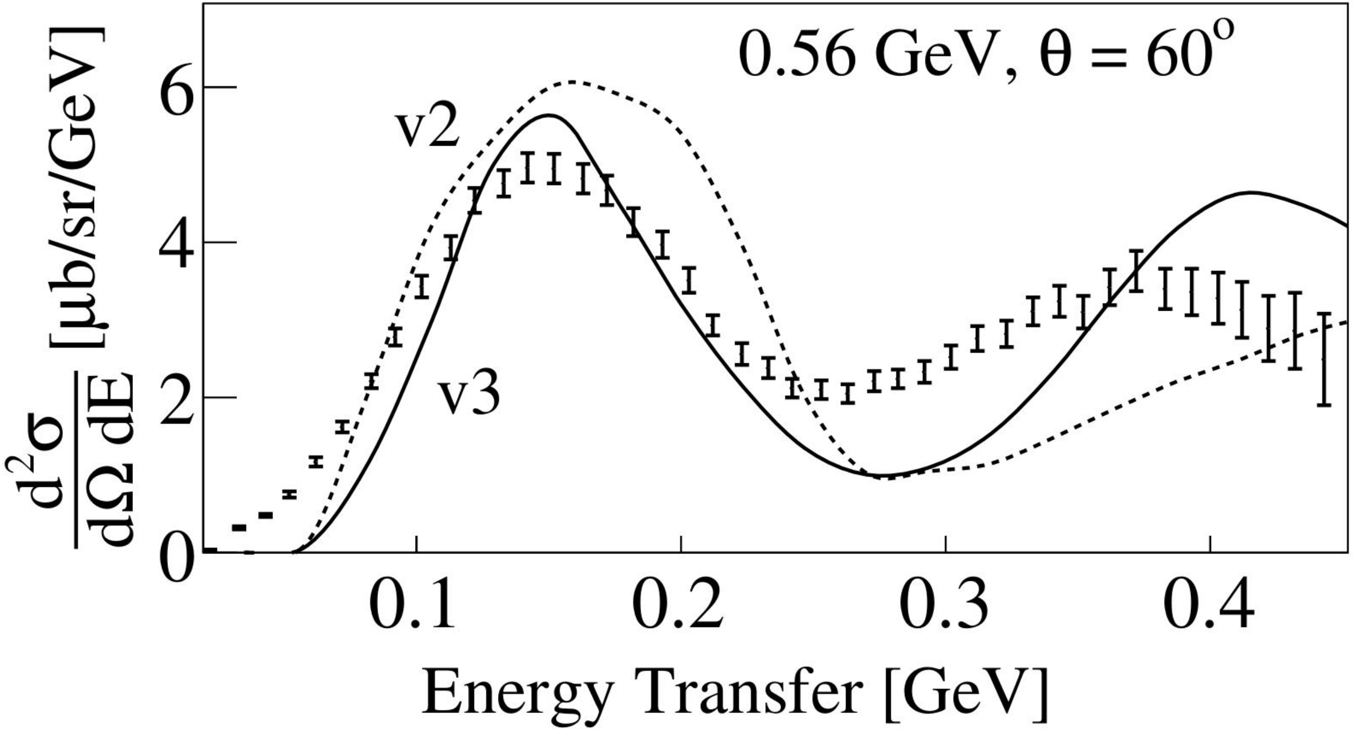

Phys. Rev. D 103, 113003 (2021)

SuSav2 Offers More Accurate Prediction

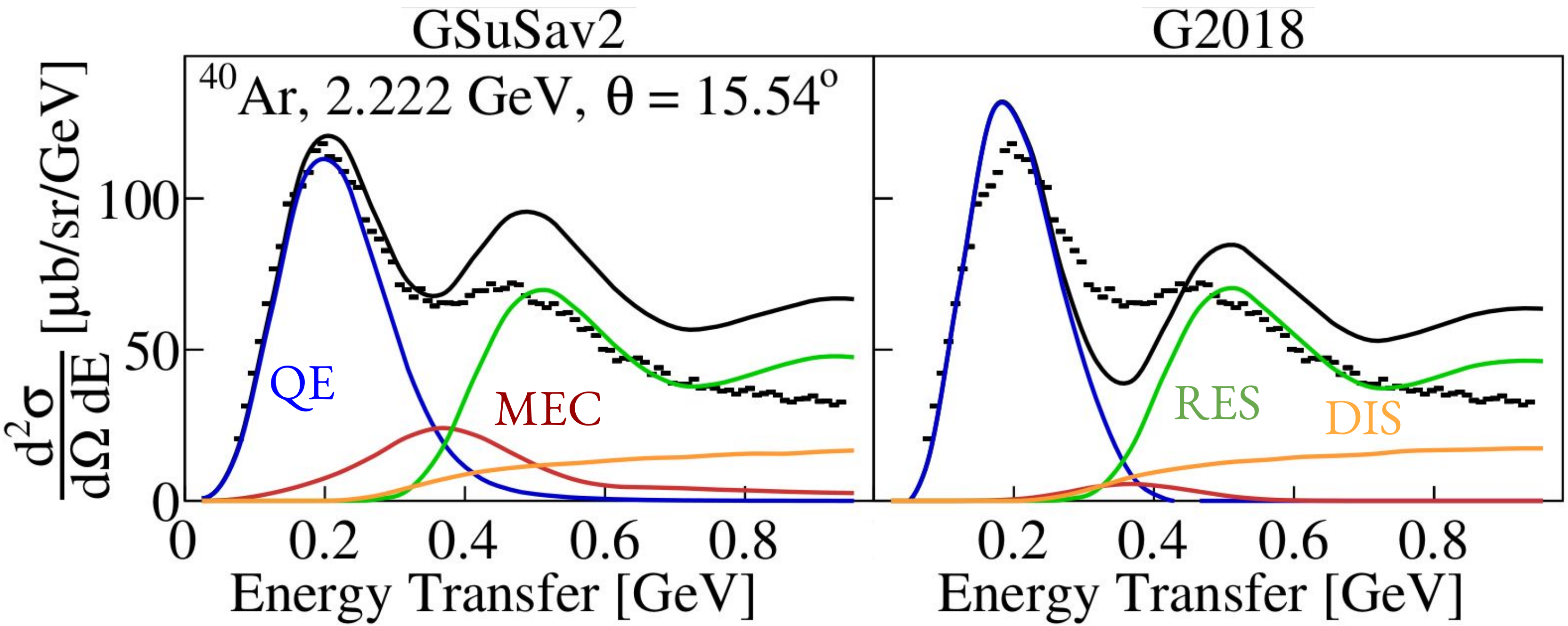

Phys. Rev. D 103, 113003 (2021)

Probing The Neutrino Phase-Space With Electrons

QE Events

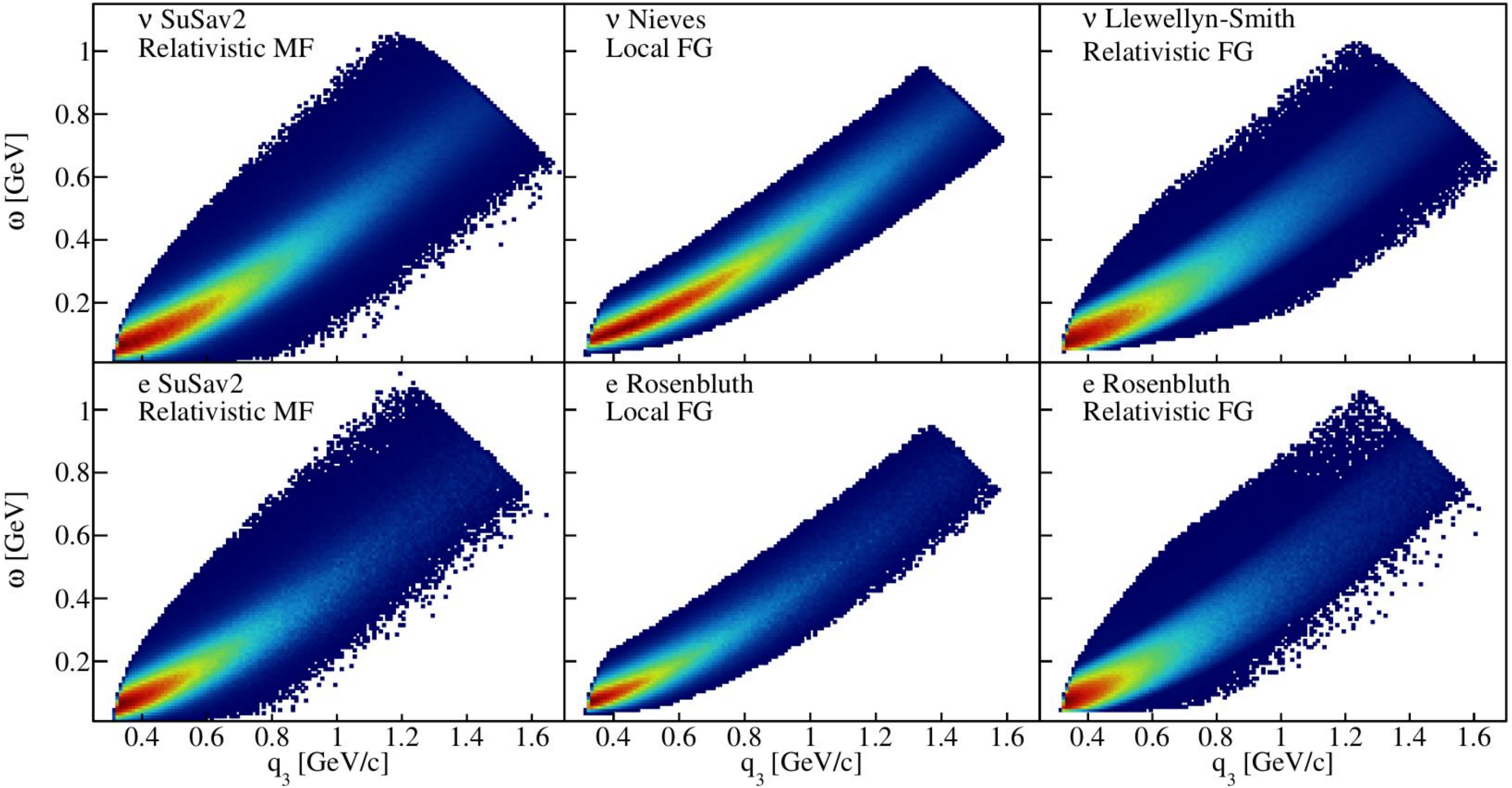

A.Papadopoulou, et al, Phys. Rev. D 103, 113003 (2021)

Electron results scaled by Q^4

Consistent Treatment Of MEC Events With SuSav2

Unique chance to constraint one of least understood interaction channels

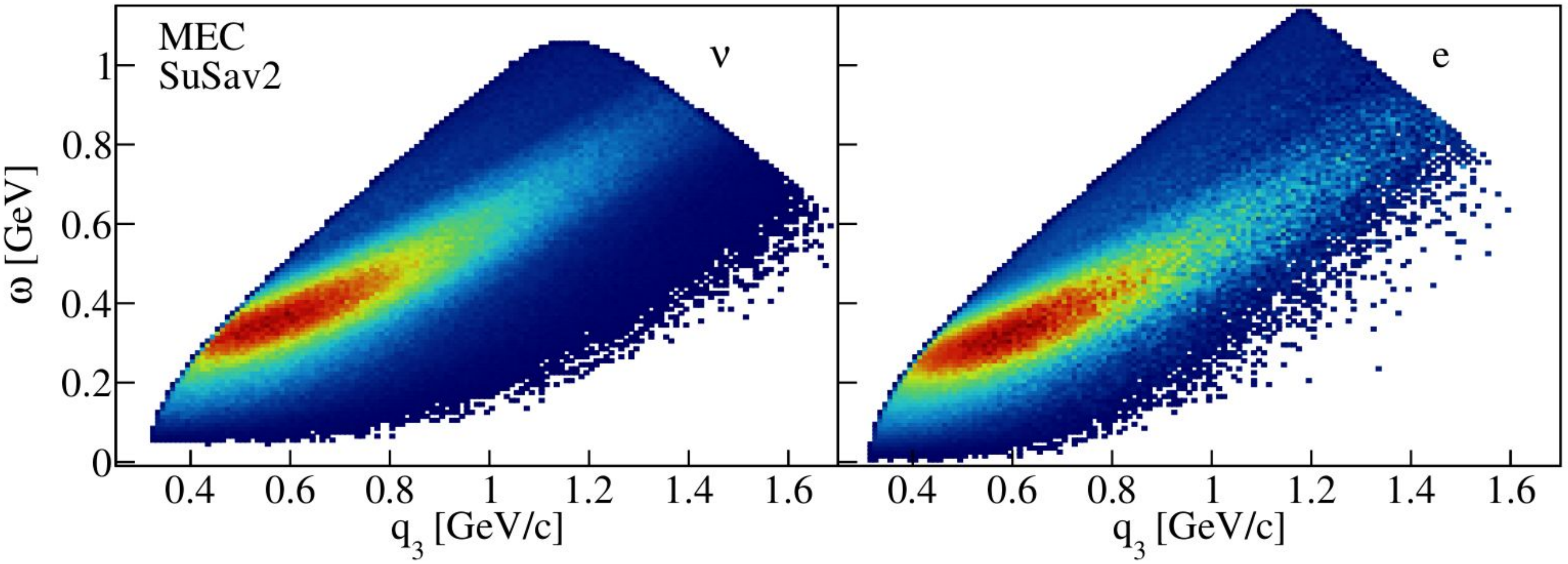

Phys. Rev. D 103, 113003 (2021)

Electron results scaled by Q^4

Inclusive C cross sections

Phys. Rev. D 103, 113003 (2021)

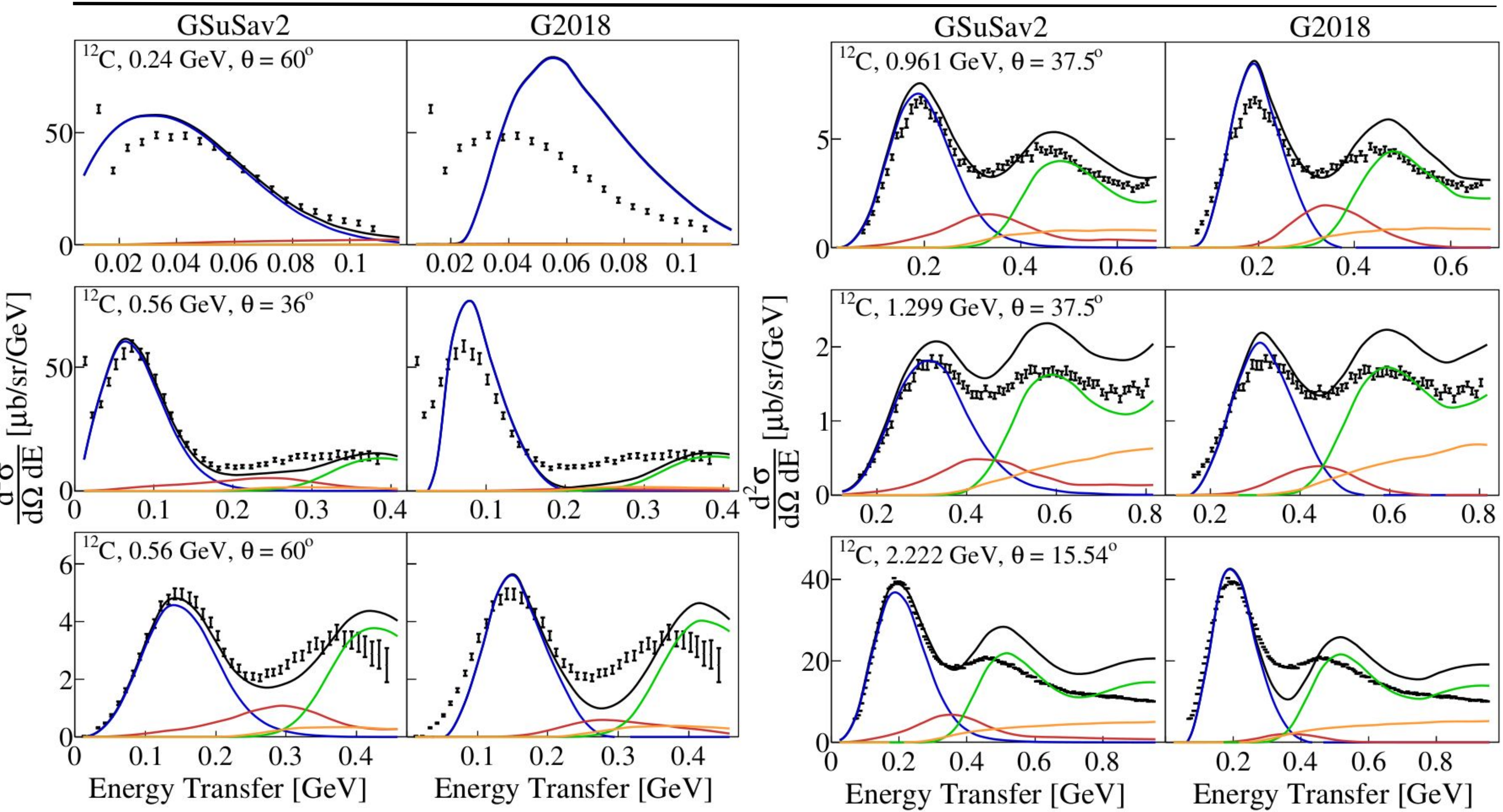

Inclusive C/Fe cross sections

Phys. Rev. D 103, 113003 (2021)

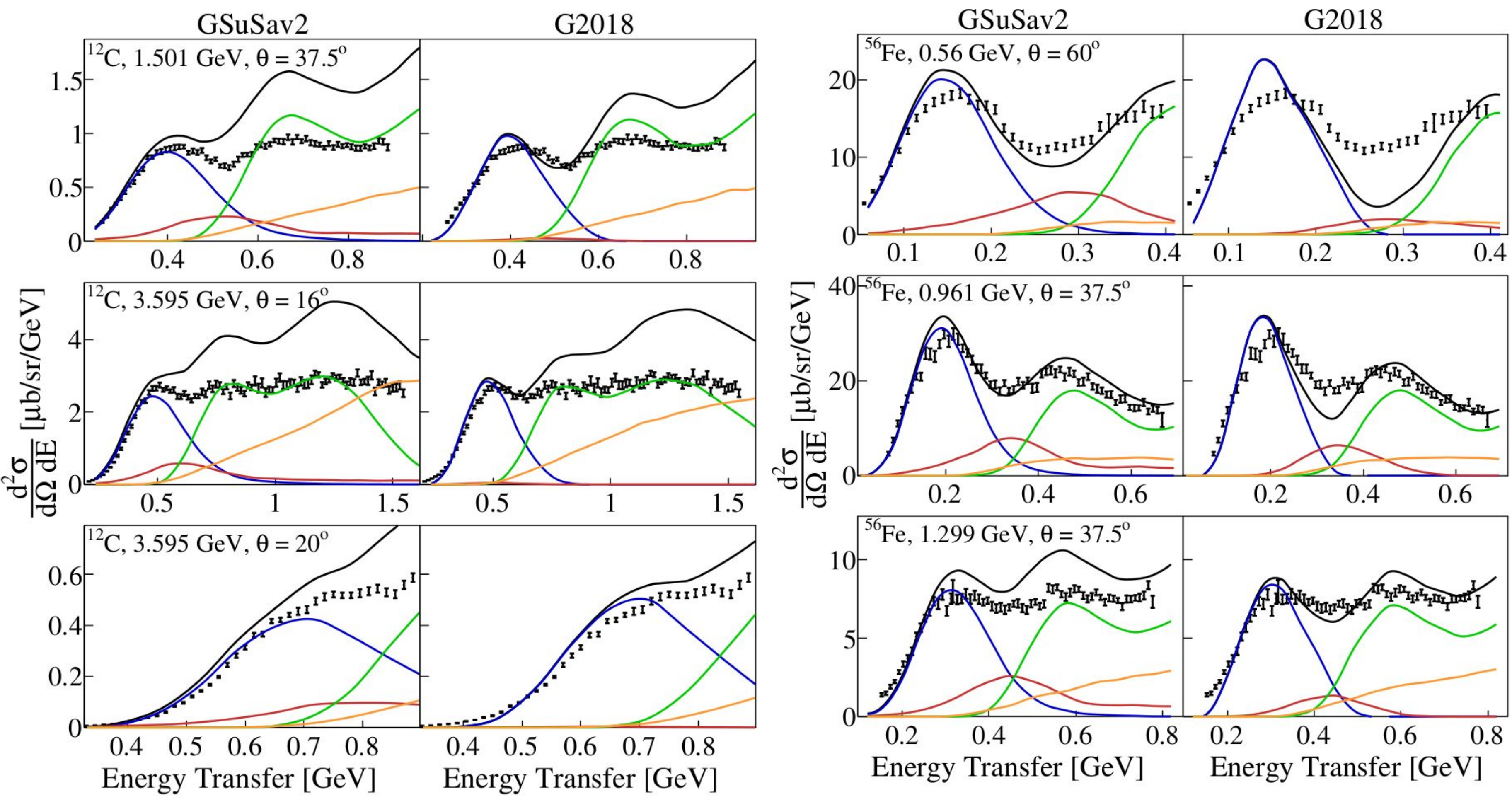

Inclusive H cross sections

Phys. Rev. D 103, 113003 (2021)

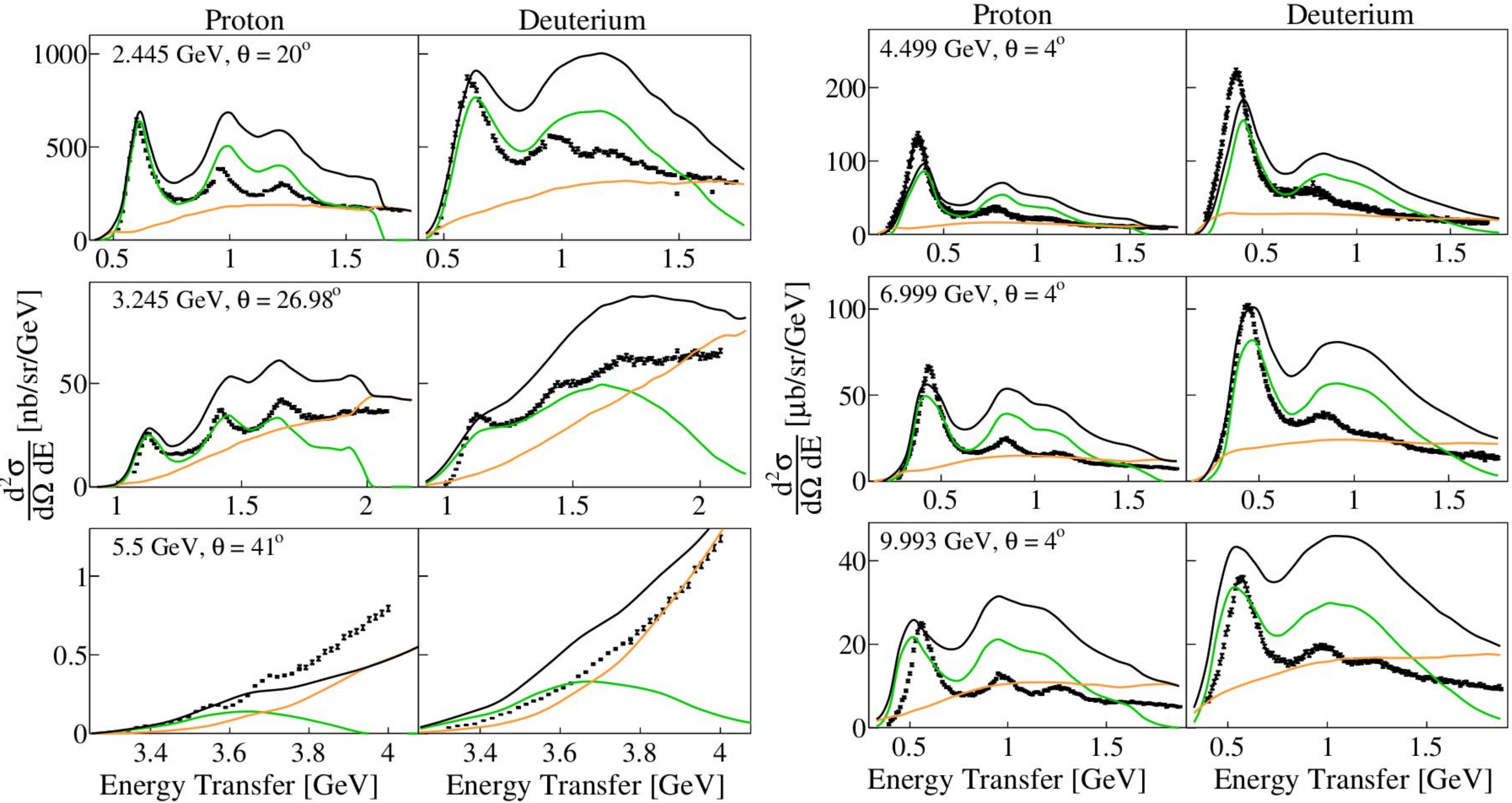

Sanity Check With Inclusive Cross Sections

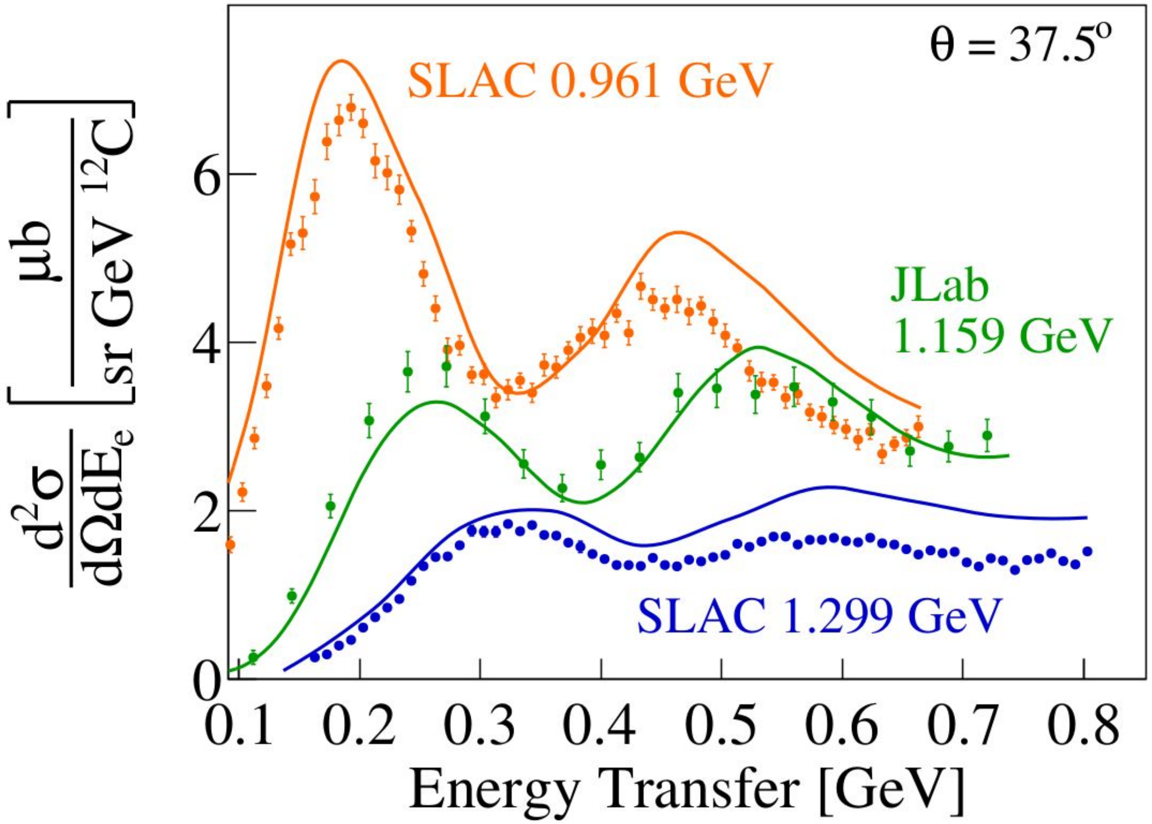

M.Khachatryan, A.Papadopoulou, et al. Nature 599, 565–570 (2021)

Detected Hadron Multiplicities

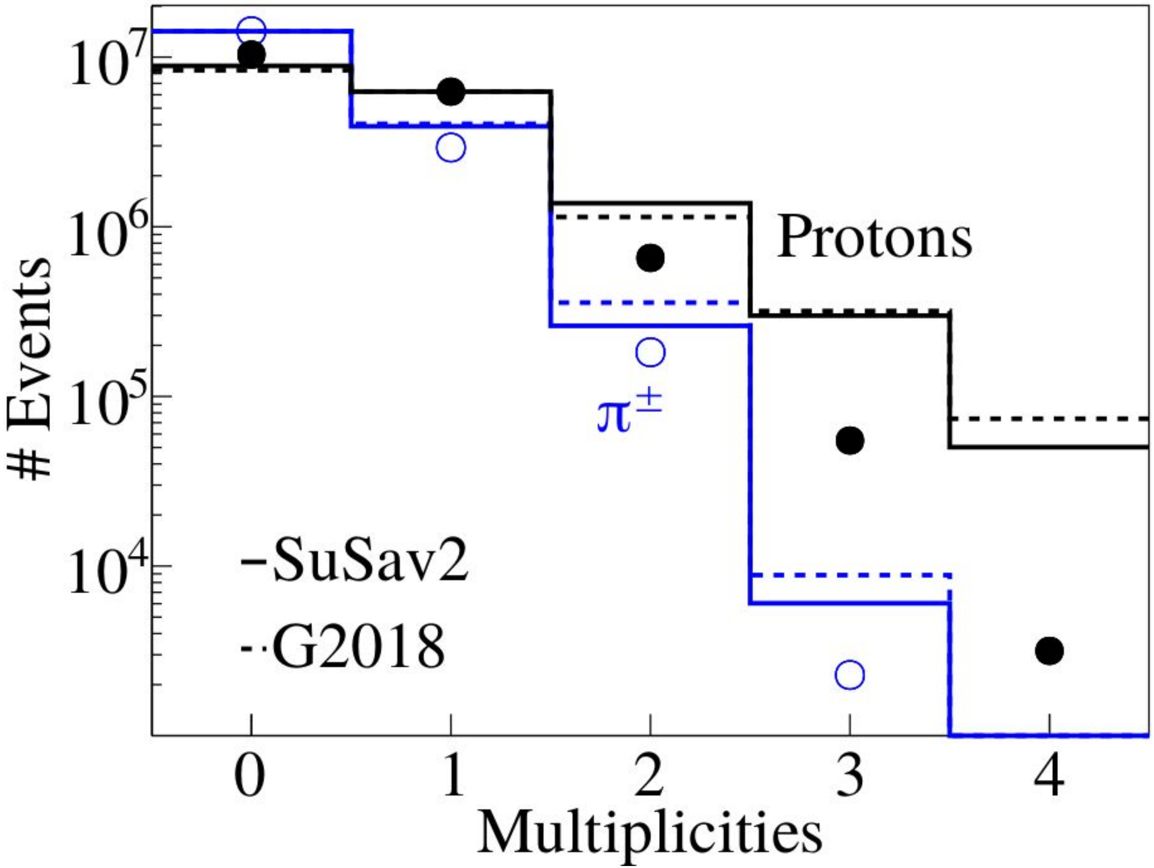

^{12}C @ 2.2 GeV

$P_p > 300$ MeV/c
$P_\pi > 150$ MeV/c

Simulation overpredicts hadron multiplicities

M.Khachatryan, A.Papadopoulou, et al. Nature 599, 565–570 (2021)

Q^4 Scaling Effect

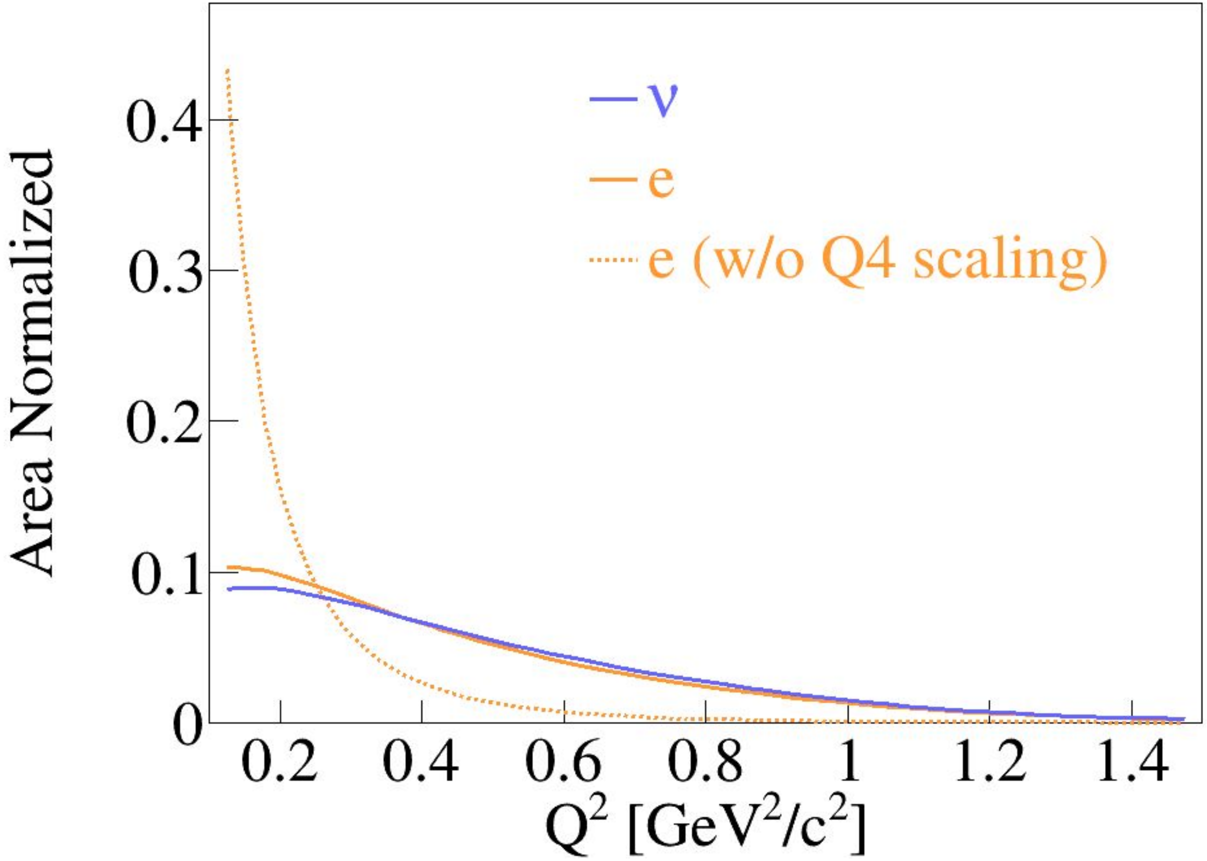

Available Nuclear Models

Phys. Rev. D 103, 113003 (2021)

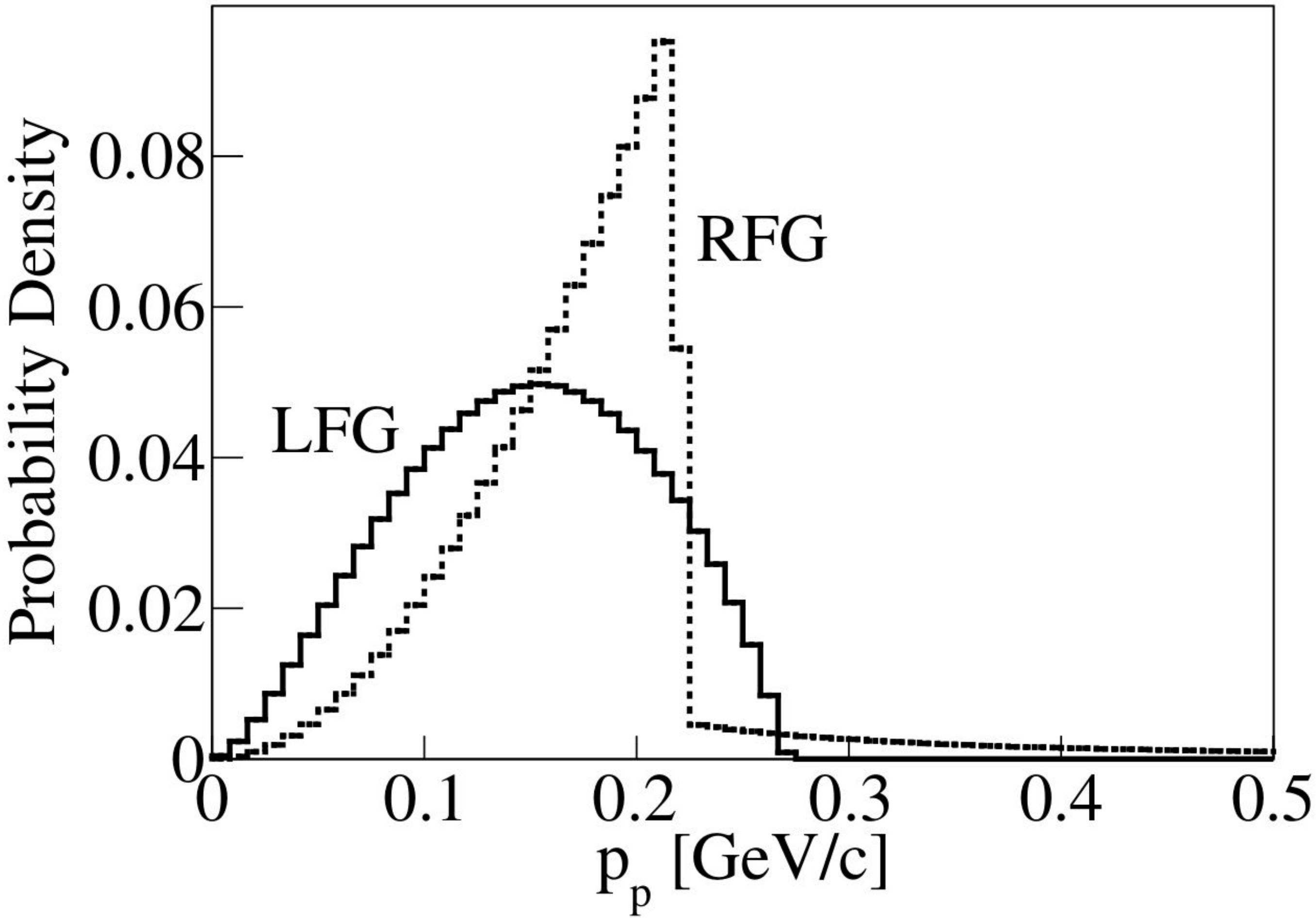

SuSav2 Configuration / GEM21_11b_00_000

	Electrons	Neutrinos
QE	SuSav2	SuSav2
MEC	SuSav2	SuSav2
RES	Berger-Sehgal	Berger-Sehgal
DIS	AGKY	AGKY
FSI	hN2018	hN2018
Nuclear Model	Relativistic Mean Field	Relativistic Mean Field

G2018 Model Configuration

	Electrons	Neutrinos
QE	Rosenbluth	Nieves
MEC	Empirical	Nieves
RES	Berger-Sehgal	Berger-Sehgal
DIS	AGKY	AGKY
FSI	hA2018	hA2018
Nuclear Model	Local Fermi Gas	Local Fermi Gas

Closure Test

- Use GENIE files
- Filter specific topologies (e.g. 1p0πp + 1p1π)
- Subtracted & True 1p0π are in good agreement

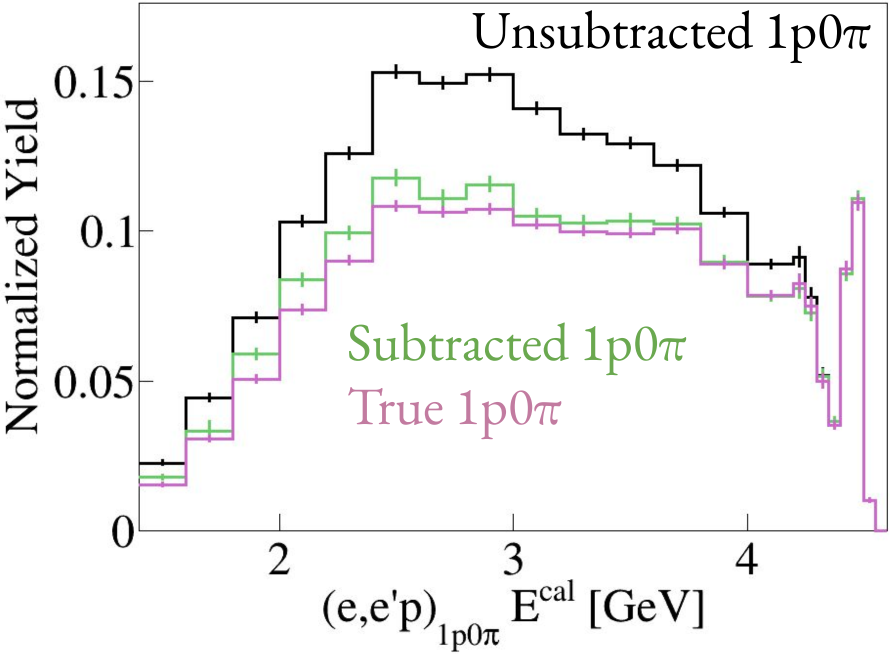

Well defined signal definition: Min θ_e Cut

@ 1.1 GeV: $\theta = 17 + 7 / P$

@ 2.2 GeV: $\theta = 16 + 10.5 / P$

@ 4.4 GeV: $\theta = 13.5 + 15 / P$

See backup for p / $\pi^{+/-}$ definitions

- We do not acceptance correct below min θ

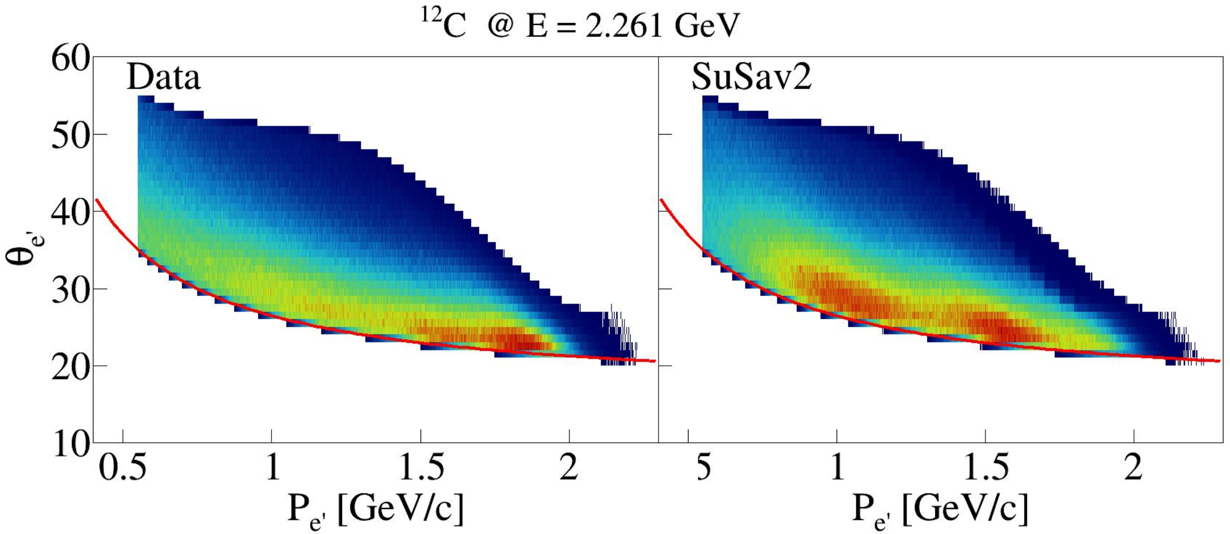

Well defined signal definition: Min θ_e Cut

@ 1.1 GeV: $\theta = 17 + 7 / P$

@ 2.2 GeV: $\theta = 16 + 10.5 / P$

@ 4.4 GeV: $\theta = 13.5 + 15 / P$

See backup for p / $\pi^{+/-}$ definitions

- We do not acceptance correct below min θ

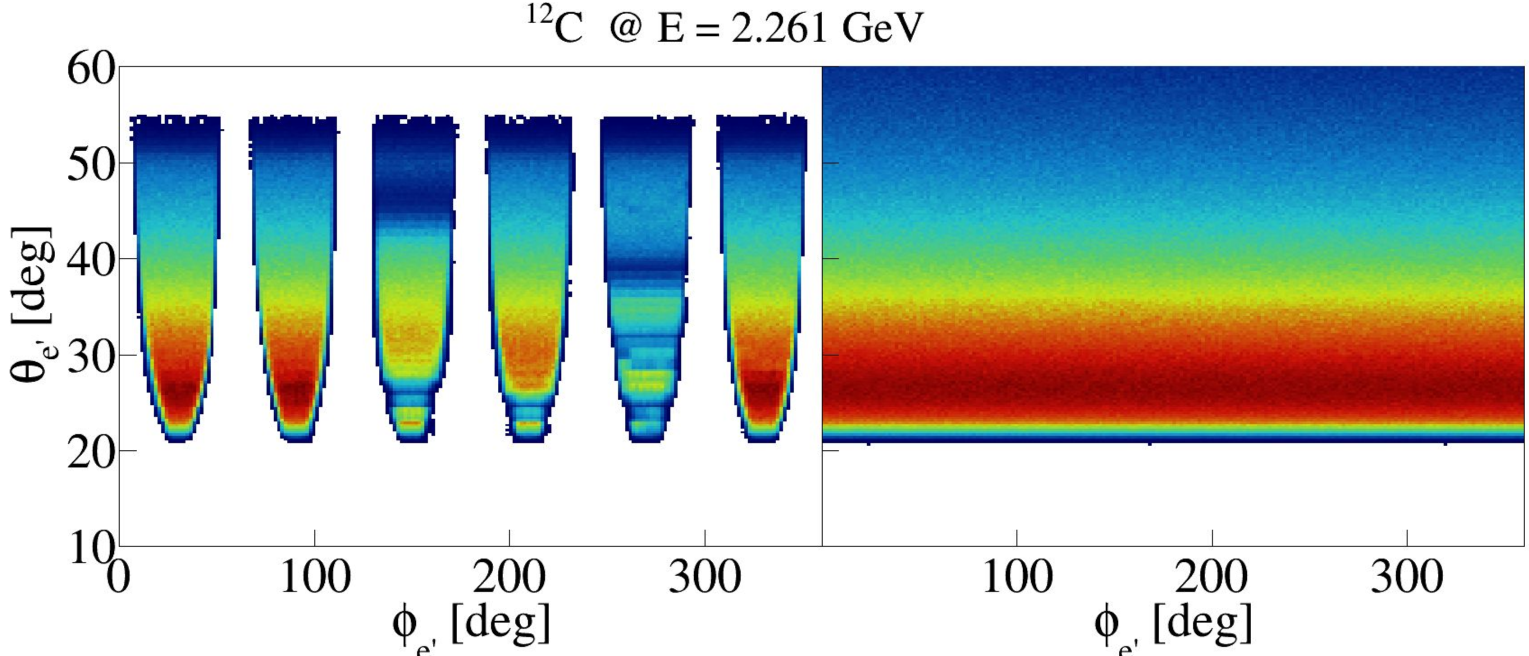

Background Subtraction

Non-(e,e'p) interactions lead to multi-hadron final states
Gaps can make them look like (e,e'p) events

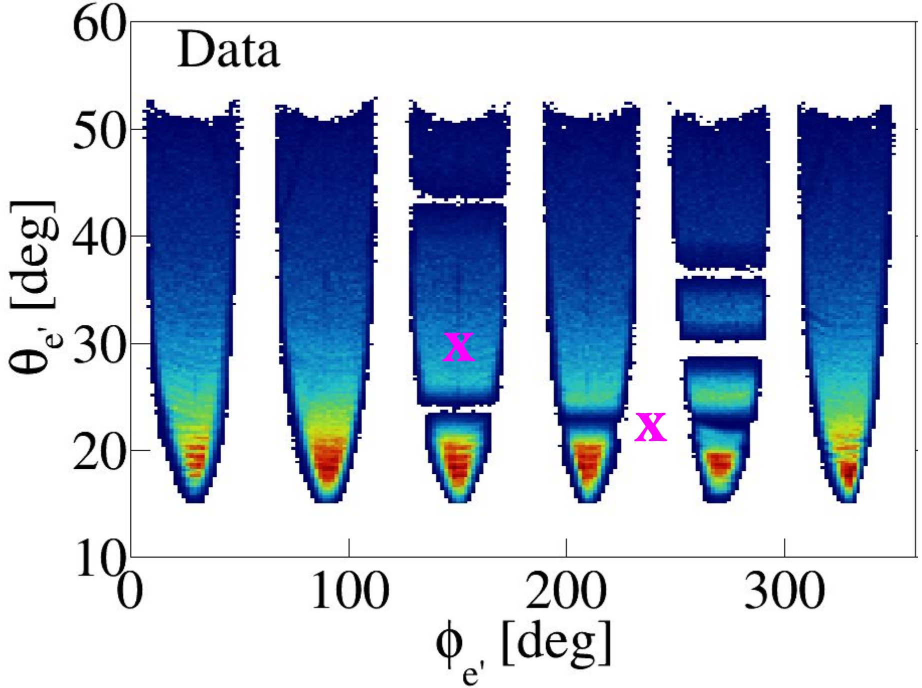

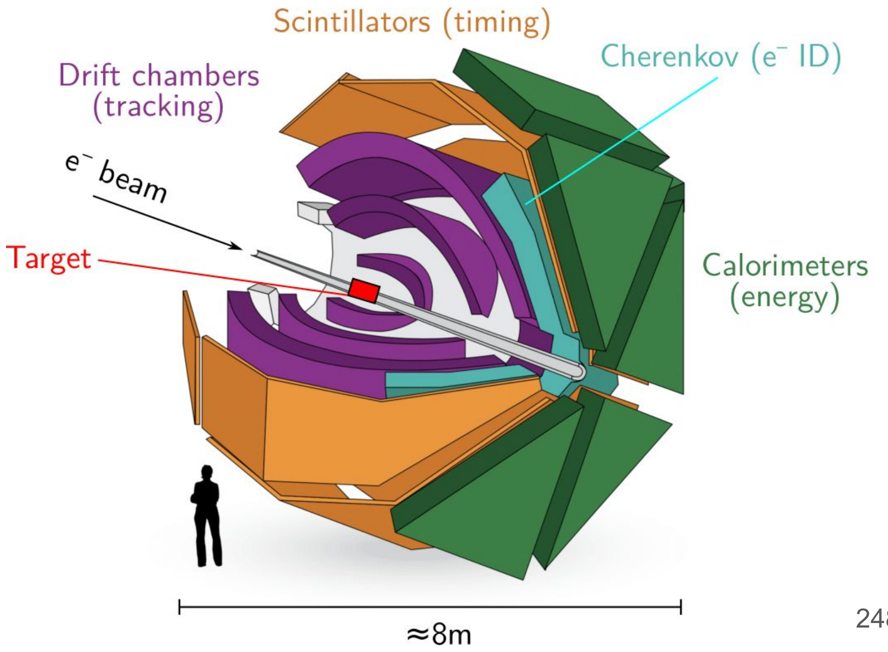

Data Driven Correction

Non-(e,e'p) interactions lead to multi-hadron final states
Gaps make them look like (e,e'p) events

- Use measured (e,e'pπ) events
- Rotate p, π around q to determine π detection efficiency
- Subtract undetected (e,e'pπ)
- Repeat for higher hadron multiplicities

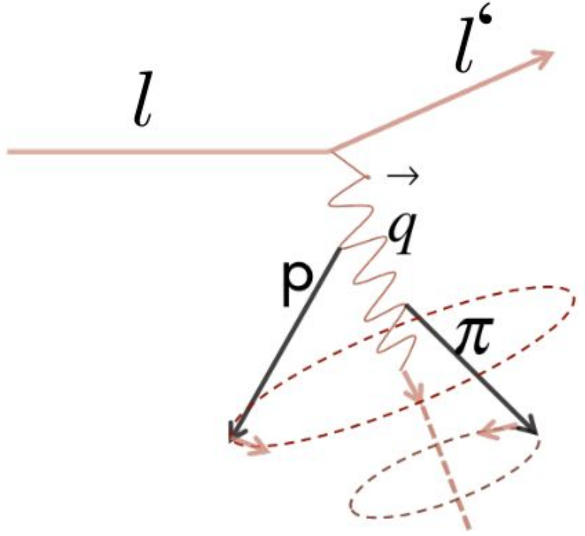

Data Driven Correction

Non-(e,e’p) interactions lead to multi-hadron final states
Gaps can make them look like (e,e’p) events

- Use measured (e,e’pπ) events
- Rotate p, π around q to determine π detection efficiency
- Subtract for undetected (e,e’pπ)
- Repeat for higher hadron multiplicities

(2p, 3p, 2p+1π, …)

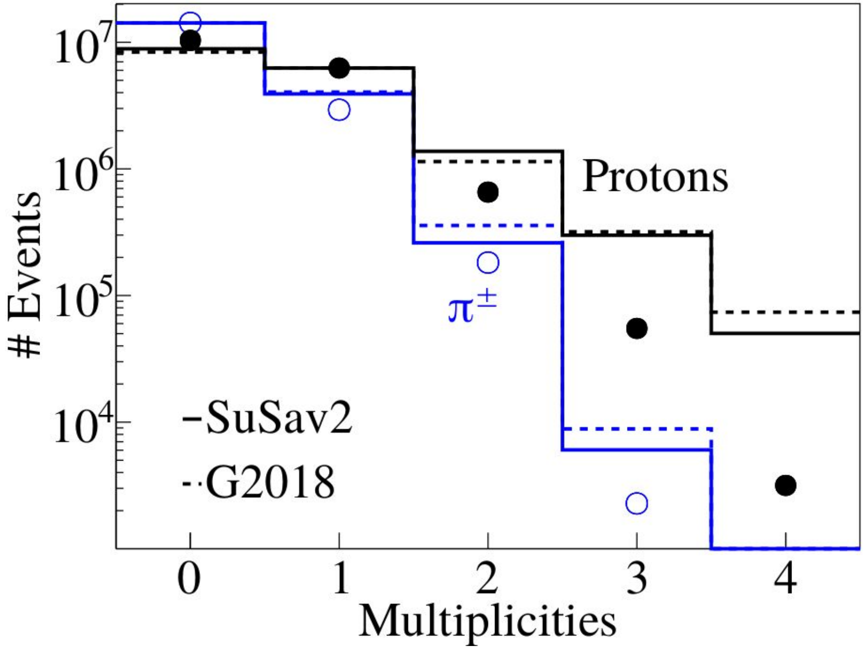

Subtraction Effect

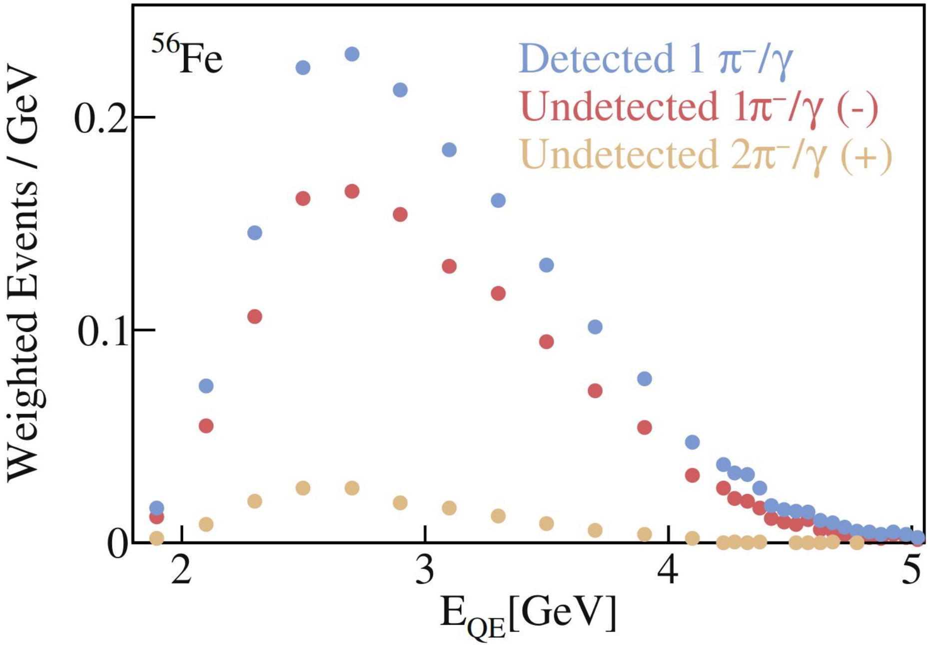

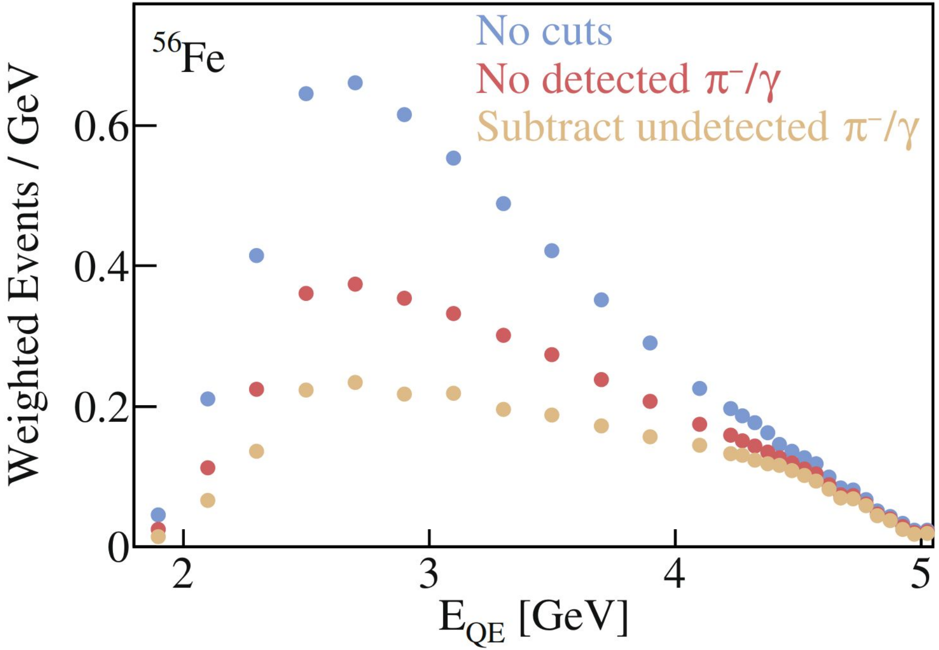

Systematics: Sector Dependence

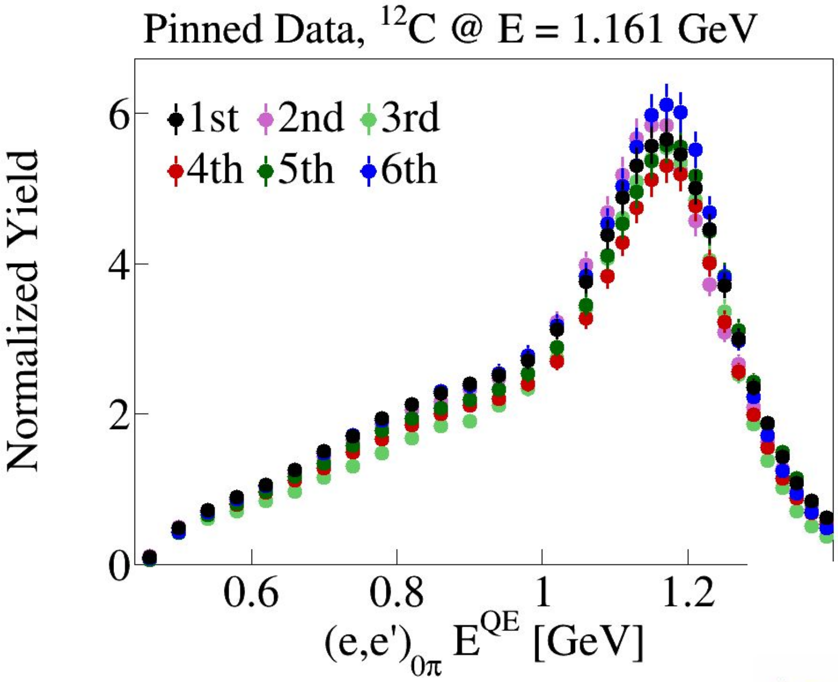

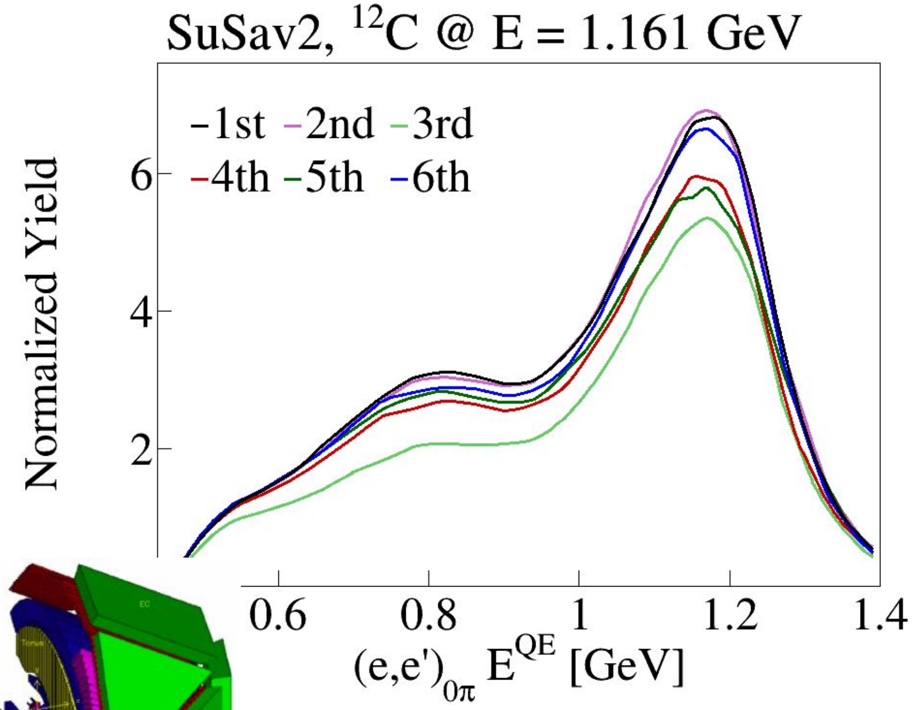

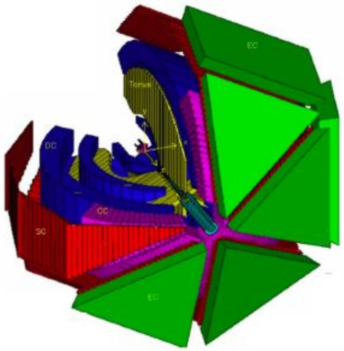

Systematics: Sector Dependence

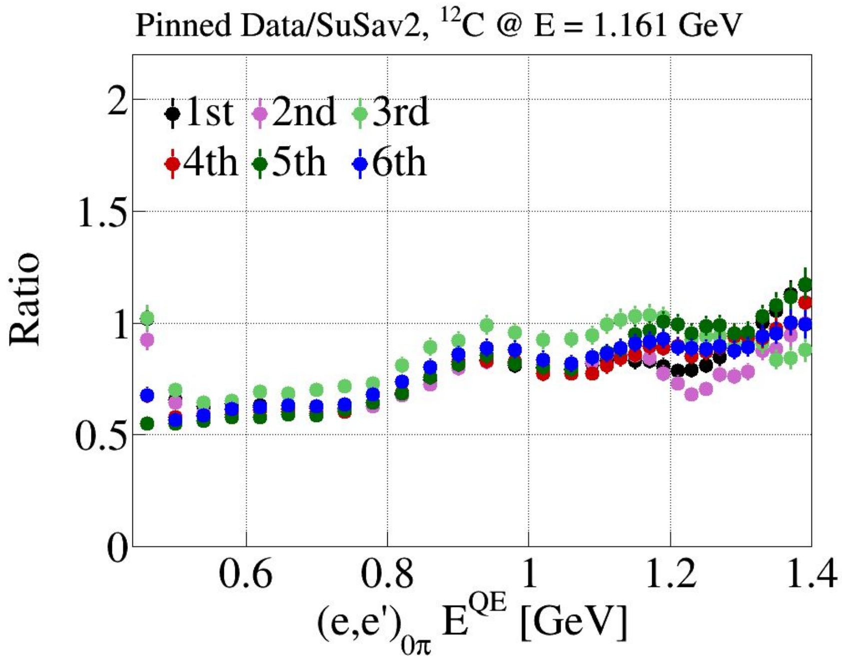

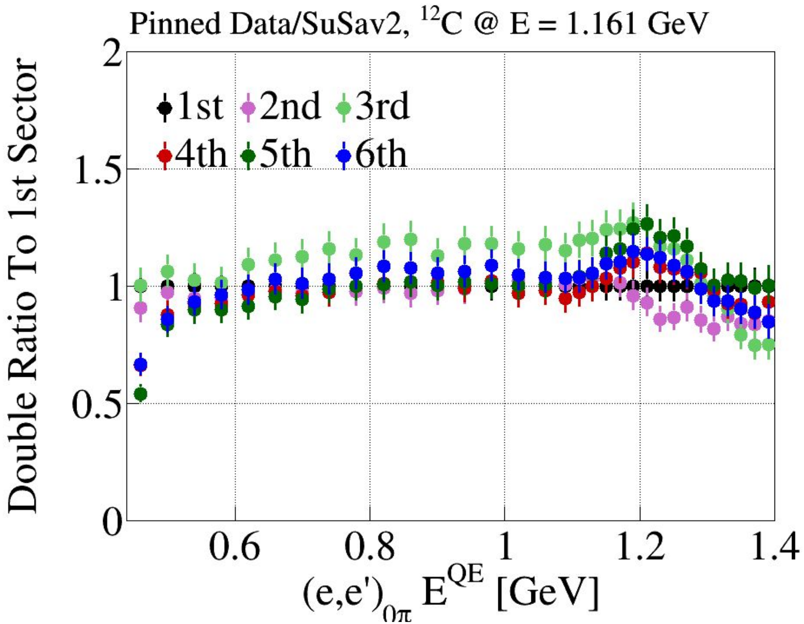

Systematics: Sector Dependence

Quantifying uncertainty by using
unweighted variance & by subtracting variance from statistical uncertainty

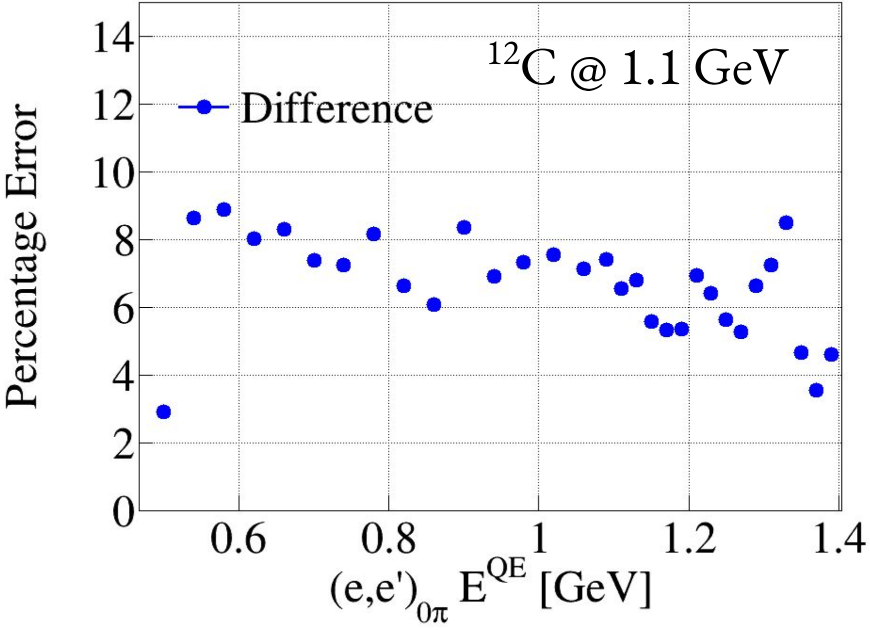

- Playing this game across all nuclei & energies
- Division by $\sqrt{N_{sectors}}$
- Flat uncertainty of 6%

1st e4ν Submission

Calorimetric energy reconstruction using the 1p0π channel

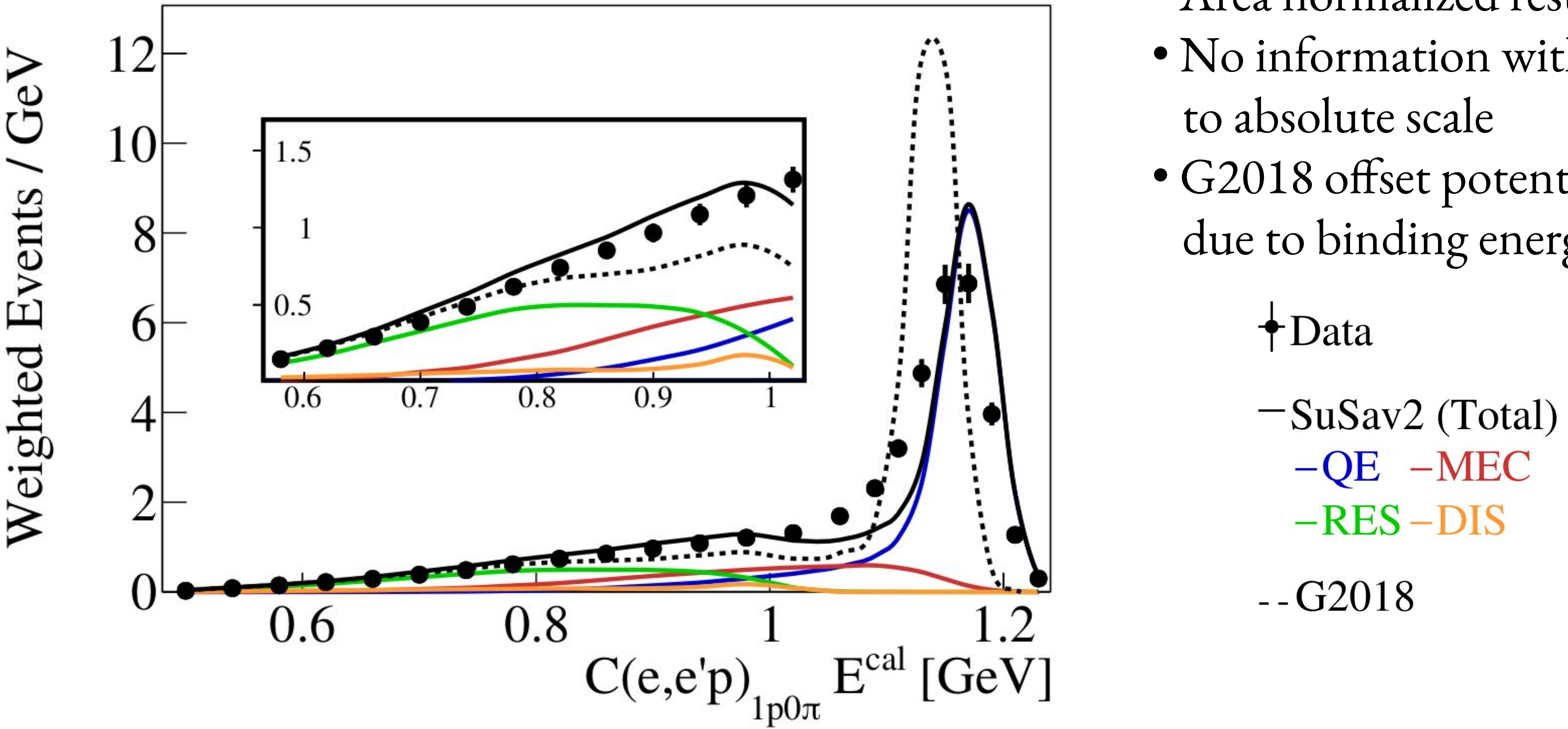

- Area normalized results
- No information with respect to absolute scale
- G2018 offset potentially due to binding energy issue

Step #2: Normalized Yield

Data

- Divide # events by integrated charge & target thickness to get xsec in μb
- Divide by bin width to get μb/GeV

Simulation

- Get GENIE total cross section for E_e / target A & Q2 > $Q2_{min}$
- xsec = (Selected detected events / all generated events) * total xsec / bin width

No corrections for CLAS acceptance or for bremsstrahlung radiation

Step #2: Normalized Yield

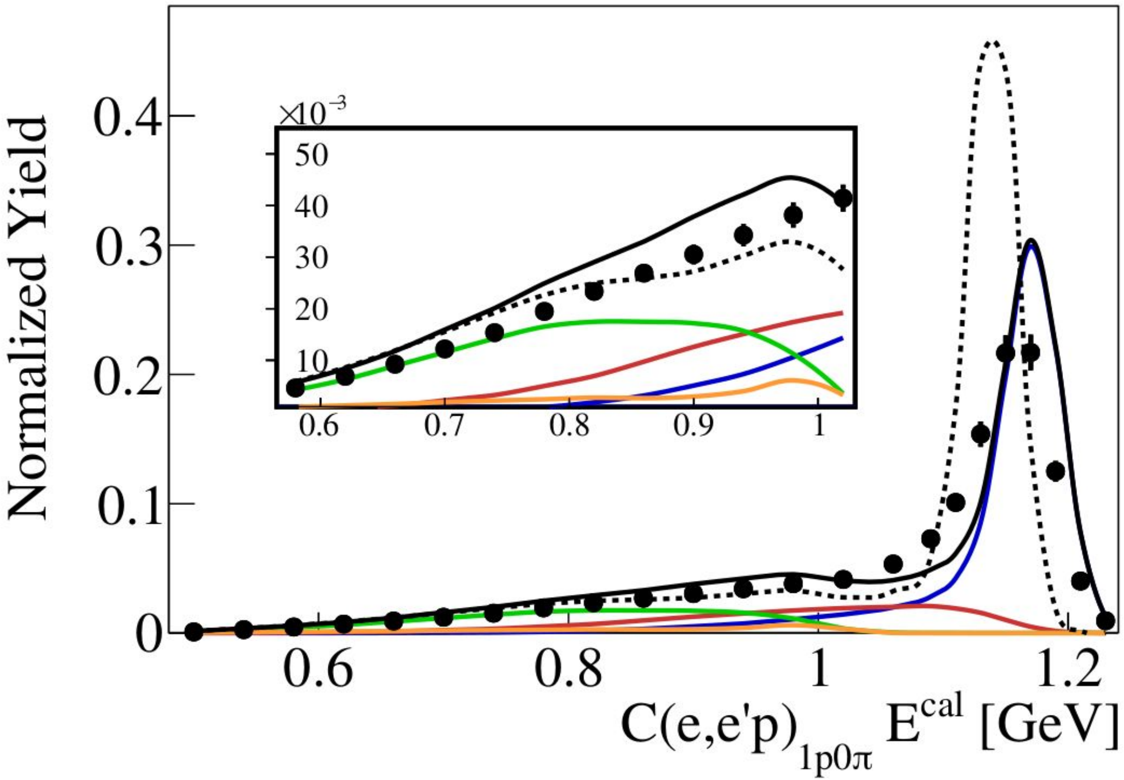

- Absolute scale comparison
- Small effect @ 1GeV

Step #3a: Acceptance Correction

- Start from reco / true ratio w/o radiation to obtain acceptance correction
- Average on a bin-by-bin basis x = |SuSav2 + G2018| / 2
- Due to offset, G2018 Ecal predictions have been shifted by 10/25/36 MeV for 4He/12C/56Fe respectively

Step #3a: Example 12C @ 1.1 GeV

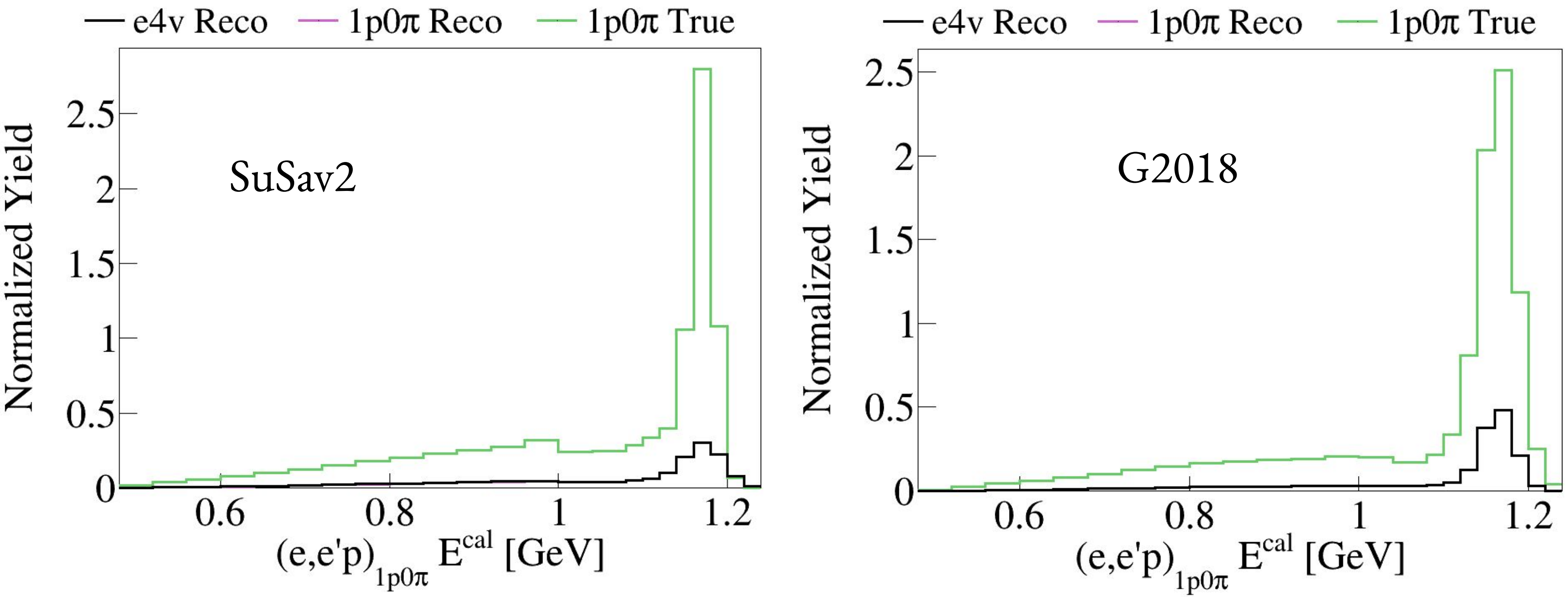

Use reco / true ratio to obtain acceptance correction

Step #3b: Radiation Correction

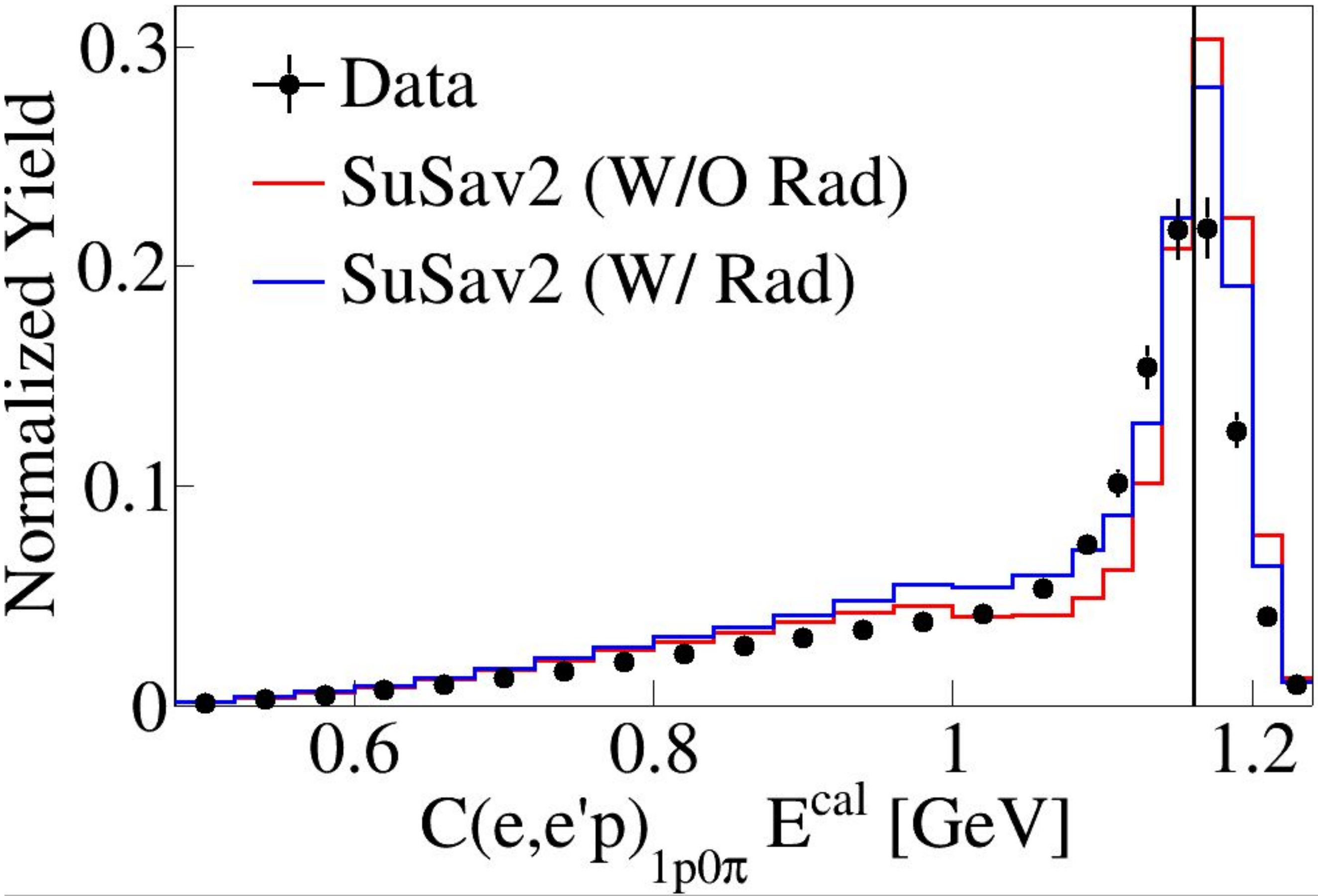

Use ratio of red / blue to correct for radiation

Averaged Acceptance Correction Uncertainty Over True Beam Energy

On a bin-by-bin basis

x = |SuSav2 - G2018| / Sqrt(12)

Bin Entry = x / Average * 100 %

Same recipe as for acceptance correction but,
to avoid infinities, will use average (1 bin) around the peak and
average(reco) / average(true) for correction factor

Excluding Radiation

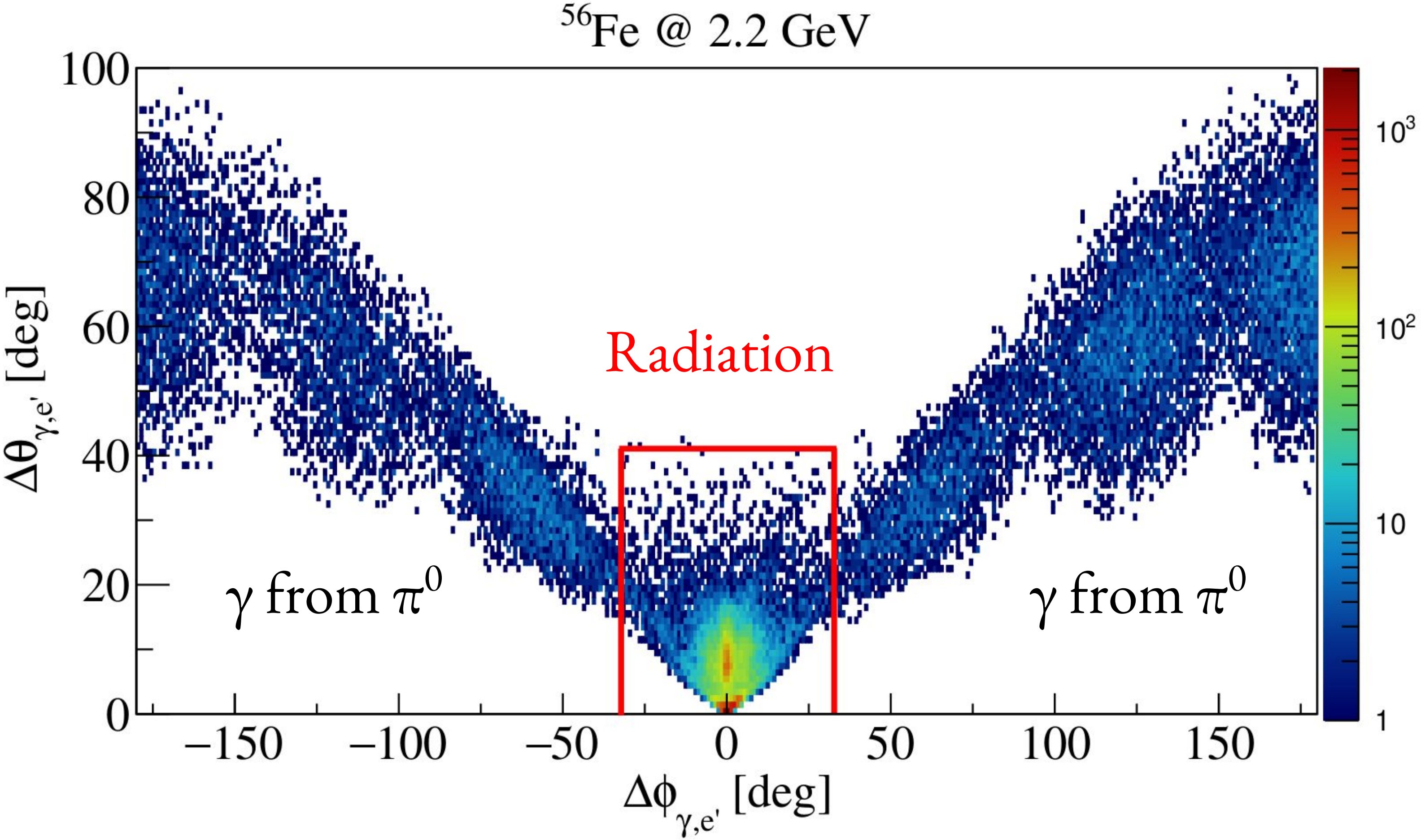

Correction Factors

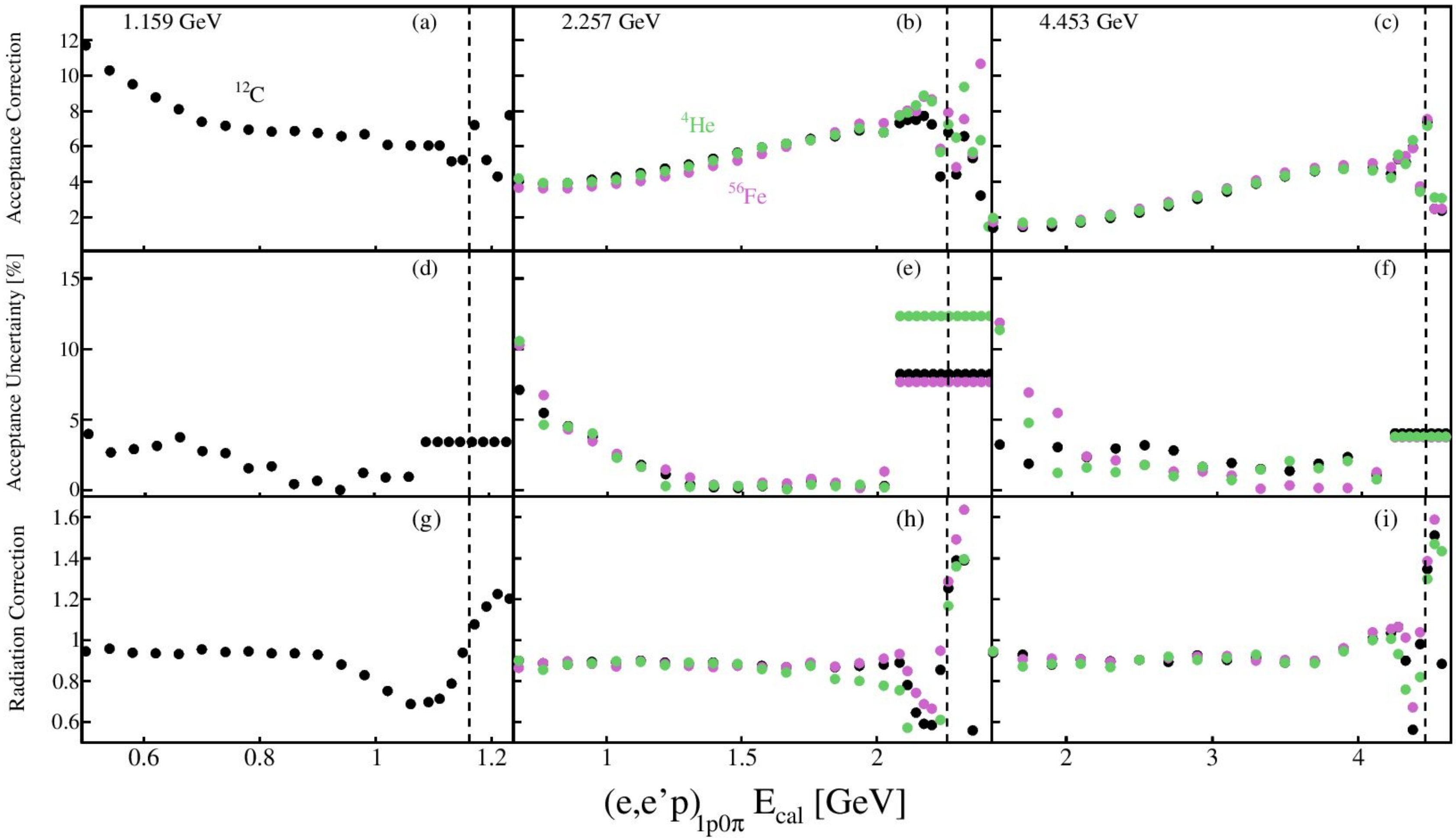

Step #4: Absolute Cross Sections

After both acceptance & radiation corrections, without systematics yet

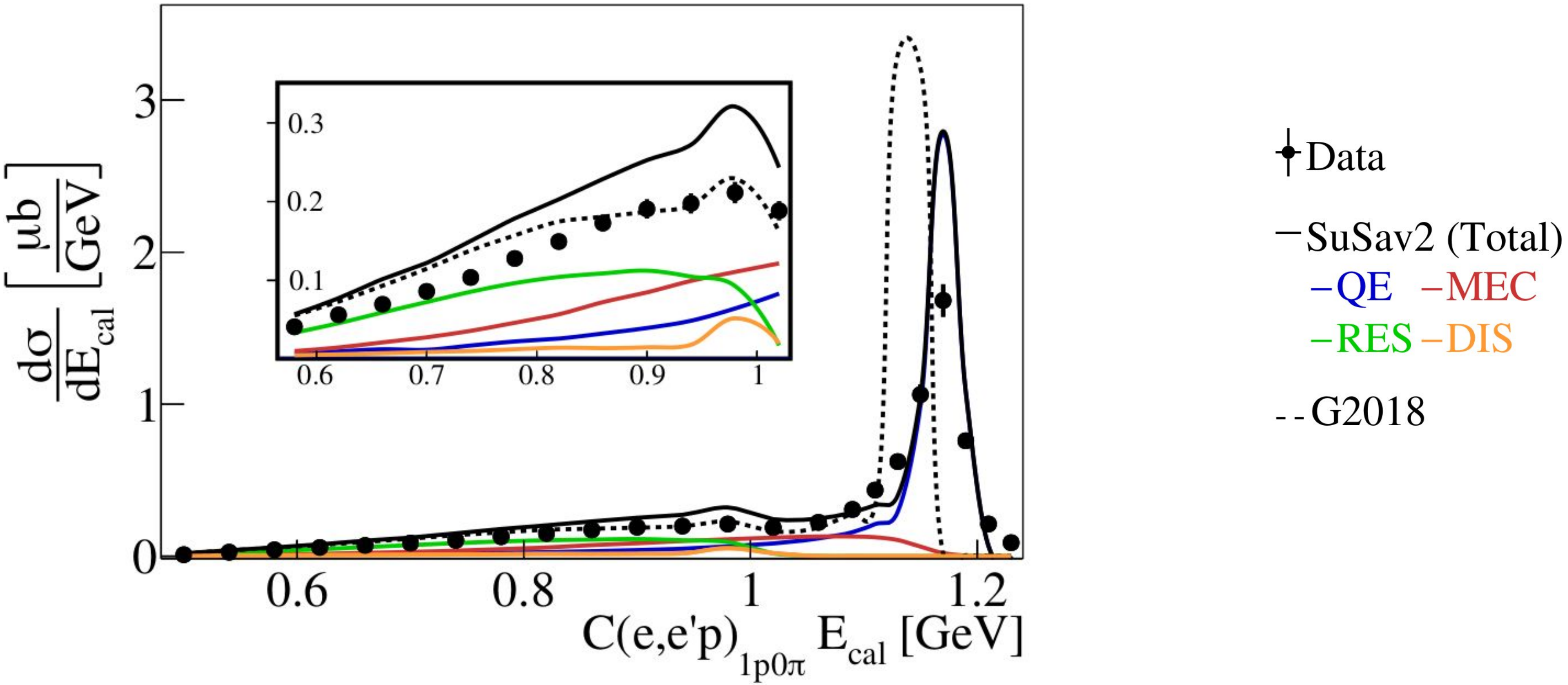

Systematics

Source	Uncertainty (%)
Detector acceptance Identification cuts $\varphi_{q\pi}$ cross section dependence Number of rotations	2,2.1,4.7 (@ 1.1,2.2,4.4 GeV)
Sector dependence	6
Acceptance correction	2-15
Overall normalization	3
Electron inefficiency	2

Energy Reconstruction Accuracy

		1.159 GeV		2.257 GeV		4.453 GeV	
		Peak Fraction	Peak Sum [μb]	Peak Fraction	Peak Sum [μb]	Peak Fraction	Peak Sum [μb]
^{4}He	Data	-	-	41	0.48	38	0.15
	SuSAv2	-	-	45	1.31	22	0.14
	G2018	-	-	39	0.93	24	0.16
^{12}C	Data	39	4.13	31	1.26	32	0.34
	SuSAv2	44	5.33	27	1.76	12	0.20
	G2018	51	6.53	37	2.44	23	0.43
^{56}Fe	Data	-	-	20	3.73	23	1.01
	SuSAv2	-	-	21	5.28	10	0.58
	G2018	-	-	30	8.22	19	1.48

E_{QE} Nucleus & Energy Dependence

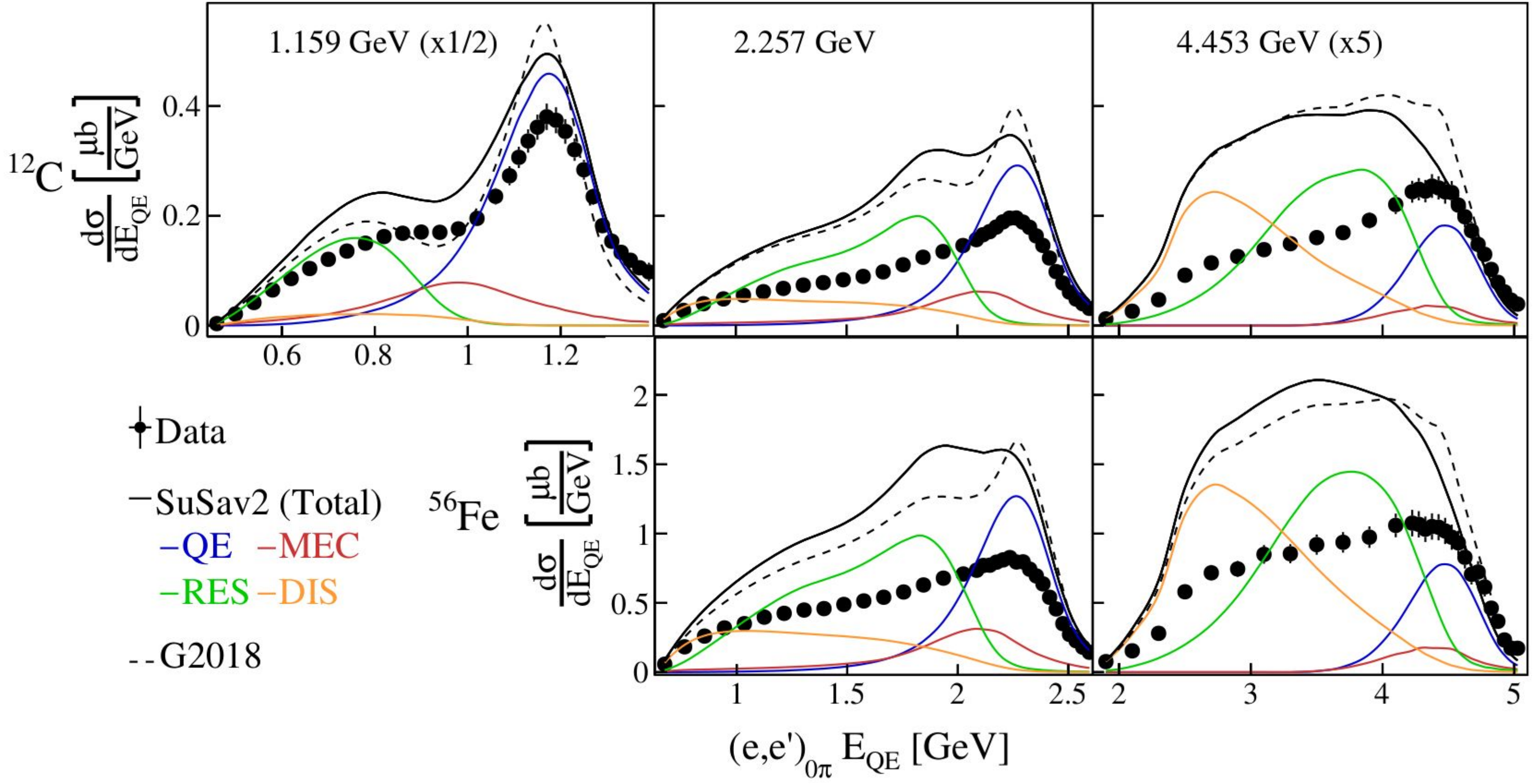

$$E_{QE} = \frac{2M\epsilon + 2ME_l - m_l^2}{2(M - E_l + |k_l|\cos\theta_l)}$$

A.Papadopoulou, et al,
In preparation

P_T Nucleus & Energy Dependence

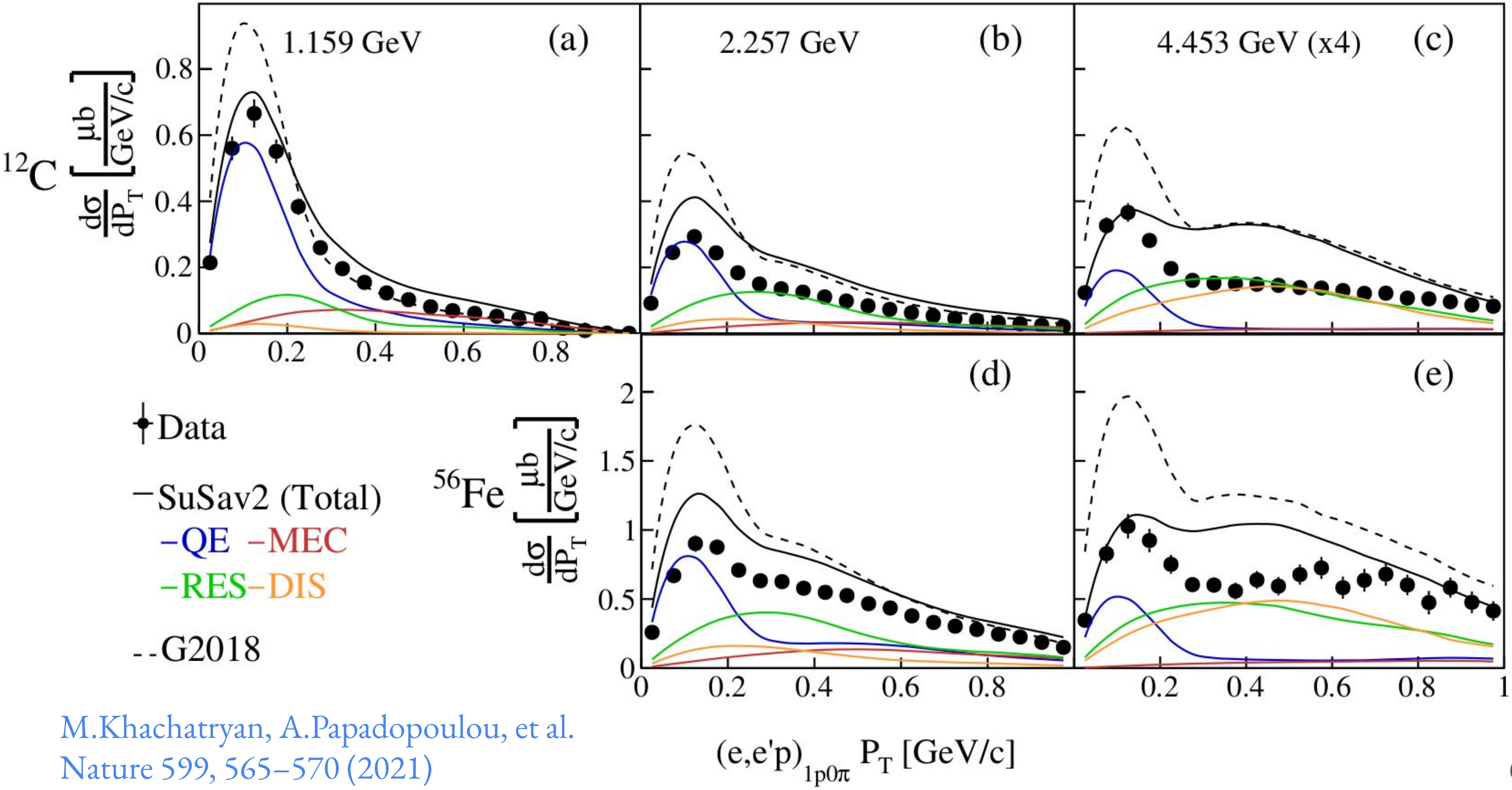

M.Khachatryan, A.Papadopoulou, et al.
Nature 599, 565–570 (2021)

$\delta\alpha_T$ Nucleus & Energy Dependence

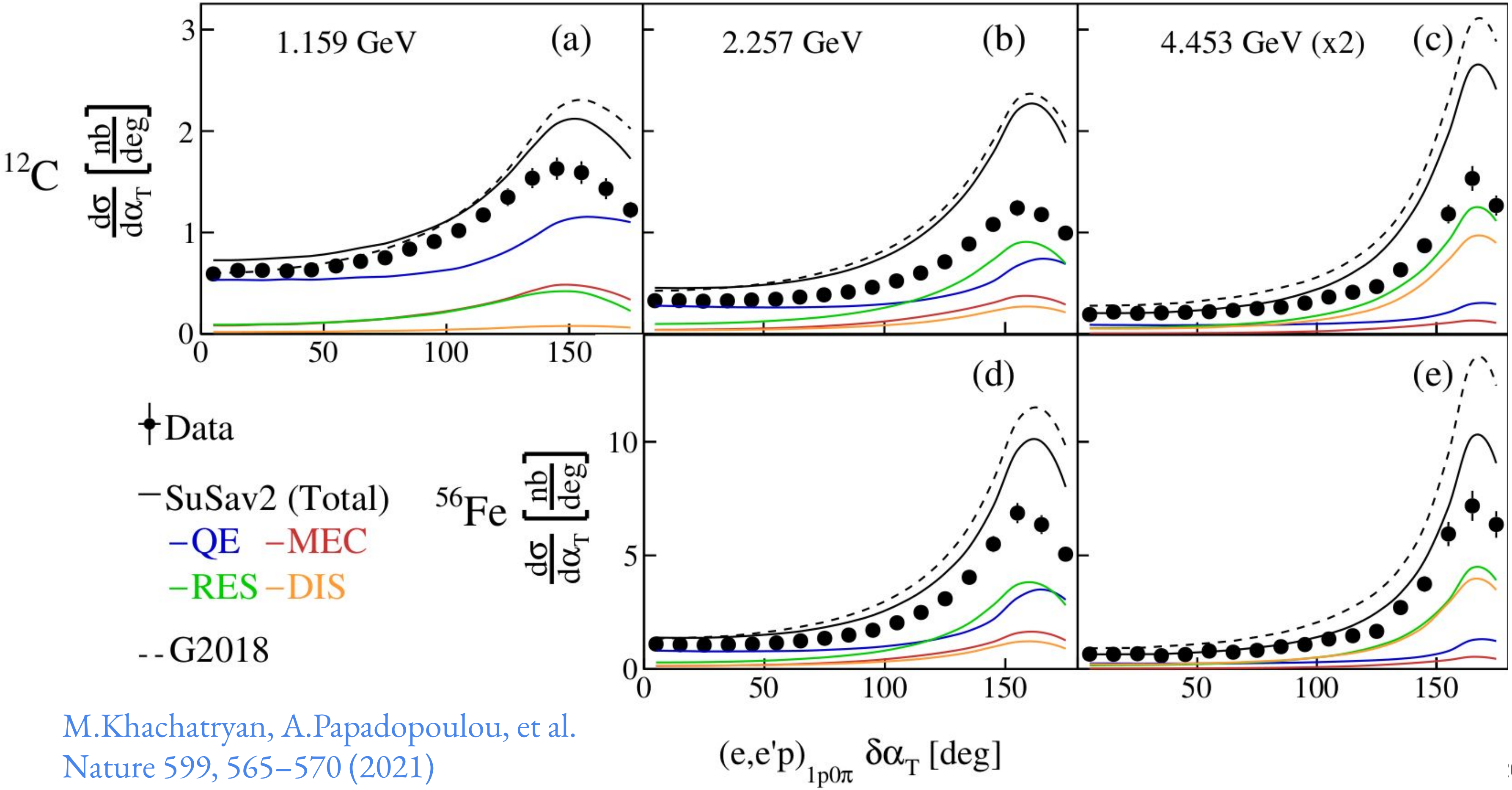

M.Khachatryan, A.Papadopoulou, et al.
Nature 599, 565–570 (2021)

$\delta\varphi_T$ Nucleus & Energy Dependence

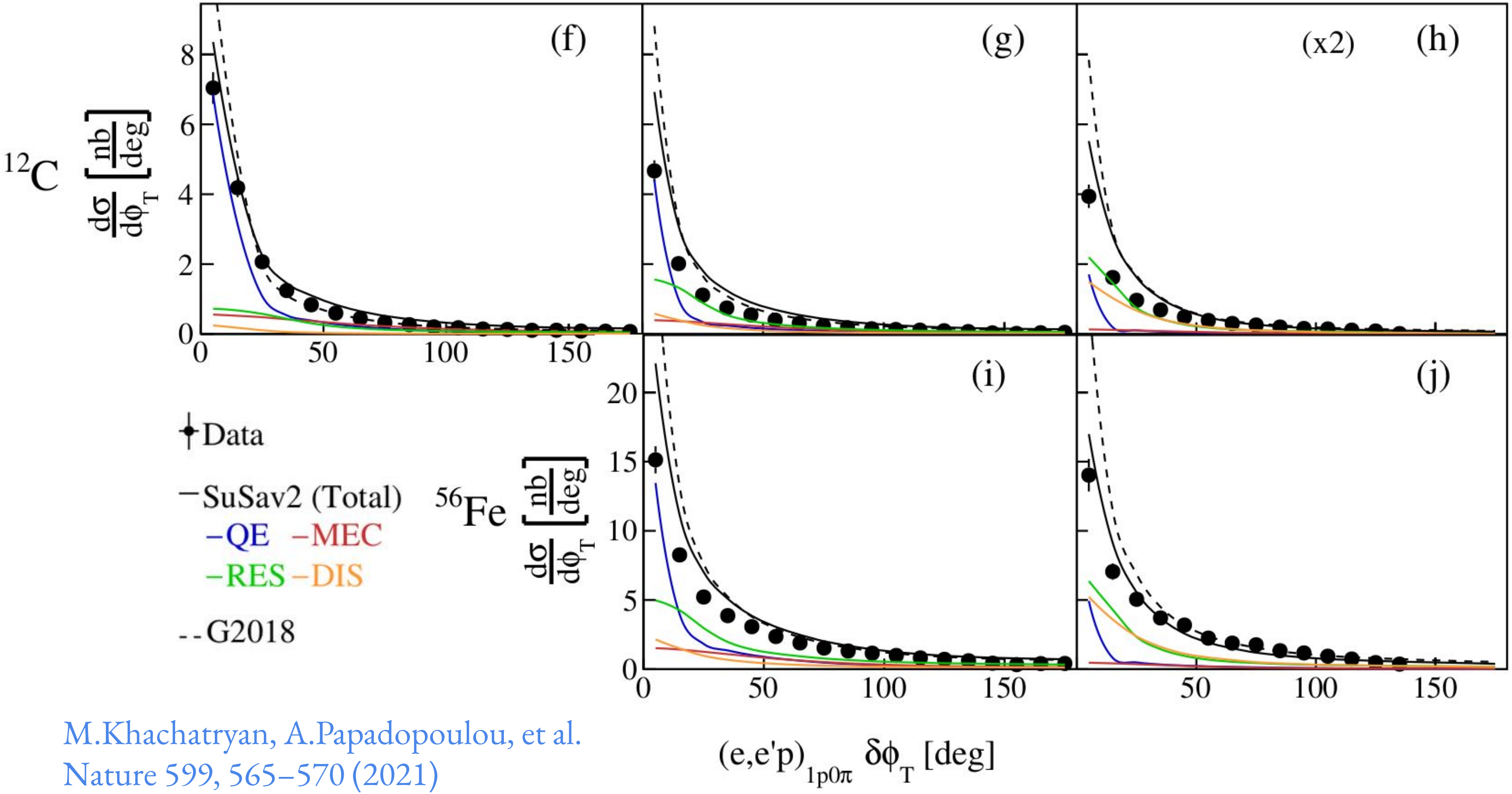

M.Khachatryan, A.Papadopoulou, et al.
Nature 599, 565–570 (2021)

Into The 3D e4ν Multiverse!

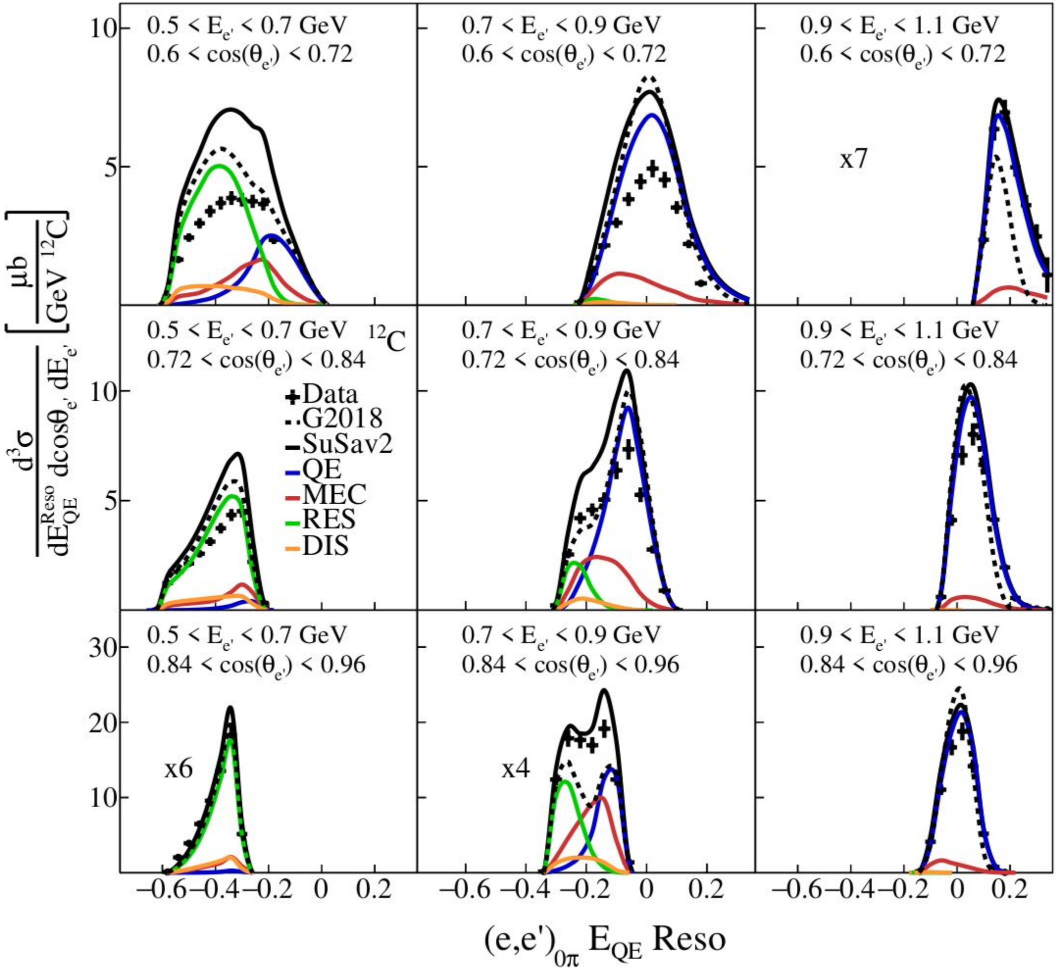

A.Papadopoulou, et al,
In preparation

Nuclear Sensitivity Variables

$\delta p_{T_x} = (\hat{p}_\nu \times \hat{p}_T^l) \cdot \delta\vec{p}_T = |\delta\vec{p}_T| \sin(\delta\alpha_T)$

Sensitivity to Fermi motion

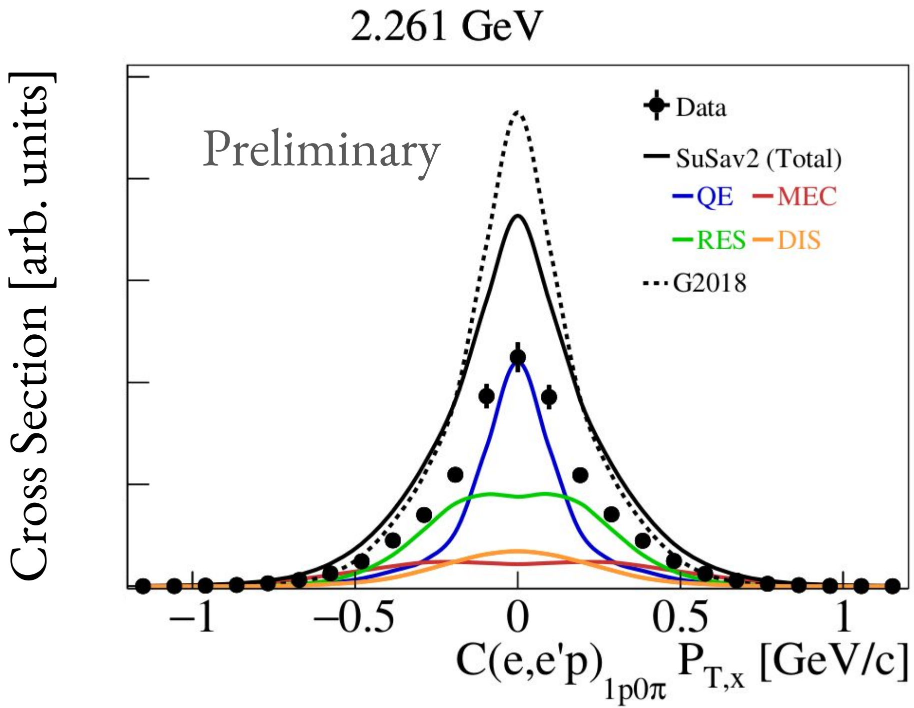

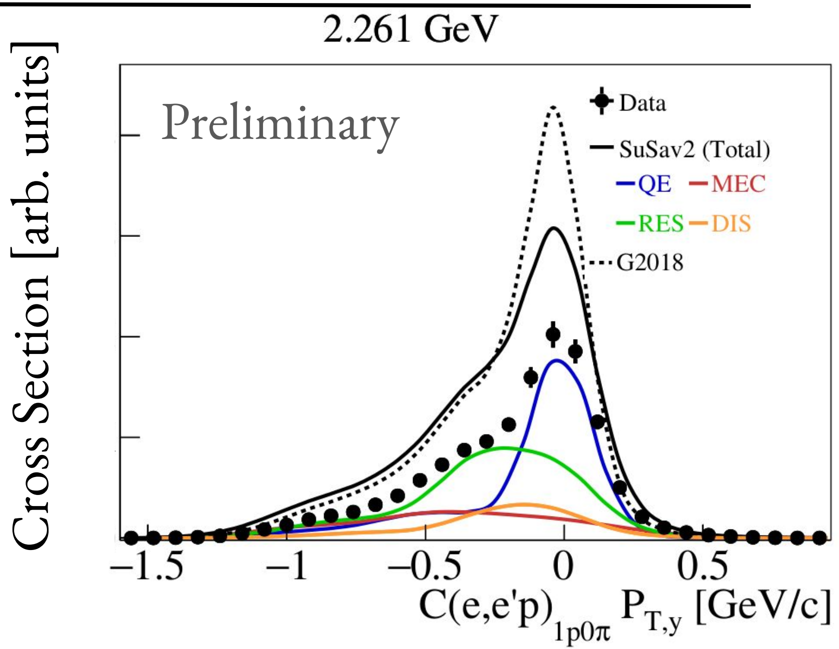

$\delta p_{T_y} = -\hat{p}_T^l \cdot \delta\vec{p}_T = |\delta\vec{p}_T| \cos(\delta\alpha_T)$

Sensitivity to final state interactions

A.Papadopoulou, et al, In preparation

Missing Momentum Approximation

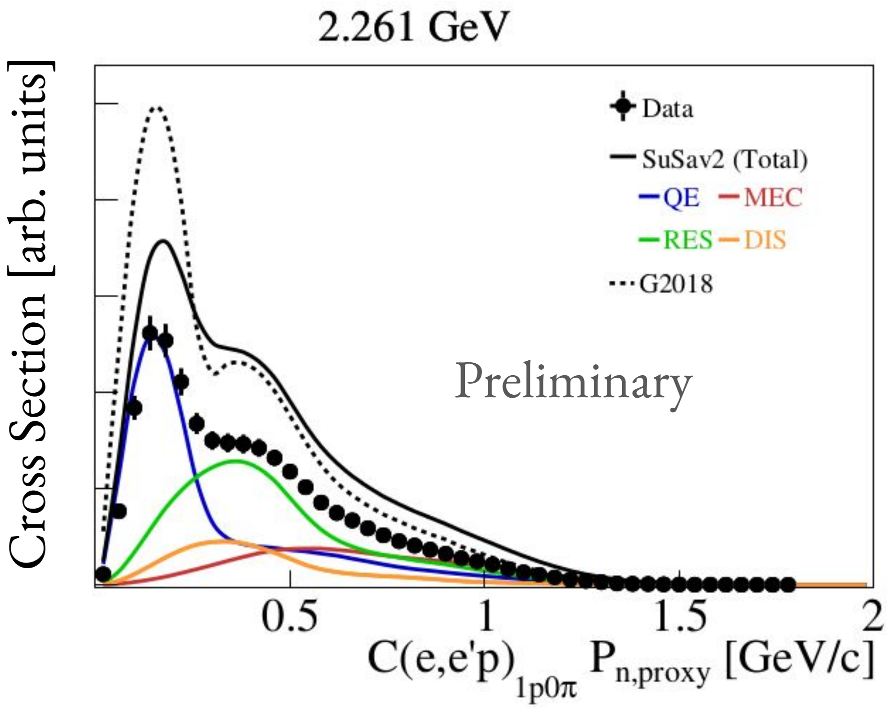

A.Papadopoulou, et al, In preparation

$$p_{n,proxy} = \sqrt{\delta p_L^2 + \delta p_T^2}$$

Under QE assumption

Phys. Rev. Lett. 121, 022504 (2018)

Fails To Reproduce True Missing Momentum

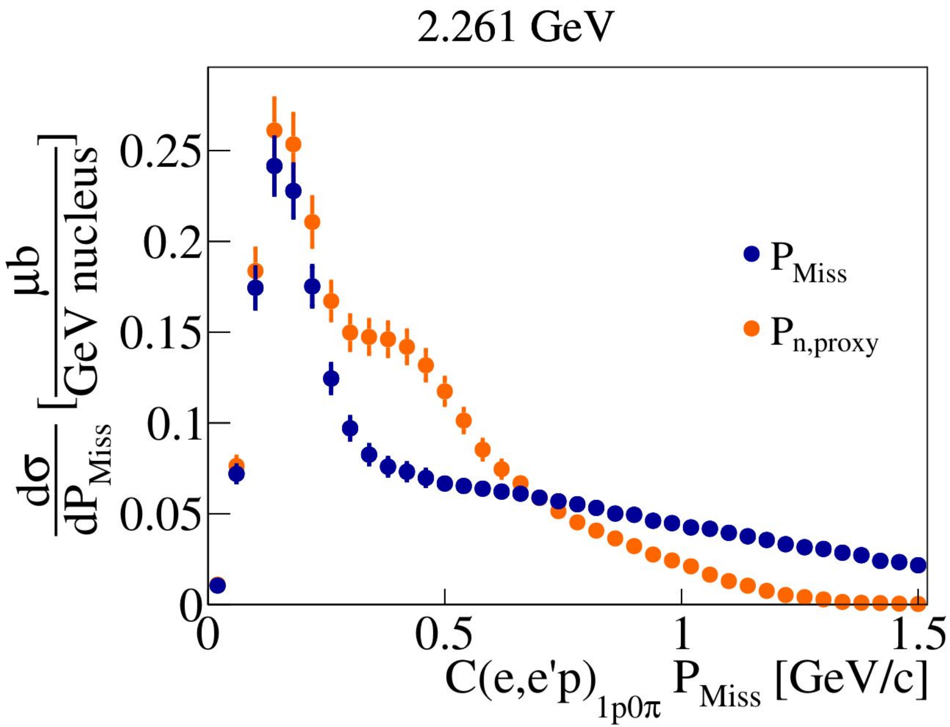

A.Papadopoulou, et al, In preparation

$$p_{n,proxy} = \sqrt{\delta p_L^2 + \delta p_T^2}$$

Under QE assumption

Phys. Rev. Lett. 121, 022504 (2018)

True missing momentum

$$P_{miss} = |p - q|$$

p = proton 3-vector
q = momentum transfer

The e4ν Result Factory Continued!

- More inclusive results
- More complex channels
- Nuclear sensitivity variables
- Multi-differential results

e4ν Collaboration, In preparation

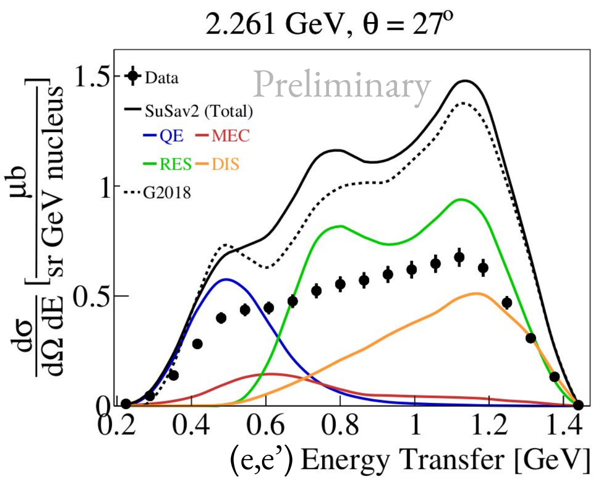

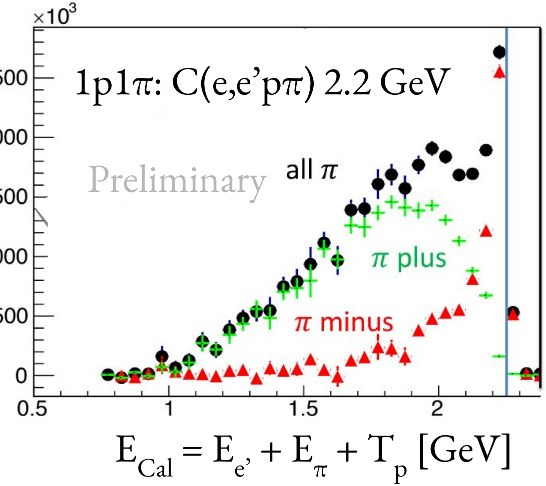

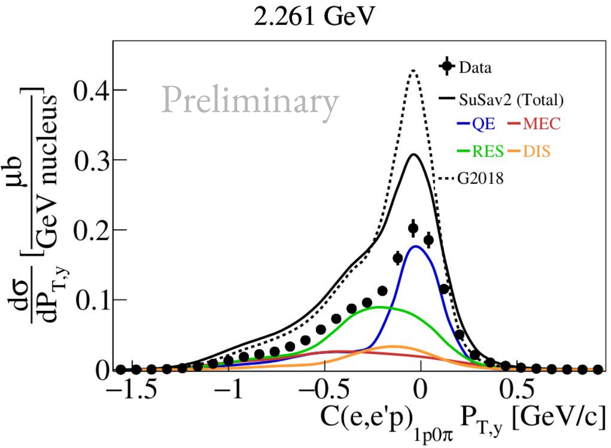

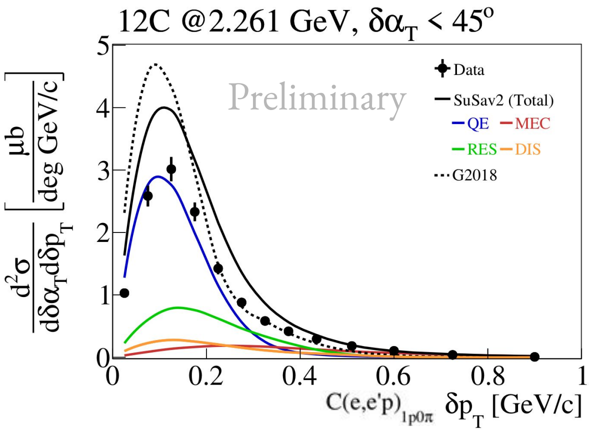

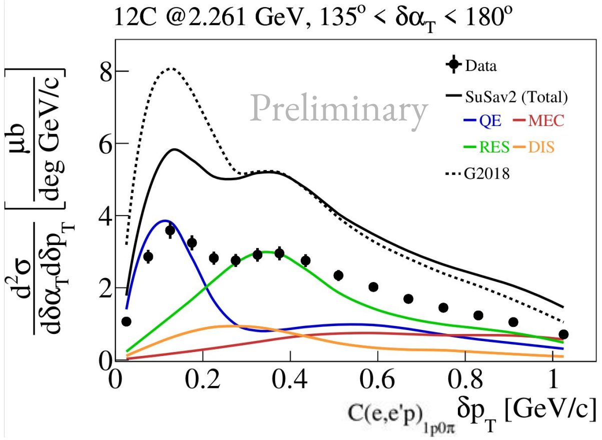

Inclusive Results

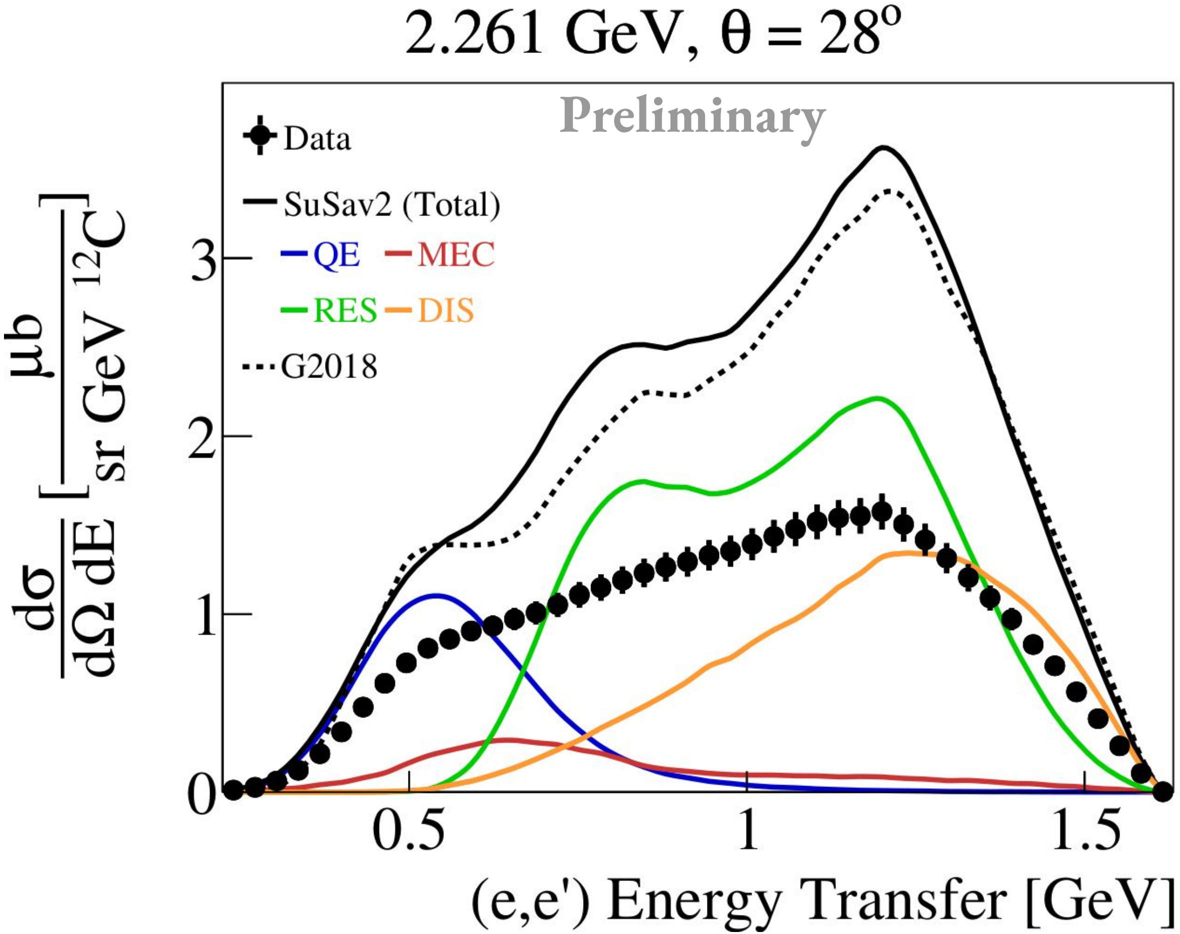

The e4ν Result Factory Continued!

- Scan over multiple angles
- Results on Argon soon

e4ν Collaboration
In preparation

Nuclear Sensitivity Variables

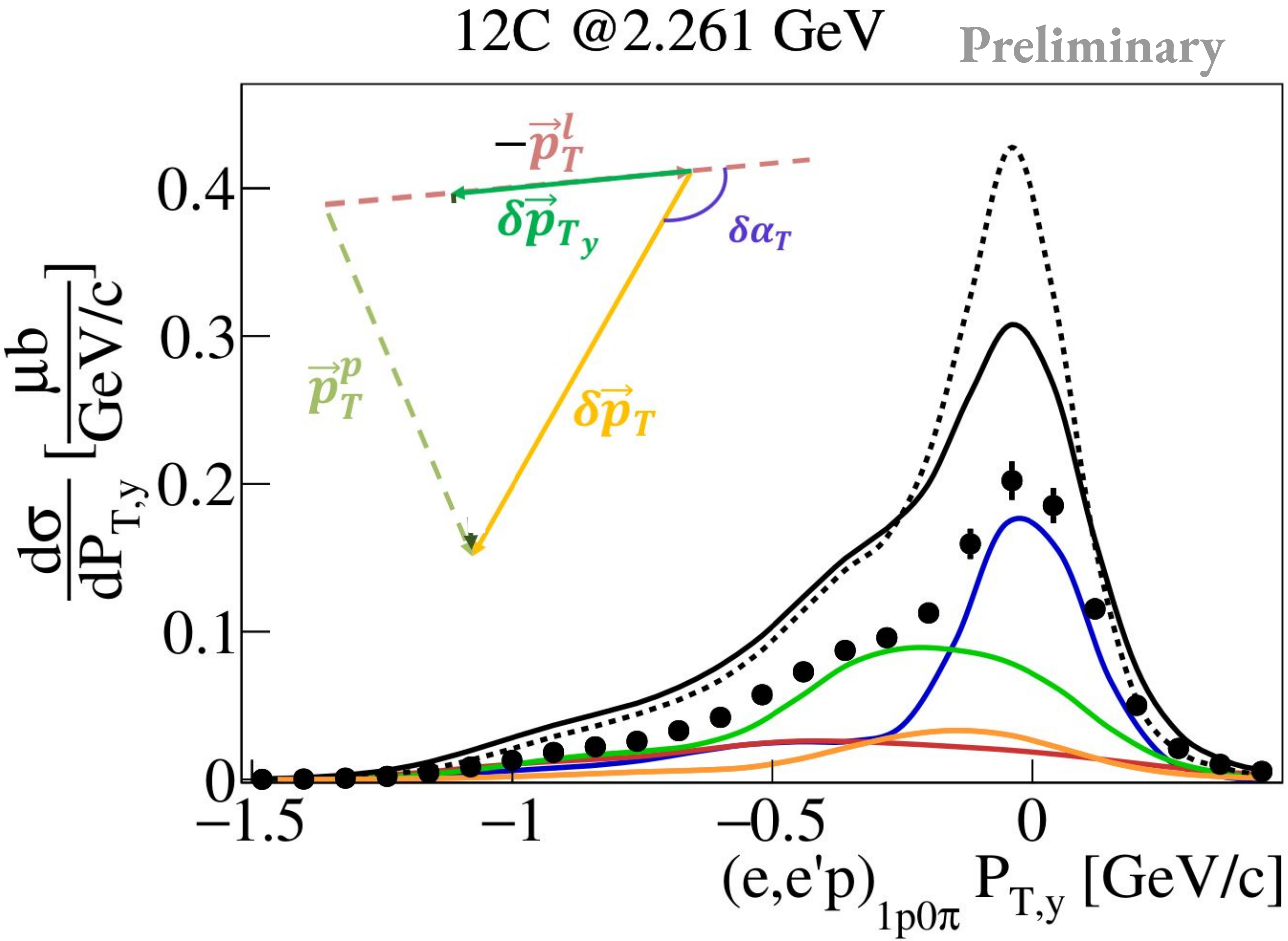

$\delta p_{T_y} = -\hat{p}_T^{\,l} \cdot \delta\vec{p}_T = |\delta\vec{p}_T| \cos(\delta\alpha_T)$

The e4ν Result Factory Continued!

- Fermi motion
- Final state interactions (FSI)

e4ν Collaboration
In preparation

Double Differential Results

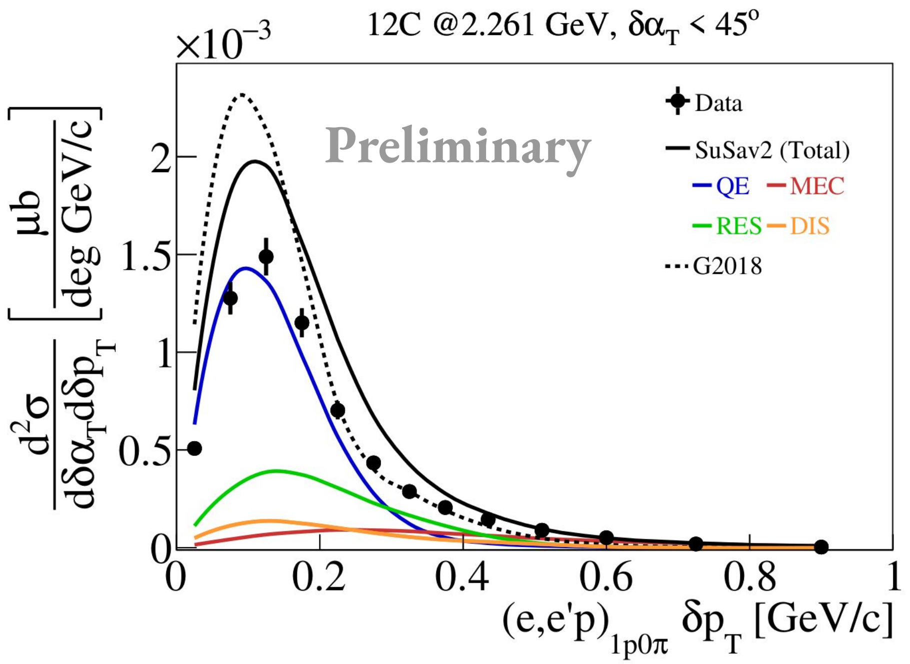

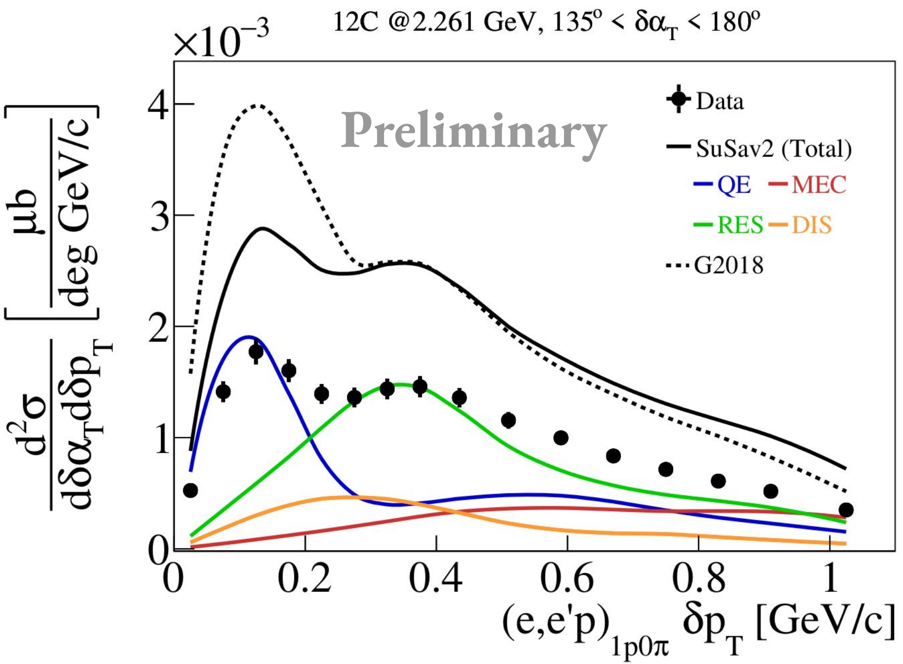

The e4ν Result Factory Continued!

e4ν Collaboration
In preparation

- Handle over FSI / initial state effects
- Tuning potential